THE DEVELOPMENT OF ANALYTICAL TECHNIQUES FOR STUDYING DEGRADATION IN IMPACT POLYPROPYLENE COPOLYMERS

by

ELANA DE GOEDE

Dissertation presented for the degree of
Doctor of Science (Polymer Science)

at the
University of Stellenbosch

Study leader: Prof H Pasch
Co-study leader: Dr PE Mallon

University of Stellenbosch
March 2009

DECLARATION

I, the undersigned, hereby declare that the work contained in this dissertation is my own original work and has not previously been submitted in its entirety or in part at any university for a degree.

Signature:_____ Date:_____

ABSTRACT

Unstabilised polyolefins are susceptible to degradation when exposed to molecular oxygen, heat, irradiation as well as chemical and mechanical stimuli. Oxidation leads to changes in molecular properties such as molecular weight, molecular weight distribution, chemical composition, chemical composition distribution and crystallisability. Conventional analytical techniques are of limited use when studying the degradation of heterogeneous materials such as impact polypropylene copolymers (ICPP). These copolymers consist of a number of components of different monomer contents, isotacticity and crystallinity, ranging from amorphous EPR to highly crystalline polypropylene. The individual components are affected differently by degradation, leading to heterogeneity within the degradation of impact copolymers. Novel analytical approaches that acknowledge the heterogeneity in sample composition are needed to study the degradation behaviour of such heterogeneous materials.

This study describes the combination of fractionation and hyphenated techniques with conventional analyses for extensive structural characterisation of complex impact copolymers as well as their degradation behaviour. Temperature rising elution fractionation (TREF) coupled to conventional techniques such as size exclusion chromatography (SEC), Fourier-Transform infrared spectroscopy (FTIR), Carbon-13 nuclear magnetic resonance (^{13}C-NMR) and differential scanning calorimetry (DSC) indicated the ICPPs in question to consist of four main components, namely ethylene-propylene random copolymers (EPR), isotactic PP (iPP), as well as semi-crystalline ethylene-propylene copolymers (EPC) and lower isotacticity PP. The degradation of an ICPP was studied by a multi-component analysis procedure consisting of TREF coupled to SEC, ^{13}C-NMR, as well as SEC-FTIR. Results obtained by this procedure indicated the change in crystallisability of the bulk sample observed by TREF, crystallisation analysis fractionation (CRYSTAF) and DSC to be the result of the preferential degradation of the iPP phase. Degradation of ICPPs initiates within this phase where chain scission and carbonyl group insertion leads to a change in the crystallisability of iPP chains. During TREF of degraded bulk ICPPs, the degraded iPP molecules elute at lower elution temperatures, depending on their degree of degradation. The other components of the copolymer were degraded to a lesser extent. Degradation products were also found to be heterogeneously distributed across the molecular weight distribution of each fraction, with a higher concentration appearing at the low molecular weight side. The multi-component analysis procedure was also used to study the difference in degradation behaviour between ICPPs of different comonomer content, isotacticity and crystallinity.

The spatial heterogeneity of degradation within ICPPs was studied by Fourier-Transform infrared microspectroscopy (FTIR-μS). A heterogeneous distribution of degradation products was found across the depth of thicker sample specimens. These results were compared to those obtained by conventional layer-by-layer milling followed by SEC, FTIR and CRYSTAF. The principles of degradation within thick samples were similar to that observed for thin films, although additional contributions by sample morphology and oxygen diffusion were detected.

OPSOMMING

Ongestabiliseerde poli-olefiene degradeer in die teenwoordigheid van suurstof, hitte, radiasie, asook chemiese en meganiese stres. Oksidasie lei tot veranderinge in moleculêre massa, moleculêre massaverspreiding, chemiese samestelling, chemiese samestellingverspreiding asook kristalliniteit. Konvensionele analitiese tegnieke is onvoldoende vir die studie van degradasie van heterogene materiale soos impak polipropileen kopolimere. Hierdie kopolimere bestaan onder andere uit etileen-propileen statistiese kopolimere en hoogs kristallyne polipropileen. Degradasie van impak copolimere is heterogeen aangesien die onderskeie komponente verskillend geaffekteer word. Innoverende analitiese tegnieke word tans benodig om die degradasie van hierdie heterogene sisteme te bestudeer.

Tydens hierdie studie is fraksionering- en koppelingstegnieke gekombineer met konvensionele analises ten einde impak kopolimere te karakteriseer en hul degradasie te bestudeer. Temperatuurstygings eluering fraksionering (TREF) gekoppel aan grootte-uitsluitings chromatografie (SEC), infrarooi specktroskopie (FTIR), koolstof-13 kern magnetise resonansie spektroskopie (^{13}C-NMR) en differensiële skandeerkalorimetrie (DSC) het aangedui dat die betrokke impak kopolimeer bestaan uit statisitese etileen-propileen kopolimere (EPR), isotaktiese polipropileen (iPP), semi-kristallyne etileen-propileen kopolimere (EPC) en lae isotaktisiteit polipropileen. Die degradasie van die impak kopolimeer is bestudeer deur middle van ‘n multi-dimensionele analitiese metode bestaande uit TREF gekoppel aan SEC, ^{13}C-NMR en SEC-FTIR. Resultate het aangedui dat die verandering in kristallinitiet van die impak kopolimeer soos aangedui deur TREF, kristallisasie-analise fraksionering (CRYSTAF) en DSC spruit uit die degradasie van die isotaktiese polipropileen komponent. Degradasie van impak kopolimere ontstaan binne hierdie komponent en beide die verkorting en invoeg van karbonielgroepe in kettings lei tot veranderinge in die kristallinitiet van iPP molecules. Gedegradeerde iPP molekules elueer by laer temperature in die TREF eksperiment, afhangend van hulle graad van modifikasie deur degradasie. Alle ander komponente toon ‘n meer geringe mate van degradasie as iPP. ‘n Heterogene verspreiding van degradasieprodukte is ook opgemerk oor die molekulêre massaverspreiding van elke komponent, waar die hoogste konsentrasie aangetref is aan die lae molekulêre massa sy van elke verspreiding. Die betrokke multi-dimensionele prosedure is ook aangewend ten einde die verskil in degradasie van twee impak kopolimere met verskillende komonomeer konsentrasie en isotaktisiteit te bestudeer.

Die ruimtelike heterogeniteit van degradasie binne dikker monsters van die twee kopolimere is bestudeer met behulp van infrarooimikroskopie (FTIR-μS). ‘n Heterogene verspreiding van degradasieprodukte is opgemerk oor die diepte van die dikker monsters, met die hoogste konsentrasie naby die oppervlak. Hierdie resultate is vergelyk met dié bekom deur ‘n laag-op-laag afskilferingstegniek gevolg deur SEC, FTIR en CRYSTAF analise van die lae. Die degradasie beginsels soos vasgelê vir dun films, is ook hier van pas, alhoewel morfologie van die monsters en suurstofdiffusie ook ‘n rol speel.

Dedicated to my parents,
your guidance will always be my cornerstone

and to Phillip,
for your never-ending love and support

ACKNOWLEDGEMENTS

I wish to express my sincerest gratitude to the following people and institutions for their contribution towards this study:

My study leader, **Prof Harald Pasch**, for supervising this study and for giving me the opportunity to spend research visits in Germany.

My co-promoter **Dr Peter Mallon** for his endless patience and guidance during this study and for his many innovative ideas.

Sasol Polymers (Modderfontein) for providing me with the samples studied and the opportunity to use their compounding facilities.

The financial assistance of the **National Research Foundation (NRF)** towards this research is hereby acknowledged. Opinions expressed and conclusions arrived at, are those of the author and are not necessarily to be attributed to the NRF.

I would also like to thank the **German Ministry of Education and Research (BMBF**, Jülich), for the grants received for research in Germany.

Jean McKenzie and **Elsa Malherbe** for their assistance with the high-temperature NMR measurements.

Christoph Brinkmann, **Christel Hock**, **Andreas Albrecht** and **Robert Bruell** for their assistance with SEC, FTIR, LC-FTIR and CRYSTAF analyses at the DKI, Germany.

Gareth Harding for his assistance with high-temperature GPC and CRYSTAF in Stellenbosch as well as **Margaretha Brand** and **Liesl Keulder** for TCB distillation.

The members of **Lab 134** (Stellenbosch) and the **'Analytik' group** (Darmstadt) for creating a pleasant working environment within which to perform this study and for sharing scientific knowledge.

Erinda, **Aneli**, **Margie** and **Calvin** for administrative assistance during my studies.

On a more personal note I would like to thank **my parents** for their love and support throughout my studies. Also, I would like to thank my **brothers** for their interest in my studies.

My South African friends, **Margaretha**, **Gareth**, **Jerrie**, **Celeste**, **Kenneth**, **Marius**, **Nadine**, **Liesl** and **Aimee** are thanked for their friendship, support and scientific contributions during this study. **Jacques**,

Pritish, **Birgit**, **Tobias**, **Laura**, **Mats** and **Sawa** are also thanked for making my time overseas enjoyable.

Finally I would like to thank **Phillip** for his love, support and tolerance during my post-graduate studies.

Table of contents

LIST OF FIGURES

Chapter 4

Chapter 5

Appendix

LIST OF SCHEMES

Chapter 2

Chapter 3

Chapter 4

LIST OF TABLES

Chapter 2

Chapter 3

Chapter 4

Appendix

Glossary

List of Abbreviations

^{13}C-NMR	Carbon-13 nuclear magnetic resonance
AFM	Atomic force microscopy
aPP	Atactic polypropylene
ATR	Attenuated total reflectance
ATR-FTIR	Attenuated total reflectance-Fourier transform infrared
BHT	Butylhydroxytoluene
CL	Chemiluminescence
CO	Carbonyl group
CRYSTAF	Crystallisation analysis fractionation
DMA	Dynamic mechanical analysis
DSC	Differential scanning calorimetry
d-TCE	Deuterated tetrachloroethane
E	Ethylene monomer unit
EH	Ethylene-1-hexene
ELSD	Evaporative light scattering detector
EPC	Ethylene-propylene copolymer
EPDM	Ethylene-propylene diene monomer
EPR	Ethylene-propylene rubber
ESR	Electron spin resonance
ESRI	Electron spin resonance imaging
FTIR	Fourier-transform infrared
FTIR-μS	Fourier-transform infrared-microspectroscopy
FWHM	Full width at half maximum
GC-MS	Gas chromatography-mass spectrometry
GPC	Gel permeation chromatography
GS	Gram-Schmidt
HAS	Hindered amine stabiliser
HPLC	High performance liquid chromatography
HT-SEC	High-temperature size exclusion chromatography
ICPP	Impact polypropylene copolymer or impact copolymer polypropylene
iPP	isotactic polypropylene
IR	Infrared
LC-FTIR	Liquid chromatography-Fourier-transform infrared
LDPE	Low density polyethylene
LLDPE	Linear low density polyethylene
MWD	Molecular weight distribution
MWDCA	Molecular weight distribution computer analysis
NMR	Nuclear magnetic resonance
NOE	Nuclear Overhauser effect

o-DCB	*Ortho*-dichlorobenzene
OIT	Oxidation induction time
P	Propylene monomer unit
PAS-FTIR	Photoacoustic Fourier-transform infrared
PB-1	Polybutene-1
PDI	Polydispersity index
PE	Polyethylene
PLM	Polarised light microscopy
PP	Polypropylene
prep-TREF	Preparitive temperature rising elution fractionation
R•	Alkyl radical
ROO•	Peroxy radical
ROOH	Hydroperoxide
SBS	Styrene-butadiene-styrene
SEC	Size exclusion chromatography
SEC-FTIR	Size exclusion chromatography-Fourier-transform infrared
SEM	Scanning electron microscopy
TCB	Trichlorobenzene
TEM	Transmission electron microscopy
TGA	Thermo-gravimetric analysis
TGEF	Temperature-gradient extraction fractionation
TREF	Temperature rising elution fractionation
TREF-SEC	Temperature rising elution fractionation-size exclusion chromatography
UV	Ultraviolet
WAXD	Wide-angle X-ray diffraction

List of Notations

Tg	Glass transition temperature
[Ethylene]	Ethylene concentration
A	Area
CH	Methine group
C-H	Carbony-hydrogen bond
CH_2	Methylene group
CH_3	Methyl group
ΔH_m	Melt enthalpy
H	Height
MH_z	Megahertz
μm	micrometer
$\overline{M_n}$	Number-average molecular weight
$\overline{M_{n0}}$	Initial number-average molecular weight
$\overline{M_{nf}}$	Final number-average molecular weight

μS	microspectroscopy
μs	microseconds
$\overline{M_w}$	Weight-average molecular weight
$\overline{n_E}$	Number-average sequence length for ethylene
$\overline{n_P}$	Number-average sequence length for propylene
n_R	Number of chain scissions
$\Sigma W_i\%$	Accumulative weight percentage
T_c	Crystallisation temperature
T_e	Elution temperature
T_m	Melting temperature
T_{ox}	Oxidation temperature
$W_i\%/\Delta T$	Weight fraction per temperature increment
Wt% or $W_i\%$	Weight percentage

Chapter 1

General introduction and Objectives

This chapter provides a general introduction to impact polypropylene copolymers, including their synthesis, properties and the analytical techniques most frequently used for their characterisation. The objectives for this study are formulated and the layout of this dissertation is explained.

1.1 Introduction

Polyolefins are the most widely used class of commodity thermoplastics in the world and constitute more than 50% of all synthetic polymers produced annually. Polyolefin consumption has grown at a substantial rate over the past few years, and is expected to continue to do so in future, as new technologies and synthesis procedures are developed constantly to satisfy commercial demands. Polypropylene is one extremely versatile member of the polyolefin family, which, due to the prochiral nature of the propylene monomer, can be produced as a variety of different structures, ranging from atactic PP which is non-crystalline in nature, to highly crystalline isotactic PP[1]. Although polypropylene is one of the most important commercial polyolefins, it has been reported to lack impact strength at low temperatures, mainly due to its relatively high Tg and large spherulite dimensions. Impact polypropylene copolymers (ICPP) or heterophase ethylene-propylene copolymers are a unique group of polyolefin materials produced to extend the application range of the polypropylene homopolymer through improvement of its impact strength at temperatures below 0ºC. These impact copolymers can be produced either by blending of polypropylene homopolymer with elastomers[2-4], or by copolymerisation of polypropylene with ethylene in the presence of a Ziegler-Natta catalyst. Copolymerisation is performed *in-situ* via a two-reactor sequential gas-phase process where propylene is polymerised within the first reactor and transferred to the second reactor where the monomer feed consists of both ethylene and propylene[5]. This sequential polymerisation procedure, together with the heterogeneous nature of the catalyst, possessing multiple active sites with different selectivity towards ethylene and propylene polymerisation[6, 7], leads to the formation of a complex mixture of reaction products ranging from amorphous random ethylene-propylene copolymers (EPR), to highly isotactic polypropylene (iPP) as well as a range of semi-crystalline ethylene-propylene copolymers (EPC) with different monomer sequence distributions and lengths[8-10]. These copolymers as sometimes mistakenly referred to as ethylene-propylene block copolymers[11-13], although this terminology is misleading, regarding the nature of the mixture of end products obtained. The presence of true block structures within impact copolymers is still disputed[12, 14-16]. Depending on the nature of the application for which the ICPP is intended, the comonomer concentration and reactor conditions can be varied during copolymerisation to ensure the desired properties for a specific end use[17].

The properties of impact PP copolymers strongly depend on their microstructure, e.g., distribution of ethylene monomer, taciticity distribution as well as ethylene and propylene sequence distributions and average sequence lengths. ^{13}C-NMR spectroscopy has long been the method of choice for determining these structural parameters in bulk EP copolymers[18], whereas FTIR spectroscopy can also supply information on comonomer contents, isotacticity and the distribution of the two monomers within EP copoylmers[19]. Differential scanning calorimetry (DSC) is the thermal method most often used to study the melting and crystallisation temperatures of ICPP, while it is also used to distinguish random copolymers from blends and block structures found in EP copolymers[20]. With the realisation of the complexity of the products formed during ICPP synthesis, it has become evident that fractionation techniques would form an integral part of the characterisation of impact copolymers. Although ICPP

fractions of different crystallinity could be obtained by temperature-gradient extraction fractionation (TGEF)[10, 21, 22], analytical and preparative temperature rising elution fractionation (TREF) have become the preferred methods for separation of the different components[8, 11, 13, 23, 24]. Preparative TREF combined with offline analysis of the fractions by ^{13}C-NMR, FTIR and DSC are the methods most often employed for comprehensive structural analysis of impact PP copolymers.

Impact polypropylene copolymers, like all polyolefins, are susceptible to degradation when exposed to molecular oxygen, elevated temperatures, irradiation and mechanical processes. As a result of the structural and morphological complexity of impact PP copolymers, their thermo-oxidative and photo-degradation has only been studied in a number of cases[25-27]. Some publications reported the similarities in ICPP degradation behaviour to that of PP homopolymer, which is not surprising in copolymers containing $\geq$ 85% PP[25, 26]. The individual components of impact PP copolymers degrade non-identically due to differences in ethylene contents, isotacticity, morphology as well as monomer sequence lengths and distributions[28-33]. Bulk characterisation techniques such as SEC or FTIR are of limited use when studying the degradation of heterogeneous materials, since they provide only the average value of a certain property measured, e.g., molecular weight and carbonyl concentration for the bulk material, without any indication of the degradation behaviour of the individual components or morphologies. The insufficiency of these techniques has been realised over the past few years, with the result that new techniques, that acknowledge the heterogeneity of this unique group of polyolefins, have been utilised for the purpose of understanding the structure and degradation within the individual components of impact PP copolymers. Very recently, the potential of TREF for studying the degradation of impact PP copolymers, has been demonstrated[27, 34, 35]. Differences in degradation behaviour between bulk ICPP samples were related to the tacticity distribution within the TREF fractions of the undegraded materials[36, 37]. TREF separation, followed by degradation of the individual fractions are usually performed in order to assess the degradation behaviour of the individual components[2, 27]. Such procedures do, however, destroy the unique morphology of these heterophase materials, and the degradation behaviour of each component studied independently, does not necessarily reflect the degradation behaviour of the bulk ICPP material. In this study, fractionation and hyphenated techniques will be combined with conventional techniques in novel ways to study the microstructure of impact PP copolymers as well as their degradation behaviour. The individual components will only be separated after degradation of the bulk sample, and changes in the composition, molecular weight and crystallisability within the fractions will be correlated to the degradation behaviour of the bulk material.

1.2 Objectives and methodology

The main objective of this study was to develop novel analytical approaches for studying the thermo-oxidative degradation of low ethylene content impact PP copolymers. For this purpose, fractionation (CRYSTAF and TREF) and hyphenated (SEC-FTIR) techniques were to be combined with

conventional analyses such as SEC, FTIR and ^{13}C-NMR to simultaneously characterise the changes in chemical composition, molecular weight and crystallisability caused by accelerated degradation. An unstabilised commercial impact PP copolymer produced by sequential gas-phase polymerisation in the presence of a Ziegler-Natta catalyst, was to be used to investigate the suitability of fractionation and hyphenated techniques for studying ICPP degradation. Conventional SEC and FTIR analysis of the bulk ICPP would still be performed to monitor molecular weight and chemical composition changes during the degradation process, whereas SEC-FTIR was to be carried out in order to determine the distribution of carbonyl-containing degradation products as a function of the molecular weight distribution of the samples. CRYSTAF would also be used to study changes in crystallisability during degradation. Samples obtained at different stages of the degradation process were to be fractionated by prep-TREF, also to study changes in crystallisability as a function of degradation time. The next step in the multi-component analysis procedure would be off-line SEC analysis for studying the molecular weight distribution shifts within the individual fractions and ^{13}C-NMR for determining changes in tacticity and monomer sequence lengths and distributions upon degradation. TREF was also to be combined with off-line SEC-FTIR analysis for the determination of the distribution of degradation products and chemical composition changes as a function of the molecular weight distribution of each fraction upon degradation. This multi-component analysis procedure should provide valuable information on the influence of degradation on the crystallisability of the bulk sample, as well as the stability of the different components to degradation, as studied by molecular weight and chemical composition changes. It will also, within each component, be able to indicate the heterogeneity in the distribution of degradation species as a function of molecular weight. TREF combined with ^{13}C-NMR, SEC and FTIR should also be used to extensively characterise the undegraded material, i.e., its distributions in comonomer content, isotacticity, ethylene and propylene sequences as well as their sequence lengths as a function of TREF elution temperature. The possibility of combining TREF with SEC-FTIR for studying the ethylene and propylene crystallinity distributions within each fraction of the undegraded material, as a function of molecular weight, should also be investigated.

The second objective of this study was to extend the ICPP degradation study to a second, higher ethylene content copolymer. It was proposed to investigate the difference in degradation behaviour between this ICPP sample and the one studied in the first section, based on their chemical composition (ethylene content), microstructure (monomer sequence distributions and average sequence lengths) and crystallinity. It was once again the aim to use a combination of TREF fractionation and conventional techniques for analysing the differences in composition between the two undegraded samples, as well as the difference in their degradation behaviour.

After completion of the investigation of the compositional heterogeneity of degradation within ICPPs based on differences in chemical composition, microstructure and crystallinity, the study will be extended to thicker specimens of the two ICPPs studied in the foregoing two sections. Since oxygen diffusion effects are expected to play a more significant role in the degradation of these samples, the spatial heterogeneity of the degradation process within the two samples will be compared by means of

FTIR-microspectroscopy (FTIR-μS). The concentration profiles of degradation products will be constructed as a function of depth into the sample. These results will be compared to a conventional technique comprising the abrasion of layers of specific thickness from the surface of a thick specimen and subsequent analysis of the layers by SEC, FTIR and CRYSTAF to determine the molecular weight, chemical composition and morphology or crystallisability influence on the spatial heterogeneity of the degradation process.

1.3 Layout of this dissertation

This dissertation is divided into the following five chapters:

Chapter 1

A general introduction has been presented in the first section of this chapter and the objectives for this study have been formulated.

Chapter 2

The historical section of this chapter summarises the most important contributions made by scientists in the field of polyolefin degradation. Special emphasis is placed on the analytical techniques used to study degradation over the past few decades. The characterisation of impact polypropylene copolymers, in particular, is discussed and an overview of their degradation behaviour is presented.

Chapter 3

The procedures followed during sample preparation, oven aging and characterisation are discussed. The experimental conditions for all analytical instrumentation is supplied, together with a brief discussion on the principles of TREF, CRYSTAF and SEC-FTIR operation.

Chapter 4

The results of this study are divided into three sections within this chapter, according to the three main objectives of this study. The first section contains the results obtained by the multi-component analysis procedure developed for characterising an undegraded low ethylene content impact PP copolymer and for studying its degradation behaviour. The second section contains the results on the comparison of the degradation behaviour of two copolymers of different ethylene contents and the third section illustrates the difference in the spatial heterogeneity of the degradation process within the two copolymers.

Chapter 5

The conclusions of all three sections of this study are summarised and recommendations are proposed for future studies within this field of research.

1.4 References

1. Monasse, B.; Haudin, J. M., Molecular structure of polypropylene homo- and copolymers. In *Polypropylene: Structure, blends and composites*, Karger-Kocsis, J., Ed. Chapman & Hall: London, 1995; p 3.
2. Paul, S.; Kale, D. D. *J. Appl. Polym. Sci.* (2000) 76, p 1480.
3. Greco, R.; Mancarella, C.; Martuscelli, E.; Ragosta, G.; Yin, J. *Polymer* (1987) 28, p 1929.
4. D'Orazio, L.; Mancarella, C.; Martuscelli, E.; Sticotti, G. *J. Mater. Sci.* (1991) 26, p 4033.
5. Galli, P.; Haylock, J. C.; Simonazzi, T., Manufacturing and properties of polypropylene copolymers. In *Polypropylene: Structure blends and composites*, Karger-Kocsis, J., Ed. Chapman & Hall: London, 1995; Vol. 2, p 1.
6. Kakugo, M.; Miyatake, T.; Mizunuma, K.; Kawai, Y. *Macromolecules* (1988) 21, p 2309.
7. Locatelli, P.; Sacchi, M. C.; Tritto, I. *Macromolecules* (1990) 23, p 2406.
8. Mirabella, F. M. *Polymer* (1993) 34, p 1729.
9. Usami, T.; Gotoh, Y.; Unemoto, H.; Takayama, S. *Appl. Polym. Sci.: Appl. Polym. Symp.* (1993) 52, p 145.
10. Fan, Z.; Zhang, Y.; Xu, J.; Wang, H.; Feng, L. *Polymer* (2001) 42, p 5559.
11. Xu, J.; Feng, L.; Yang, S.; Wu, Y. *Polymer* (1997) 38, p 4381.
12. Sun, Z.; Yu, F.; Qi, Y. *Polymer* (1991) 32, p 1059.
13. Feng, Y.; Hay, J. N. *Polymer* (1998) 39, p 6723.
14. Ke, B. *J. Polym. Sci.* (1962) 61, p 47.
15. Cogswell, F. N.; Hanson, D. E. *Polymer* (1975) 16, p 937.
16. Ke, B. *J. Polym. Sci.* (1960) 42, p 15.
17. Fan, Z.; Deng, J.; Zuo, Y.-M.; Fu, Z.-S. *J. Appl. Polym. Sci.* (2006) 102, p 2481.
18. Randall, J. C. *JMS-Rev. Macromol. Chem. Phys.* (1989) C29, p 201.
19. Tosi, C.; Ciampelli, F. *Adv. Polym. Sci.* (1973) 12, p 87.
20. Baker, B. B.; Bonesteel, J. K.; Keating, M. Y. *Thermochim. Acta* (1990) 166, p 53.
21. Hongjun, C.; Xiaolie, L.; Dezhu, M.; Jianmin, W.; Hongsheng, T. *J. Appl. Polym. Sci.* (1999) 71, p 93.
22. Tan, H.; Li, L.; Chen, Z.; Song, Y.; Zheng, Q. *Polymer* (2005) 46, p 3522.
23. Xu, J.; Fu, Z.-S.; Fan, Z.; Feng, L. *Eur. Polym. J.* (2002) 38, p 1739.
24. Zacur, R.; Goizueta, G.; Capiati, N. *Polym. Eng. Sci.* (1999) 39, p 921.
25. Delprat, P.; Duteurtre, X.; Gardette, J.-L. *Polym. Degrad. Stab.* (1995) 50, p 1.
26. Tocháchek, J.; Jancár, J.; Kalfus, J.; Zborilová, P.; Burán, Z. *Polym. Degrad. Stab.* (2008) 93, p 770.
27. Nakatani, H.; Manabe, N.; Yokota, Y.; Minami, H.; Suzuki, S.; Yamaguchi, F.; Terano, M. *Polym. Int.* (2007) 56, p 1152.
28. Schlick, S.; Kruczala, K. *JCT Research* (2005) 2, p 389.
29. Manabe, N.; Yokota, H.; Suzuki, S.; Liu, b.; Terano, M. *J. Appl. Polym. Sci.* (2006) 100, p 1831.
30. Manabe, N.; Yokota, H.; Nakatani, H.; Suzuki, S.; Liu, B.; Terano, M. *Polym. Bull.* (2005) 54, p 141.
31. Singh, R. P.; Mani, R.; Sivaram, S.; Lacoste, J.; Lemaire, J. *Polym. Int.* (1993) 32, p 189.
32. Kruczala, K.; Aris, W.; Schlick, S. *Macromolecules* (2005) 38, p 6979.
33. Kruczala, K.; Bokria, F. G.; Schlick, S. *Macromolecules* (2003) 36, p 1909.
34. Nakatani, H.; Suzuki, S.; Tanaka, T.; Terano, M. *Polymer* (2005) 46, p 12366.
35. Nakatani, H.; Suzuki, S.; Tanaka, T.; Terano, M. *Polym. Int.* (2007) 56, p 1147.
36. Suzuki, S.; Nakamura, Y.; Kamrul Hasan, A.; Liu, B.; Terano, M.; Nakatani, H. *Polym. Bull.* (2005) 54, p 311.
37. Nakatani, H.; Matsuoka, H.; Suzuki, S.; Taniike, T.; Boping, L.; Terano, M. *Macromol. Symp.* (2007) 257, p 112.

Chapter 2

Historical overview and Theoretical background

This chapter gives a general overview on impact polypropylene copolymers and polyolefin degradation. Special emphasis is placed on the analytical techniques used in literature to study the properties of these copolymers, as well as their degradation.

2.1. Polyolefins: An overview

The term olefin originates from 'olefiant' (oil-forming gas), the word first used by four pioneer Dutch chemists to describe the gas (ethylene) that produced an oil (ethylene dichloride) by the addition of chlorine[1]. It was as early as 1858 that Goryainov and Butlerov reported on producing polypentene by addition of boron trifluoride to pentene[2]. The same approach was used to successfully polymerise propylene and isobutylene, but the same success could not be achieved with ethylene[3]. In 1894 von Pechman made use of the decomposition of diazomethane for producing a linear, low molecular weight ethylene polymer[4]. This technique was also used by several authors to prepare crystalline polymethylene[5-8].

It was only much later, during the 1930's that the polymerisation of high molecular weight polymers became a topic of interest. In 1931 Taylor and Jones reported on the polymerisation of ethylene in the presence of diethylmercury and the condensation of decamethylene bromine was used by Carothers and co-workers to produce linear polyethylene[9] A few years later, in 1935 the Fischer-Tropsch reduction of carbon monoxide by hydrogen was used by Koch and Ibing to produce linear polyethylene[10]. In 1940 Pitchler and Buffleb repeated this synthesis using a ruthenium catalyst, a process later patented by Du Pont in 1955[11].

In 1952 Fontana attempted the cationic polymerisation of propylene, but his product could only be used as an additive for lubricating oil, since it was of limited use as a structural material. A significant step forward in the polymerisation of high molecular weight polyolefins was taken when Ziegler managed to produce high density polyethylene in 1953. The following year Natta managed to synthesise polypropylene, followed shortly by Ziegler[12]. Stereoregularity in polyolefins only became acknowledged during the late 1940's when the stereoregularity of natural rubber was observed. During this time the terms isotactic, syndiotactic and atactic were cloned, and have ever since become part of the accepted nomenclature[13].

The first commercial production of polyolefins was that of low density polyethylene by ICI in 1933[12]. It was during the time of World War II that high pressure plants appeared in both the United States (Du Pont and Union Carbide) and Germany. The commercial production of linear polyethylene was started in the late 1950s by Phillips in the United States. After having realised the importance of branch structures in lowering the density of polyolefins, Du Pont succeeded in producing a copolymer of ethylene and 1-butene, known as linear low density polyethylene[14]. At the time however, there was limited demand for such materials and the technology was still in its infancy. The first commercial production of crystalline polypropylene was only done by Hercules, Montecatini and Farbwerke-Hoechst in 1957[1]. Soon thereafter, in 1965, two other polyolefins, namely poly(4-methyl-1-pentene) and poly-1-butene were also synthesised successfully in small quantities. From here onwards the production of polyolefins escalated and improved as traditional materials such as metals, glass and

wood were replaced by polymers due to their superior properties. A 6.9% growth in the production of polypropylene was reported between 1993 and 2000, with the other major polyolefins showing similar trends (LDPE 3.5%, LLDPE 9.7%, HDPE 6.1%)[12]. The polyolefin market continues to grow at a steady rate and technologies are adjusted and improved in order to supply materials for demanding applications. The invention of blends and copolymers comprising polyolefins have opened up a whole new field of applications and are being used in increasing amounts in our daily lives.

2.2 Commercial Polypropylene

As early as 1869, propylene has been polymerised by Berthelot by reaction with concentrated sulphuric acid to yield a viscous oil product that was not considered of economic or industrial importance. The first industrially important crystalline, high molecular weight polypropylene was synthesised by Natta in 1955 from organo-metallic catalysts based on titanium and aluminium[15]. The mechanical properties of this semi-crystalline material made it a favourite to be introduced into the market by Hoechst in 1965. A wide variety of polypropylene homopolymers, and versatile random and block copolymers with various molecular weight distributions were also manufactured for numerous applications[16].

Polypropylene is widely used in injection moulding applications for supplying bumpers and dashboards for the automotive industry. A high percentage of the overall polypropylene produced is also used for packaging produced by blow moulding and thermoforming. Pipes, profiles and sheets are produced by extrusion, while textile fibres and non-woven fibres are also possible via melt spinning, in the case of sufficiently high molecular weight. Furthermore, the high melting temperature of isotactic polypropylene allows the exploitation of its properties over a wide temperature range[17-19]. Its overall crystallinity, which is related to both stereoregularity and molecular weight, promotes some properties such as stiffness, hardness and high-temperature mechanical characteristics. However, its fairly high glass transition temperature results in it being too brittle at application temperatures below 0ºC. The homopolymer has also proven to be too rigid and lacks the transparency desired for some applications. The application range can, therefore, be expanded if its flexibility and clarity is improved together with a reduction of its melting point, which would promote its weldability. Improved impact resistance and elongation properties at low temperatures combined with good stiffness would also be an asset to this already versatile polyolefin material.

2.3 Impact-modified Polypropylenes

The toughness of polypropylene can be improved in several ways, i.e., blending with a variety of elastomers[20-24], addition of a nucleating agent to reduce the average size of the spherulites [25-27] or by multi-stage copolymerisation. Copolymerisation with another olefin such as ethylene or butene simultaneously lowers the melting point of polypropylene and ensures higher flexibility. Adequate

stiffness and improved low temperature impact resistance is generally achieved by incorporation of an elastomeric copolymer component as a dispersed phase in the polypropylene matrix[28-31]. Thus, blending and copolymerisation can alter the polymer structure and morphology and, therefore, the end-use properties and applications of polymeric materials. These approaches have been employed for decades in the polymer industry, but growing demands in the field leads to continuous developments, and interest in this topic still continues.

2.3.1 Polypropylene-elastomer blends

The application range of isotactic polypropylene as an engineering plastic has expanded significantly over the last few decades due to blending with elastomers such as ethylene-propylene copolymer (EP) [32-34], butyl rubber[35], styrene-butadiene-styrene copolymer (SBS)[36], ethylene-1-hexene copolymer (EH), ethylene-propylene rubber (EPR)[37, 38] and ethylene-propylene-diene terpolymer (EPDM)[39-41]. Blends can be prepared by post-reactor mechanical mixing of the two materials, or by in-situ or in-reactor blending. In-situ blending is considered to be more advantageous both in terms of mechanical properties and production costs[42].

It is well known that addition of a low-Tg rubber-like material to a high-Tg, hard polymer may result in dramatic improvement in the toughness of the hard polymer[43] . The elastomer is typically added at low concentrations, and exists either as a discrete phase in the continuous matrix of the hard phase or as a continuous phase throughout the matrix. In PP/EPDM blends it was observed that an impact modifier content below 20% leads to the formation of a dispersed elastomer phase in the polypropylene matrix, whereas the incorporation of 50% EPDM constitutes the formation of a continuous elastomer phase[44]. The properties of blends, i.e., mechanical strength, surface bonding and impact resistance are dependent on the blend morphology which, in turn, depends strongly on the miscibility of PP and the elastomer in question. Owing to the negligibly small entropy of mixing[45-47] as well as unfavourable enthalpic interactions[48], the majority of polymer blends are immiscible. The only miscible PP blends are those of atactic polypropylene (aPP) with EPR containing less than 10 wt% ethylene, and with polybutene-1(PB-1)[49, 50]. Even in these cases miscibility is limited due to the strong tendency of polypropylene to crystallise out from the mixtures. Therefore, compatibilisation by means of compatibilizer addition or reactive blending (usually accomplished by the addition of a peroxide) is needed to promote miscibility in polyolefin blends.

2.3.2 Random and sequential copolymerisation

As has been mentioned before, the unsatisfactory impact behaviour of isotactic PP at low temperatures, can be improved via copolymerisation with ethylene. Ethylene-propylene copolymers are the most widely investigated of the Ziegler-Natta copolymers and undoubtedly illustrate the benefits that comonomer incorporation can bring[51]. Commercially, the copolymerisation of ethylene and propylene can be accomplished in two ways, i.e., random or statistical copolymerisation, or sequential

copolymerisation. In random copolymers the ethylene comonomer units are, as the name suggests, incorporated in a purely random manner, thereby acting as defects in the long macromolecular chains of polypropylene. This decrease in the length of the isotactic segment leads to different thermal, mechanical and processing properties compared to polypropylene homopolymer (i.e. lowering of melting and sealing temperatures, flexural modulus, broadening of the melting range). Another very important effect is the improvement of optical properties such as haze and clarity, by the reduction of the refractive index difference between the amorphous and crystalline zones[52]. These effects do, however, depend on the amount of comonomer added and its distribution within the copolymer[53].

Random ethylene-propylene copolymers are synthesised when a small amount of ethylene is polymerised together with propylene in a single reactor. The degree of randomness within the copolymer depends on various factors such as the polymerisation conditions, catalyst system and the reactivity ratio of ethylene relative to propylene. The influence of the mentioned parameters on the resulting copolymer, has also been discussed by Tait and Berry[54].

The second means of copolymerising ethylene and propylene is called sequential copolymerisation or *in-situ* polymerisation[55] and the copolymer produced is generally referred to as impact polypropylene copolymer[30, 31, 56-61]. Other terms also used to describe the copolymers formed by sequential polymerisation of ethylene and propylene, are heterophasic PP[62] and EP block copolymer[63, 64]. For the purpose of consistency/uniformity, the term 'impact PP' or 'impact PP copolymers' will be used throughout this dissertation.

2.3.3 Impact PP copolymers

2.3.3.1 Synthesis and morphology

The sequential copolymerisation of ethylene and propylene to form impact PP is a two-step, two-reactor process described by various authors[40, 65-68]. In the first reactor isotactic PP polymerisation takes place in liquid propylene in the presence of a Ziegler-Natta catalyst. After a predetermined time, the PP pre-block, along with the living catalyst and some unreacted monomer is transferred to the second stage, a gas-phase fluidised reactor containing a mixture of ethylene and propylene, where EPR is mainly formed[69] within the PP matrix[59]. Since a heterogeneous catalyst is used, the resultant copolymer system is a highly complex mixture of isotactic PP, EPR, a series of EP segmented copolymers with different sequence lengths of ethylene and propylene as well as an ethylene homopolymer component[64, 70, 71]. The presence of propylene homopolymer is obviously explained by the production within the first reactor where only catalyst, propylene homopolymer and hydrogen are present. The EPR is the result of its deliberate production in the second reactor where ethylene, propylene, catalyst and hydrogen are all present. It is however, unexpected to find semicrystalline copolymers of ethylene and propylene besides the non-crystallisable EPR. The monomer ratio of ethylene and propylene in the second reactor is such that a copolymer equally rich in both monomers

should theoretically be produced. These requirements are fulfilled by the EPR being present in the final mixture. The reason for the presence of the semi-crystalline copolymers that contain small quantities of propylene in an ethylene-rich copolymer and small amounts of ethylene in a propylene-rich copolymer, is however, not straightforward, but it is believed to be related to the heterogeneous nature of the catalyst which contains a spectrum of active sites governing different processes[56, 72]. The small amount of PE homopolymer always present in the final mixture is the result of the Ziegler-Natta catalyst's ability to polymerise ethylene at a much higher rate than propylene[55]. If some catalyst active sites have no active chains attached to them when it is transferred to the second reactor, ethylene, with its higher reactivity ratio may readily polymerise to yield PE homopolymer as a by-product.

Although impact polypropylene copolymers are often referred to as EP block copolymers, the existence of true block structures are still disputed[73-75]. In order to successfully synthesise true blocks of ethylene and propylene, a number of requirements should be met,[12, 54, 76] (a) catalyst active sites should have equal activity towards ethylene and propylene, (b) all polymerisation centres should be activated at the same time, (c) active centres should remain alive during polymerisation (i.e. all chains must remain attached to active centres during polymerisation, (d) the crossover propagation rates must be high for all centres and (e) centres must be isospecific for polypropylene polymerisation and be able to produce linear polyethylene segments. These requirements were formulated for typical anionic initiators and it is clear that many of them do not hold for heterogeneous Ziegler-Natta catalysts, where a number of transfer reactions (to metal alkyl and hydrogen) take place, resulting in growing chains having very short lifetimes[76-78]. Therefore a more suitable nomenclature such as heterophasic or impact polypropylene should be used for these copolymers.

The dispersed EPR phases in these copolymers act as stress concentrators to relieve the strain on impact by cavitation at the particle/matrix interface as well as within the copolymer particles, leading to large deformations of the surrounding matrix[79-82]. It is also known that polyethylene and polypropylene are generally immiscible in a blend, and, therefore, the ethylene-propylene segmented copolymers are proposed to act as the compatibiliser that enhances the interfacial adhesion between the disperse phase and the matrix[30, 70]. Although the process of sequential copolymerisation of ethylene and propylene is commercially successful, the mechanism of polymer growth is poorly understood, mainly due to a lack of thorough characterisation of the resulting product.

Debling and Ray[83] based their description of the growth process on the double grain structure proposed by Kakugo *et al*.[84, 85] for the polypropylene particles formed in the first reactor. According to this model the PP particle is formed by mesoparticles, also referred to as polymer globules. Mesoparticles are formed by primary polymer particles containing catalyst crystallites. These structures also contain macropores separating the mesoparticles and micropores that separate the microparticles. The EPR formed in the second reactor does not remain encapsulated within the PP microparticles but progressively expands into the small micropores and into the large macropores. According to McKenna *et al*.[86] the EPR is formed on the active sites on the surface of the catalyst

crystallites underneath a PP homopolymer layer. The EPR creates stresses in the viscoelastic PP homopolymer, leading to crack formation in the PP after which the EPR flows through the cracks, into the micro and macropores and onto the surface of the polymer particle. Cecchin *et al*. [87] proposes that homopolymerisation within the first reactor results in PP particles consisting of a number of polymer mesoparticles. Catalyst fragments are believed to exist at the surface of these mesoparticles, where they have migrated to during homopolymerisation. Therefore, the EPR polymerised in the second reactor is located at the surface of these mesoparticles, filing the pores between them, thereby accounting for the continuous EPR network found within the PP matrix. Urdampilleta *et al*.[59] proposed that the PP particles are formed by a relatively small number of mesoparticles, in which the catalyst fragments are well dispersed. No proof of a finer morphology was observed. EPR in the second reactor is formed around the catalyst fragments, yielding a composite of finely dispersed EPR within the PP matrix. Most of the EPR is located within the mesoparticles, while some of it breaks through the PP matrix and flows to the pores. A part of the EPR reaches the surface of the particle, thereby smoothing the particle surface. It is however, uncertain whether the catalyst fragments encapsulated by elastomer migrate to the surface of the mesoparticle together with the elastomer, and once there, contribute to the formation of EPR within the pores. Understanding of the growth process of nascent impact PP copolymers is by no means conclusive and the growth mechanism is still the subject of ongoing investigation.[61]

2.3.3.2 Characterisation

Impact PP copolymers are known to exist as highly complex mixtures consisting of polypropylene homopolymer and ethylene-propylene copolymers, random and segmented, with different chemical compositions and monomer sequence distributions. The complete assessment of the compositional heterogeneity and chain structure of such systems is undoubtedly a formidable task. However, detailed analysis of the microstructure of impact PP copolymers is necessary to obtain a better understanding of the impact performance of the material as a whole as well as the location and function of each of the components. Owing to the presence of a multiplicity of different components, fractionation techniques are often employed in the analysis of impact PP copolymers. Such techniques can separate the various chemically distinct components from each other, yielding more homogeneous fractions that can subsequently be analysed by a number of well-established ancillary techniques in order to obtain detailed structural information. Fractionation techniques so far employed in the analysis of impact PP copolymers, include Soxhlet extraction[63], successive solvent extractions [30, 88, 89], temperature-gradient extraction fractionation (TGEF) [31, 70] and temperature rising elution fractionation (TREF). TREF fractionation of impact PP for structural analysis was first performed by Mirabella in 1992 and 1993[56, 72]. Ever since, both preparative[55, 60, 64, 90-93] and analytical TREF procedures have been employed [56, 72] in this regard. A novel online TREF-SEC analysis procedure, reported by Usami *et al*. in 1993 was also applied to the characterisation of impact PP copolymers[94].

One aspect of the characterisation of impact PP copolymers is the identification of the major components on the basis of their unique chemical structure. By far the most popular techniques for this purpose are ^{13}C-NMR and FTIR spectroscopy. Certain pre-defined bands in the FTIR spectrum are known to be characteristic of crystalline and amorphous polyethylene and polypropylene [95, 96]. Through the evaluation of the presence as well as the ratio of these bands, certain assumptions can be made with regard to the crystallinity and microstructure of a polymer. FTIR analysis of TREF-fractionated impact PP copolymers has been performed by a number of authors[30, 70, 90, 96]. FTIR spectroscopy can even be used to study the amount of ethylene in each TREF fraction in cases where ^{13}C-NMR calibration data is available[70].

However, the preferred method for reliable evaluation of the molecular structure of impact polypropylenes is ^{13}C-NMR spectroscopy. The most important factors influencing the performance and properties of impact PP are tacticity, and monomer sequence distribution, both of which are reliably detected by ^{13}C-NMR spectroscopy. While the amount of ethylene in each TREF fraction can be determined using the relationship suggested by Cheng[97] and Ray *et al*.[98] and Carman and Wilkes[99] have proposed the assignments widely used for the sequential analysis of both monomers in EP copolymers. The quantitative NMR measurement of EP copolymers with low ethylene content has also been confirmed by Paxon and Randall[100] and a review article was published by Randall in 1989, on the detailed extraction of triad concentrations from ^{13}C-NMR data of ethylene-based copolymers[101]. Most studies allowed the determination of sequence distribution only as far as triad level, until Hayashi *et al* accurately determined tetrad and hexad sequence distributions in stereoregular EP copolymers[102].

Monomer sequence distribution determinations have been successfully applied to bulk impact PP samples[102-105] as well as TREF-fractionated impact PP copolymers have been reported[58, 90]. Even if determinations are done only up to diad or triad concentrations, one can still obtain valuable information on the distribution of both short and long ethylene and propylene sequences within each fraction, as well as the amount of EP junctions. By determining the mole fraction of long ethylene and propylene (EE, EEE, PP, PPP) sequences in each fraction, together with the amount of junctions between them (PE, PPE, EPE, EEP, and PEP), one can easily distinguish between fractions of EPR, those containing isotactic PP and PE homopolymer, and those containing the range of EP copolymers of varying ethylene and propylene segment lengths[30, 31, 64, 70, 106]. The average length of long ethylene and propylene sequences can also be calculated using the PPP, PPE, EEE and EEP triad information[30]. Monomer sequence distributions within impact PP copolymers clearly illustrate the continuity in the change of composition and chain sequence from low to higher elution temperatures. This continuity in properties as a function of TREF elution temperature is an undeniable characteristic of impact PP copolymers[30].

Another popular technique for studying the composition of TREF-fractionated impact PP copolymers on the basis of their thermal behaviour and crystallinity, is DSC[31, 58, 63, 64]. The observation of thermal transitions and their change observed upon increasing elution temperature may be used to gain insight

into the microstructure of fractions. Results on microstructure obtained by DSC were in good agreement with those obtained by NMR and FTIR[70], although DSC results are typically reported in conjunction with ^{13}C NMR for the purpose of identification[56, 60, 64, 72]. Wide-angle X-ray diffraction (WAXD) is also sometimes used together with DSC for studying the microstructure of impact PP copolymer fractions[90, 91].

The final aspects of importance in the characterisation of impact PP copolymers, are their morphology and impact behaviour. Morphological aspects such as the size and dispersion of EPR inclusions in the PP matrix and the compatibilisation between the phases, are usually studied by scanning electron microscopy (SEM)[57, 59, 63, 71, 89], transmission electron microscopy (TEM)[44, 57, 61, 94] or atomic force microscopy (AFM) [62] in order to gain knowledge of the relationship between the chain structure and morphology and the impact behaviour of impact polypropylenes. Polarised light microscopy (PLM) has also been used to study crystalline morphology of impact PP fractions as a function of their chain structure[71, 89], while dynamic mechanical analysis (DMA) provided useful information on the compatibility between dispersed particles and the matrix[44, 63, 89].

2.5 Polyolefin Degradation

Polyolefins, most notably PE and PP, have gained considerable popularity over the past few decades due to their versatility in terms of affordable petrochemical stocks serving as raw materials, the efficient catalytic polymerisation processes for their production and the ease of processing of the final products. This success has occurred in spite of polyolefins being susceptible to degradation when exposed to elevated temperatures, radiation, chemicals, molecular oxygen and other stimuli. Polymer degradation has long been recognised as the Achilles' heel in polymer applications, therefore causing it to become an active area of research, together with stabilisation studies. Polyolefins are normally subjected to high temperature manufacturing and processing operations, and are, like all other hydrocarbon polymers, susceptible to degradation during every stage of their lifecycle, i.e., during synthesis, processing and end-use. Degradation is defined as the process that brings about several physical and chemical changes in a polymeric material[107, 108], that leads to significant deterioration in the quality of the material (i.e., deterioration of mechanical, electrical, and aesthetic properties) and finally to it failing prematurely and becoming unsuitable for its intended application[109, 110]. Decomposition is closely related to degradation, but is generally conceived as the processes induced by heat, oxygen, chemicals etc. that leads to the formation of non-polymeric products or a structure completely different from the original material[109] It is accepted as the advanced stage of degradation and distinction between these terms is rarely made. 'Weathering' is another concept closely related to the topic of polymer degradation but it normally refers to the process where oxygen, heat, wind, humidity, micro-organisms, rain, atmospheric pollutants and UV irradiation alters the properties of a material during outdoor use, leading to failure[109, 111, 112].

Except for a few instances where controlled degradation can lead to improved properties of a material for a certain application (i.e., adjustment of the molecular weight of a polymer through controlled backbone scission and the controlled cross-linking of surface coatings), degradation is usually treated as an unwanted occurrence leading to irreversible changes in the physical, mechanical and chemical characteristics of polymeric materials. The usefulness of polyolefins strongly depends on the retention of their properties during a prolonged service life and thus studies of polyolefin degradation and the influence of various factors on their degradation behaviour is of appreciable commercial importance. Polypropylene is one of the most oxidatively unstable of the polyolefins due to its chemical structure, but it is commercially very successful as a commodity thermoplastic, thereby reflecting the extent to which a detailed understanding of the degradation process has led to strategies of successful stablisation[113-116].

2.5.1 Types of degradation

The most common types of degradation occur through chemical reactions that modify the chemical structure of the polyolefin, leading to a change in its chemical, mechanical and physical properties[107, 108, 117, 118]. Such reactions include (a) chain scission, (b) cross-linking, (c) modification of the chemical structure of the main polymer chain, (d) modification of branched chains, or (e) a combination of all of these reactions. The overall effect of degradation on a material is usually the summation of all of these reactions and may vary widely depending on the relative rates of these reactions as well as exposure conditions. The agent(s) initiating the degradation process defines the type of degradation or decomposition of a material. A summary of the different types of degradation and their initiating agents are given in Table 1[109]. Oxidative degradation is the prime agent causing deterioration of products fabricated from polyolefins, and even very small amounts of oxygen can cause drastic changes in the polymer and destroy its useful properties[119, 120].

Table 2.1: The types of degradation induced by various degrading agents

Degrading agent	Type of degradation
Light (UV, visible)	Photochemical degradation
X-rays, γ-rays, fast electrons	High-energy radiation-induced degradation
Laser light (pulsed mode)	Ablative Photodegradation, involving photothermal and/or photochemical processes
Electrical field	electrical ageing
Plasma	Corrosive degradation, etching
Microorganisms	Biodegradation / biological degradation
Abrasive forces	Physical degradation, physical wear, environmental stress cracking
Stress forces	Mechanical degradation, fatigue
Chemicals (acids, alkalis, salts reactive gases, solfents, water)	Chemical degradation and/or decomposition
Heat	Thermal degradation and/or decomposition
Oxygen, ozone	Oxidation, oxidative degradation and/or decomposition
Heat and oxygen	0Thermo-oxidative degradation and/or decomposition
Light and oxygen	Photooxidation

It is very difficult to study a 'pure' type of degradation, since various factors often act simultaneously to induce the degradation process within polymers. The types of degradation most commonly studied are thermal and photo-oxidation. The chemical reactions in both cases are fairly similar, with only minor differences owing to variations in the initiation mechanism and secondary photochemistry[121]. In thermal oxidation, initiation results form thermal dissociation of chemical bonds, whereas in photo-oxidation, photophysical processes such as the formation of electronically excited species, energy transfer and photo-dissociation, all induced by UV radiation, lead to bond cleavage. The degradation of weathering of polymers during outdoor use is usually initiated by UV radiation, and referred to as photooxidation[112]. The process ultimately leads to surface embrittlement and failure due to brittle fracture, unless photo-stabilisers are incorporated to prolong the lifetime of the polymeric material[116]. Under conditions of outdoor use, elevated temperatures close to the crystalline melting points of polymers are usually not reached, therefore, photo-oxidation is seen as the major type of oxidation to prevent or restrict during outdoor use of polymers.

Polymers may however, also degrade in the absence of light when they are exposed to elevated temperatures. In the presence of molecular oxygen this is referred to as thermo-oxidative degradation[110] In both photo- and thermo-oxidative degradation, the process is considered to be a free radical oxidation process, also known as autoxidation. The earliest work on the free radical chain theory of polymer oxidation was done by Morou and Dufraisse[122] when they realised that small quantities of substances they called 'antioxygens', could retard oxidation. Also in the 1920's, Christiansen[123] and Bäckström[124] obtained evidence for the existence of a chain reaction mechanism during degradation. This was followed in the early 1940's, by the discovery that free radicals were responsible for initiation and autocatalysis was related to the presence of hydroperoxides[125]. Detailed studies by Bolland and Gee at the British Rubber Producers Research Association in 1946, gave birth to the generally-accepted oxidation model for olefins, consisting of radical initiation, propagation and termination still used in present times[126]. Polyolefin degradation is often described by making use of the Ciba cycle for themo-oxidative degradation in polyolefins[113], as seen in Scheme 1.

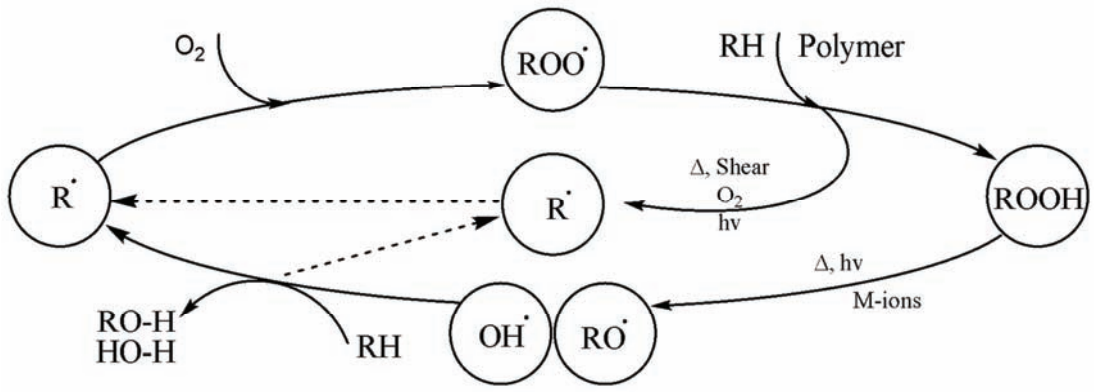

Scheme 2.1: Schematic representation of the cyclical autoxidation process taking place during polyolefin degradation

2.5.2 Oxidation mechanisms for polyolefins

The autoxidation process of polyolefin degradation is best described by the classical free-radical chain reactions depicted in Scheme 2[113, 127], consisting of individual steps of initiation, propagation and termination.

2.5.2.1 Initiation:

During the initiation stage of polyolefin degradation, stimuli such as heat or UV radiation are responsible for the formation of macro-alkyl radicals due to the abstraction of a hydrogen atom from the polymer backbone or cleavage of a polymer chain. Radicals formed during this stage may either react with each other (as is the case during cross-linking), or with other molecules in the polymer matrix, e.g., molecular oxygen to continue the cycle of degradation.

Cleavage of the polymer chains (reactions 2.1, 2.2) is usually caused by severe deformation of a polymer by physical means or high temperature, high-shear processes in the molten state such as extrusion, injection moulding, blow moulding and internal mixing. This process is less likely to occur, as the majority of polyolefin degradation is initiated by scission of a C-H bond.

2.5.2.2 Propagation:

During propagation, the radicals formed during initiation react with molecular oxygen and are transformed into macro-alkylperoxyl radicals (reaction 2.4). This is followed by the abstraction of a hydrogen atom from another polymer molecule, (or the same molecules, through backbiting) giving rise to macro-hydroperoxides (reaction 2.5) and more alkyl radicals. Hydroperoxides formed during this stage of degradation may be cleaved homolytically to yield both an alkoxy and a hydroxyl radical (reaction 2.8). Both these species are capable of abstracting hydrogens form adjacent polymer chains, resulting in the formation of water, an alcohol and more alkyl radicals capable of initiating degradation. These reactions are known as chain branching reactions and are detrimental to the long-term stability of polyolefin materials during use, leading to catastrophic failure. Free radicals formed during the first two steps may also undergo further reactions leading to the insertion of various oxygen-containing groups in the oxidised polymer, leading to changes in molecular structure and deterioration of properties. One example of such a reaction is the unimolecular decomposition of polypropylene alkoxy radicals, also known as β-scission (reaction 2.12). Scission reactions decrease the molecular weight of chains and also influence the crystallinity of samples through an effect known as chemi-crystallisation[128]. Since amorphous regions of semi-crystalline polymers degrade more readily than the crystalline phase[129-131], the scission of tie molecules, responsible for linking two adjacent crystalline areas, will cause a rapid impairment of the physical and mechanical properties of a polymer. The higher mobility of oxygen in non-crystalline material leads to propagation within amorphous regions, but without the presence of oxygen, alkyl radicals will migrate until they react with other radical species.

This step of the degradation is autocatalytic and is a continuous process, which will sustain itself until all radicals are terminated.

Initiation:	RH	→	R· + H		(2.1)
	RR	→	R· + R·		(2.2)
Propagation:	R· + R'H	→	RH + R'·		(2.3)
	R· + O_2	→	ROO·		(2.4)
	ROO· + R'H	→	ROOH + R'·		(2.5)
	ROOH + R'OOH	→	RO· + R'OO· + H_2O	*Chain Branching*	(2.6)
	ROOH + R'H	→	RO· + R'· + H_2O		(2.7)
	ROOH	→	RO· + HO·		(2.8)
	RO· + R'H	→	ROH + R'·		(2.9)
	HO· + R'H	→	H_2O + R'·		(2.10)

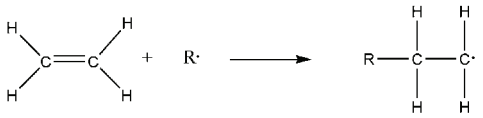

(2.11)

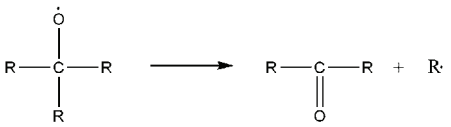

(2.12)

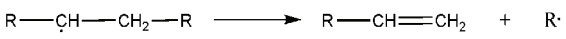

(2.13)

Termination:	R· + R·	→	RR		(2.14)
	R· + RO·	→	ROR		(2.15)
	R· + ROO·	→	ROOR		(2.16)
	R· + R·	→	RH + Olefin		(2.17)
	ROO· + ROO·	→	Ketone + alcohol + O_2		(2.18)

Scheme 2.2: Possible oxidation reactions during the autoxidation cycle of polyolefins

2.5.2.3 Termination:

The reactions taking place during termination are highly dependent on the molecular structure of the polymer as well as the prevailing degradation conditions. Under normal oxygen pressure (oxygen saturation) ROO· radicals are the abundant species, i.e., [ROO·]>[R·][113] and termination reactions 2.16 and 2.18 (scheme 2) predominate. However, in the case of oxygen starvation (during processing and in thick polymer sheets) alkyl radical predominate, i.e., [ROO·]<[R·] and bimolecular termination reactions are of greater significance. This leads to cross-linking which is evidenced by an increase in molecular weight, (especially in PE) and /or disproportionation without a change in molar mass.

2.5.3. Degradation mechanism of polypropylene

Polypropylene also degrades by means of the generally accepted free radical chain reaction mechanism consisting of the steps of initiation, propagation, branching and termination. During the initiation step, heat-facilitated hydrogen abstraction from either the tertiary or secondary carbons may lead to the formation of either tertiary of secondary alkyl radicals (reaction 3.1). In PP, tertiary radicals are formed predominantly, due to the lower dissociation energy of a tertiary C-H bond (ca. 373 kJ.mol^{-1} at 25ºC), compared to that of a secondary C-H bond (ca. 394 kJ.mol^{-1} at 25ºC)[132]. During the subsequent propagation step, secondary and tertiary radicals will follow separate reaction paths. The reaction paths followed by tertiary and secondary radicals are depicted in Schemes 2.3 and 2.4, respectively.

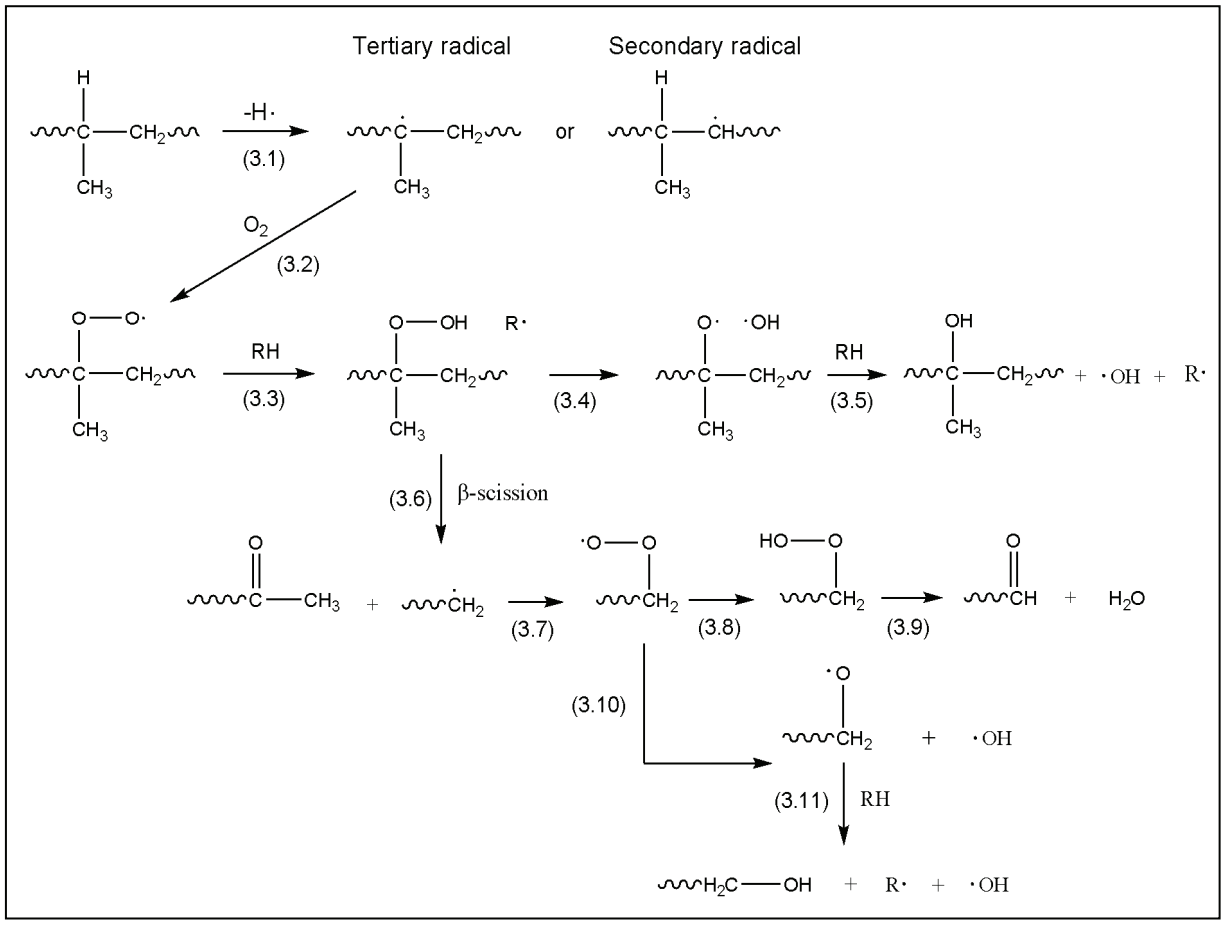

Scheme 2.3: Initiation, propagation and termination reactions involving the tertiary alkyl radical

In the presence of oxygen, tertiary radicals will react with molecular oxygen to form tertiary peroxides (reaction 3.2). The next propagation step involves the abstraction of a hydrogen atom from an adjacent polymer chain to form a tertiary hydroperoxide (reaction 3.3) and another active alkyl radical species capable of continuing the cycle of degradation. Subsequently, the tertiary hydroperoxide may follow one of two possible degradation pathways. It may either react with a hydrogen atom to form a tertiary alcohol (reaction 3.5) or it may undergo β-scission to form an inactive ketone and a macroalkyl

radical (reaction 3.6)[133]. The primary chain end formed in this step can be oxidised further to produce an aldehyde (reaction 3.9) or an alcohol and water (reaction 3.11).

Although PP degrades preferentially via the formation of tertiary radicals, secondary radical species may also originate during the initiation step. Similar to the first propagation steps followed by the tertiary radical, secondary radicals also react with molecular oxygen to form secondary peroxides (reaction 4.2), followed by the formation of secondary hydroperoxides (reaction 4.3) after hydrogen abstraction. Hydroperoxides can degrade in a similar fashion to their tertiary counterparts, extracting either another hydrogen atom to form a secondary alcohol and a chain radical (reaction 4.5), or undergoing β-scission to yield an aldehyde and a macroalkyl radical (reaction 4.6).

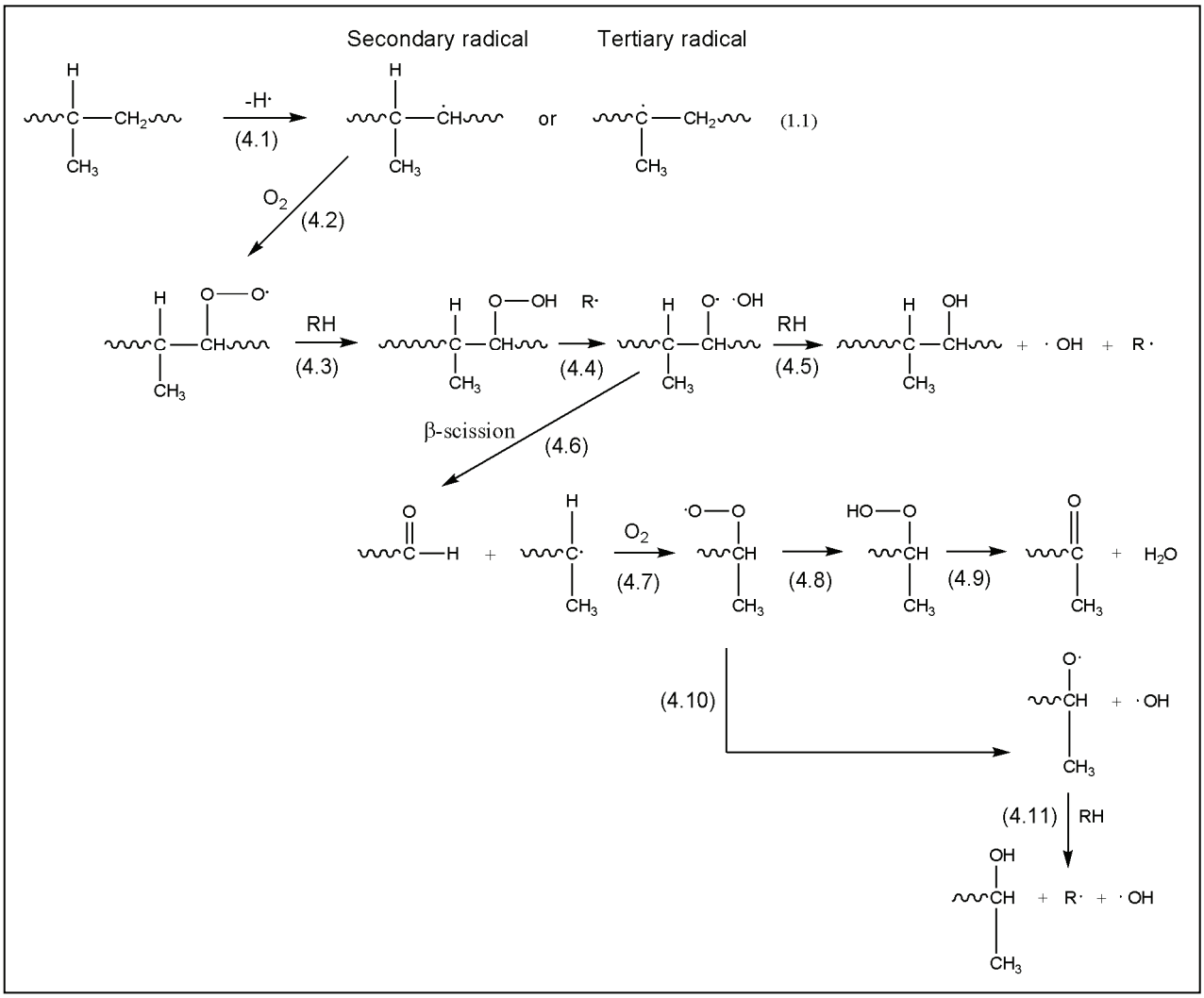

Scheme 2.4: Initiation, propagation and termination reactions involving the secondary alkyl radical

Secondary chain ends are also capable of further degradation, leading to the formation of inactive ketones (4.9), alcohols (4.11) and water. According to Adams *et al*.[134], these degradation cycles should lead to the formation of equal amounts of methyl ketones and aldehydes, but Costa[135] used a

combination of FTIR spectroscopy and derivatisation techniques to illustrate that the main degradation products detected were tertiary and secondary hydroperoxides (products of reactions 3.3 and 4.3), alcohols (reactions 3.5; 3.11; 4.5; 4.11), ketones (reactions 3.6 and 4.9), carboxylic acids (reactions 5.8 and 5.6, Scheme 2.5), γ-lactones and γ-perlactones. A very low concentration of aldehydes was detected, since they are highly reactive and quickly undergo further oxidation into peracid groups (reactions 5.2 and 5.3).

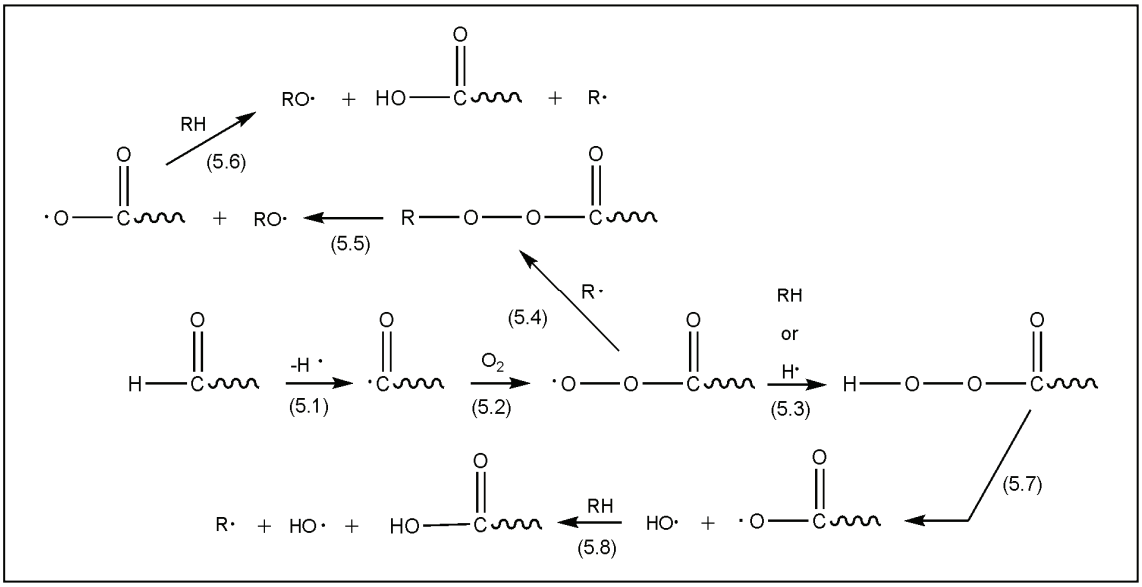

Scheme 2.5: Oxidation of aldehydes into peracids and peresters

During the termination steps, several reactions may occur, some of which have been illustrated in the propagation section, where the formation of ketones, aldehydes, peracids and other inactive carbonyl-containing species is discussed. Termination of polymer radicals occurs through various bimolecular recombinations which are very much dependent on the availability of oxygen and prevailing conditions. When sufficient oxygen is present, termination proceeds almost exclusively via reactions 2.18 and 2.16[113]. At low oxygen pressure other termination reactions involving radicals or macroradicals may take place, e.g., cross-linking reaction 2.14[113], as evidenced by an increase in molecular weight. Recombination is influenced by cage effects, steric control, mutual diffusion and the molecular dynamics of the polymer matrix[136-138]. In solid PP samples the recombination of polymer peroxy radicals is subject to the rate of their encounter with each other and is influenced by the intensity of molecular motion within the polymer.

2.5.4 Comparison of the degradation mechanisms of PP and PE

Although polyethylene and polypropylene oxidise via similar propagation reactions, there are some marked differences in their oxidative degradation processes. Propagation reaction 2.4 is approximately 20 times faster at the tertiary carbon in polypropylene than at the secondary carbon in PE[113]. Similarly, reaction 2.5 is about 6 times faster in PP than in PE due to the ease of abstraction of a tertiary carbon.

However, the conventional termination reaction 2.18 is approximately three orders of magnitude faster when the secondary peroxyl radicals of PE are involved, relative to that of PP. This accounts for the kinetic chain length of autoxidation in PE being 10 times shorter than in the case of PP[139, 140].

A marked difference is seen between the degradation mechanism in PE and PP under conditions of high temperature and high shear (i.e., extrusion, injection moulding, mixing). In the case of PE, cross-linking reactions predominate at temperatures up to about 290ºC[141]. Low concentrations of various unsaturated groups, e.g., terminal vinyl, in-chain vinylidene and pendant trans-vinylene groups are present in PE that affects its overall degradation. High concentrations of vinyl groups with respect to other types of unsaturation, often present in Ziegler-catalysed LLDPE, would promote cross-linking reactions through addition of macro-alkyl radicals to vinylic double bonds. Degradation by chain scission is less favourable in PE and only becomes important at higher temperatures and proceeds to a large extent via β-scission of alkoxy radicals. PP, however, predominantly undergoes chain scission under all processing conditions, accompanied by a reduction of molecular weight and melt viscosity. The propagation reaction is facilitated by intramolecular hydrogen abstraction leading to the formation of adjacent hydroperoxides that are less stable than the isolated kind, leading to an increase in the rate of initiation.

A difference in the photo-oxidation behaviour of PE and PP is also observed due to fundamental differences in the behaviour of hydroperoxides in the two polyolefin materials. Hydroperoxides are known not to accumulate during the photo-oxidation of PE, whereas the concentration increases steadily during the photo-oxidation of PP. This is in contrast with observations made under conditions of thermal oxidation, where hydroperoxides accumulate in both polymers. Carbonyl-containing products become more important during the later stages of photo-oxidation. PE undergoes Norrish types I and II photo-cleavage processes that result in backbone scission to give free radicals capable of initiating photo-oxidation or undergo rearrangements to give molecular products with backbone scission (scheme 6). Photo-oxidation of PE leads to the formation of acids, ketones, γ-lactones, esters and vinyl-alkenes, with an overall higher concentration of vinyl groups and acids formed in PE than PP.

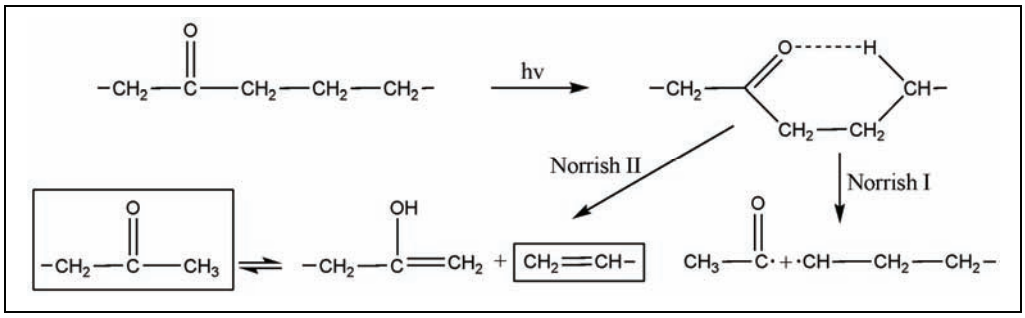

Scheme 2.6: Photolysis of polyethylene, the Norrish reactions

2.5.5 Degradation of impact polypropylene copolymers

As has been mentioned in section 2.3, impact PP copolymers were developed to compensate for the poor impact toughness of PP homopolymer at low temperatures. Impact PP copolymers, like PP and PE, are also readily degraded by stimuli such as elevated temperatures and UV radiation when insufficiently stabilised. The degradation chemistry of impact PP is complicated to a great extent by the presence of multiple components of different chemical composition (isotactic PP, EPR, PE homopolymer and a range of semi-crystalline EP copolymers) composing this heterophasic material. Degradation studies of impact PP copolymers are concerned with the oxidative stability of the respective phases based on chemical composition and morphology or crystallinity. From the viewpoint of primary structure, PP is considered less stable than PE and EPR due to the presence of many highly reactive tertiary carbons capable of undergoing hydrogen abstraction during the initiation stage of oxidation[142]. Oxidative degradation is however, dependent on morphology of polymers in the solid state and is known to originate in amorphous regions of semi-crystalline samples[131] due to the higher diffusion and solubility of oxygen within these regions. This will lead to EPR being oxidised preferentially and the overall degradation process being heterogeneous. These contradictory tendencies are responsible for only a limited number of studies on the degradation of impact PP copolymers having been performed so far. Authors such as Manabe, Suzuki, Nakatani Terano and some co-workers have performed a number of successive studies on the degradation of impact PP. They concluded that the degradation behaviour of the different phases could be linked directly to their primary structure. EPR was found to have higher oxidative stability compared to PP due to the lower concentration of tertiary carbons, regardless of the higher oxygen diffusion and solubility[143, 144]. They also investigated the effect of comonomer content and tacticity on degradation behaviour of a range of impact PP materials and found that the rate of oxidation decreased with increasing ethylene content and decreasing isotacticity[145, 146].

Their investigations continued with the fractionation of impact PP into a xylene-soluble and -insoluble fraction prepared via precipitation form boiling xylene[144]. Characterisation of these fractions by GPC, TGA and AFM also indicated that degradation is confined to the PP matrix, thereby confirming the belief that the concentration of tertiary carbon atoms is of greater importance than oxygen permeability. They also speculated that this might be due to catalyst residues initiating oxidation in the PP matrix after their migration from their initial location in the amorphous EPR phase, but no experimental evidence was supplied to support this assumption. Their most recent publication involves the thermal oxidation of 8 individual fractions obtained by TREF-fractionation of an impact PP sample[147]. It was once again observed that the degradation behaviour of each fraction depends on two factors, namely the chemical constitution (i.e., number of tertiary carbons) and the concentration of 3_1 helix conformation, corresponding to isotacticity. When degradation takes place in the 3_1 helix conformation, the peroxy radical is adjacent to the tertiary C-H and hydroperoxide formation via bimolecular decomposition occurs with great ease.

The most important factors governing the degradation of impact PP copolymers are therefore, (i) the chemical structure (number of tertiary carbon atoms), (ii) comonomer content, (iii) isotacticity and (iv) existence of 3_1 helix conformation corresponding to the PP crystalline part.

Some of the earliest investigations of the degradation behaviour of impact PP copolymers were done by Singh *et al*. who investigated the products formed via thermo-oxidation by FTIR spectroscopy[148]. Derivatisation reactions were used to resolve the overlapping bands in the carbonyl region of the FTIR spectrum and degradation products were compared to those formed by PP and LLDPE homopolymers. They also investigated the concentration profile of products from the surface to the bulk and found that thermo-oxidative degradation was concentrated within the first 125 µm, with the inner layers being impermeable to oxygen. Oxygen consumption results indicated that the presence of ethylene sequences delayed the initiation of degradation and caused a decrease in the degradation rate with increasing ethylene content. As was also confirmed at a later stage[149], degradation takes place at a faster rate in the PP phase, in spite of its crystalline nature and ethylene acts as a moderator for oxidation in impact PP copolymers.

During later years they also compared the degradation products formed under natural and artificial weathering[111]. It was found that the same relative amounts of photo-products such as alcohol, ketone, and ester groups were formed in both degradation scenarios, which indicated that the mechanism of the formation of these products were independent of temperature and the flux of photons in the degradation environment.

The morphological aspects of oxidation of impact PP copolymers were investigated in a series of publications by Kruczala *et al.*[130, 150-152] They've made use of 1D and 2D electron spin resonance (ESR) and electron spin resonance imaging (ESRI) for studying the degradation behaviour of the phases in impact PP copolymers containing a hindered amine stabiliser (HAS)[130, 150-152]. The nitroxides are derived from the HAS and are extremely sensitive to polymer morphology. Comparison of the thermo- and photo-oxidation behaviour of impact PP copolymers with different ethylene contents (10% and 25%) yielded the opposite result. FTIR and ESRI indicated a higher rate of thermo-oxidation in the sample containing 25% ethylene than the samples containing only 10%[151]. This was explained by the enhanced rate of oxygen diffusion and reactant mobility at ageing temperatures of 393 and 433K in copolymers containing more ethylene. UV-irradiation of the same samples suggested a higher rate of degradation in the sample containing 10% ethylene[150]. It is agreed that, although PP tertiary carbons are the point of attack, the rate of oxidation is sensitive to the amount of EPR in the sample, which influences the diffusion of oxygen and reactant mobility. A difference in the oxidation mechanism of PP under thermal and UV-irradiated conditions has also been reported in recent papers, using $^{32}O_2$ and $^{34}O_2$[153, 154] where a difference in temperature is proposed to cause the two different mechanisms in thermal (high temperatures) and photo-oxidation (lower temperatures).

2.5.6 Factors influencing the oxidation of polyolefins

For many years the free radical chain reaction mechanism has provided the framework for interpreting the oxidation of hydrocarbon polymers. This model treats oxidation reactions as though they were homogeneous, i.e., occurring in the liquid phase for all polymers. Although this model is suitable for polymers in the molten state, the oxidation of solid polymers is far more complicated and several reports have indicated the heterogeneous nature of the degradation process[131, 155-162]. Visual evidence for heterogeneity of the degradation process was observed by Knight *et al*.[131] when macroscopic cracks became visible in thermally oxidised PP. The heterogeneous distribution of oxidation products as studied by UV microscopy and staining techniques confirmed the heterogeneity of the process. Several authors have confirmed the inhomogeneous distribution of degradation products in polymer samples by making use of FTIR microscopy and other techniques for depth profiling of oxidation products such as carbonyl species[163-166], hydroperoxides[164, 167], double bonds[168] and carboxylic groups[169] across the thickness of samples. The heterogeneity is caused by several factors such as the morphology and structure of the material[170], catalyst residues[131, 171, 172] and specific properties of free radicals in the solid state, such as recombination and migration probabilities[173-175]. The influence of the most important factors responsible for heterogeneous degradation will now be discussed.

2.5.6.1 Solubility and diffusion of oxygen

Many studies have proven that degradation is a heterogeneous process controlled by oxygen diffusion[130, 155, 163-169, 176]. It has been observed that degradation at polymer surfaces is more severe than in the interior or bulk[176-181]. This is generally attributed to oxygen starvation in the interior. The reaction rate near the surface is very high and most oxygen available at the surface is consumed in free radical reactions before it can be replenished by diffusion from the environment, and subsequently diffuses into the bulk of the sample[182, 183]. Only with sufficient stabilisation will the reaction rate near the surface be lower and oxygen will penetrate the layers underneath the surface to initiate degradation here[184].

The solubility and diffusion of oxygen and other reactants is largely influenced by the density of the material which varies with the degree of crystallinity and compactness of amorphous and crystalline regions of semi-crystalline materials. As the degree of crystallinity and the size of spherulites increase, oxygen permeability decreases due to changes in the relative content of the crystalline phase and the lowering of the diffusion constant which is related to an increased impedance factor[185, 186]. In most polyolefins, degradation initiates in the amorphous region where oxygen diffusion is much less restricted than in crystalline domains[129]. Michaels and Bixler have shown that the solubility of oxygen was proportional to the volume fraction of the amorphous material in PE, as well as the size, shape and size distribution of crystallites[187].

Another factor influencing the diffusion of oxygen in semi-crystalline polymers, is film thickness. It was illustrated that thin samples (less than 40 µm thick) were independent of oxygen diffusion effects, whereas samples between 40 and 200 µm showed an intermediate dependence and films of more than 200 µm was subject to diffusion-controlled processes[188]. Vink[189] concluded that, for films of less than 100µm, the effect of diffusion on photo-oxidation seemed negligible. Still underinvestigated is the effect of oxidation on chemical composition and, therefore, oxygen diffusion.

2.5.6.2 Comonomer content and stereoregularity

A number of studies on the effect of stereoregularity on degradation behaviour of PP has been performed[131, 171, 174, 190-192]. Although Iring *et al*.[193] demonstrated a longer induction period and more rapid oxidation in aPP compared to iPP, Dulog *et al*.[194, 195] were the first authors to indicate that iPP was more prone to degradation than aPP, mainly due to the difference in the chain initiation step, where iPP undergoes a bimolecular chain initiation reaction of hydroperoxides, whereas a unimolecular reaction occurs in aPP. Various other works have also indicated that isotactic PP is much more susceptible to oxidation than syndiotactic PP[196, 197] or atactic PP[194, 195, 198]. The resistance of the different PP structures to oxidation has been found to decrease in the following order: sPP >> aPP >>> iPP[199]. Degradation in iPP proceeds via a bimolecular chain initiation step and random scission events dominate the degradation process, whereas unimolecular chain initiation takes place in aPP and the process is non-random[193]. Mori *et al.*[197] and Hatanaka[199] gave the following explanation for the difference in oxidative stability between syndiotactic and isotactic PP. In isotactic PP all methyl groups are situated on the same side of the polymer backbone and most of the configurational repeat units show meso-diads. During the oxidation of iPP, where hydrogen abstraction preferentially occurs at the tertiary carbons, the hydroperoxide species formed upon reaction with molecular oxygen is situated on the same side as the hydrogen atom connected to the adjacent tertiary carbon. Therefore, intramolecular hydrogen abstraction occurs with greater ease than in the case of syndiotactic PP where the process is complicated by the steric hindrance of the methyl group, and where the peroxy radical and tertiary C-H bond are located on opposite sides of the backbone. It, therefore, seems probable that the thermo-oxidative degradation is depressed significantly due to the existence of racemic configurations in sPP. The high thermo-oxidative stability of sPP has also been reported by other authors[200, 201]. Suzuki continued the investigation of the effect of tacticity on the rate of oxidation. In this study TREF was used to study the effect of tacticity distribution on the ease of oxidation of two PP samples[146]. It was seen that fractions of the same molecular weight but different tacticities degraded differently, and the explanation given above for the higher degradation rate in samples of higher tacticity, was confirmed.

Suzuki *et al.* investigated the effect of comonomer content and tacticity on a series of impact PP copolymers with different ethylene contents[145, 146]. It was seen that a decreasing tacticity and increasing ethylene content lead to an increase in oxidation resistance in this series of copolymers. Alam *et al*.[142] studied the photo-oxidation of iPP and s-PP and also found that sPP had higher

photostability. This study has lead to the proposal for increasing the photostability of iPP by copolymerisation with ethylene. Incorporation of ethylene is supposed to eliminate a number of highly reactive tertiary carbons in PP, thereby improving its resistance to photo-oxidation.

2.5.6.3 Mobility of radicals

One of the main reasons for the heterogeneous oxidation of solid polymers is the limited mobility of radical species. It is accepted that kinetic treatments developed for liquid phases are not suitable for solid systems where radical mobility is impaired. Radicals formed in close proximity to each other in highly viscous melts and solid systems have little chance of migrating away from one another, leading to a high frequency of recombination and disproportionation reactions. These reactions result in a significant change in molecular weight of polymers[138]. Cage recombination is considered the main difference between liquid- and solid-state photo-oxidation process[174]. Liquid state radicals are capable of quick randomisation whereas solid-state radicals will only separate by slow segmental diffusion. Kinetics of solid polymer reactions is limited by this problem, which complicates predictions of polymer lifetimes.

It has been demonstrated that the mobility of radicals varies significantly between crystalline and amorphous phases in semicrystalline polymers. Chien and Wang investigated the initiation efficiency of polyolefin oxidation and concluded that initiation was around ten times lower for semicrystalline polymers than for amorphous systems[202]. Crystallinity and orientation undoubtedly influence the mobility of radicals and, therefore, control the rate of termination through recombination and/or disproportionation. Increased crystallinity and/or orientation reduce the mobility of radicals, and the rate of termination, causing an increase in propagation reactions involving chain scission[203]. This effect is the opposite of that caused by reduced oxygen mobility and it is very difficult to predict whether the restriction of oxygen or radical mobility will dominate. Thus, some studies proved an increase in the rate of degradation with crystallinity, [204], or with orientation[205], while in others the opposite effect was observed[175, 206, 207].

Another aspect of importance in oxidation kinetics is secondary cage recombination, whereby radicals that escape the initial cage still have very high probabilities of recombining even after several propagation steps[173]. Limited migration of radicals clearly is a very important factor in heterogeneous degradation of semicrystalline polymers, but the extent to which it affects the degradation process, strongly depends on polymer morphology and structure as well as molecular mobility of the matrix.

2.5.6.4 Catalyst residues

Celina *et al.*[159] have demonstrated that individual PP particles have different intrinsic stabilities, possibly due to different concentrations of catalyst residues or residual stabilisers in each particle. The spreading of oxidation from one particle to another was also demonstrated. This has lead to the

proposal of 'the spreading model' for heterogeneous oxidation of solid PP[161]. This model proposes that oxidation originates in localised domains of possible higher catalyst concentration, and subsequently spreads to other regions of the polymer. It has been confirmed that it is, in fact, the ions of the transition metals of the polymerisation catalysts that are responsible for initiating degradation[190, 208, 209]. Residual titanium concentrations of 1-20 ppm were detected in polymers prepared by second-generation Ziegler-Natta catalytic systems[210]. It has been demonstrated that metal chelates such as *n*-butyl-*o*-titanate, *n*-octadecyl-*o*-titanate and titanium tetrastearate could act as oxidation initiators in PP at low concentrations but also as inhibitors at high concentrations, depending on the nature of the ligand[211]. Several other studies have also been undertaken to evaluate the initiation of oxidation in areas of higher catalyst concentrations[157, 159, 160, 162]. One study of particular interest was the study done by Blakey and George[212], where it was found that catalyst residues had an inhibiting effect on oxidation in the exact spot where they are found, but they do generate migratable oxidant species that can initiate oxidation some distance from the original catalyst particles. Superoxide and hydroperoxy radicals formed at the location of catalyst particles, spread to other areas where they take part in the formation of highly reactive hydroxyl radicals that subsequently abstract hydrogen atoms from polymer chains, thereby initiating oxidation in this area.

2.5.6.5 Inhomogeneous distribution of stabilisers

Before any degradation occurs, there is already an inhomogeneous distribution of pigments, plasticisers and additives or stabilisers in all freshly produced polymers. Furthermore, the migration of these entities, especially those stabilisers affecting the long-term stability of materials, is an important factor governing the heterogeneity within degraded materials. The migration of stabilisers to their surrounding medium (physical loss) and the oxidation of stabilisers themselves (chemical loss), are two important causes for the loss of stability in polymeric materials[213-215]. The physical loss of stabilisers/antioxidants is controlled either by the rate of diffusion in the polymer or by its escape rate at the material boundary. The latter can be the result of either evaporation in a gas phase medium or dissolution in a liquid phase like water. The migration of phenolic antioxidants in polyolefins used in hot-water applications was studied[216, 217] and it was found that the chemical consumption of phenolic antioxidants is negligible compared to their physical loss at temperatures between 70 and 110ºC[216, 217]. The rate of antioxidant diffusion within the polymer matrix should be fast enough to compensate for their consumption in the reactive layers. If this is not the case, antioxidant supplies cannot be replenished in the areas where they are needed and degradation will proceed very quickly into the bulk of a sample. Due to the practical importance, numerous investigations on the diffusion and extraction of stabilisers in and from polymers have been performed[218-220].

The migration of additives leads to a change in their concentration profile across the thickness of polymer samples. This concentration profile changes with time and can be studied by a number of techniques. One way to study additive concentration profiles is by stacking many individual film layers together and to allow sufficient time for stabilisers to diffuse between the layers [221]. The layers are

then separated and the amount of stabiliser can be determined by means of spectroscopy or solvent extraction followed by chromatography. In the case of a single film, successive layers may be microtomed from the surface into the bulk and then analysed by microscopy or spectroscopy. An alternative to successive microtoming is depth-profiling using attenuated total reflectance Fourier-transform infrared spectroscopy (ATR-FTIR)[222-224], but ATR only probes a fraction of the thickness of a film and quantification is a challenge with ATR-FTIR. Photoacoustic FTIR spectroscopy (PAS-FTIR) can also be used for the purpose of examining the heterogeneity of degraded surface layers[225]. Depending on the optical and thermal properties of the sample, as well as the frequency at which the IR light is modulated, the penetration depth may vary from only a few microns to several tens of micrometers.

A more favourable approach is to microtome cross sections of a film and subsequently scan the concentration profile across the thickness of the film by UV microscopy[226], although this technique is limited to those additives that absorb sufficiently in the UV region. Therefore, Raman-[212] and FTIR microspectroscopy[155, 227-230] are considered among the key innovations in studying the heterogeneity of the degradation process.

2.6 Characterisation techniques for studying degradation

As it has been mentioned before, polyolefin materials are of extreme importance commercially, but unfortunately they are also vulnerable to attack by oxygen, radiation, heat, chemicals and other stimulants. It is extremely important to analyse the degradation process i.e., to establish the mechanisms at work during oxidation, the products formed as well as the influence of molecular structure on the stability of materials. A full understanding of degradation is of extreme importance, since without this, successful stabilisation approaches and superior methods of lifetime prediction would not have been possible. It is, therefore, necessary to pay careful consideration to the analytical techniques employed to study the degradation process. The field of analytical chemistry possesses a powerful arsenal of conventional techniques that have been used for the purpose of studying polyolefin degradation over the years, some of which include size exclusion chromatography (SEC), Fourier transform infrared spectroscopy (FTIR), differential scanning calorimetry (DSC), nuclear magnetic resonance spectroscopy (NMR), chemiluminescence (CL), ultraviolet spectroscopy (UV) and gas chromatography coupled to mass spectrometry (GC-MS). A number of more recently developed techniques have also found application in the field of polymer degradation studies over the past few years. Such techniques include temperature rising elution fractionation (TREF), crystallisation analysis fractionation (CRYSTAF) and liquid chromatography coupled to Fourier transform infrared spectroscopy (LC-FTIR). A brief overview on the use of some of these techniques for the purpose of studying polyolefin degradation will now be presented.

2.6.1 Conventional techniques

2.6.1.1 Size Exclusion Chromatography

Size exclusion chromatography separates molecules according to their hydrodynamic volume and is the preferred method for the determination of molecular weight and molecular weight distribution of synthetic polymers. During the degradation of polyolefins, changes in average molecular weight and molecular weight distribution (MWD) are often observed[231-234]. Depending on the polymer in question and the degradation conditions, many radical reactions can take place. In the case of polyethylene, branching and recombination reactions predominate at lower temperatures, yielding a cross-linked material, which leads to an increase in the average molecular weight of the material[234]. Polypropylene degrades almost exclusively by means of chain scission, leading to a reduction of its average molecular weight[235].

Chain scission during degradation results in continuous breaking of polymer chains, yielding chains of shorter lengths. The average result is that the number of short chains increases with degradation time and is accompanied by a broadening of the molecular weight distribution. The molecular weight curve obtained from SEC measurements, therefore, shifts towards the region of lower molar mass when chain scission is the dominant degradation mechanism[142, 144, 147]. As degradation proceeds and chain scissions continue, the molecular weight curve will exhibit bimodality with the portion of highly degraded short molecules appearing as a narrow distribution on the lower molecular weight side of the original material.

The following equation was proposed by David *et al.*[236] for determining the number of chain scissions in degraded samples, by determining the numerical average of the initial and final number-average molecular weights.

$$n_R = \frac{\overline{M_{no}}}{\overline{M_{nf}}} - 1$$

where: n_R is the number of chains scission

$\overline{M_{no}}$ is the initial number-average molecular weight ($\overline{M_n}$) determined by SEC, and

$\overline{M_{nf}}$ is the final $\overline{M_n}$ value after degradation

As explained in Section 2.5.5, polyolefin degradation in the solid state is a heterogeneous process that leads to varying depth levels of oxidation products in thick samples. Size exclusion chromatography can be used to register molecular weight changes over a cross-section of a thick polymer sample by means of microtoming[163] or layer-by-layer milling[184]. Computer-aided analysis procedure called molecular weight distribution computer analysis (MWDCA) has also proven to be useful for the

comparison of degradation rates in polyolefins[176, 237, 238]. This technique uses molecular weight data, obtained by comparison of experimental SEC molecular weight distribution profiles with computer simulations for determining the scission or crosslink ratio of layers milled from the surface into the core of the sample. Shyichuk investigated scission and crosslink concentrations in photo-degraded LDPE, PP homopolymer and an ethylene-propylene copolymer and found that there was much less variation in these concentrations for LDPE with depth and ongoing degradation times[176]. The lower degree of stratification in PE suggested that oxidation of PE is less dependent on oxygen diffusion than PP.

2.6.1.2 Fourier Transform Infrared Spectroscopy

IR spectroscopy is one of the most popular techniques for studying the chemical changes brought about by polymer degradation. It has been used for both qualitative and quantitative characterisation of degradation products[166, 239-242]. The chemical changes resulting from polymer ageing involve the formation of various functional groups at rates that are strongly dependent on the chemical structure of the polymer. The main chemical species detectable by infrared spectroscopy are hydroxyl and carbonyl groups[243]. The formation of these groups generally leads to visible changes in the infrared spectrum, with carbonylated products and hydroxy and hydroperoxy compounds appearing in the regions of 1850-1550 cm^{-1} and 3700-3200 cm^{-1}, respectively[111, 239, 244]. Associated hydroperoxides and hydrogen-bonded hydroxyl groups are known to give rise to a band around 3400 cm^{-1} in the infrared spectrum [243-245], with free hydroperoxides appearing at around 3560 cm^{-1} [245]. The wavenumbers (cm^{-1}) of the degradation products strongly depend on the mechanism of degradation and the polymer matrix. Differences can be observed in the degradation products of natural and artificial ageing[111] detected by FTIR spectroscopy, as well as thermo- and photo-oxidation[242] conditions. Furthermore, differences in the FTIR absorption of degradation products in PE and PP can also be observed and used for studying the difference in their oxidation mechanisms[246].

The absorption bands of the degradation products often overlap to form complex absorption bands, which complicates their identification. From the hydroxyl and carbonyl groups, degradation products such as peroxides, alcohols, carboxylic acids, ketones, aldehydes, esters and γ-lactones can be identified by means of derivatisation reactions[239, 247]. This method usually involves the treatment of oxidised samples with a reactive gas that can selectively convert degradation products. This leads to the disappearance of some bands in the infrared spectrum and the appearance of some new bands of the derivated products. Derivatisation methods for this purpose were first applied to polyolefins by Carlsson *et al.*[248]. The reagents used are diazomethane for conversion of acids and peracids to their respective methylesters, sulphur tetrafluoride to convert acids to acyl fluorides, nitric oxide to convert alcohols and hydroperoxides to nitrites and nitrates respectively, and phosgene to convert alcohols and hydroperoxides to chloroformates[248].

FTIR has also been useful in determining changes in unsaturation of PE during degradation[243, 249]. The unsaturated groups typically detected, include vinylidene end groups (characteristic bands at 889 and 1684 cm^{-1}) terminal vinyl groups appearing at 910 cm^{-1} and trans-vinylenes at 965 cm^{-1}.

The extent of degradation within polymer samples is often determined on the basis of their carbonyl index[240, 250-252]. The carbonyl index is defined as the ratio of the carbonyl absorbance band around 1714 cm^{-1} with respect to a certain reference band that is not affected by the degradation process. In the case of PE, the band around 1470 cm^{-1} can be used, whereas the bands at 1892 cm^{-1} [250], 974 cm^{-1} [251] 2720 cm^{-1} [203] and 840 cm^{-1} [252], have all been used as reference bands for determining the carbonyl index in PP. Plotting the carbonyl index against degradation time (hours), permits assessment of the kinetics of oxidation[244]. These kinetic curves usually present two phases during the degradation process. The induction stage of degradation is seen in the first region of these plots, where the curve has a very low slope. This stage is characterised, in part, by the consumption of residual processing stabiliser still present in the sample and the diffusion of oxygen into the top layers of the sample, thereby kicking off the degradation process. The second stage is characterised by a steep increase in the carbonyl index of the material as the autoxidation process continues. Changes in the carbonyl index of different polymer materials as a function of degradation time or temperature, are therefore a convenient way for comparing the degradation behaviour of different polymer systems.

2.6.1.3 Nuclear Magnetic Resonance Spectroscopy

^{13}C-NMR has the potential to differentiate between all the major degradation products such as ketones (both methyl and chain-ketones), primary and secondary peroxy radicals, hydroperoxides, alcohols, ketones and acids based on their chemical shifts. The major disadvantage is the insufficient sensitivity to detect products at very low concentrations. Even in highly oxidised polymers, where a considerable loss in mechanical properties is observed, only moderate levels of oxidation products might be present. Jelinski *et al*.[253] reported on the detection and quantification of thermo-oxidation products at the 0.05% level. Ketones, secondary alcohols, secondary hydroperoxides and carboxylic acids were found as the primary oxygen-containing degradation products. It was also possible to distinguish between the degradation patterns and distribution of degradation products in LDPE and LLDPE, originating from different branch contents and thermal treatment procedures. Some of the most difficult species to detect are quaternary carbons due to their low Nuclear Overhauser effect (NOE) and long relaxation times. These complications have been overcome by acquisition of a large number of scans, long pulse delays and large NMR tube diameters. Valuable results on the thermo-oxidation of PE[254] and γ-irradiated PP[255] have been reported. Vaillant *et al*.[256] identified the chemical shifts between 60 and 250ppm in the NMR spectrum as the area of interest with regard to oxidation products. It was shown that the tertiary carbons of alcohols, hydroperoxides and ester were found in the region between 60 and 120ppm, with carboxylic acids and methyl- and in-chain ketones appearing between 140 and 240ppm.

Unsaturated chain ends produced by degradation can also be identified and quantified by means of ^{1}H and ^{13}C-NMR. Kolbert *et al.* studied all the possible chain ends that could form during mechano-chemical degradation of ethylene-propylene (EP) copolymers and found that vinyl, vinylidene and vinylene groups were the main unsaturated species formed[257]. By assigning the olefin region of the NMR spectrum, it was clear that the mechanism of shearing is hydrogen abstraction followed by disproportionation. The methine proton is preferentially abstracted by a ratio of 6:1, compared to a proton linked to a secondary carbon and there is a preference toward main chain scission following C-H scission, at the β-position relative to the radical by over 2:1.

2.6.1.4 Differential Scanning Calorimetry

Differential scanning calorimetry is another technique often used to obtain information on the degradation behaviour of polymers[258-260]. Changes in the peak temperatures and shape of melt endotherms as well as the overall percentage crystallinity, can supply information on the susceptibility of different crystalline phases or arrangements to degradation[260].

DSC is very useful in determining the oxidative induction time (OIT)[261-263] and oxidative temperature (T_{ox})[261, 264] of polymers. OIT measurements are often used to assess the thermal stability, antioxidant effectiveness and degree of degradation of polymers under high temperature conditions. The thermal stability is determined by measuring the time needed until the onset of degradation in a polymer at a given temperature within an oxidative atmosphere. Rosa *et al.*[259] investigated the influence of several parameters on OIT data and found that sample preparation (shape and size), oxygen flow and heating rate of the OIT experiment had a significant influence on the data obtained.

2.6.2 Fractionation and hyphenated techniques

Although conventional techniques such as these mentioned in the previous section are still of undeniable value for studying degradation of polymers, some techniques specifically suited for studying the chemical heterogeneity within polyolefin materials have also recently found application in the field of degradation studies. TREF is a highly effective technique for separating semi-crystalline polymers according to their crystallisability, which is directly related to their molecular structure[58, 92, 265, 266]. Although it has been a technique of choice for characterisation of semi-crystalline materials for several years already, it has only recently been employed for the purpose of studying degradation[146, 147, 267, 268]. TREF supplied valuable information on the influence of tacticity and tacticity distribution[146] as well as molecular weight[147] on the degradation of polyolefins.

Crystallisation analysis fractionation (CRYSTAF), another technique used for solution crystallisation of semi-crystalline polymers[265, 269], has only recently been employed for studying degradation[270, 271]CRYSTAF also fractionates polymers according to their crystallisability, which is a function of their chemical composition. The depth profile of degradation across thick PP samples, based on their

crystallisability, was determined by CRYSTAF analysis of abrased layers, taken from the surface towards the sample core. Depending on the level of degradation, samples will change in their ability to crystallise out at higher temperatures, due to impurities incorporated in chains (e.g., carbonyl and hydroxyl groups). Surface layers comprised of highly degraded, amorphous material, that was altered by degradation to such a large extent that crystallisation was no longer possible. The crystallisability increases towards the bulk where chain molecules have been altered to a smaller extent, rendering them still crystallisable to a large extent. Apart from a shift in the CRYSTAF crystallisation peak towards lower temperatures, a decrease in the intensity of the main crystallisation peak (i.e., concentration of crystallisable material) and an increase in the soluble fraction of each layer was also observed upon higher degrees of degradation.

Another very effective technique for assessing the heterogeneity within complex polymers such as polyolefins, is SEC coupled to FTIR (SEC-FTIR), which can supply information on the chemical composition as a function of molecular weight distribution[272, 273]. It is especially useful for studying copolymers where the chemical heterogeneity across the molecular weight distribution can be studied by determining the ratio of two specific functional groups of interest[274-280]. Its benefits have also recently been exploited as a tool for studying polymer degradation[270, 271, 281]. SEC-FTIR analysis was also performed on the abrased layers of a degraded thick PP sample[270, 271]. The Gram-Schmidt plot shifted towards lower molecular weight in the surface layers compared to the core, and the highest concentration of carbonyl functionalities was found in the low molecular weight region of each layer. The heterogeneous degradation of polyolefins can therefore be successfully studied by techniques such as TREF, CRYSTAF and SEC-FTIR to obtain information that is not possible with conventional analytical techniques. It will be the aim of this study to demonstrate further applications of these techniques in studying polyolefin degradation.

2.7 References:

1. Seymour, R. B., History of Polyolefins. In *Handbook of Polyolefins*, Vasile, C.; Seymour, R. B., Eds. Marcel Dekker: New York, 1993; p 1.
2. Monasse, B.; Haudin, J. M., Molecular structure of polypropylene homo- and copolymers. In *Polypropylene: Structure, blends and composites*, Karger-Kocsis, J., Ed. Chapman & Hall: London, 1995; p 3.
3. Zimm, B. H. *J. Chem. Phys.* (1948) 16, p 1099.
4. Grinshpun, V.; O'Driscoll, K. F.; Rudin, A. *J. Appl. Polym. Sci.* (1984) 29, p 1071.
5. Grinshpun, V.; Rudin, A. *J. Appl. Polym. Sci.* (1985) 30, p 2413.
6. Utracki, L. A.; Dumoulin, M. M. *ACS Symp. Ser.* (1984) 145, p 91.
7. Lew, R.; Suwunda, D.; Balke, S. T. *J. Appl. Polym. Sci.* (1988) 35, p 1049.
8. Chiang, R., In *Newer methods of polymer characterisation*, Ke, B., Ed. Wiley-Interscience: New York, 1964; p 471.
9. Horska, J.; Stejskal, J.; Kratochvil, P. *J. Appl. Polym. Sci.* (1979) 24, p 1845.
10. Horska, J.; Stejskal, J.; Kratochvil, P. *J. Appl. Polym. Sci.* (1983) 28, p 3873.
11. Mays, J. W.; Fetters, L. J. *Macromolecules* (1989) 22, p 921.
12. Moore, E. P. J., *Polypropylene handbook*. Hanser/Gardner Publishers Inc.: Cincinnati, 1996; p 89.
13. Atkins, J. L.; Muus, L. T.; Smith, C. W.; Pieski, E. T. *J. Am. Chem. Soc.* (1957) 79, p 5089.

14. Schulz, G. V. *Phys. Chem.* (1940) B46, p 173.
15. Natta, G.; Pino, P.; Corradini, P. *J. Am. Chem. Soc.* (1955) 77, p 1708.
16. Galanti, A. V.; Mantell, C. L., *Polypropylene fibers and films*. Plenum press: New York, 1965.
17. Natta, G. J. *J. Polym. Sci.* (1959) 34, p 531.
18. Natta, G.; Pasquon, I.; Zambelli, I.; Gatti, G. *Makromol. Chem.* (1964) 70, p 191.
19. Van der Ven, S., *Polypropylene and other polyolefins*. Elsevier Science Publishers: Amsterdam, 1990.
20. Greco, R.; Mancarella, C.; Martuscelli, E.; Ragosta, G.; Yin, J. *Polymer* (1987) 28, p 1922.
21. D'Orazio, L.; Mancarella, C.; Martuscelli, E.; Sticotti, G. *J. Mater. Sci.* (1991) 26, p 4033.
22. Zhang, X. F.; Xie, F.; Pen, Z. L.; Zhang, Y.; Zhang, Y. X.; Zhou, W. *Eur. Polym. J.* (2002) 38, p 1.
23. Jang, B. Z.; Uhlman, D. R.; Vander Sande, J. B. *J. Appl. Polym. Sci.* (1984) 29, p 3409.
24. Jang, B. Z.; Uhlman, D. R.; Vander Sande, J. B. *Polym. Eng. Sci.* (1985) 25, p 643.
25. Premphet, K.; Horanont, P. *Polymer* (2000) 41, p 9283.
26. Rybuikar, F. J. *J. Appl. Polym. Sci.* (1969) 13, p 827.
27. Binsbergen, F. L.; Delarge, B. G. M. *Polymer* (1970) 11, p 309.
28. Ito, J.; Mitani, K.; Mizatani, Y. *J. Appl. Polym. Sci.* (1992) 46, p 1221.
29. Yokoyama, Y.; Ricco, T. *J. Appl. Polym. Sci.* (1997) 66, p 1007.
30. Hongjun, C.; Xiaolie, L.; Dezhu, M.; Jianmin, W.; Hongsheng, T. *J. Appl. Polym. Sci.* (1999) 71, p 93.
31. Tan, H.; Li, L.; Chen, Z.; Song, Y.; Zheng, Q. *Polymer* (2005) 46, p 3522.
32. Yang, D. C.; Zhang, B. L.; Yang, Y. K.; Fang, Z.; Sun, G. F. *Polym. Eng. Sci.* (1984) 24, p 612.
33. Jang, B. Z.; Uhlman, D. R.; Vander Sande, J. B. *J. Appl. Polym. Sci.* (1985) 30, p 2485.
34. Van Gisbergen, J. G. M.; Hoeben, W. F. L. M.; Meijer, H. E. H. *Polymer* (1991) 31, p 1539.
35. Van Gisbergen, J. G. M.; Meijer, H. E. H.; Lemstra, P. J. *Polymer* (1989) 30, p 2153.
36. Choudhary, V.; Varma, H. S.; Varma, I. K. *Polymer* (1991) 32, p 2534.
37. D'Orazio, L.; Mancarella, C.; Martuscelli, E.; Sticotti, G.; Massari, P. *Polymer* (1993) 34, p 3671.
38. Choudhary, V.; Varma, H. S.; Varma, I. K. *Polymer* (1991) 32, p 2541.
39. D'Orazio, L.; Mancarella, C.; Martuscelli, E. *Polymer* (1991) 32, p 1186.
40. Prentice, P.; Williams, J. G. *Plast. Rubber Compos Process. Appl.* (1982) 2, p 27.
41. Chiang, W. Y.; Yang, W. D.; Pukanszky, B. *Polym. Eng. Sci.* (1991) 32, p 641.
42. Wang, L.; Huang, B. *J. Polym. Sci., Part B: Polym. Phys.* (1990) 28, p 937.
43. Whelan, T., *Polymer technology dictionary*. Chapman & Hall: London, 1994; p 439.
44. Karger-Kocsis, J.; Kallo, A.; Kuleznev, V. N. *Polymer* (1984) 25, p 279.
45. Sheffold, F.; Budkowski, A.; Steiner, U.; Eiser, E.; Klein, J. *J. Chem. Phys.* (1996) 104, p 8795.
46. Graessley, W. W.; Krishnamoorti, R.; Balsara, N. P.; Butera, R. J.; Fetters, L. J.; Lohse, D. J.; Schulz, D. N.; Sissano, J. A. *Macromolecules* (1994) 27, p 3896.
47. Weimann, P. A.; Johnes, T. D.; Hillmyer, M. A.; Bates, F. S.; Londono, J. D.; Melnichenko, Y.; Wignall, G. D.; Almdal, K. *Macromolecules* (1997) 30, p 3560.
48. Fredrickson, G. H.; Liu, A. J.; Bates, F. S. *Macromolecules* (1994) 27, p 2503.
49. Lohse, D. J., Miscibility and phase separation in polypropylene blends. In *Polypropylene: An A-Z reference*, Karger-Kocsis, J., Ed. Kluwer Publishers: Dordrecht, 1999; p 484.
50. Lohse, D. J.; Wissler, G. E. *Jnl. Mater. Sci.* (1991) 26, p 743.
51. Baldwin, F. P.; Ver Strate, G. *Rubber Chem. Technol.* (1972) 45, p 709.
52. Del Duca, D.; Moore, E. P. J., End-use properties. In *Polypropylene handbook*, Moore, E. P. J., Ed. Hanser/Gardner Publications Inc.: Cincinnati, 1996; p 237.
53. Galli, P.; Haylock, J. C.; Simonazzi, T., Manufacturing and properties of polypropylene copolymers. In *Polypropylene: Structure, blends and composites*, Karger-Kocsis, J., Ed. Chapman & Hall: London, 1995; p 1.
54. Tait, P. J. T.; Berry, I. G., Monoalkene polymerisation: Copolymerisation. In *Comprehensive Polymer Science*, Allen, G. F.; Bevington, J. C., Eds. Pergamon Press plc: Oxford, 1989; Vol. 4.
55. Pires, M.; Mauler, R. S.; Liberman, S. A. *J. Appl. Polym. Sci.* (2004) 92, p 2155.
56. Mirabella, F. *Polymer* (1993) 34, p 1729.
57. Zacur, R.; Goizueta, G.; Capiati, N. *Polym. Eng. Sci.* (2000) 40, p 1921.
58. Soares, J. B. P.; Hamielec, A. E. *Polymer* (1995) 36, p 1639.
59. Urdampiletta, I.; González, A.; Iruin, J. J.; de la Cal, J. C.; Asua, J. M. *Macromolecules* (2005) 38, p 2795.
60. Xu, J.; Fu, Z.; Fan, Z.; Feng, L. *Eur. Polym. J.* (2002) 38, p 1739.

61. Chen, Y.; Chen, Y.; Chen, W.; Yang, D. *Polymer* (2006) 47, p 6808.
62. Tanem, B. S.; Kamfjord, T.; Augestad, M.; Løvgren, T. B.; Lundquist, M. *Polymer* (2003) 44, p 4283.
63. Sun, Z.; Yu, F.; Qi, Y. *Polymer* (1991) 32, p 1059.
64. Xu, J.; Feng, L.; Yang, S.; Wu, Y. *Polymer* (1997) 38, p 4381.
65. Fernado, P. L.; Williams, J. G. *Polym. Eng. Sci.* (1981) 21, p 1003.
66. Narisawa, I. *Polym. Eng. Sci.* (1987) 27, p 41.
67. Ma, D.; Li, X.; Luo, X.; Chin. *J. Polym. Sci.* (1994) 12, p 164.
68. Bramuzzo, M. *Polym. Eng. Sci.* (1987) 29, p 1077.
69. Prentice, P. *Polymer* (1982) 23, p 1189.
70. Fan, Z.; Zhang, Y.; Xu, J.; Wang, H.; Feng, L. *Polymer* (2001) 42, p 5559.
71. Fu, Z.-S.; Fan, Z.-Q.; Zhang, Y.-Q.; Feng, L.-X. *Eur. Polym. J.* (2003) 39, p 795.
72. Mirabella, F. J. *J. Appl. Pol. Sci., Appl. Polym. Symp.* (1992) 51, p 117.
73. Cogswell, F. N.; Hanson, D. E. *Polymer* (1975) 16, p 937.
74. Ke, B. *J. Polym. Sci.* (1960) 42, p 15.
75. Ke, B. *J. Polym. Sci.* (1962) 61, p 47.
76. Boor, J., Block copolymerisation. In *Ziegler-Natta catalysts and polymerisations*, Boor, J., Ed. Academic Press Inc.: London, 1979; p 587.
77. Barbè, P. C.; Cecchin, G.; Noristi, L. *Adv. Polym. Sci.* (1986) 81, p 1.
78. Kashiwa, N.; Yoshitake, J. *Polym. Bull.* (1984) 11, p 479.
79. Lazzeri, A.; Bucknall, C. B. *Polymer* (1995) 36, p 2895.
80. Kim, G. M.; Michler, G. H. *Polymer* (1998) 39, p 5689.
81. Kim, G. M.; Michler, G. H.; Gahleitner, M.; Fiebig, J. *J. Appl. Polym. Sci.* (1996) 60, p 1391.
82. Michler, G. H. *J. Macromol. Sci., Phys.* (1999) B38, p 787.
83. Debling, J. A.; Ray, W. H. *J. Appl. Polym. Sci.* (2001) 81, p 3085.
84. Kakugo, M.; Sadatoshi, H.; Sakai, J.; Yokoyama, M. *Macromolecules* (1989) 22, p 3172.
85. Kakugo, M.; Sadatoshi, H.; Yokoyama, M.; Kojima, K. *Macromolecules* (1989) 22, p 551.
86. McKenna, T.; Bouzid, D.; Matsunami, S.; Sugano, T. *Polymer Reac. Eng.* (2003) 11, p 177.
87. Cecchin, G.; Marchetti, E.; Baruzzi, G. *Macromol. Chem. Phys.* (2001) 202, p 1987.
88. Besomles, M.; Menguel, J.-F.; Delmas, G. J. *J. Polym. Sci., Part B: Polym. Phys.* (1988) 26, p 1881.
89. Hongjun, C.; Xiaolie, L.; Xiangxu, C.; Dezhu, M.; Jianmin, W.; Hongsheng, T. *J. Appl. Polym. Sci.* (1999) 71, p 103.
90. Feng, Y.; Hay, J. N. *Polymer* (1998) 39, p 6723.
91. Feng, Y.; Jin, X.; Hay, J. N. *J. Appl. Polym. Sci.* (1998) 68, p 381.
92. Xu, J.; Feng, L. *Eur. Polym. J.* (2000) 36, p 867.
93. Xu, J.; Feng, L.; Yang, S.; Yang, Y.; Kong, X. *Eur. Polym. J.* (1998) 34, p 431.
94. Usami, T.; Gotoh, Y.; Umemoto, H.; Takayama, S. *J. Appl. Polym. Sci., Appl. Polym. Symp.* (1993) 52, p 145.
95. Painter, P. C.; Watzek, M.; Koenig, J. L. *Polymer* (1977) 18, p 1169.
96. Baker, B. B.; Bonesteel, J. K.; Keating, M. Y. *Thermochim. Acta* (1990) 166, p 53.
97. Cheng, H. N. *Macromolecules* (1984) 17, p 1950.
98. Ray, G. J.; Johnson, P. E.; Knox, J. R. *Macromolecules* (1977) 10, p 773.
99. Carman, C. J.; Harrington, R. A.; Wilkes, C. E. *Macromolecules* (1977) 10, p 536.
100. Paxon, J. R.; Randall, J. C. *Anal. Chem.* (1978) 50, p 1777.
101. Randall, J. C. *JMS-Rev. Macromol. Chem. Phys.* (1989) C29 (2&3), p 201.
102. Hayashi, T.; Inoue, Y.; Chûjô, R.; Asakura, T. *Polymer* (1988) 29, p 1848.
103. Kakugo, M.; Naito, Y.; Mizunuma, K.; Miyatake, T. *Macromolecules* (1982) 15, p 1150.
104. Hansen, E. W.; Redford, K.; Oysaed, H. *Polymer* (1996) 37, p 19.
105. Wang, W.-J.; Zhu, S. *Macromolecules* (2000) 33, p 1157.
106. Xu, J.; Feng, L. *Polym. Int.* (1998) 47, p 433.
107. Bhuiyan, A. L. *Adv. Polym. Sci.* (1982) 47, p 43.
108. Hutchinson, J. M. *Prog. Polym. Sci.* (1995) 20, p 703.
109. Vasile, C., Degradation and Decomposition. In *Handbook of polyolefins*, Vasile, C.; Seymour, R. B., Eds. Marcel Dekker: New York, 1993; p 479.
110. Carlsson, D. J.; Wiles, D. M., Degradation. In *Encyclopedia of Polymer Science and Engineering*, Kroschwitz, J. I., Ed. John Wiley & Sons: New York, 1985; p 630.
111. Mani, R.; Singh, R. P.; Sivaram, S. *Polym. Int.* (1997) 44, p 137.
112. White, J. R., Weathering. In *Polypropylene: An A-Z reference*, Karger-Kocsis, J., Ed. Kluwer Publishers: Dordrecht, 1999; p 866.

113. Al-Malaika, S. *Adv. Polym. Sci.* (2004) 169, p 122.
114. Al-Malaika, S., Thermal antioxidants. In *Polypropylene: An A-Z reference*, Karger-Kocsis, J., Ed. Kluwer Publishers: Dordrecht, 1999; p 821.
115. Hawkins, W. L.; Winslow, F. H., Degradation and stabilisation. In *Crystalline olefin polymers* Raff, R. A. V.; Doak, K. W., Eds. John Wiley & Sons Inc.: New York, 1964; p 361.
116. Dragutan, I., Photostabilisation of Polyolefins. In *Handbook of polyolefins*, Vasile, C.; Seymour, R. B., Eds. Marcel Dekker: New York, 1993; p 605.
117. Azizi, H.; Ghasemi, I. *Polym. Test.* (2004) 23, p 137.
118. Sahin, S.; Yayla, P. *Polym. Test.* (2005) 24, p 1012.
119. Hansen, R. H.; Russell, C. A.; De Benedictis, T.; Martin, W. M.; Pascale, J. V. *J. Polym. Sci.* (1964) A2, p 587.
120. Hawkins, W. L.; Matreyek, W.; Winslow, F. H. *J. Polym. Sci.* (1959) 41, p 1.
121. Wood, D. L.; Luongo, J. P. *Mod. Plast.* (1961) 38, p 132.
122. Morou, C.; Dufraisse, C. *Chem. Rev.* (1926) 3, p 113.
123. Christiansen, J. A. *J. Phys. Chem.* (1924) 28, p 145.
124. Backström, H. L. *J. Am. Chem. Soc.* (1927) 49, p 1460.
125. Farmer, E. H.; Bloomfield, G. F.; Sundralingham, A.; Sutton, D. A. *Trans. Faraday Soc.* (1942) 38, p 348.
126. Bolland, J. L.; Gee, G. *Trans. Faraday Soc.* (1946) 42, p 236.
127. George, G. A.; Celina, M., Honmogeneous and heterogeneous oxidation of polypropylene. In *Handbook of Polymer Degradation*, Hamid, S. H., Ed. Marcel Dekker Inc.: New York, 2000; p 277.
128. Rabello, M. S.; White, J. R. *Polymer* (1997) 38, p 6379.
129. Blais, P.; Carlsson, D. J.; Wiles, D. M. *J. Polym. Sci., Part A1* (1972) 10, p 1077.
130. Schlick, S.; Kruczala, K. *JCT Research* (2005) 2, p 389.
131. Knight, J. B.; Calvert, P. D.; Billingham, N. C. *Polymer* (1985) 26, p 1713.
132. Schnabel, W., *Polymer Degradation: Principles and Practical Applications*. Hanser International: Munich, 1981.
133. Gensler, R.; Plummer, C. J. G.; Kausch, H.-H.; Kramer, E.; Pauquet, J.-R.; Zweifel, H. *Polym. Degrad. Stab.* (2000) 67, p 195.
134. Adams, J. H. *J. Polym. Sci., Part A: Polym. Chem.* (1970) 8, p 1077.
135. Costa, L.; Luda, M. P.; Trossarelli, L. *Polym. Degrad. Stab.* (1997) 55, p 329.
136. Garton, A.; Carlsson, D. J.; Wiles, D. M. *J. Polym. Sci., Polym. Chem. Ed.* (1978) 16, p 33.
137. Garton, A.; Carlsson, D. J.; Wiles, D. M. *Macromolecules* (1979) 12, p 1071.
138. Al-Malaika, S. *Polym. Plast. Technol. Eng.* (1988) 27, p 261.
139. Decker, C.; Mayo, F. R. *J. Polym. Sci., Polym. Chem. Ed.* (1973) 11, p 2879.
140. Decker, C.; Mayo, F. R.; Richardson, H. *J. Polym. Sci., Polym. Chem. Ed.* (1973) 11, p 2879.
141. Rideal, G. R.; Padget. *J. Polym. Sci. Symp.* (1976) 57, p 1.
142. Alam, M. S.; Nakatani, H.; Goss, B. G. S.; Ichiki, T.; Liu, B.; Terano, M. *J. Appl. Polym. Sci.* (2002) 86, p 1863.
143. Manabe, N.; Yokota, H.; Nakatani, H.; Suzuki, S.; Liu, B.; Terano, M. *Polym. Bull.* (2005) 54, p 141.
144. Manabe, N.; Yokota, H.; Suzuki, S.; Liu, b.; Terano, M. *J. Appl. Polym. Sci.* (2006) 100, p 1831.
145. Suzuki, S.; Liu, B.; Terano, M.; Manabe, N.; Kawamura, K.; Ishikawa, M.; Nakatani, H. *Polym. Bull.* (2005) 55, p 141.
146. Suzuki, S.; Nakamura, Y.; Hasan, A. T. M. K.; Liu, B.; Terano, M.; Nakatani, H. *Polym. Bull.* (2005) 54, p 311.
147. Nakatani, H.; Manabe, N.; Yokota, Y.; Minami, H.; Suzuki, S.; Yamaguchi, F.; Terano, M. *Polym. Int.* (2007) 56, p 1152.
148. Singh, R. P.; Mani, R.; Sivaram, S.; Lacoste, J.; Lemaire, J. *Polym. Int.* (1993) 32, p 189.
149. Sarwade, B. D.; Singh, R. P. *J. Appl. Polym. Sci.* (1999) 72, p 215.
150. Kruczala, K.; Aris, W.; Schlick, S. *Macromolecules* (2005) 38, p 6979.
151. Kruczala, K.; Bokria, J. G.; Schlick, S. *Macromolecules* (2003) 36, p 1909.
152. Kruczala, K.; Varghese, B.; Bokria, J. G.; Schlick, S. *Macromolecules* (2003) 36, p 1899.
153. Philippart, J.-L.; Gardette, J.-L. *Polym. Degrad. Stab.* (2001) 71, p 189.
154. Philippart, J.-L.; Gardette, J.-L. *Polym. Degrad. Stab.* (2001) 73, p 185.
155. Jouan, X.; Gardette, J.-L. *Polym. Commun.* (1987) 28, p 329.
156. Scheirs, J.; Delatycki, O.; Bigger, S. W.; Billingham, N. C. *Polym. Int.* (1991) 36, p 187.
157. Livanova, N. M. *Polym. Sci. Ser. A* (1994) 36, p 32.
158. Lemaire, J.; Gardette, J.-L.; Lacoste, J. *Macromol. Chem., Macromol. Symp.* (1993) 70, p 419.

159. Celina, M.; George, G. A.; Billingham, N. C. *Polym. Degrad. Stab.* (1993) 42, p 335.
160. Livanova, N. M.; Zaikov, G. E. *Polym. Degrad. Stab.* (1997) 57, p 1.
161. George, G. A.; Celina, M.; Lerf, C.; Cash, G.; Weddell, D. *Macromol. Symp.* (1997) 115, p 69.
162. George, G. A.; Ghaemy, M. *Polym. Degrad. Stab.* (1991) 33, p 411.
163. Girois, S.; Audouin, L.; Verdu, J.; Delprat, P.; Marot, G. *Polym. Degrad. Stab.* (1996) 51, p 125.
164. Yu, Y.-L.; Shen, F.-W.; McKellop, H. A.; Salovey, R. *J. Polym. Sci., Polym. Chem. Ed.* (1999) 37, p 3309.
165. La Mantia, R. P.; Gardette, J.-L. *Polym. Degrad. Stab.* (2002) 75, p 1.
166. Gulmine, J. V.; Janissek, P. R.; Heise, H. M.; Akselrud, L. *Polym. Degrad. Stab.* (2003) 79, p 385.
167. Rincon-Rubio, L. M.; Fayolle, B.; Audouin, L.; Verdu, J. *Polym. Degrad. Stab.* (2001) 74, p 177.
168. Kumar, A.; Commerceuc, S.; Gonon, L.; Verney, V. *Polym. Degrad. Stab.* (2002) 75, p 509.
169. Grossetete, T.; Gonon, L.; Verney, V. *Polym. Degrad. Stab.* (2002) 78, p 203.
170. Celina, M.; George, G. A.; Lacey, D. J.; Billingham, N. C. *Polym. Degrad. Stab.* (1995) 47, p 311.
171. Billingham, N. C. *Makromol. Chem., Makromol. Symp.* (1989) 28, p 145.
172. Gijsman, P.; Hennekens, J.; Wiles, D. M. *Makromol. Chem.* (1980) 181, p 1841.
173. Garton, A.; Carlsson, D. J.; Wiles, D. M. *Makromol. Chem.* (1980) 181, p 1841.
174. Mayo, F. R. *Macromolecules* (1978) 11, p 942.
175. Chien, J. C. W.; Wang, D. S. T. *Macromolecules* (1975) 8, p 920.
176. Shyichuk, A. V.; White, J. R.; Craig, I. H.; Syrotynska, I. D. *Polym. Degrad. Stab.* (2005) 88, p 415.
177. White, J. R.; Turnbull, A. *J. Mater. Sci.* (1994) 29, p 584.
178. Gillen, K. T.; Wise, J.; Clough, R. L. *Polym. Degrad. Stab.* (1995) 47, p 149.
179. Wise, J.; Gillen, K. T.; Clough, R. L. *Polymer* (1997) 38, p 1929.
180. Schoolenberg, G. E.; Vink, P. *Polymer* (1991) 32, p 432.
181. Gonon, L.; Gardette, J.-L. *Polymer* (2000) 41, p 1669.
182. Gillen, K. T.; Clough, R. L. *Polym. Degrad. Stab.* (1989) 24, p 137.
183. Clough, R. L.; Gillen, K. T. *Polym. Degrad. Stab.* (1992) 38, p 47.
184. Turton, T. J.; White, J. R. *Polym. Degrad. Stab.* (2001) 74, p 559.
185. Michaels, A. S.; Bixler, H. J.; Fein, H. L. *J. Appl. Phys.* (1964) 35, p 3165.
186. Vieth, W.; Wuerth, W. F. *J. Appl. Polym. Sci.* (1969) 13, p 685.
187. Michaels, A. S.; Bixler, H. J. *J. Polym. Sci.* (1961) 50, p 393.
188. Kiryushkin, S. G.; Shlyapnikov, Y. A. *Polym. Degrad. Stab.* (1989) 23, p 185.
189. Vink, P. *Jnl. Appl. Pol. Sci., Appl. Polym. Symp.* (1979) 35, p 265.
190. Van Sickle, D. E. *J. Polym. Sci., Part A1* (1972) 10, p 355.
191. Garton, A.; Carlsson, D. J.; Wiles, D. M. *Makromol. Chem.* (1981) 181, p 1841.
192. He, P.; Xiao, Y.; zhang, P.; xing, C.; Zhu, N.; Zhu, X.; Yan, D. *Polym. Degrad. Stab.* (2005) 88, p 473.
193. Iring, M.; Laszlo-Hedvig, Z.; Tüdos, F.; Kelen, T. *Polym. Degrad. Stab.* (1983) 5, p 467.
194. Dulog, L.; Radlmann, E.; Kern, W. *Makromol. Chem.* (1963) 60, p 1.
195. Dulog, L.; Radlmann, E.; Kern, W. *Makromol. Chem.* (1964) 80, p 67.
196. Kato, M.; Osawa, Z. *Polym. Degrad. Stab.* (1999) 65, p 457.
197. Mori, H.; Hatanaka, T.; Terano, M. *Macromol. Rapid Commun.* (1997) 18, p 157.
198. Osawa, Z.; Saito, T.; Kimura, Y. *J. Appl. Polym. Sci.* (1968) 22, p 563.
199. Hatanaka, T.; Mori, H.; Terano, M. *Polym. Degrad. Stab.* (1999) 64, p 313.
200. Hatanaka, T.; Mori, H.; Terano, M. *Macromol. Rapid Commun.* (1997) 18, p 157.
201. Osawa, Z.; Kato, M.; Terano, M. *Macromol. Rapid Commun.* (1997) 18, p 667.
202. Verdu, J. *Macromol. Symp.* (1997) 115, p 165.
203. Rabello, M. S.; White, J. R. *Polym. Degrad. Stab.* (1997) 56, p 55.
204. Billingham, N. C.; Prentice, P.; Walker, T. *J. Polym. Sci. Symp.* (1976) 57, p 287.
205. Akay, G.; Tincer, T.; Aydin, E. *Eur. Polym. J.* (1980) 57, p 287.
206. Mucha, M. *Colloid. Polym. Sci.* (1986) 264, p 113.
207. Baumhardt-Neto, R.; De Paoli, M. A. *Polym. Degrad. Stab.* (1993) 40, p 59.
208. Richters, P. *Macromolecules* (1970) 3, p 262.
209. Billingham, N. C. *Polymer* (1985) 86, p 1713.
210. Nowlin, T. E. *Prog. Polym. Sci.* (1985) 11, p 29.
211. Cicchetti, O.; de Simone, R.; Gratani, F. *Eur. Polym. J.* (1973) 9, p 1205.
212. Blakey, I.; George, G. A. *Polym. Degrad. Stab.* (2000) 70, p 269.

213. Pickett, J. E., Permanence of UV absorbers in plastics and coatings. In *Handbook of polymer degradation*, Hamid, S. H., Ed. Marcel Dekker: New York, 2000.
214. Billingham, N. C.; Garcia-Trabajo, P. *Polym. Degrad. Stab.* (1995) 48, p 419.
215. Boersma, A. *Polym. Degrad. Stab.* (2006) 91, p 472.
216. Smith, G. D.; Karlsson, K.; Gedde, U. W. *Polym. Eng. Sci.* (1992) 32, p 658.
217. Viebke, J.; Gedde, U. W. *Polym. Eng. Sci.* (1997) 37, p 896.
218. Figge, K. *Prog. Polym. Sci.* (1980) 6, p 187.
219. Spatafore, R.; Pearson, L. T. *Polym. Eng. Sci.* (1991) 31, p 1610.
220. Allen, N. S.; Marshall, G. P.; Vasilou, C.; Moore, L. M.; Kotecha, J. L.; Gardette, J. L. *Polym. Degrad. Stab.* (1988) 20, p 315.
221. Foldes, E.; Turcsanyi, B. *J. Appl. Polym. Sci.* (1992) 46, p 507.
222. Bokria, J. G.; Schlick, S. *Polymer* (2002) 43, p 3239.
223. Ekgasit, S.; Ishida, H. *Appl. Spectrosc.* (1996) 50, p 1187.
224. Ekgasit, S.; Ishida, H. *Appl. Spectrosc.* (1997) 51, p 461.
225. Delprat, P.; Gardette, J.-L. *Polymer* (1993) 34, p 933.
226. Billingham, N. C.; Calvert, P. D.; Uzuner, A. *Eur. Polym. J.* (1989) 25, p 839.
227. Sankhe, S. Y.; Hirt, D. E. *Appl. Spectrosc.* (2002) 56, p 205.
228. Sankhe, S. Y.; Hirt, D. E. *Appl. Spectrosc.* (2003) 57, p 37.
229. Hsu, S. C.; Lin-Vien, F.; French, R. N. *Appl. Spectrosc.* (1991) 46, p 225.
230. Joshi, N. B.; Hirt, D. E. *Appl. Spectrosc.* (1998) 53, p 11.
231. Fayolle, B.; Audouin, L.; Verdu, J. *Polym. Degrad. Stab.* (2002) 75, p 123.
232. Gonzalez-Gonzalez, V. A.; Neira-Velazquez, G.; Angulo-Sanchez, J. L. *Polym. Degrad. Stab.* (1998) 60, p 33.
233. Lew, R.; Suwanda, D.; Balke, S. T. *J. Appl. Polym. Sci.* (1988) 35, p 1049.
234. Lew, R.; Suwanda, D.; Balke, S. T. *J. Appl. Polym. Sci.* (1988) 35, p 1033.
235. Ying, Q.; Zhao, Y.; Liu, Y. *Macromol. Chem.* (1991) 192, p 1041.
236. David, C.; Trojan, M.; Daro, A.; Demarteau, W. *Polym. Degrad. Stab.* (1992) 37, p 233.
237. Shyichuk, A. V.; White, J. R. *J. Appl. Polym. Sci.* (2000) 77, p 3015.
238. Shyichuk, A. V.; Stavychna, D. Y.; White, J. R. *Polym. Degrad. Stab.* (2001) 72, p 279.
239. Edge, M., Infrared spectroscopy in analysis of polymer degradation. In *Encycl. Anal. Chem.*, Meyers, R. A., Ed. John Wiley and Sons Ltd.: Chichester, 2000; p 7658.
240. Gugumus, F. *Polym. Degrad. Stab.* (1997) 55, p 21.
241. Nekhoroshev, V. P.; Turov, Y. P.; Nekhorosheva, A. V.; Ogorodnikov, V. D.; Gaevoi, K. N. *Russ. J. Appl. Chem.* (2006) 79, p 833.
242. Costa, L.; Luda, M. P.; Trossarelli, L. *Polym. Degrad. Stab.* (1997) 58, p 41.
243. Andreassen, E., Infrared and Raman spectroscopy of polypropylene. In *Polypropylene: An A-Z reference*, Karger-Kocsis, J., Ed. Kluwer Publishers: Dordrecht, 1999 p320.
244. Rivaton, A.; Gardette, J.-L.; Mailhot, B.; Morlat-Therlas, S. *Macromol. Symp.* (2005) 225, p 129.
245. Gugumus, F. *Polym. Degrad. Stab.* (1999) 66, p 161.
246. Adams, J. H.; Goodrich, J. E. *J. Polym. Sci., Part A1* (1970) 8, p 1269.
247. Piton, M.; Rivaton, A. *Polym. Degr. Stab.* (1996) 53, p 343.
248. Carlsson, D. J.; Brousseau, R.; Zhang, C.; Wiles, D. M. *A.C.S. Symp. Ser.* (1988) 364, p 376.
249. Kolbert, A. C.; Didier, J. G.; Xu, L. *Macromolecules* (1996) 29, p 8591.
250. Jansson, A.; Möller, K.; Gevert, T. *Polym. Degrad. Stab.* (2003) 82, p 37.
251. Miraftab, M.; Horrocks, A. R.; Mwila, J. *Polym. Degrad. Stab.* (2002) 78, p 225.
252. Santos, A. S. F.; Agnelli, J. A. M.; Trevisan, D. W.; Manrich, S. *Polym. Degrad. Stab.* (2002) 77, p 441.
253. Jelinski, L. W.; Dumais, J. J.; Luongo, J. P.; Cholli, A. L. *Macromolecules* (1984) 17, p 1650.
254. Cheng, H. N.; Schilling, F. C.; Bovey, F. A. *Macromolecules* (1976) 9, p 363.
255. Busfield, W. K.; Hanna, J. V. *Polym. J.* (1991) 23, p 1253.
256. Vaillant, D.; Lacoste, J.; Dauphin, G. *Polym. Degrad. Stab.* (1994) 45, p 355.
257. Kolbert, A. C.; Didier, J. G.; Xu, L. *Macromolecules* (1996) 29, p 8591.
258. Olivares, N.; Tiemblo, P.; Gòmez-Elvira, J. M. *Polym. Degrad. Stab.* (1999) 65, p 297.
259. Rosa, D. S.; Sarti, J.; Mei, L. H. I.; Filho, M. M.; Silveira, S. *Polym. Test.* (2000) 19, p 523.
260. Elvira, M.; Tiemblo, P.; Gòmez-Elvira, J. M. *Polym. Degrad. Stab.* (2004) 83, p 509.
261. Camacho, W.; Karlsson, S. *Polym. Degrad. Stab.* (2002) 78, p 385.
262. Chang, T. C.; Yu, P. Y.; Hong, Y. S.; Wu, T. R.; Chiu, Y. S. *Polym. Degrad. Stab.* (2002) 77, p 29.

263. Gröning, M.; Eriksson, H.; Hakkarainen, M.; Albertsson, A.-C. *Polym. Degrad. Stab.* (2006) 9, p 1815.
264. Ahlblad, G.; Gijsman, P.; Terselius, B.; Jansson, A.; Möller, K. *Polym. Degrad. Stab.* (2001) 73, p 15.
265. Monrabal, B., Temperature Rising Elution Fractionation and Crystallisation analysis fractionation. In *Encycl. Anal. Chem.*, Meyers, R. A., Ed. John Wiley & sons LTD: New York, 2000; Vol. 9, pp 8074.
266. Wild, L. *TRIP* (1993) 1, p 50.
267. Nakatani, H.; Matsuoka, H.; Suzuki, S.; Taniike, T.; Boping, L.; Terano, M. *Macromol. Symp.* (2007) 257, p 112.
268. Mierau, U.; Voigt, D.; Böhme, F.; Brauer, E. *J. Appl. Polym. Sci.* (1997) 63, p 283.
269. Monrabal, B. *J. Appl. Polym. Sci.* (1994) 52, p 491.
270. De Goede, S.; Brüll, R.; Pasch, H.; Marshall, N. *Macromol. Symp.* (2003) 193, p 35.
271. De Goede, S. *Novel Analytical approaches for studying Degradation in PP and PP-1-Pentene Copolymers*. University of Stellenbosch, Stellenbosch, 2006.
272. Wheeler, L. M.; Willis, J. N. *Appl. Spectrosc.* (1993) 47, p 1128.
273. Cheung, P.; balke, S. T.; Schunk, T. C.; Mourey, T. H. *J. Appl. Polym. Sci., Appl. Polym. Symp.* (1993) 52, p 105.
274. Dekmezian, A. H.; Morioka, T. *Anal. Chem.* (1989) 61, p 458.
275. Ver Strate, G.; Cozewith, C.; West, R. K.; Davis, W. M.; Capone, G. A. *Macromolecules* (1999) 32, p 3837.
276. Adrian, J.; Esser, E.; Hellmann, G.; Pasch, H. *Polymer* (2000) 41, p 2439.
277. Pasch, H.; Siewing, A.; Heinz, L.-C. *Macromol. Mater. Eng.* (2003) 288, p 771.
278. Kok, S. J.; Wold, C. A.; Hankemeier, T.; Schoenmakers, P. J. *J. Chromatogr. A.* (2003) 1017, p 83.
279. Pasch, H.; Adler, M.; Rittig, F.; Becker, S. *Macromol. Rapid Commun.* (2005) 26, p 438.
280. Kok, S. J.; Hankemeier, T.; Schoenmakers, P. J. *J. Chromatogr. A.* (2005) 1098, p 104.
281. Coulier, L.; Kaal, E.; Hankemeier, T. *J. Chromatogr. A* (2006) 1130, p 34.

Chapter 3

Experimental

This chapter describes the procedures followed during selection of samples, additive compounding, sample preparation and ageing, as well as the analytical instrumentation and conditions used for characterisation purposes.

3.1 Sample selection and preparation

3.1 1 Impact PP Copolymer grades

Two commercial Ziegler-Natta-based impact PP copolymer samples with different ethylene contents were supplied by SASOL Polymers (Secunda, South Africa) as unstabilised reactor grades. The ethylene content, tacticity and molecular weight data of both copolymers are presented in Table 3.1. The two samples are labelled 3V and 4V, respectively.

Table 3.1: Properties of the two impact PP copolymer samples

Sample	[Ethylene] (mole%)	Isotacticity (%mmmm)	$\overline{M_w}$ (g.mol^{-1})	$\overline{M_n}$ (g.mol^{-1})	PDI
3V	10.48	88.82	354 400	114 600	3.18
4V	16.42	83.17	351 900	86 600	4.06

Ethylene content and isotacticity (%mmmm): determined by ^{13}C-NMR

$\overline{M_n}$, $\overline{M_w}$ and PDI: measured by HT-SEC

3.1.2 Compounding

A phosphite processing stabiliser, Irgafos 168, was added to both grades at a concentration of 0.05%, in order to prevent degradation during film extrusion and sample preparation. Processing stabilisers are efficient in preventing degradation during processing procedures, without having any influence on the long-term stability of polyolefin materials, and should therefore not influence long-term stability studies. The impact polypropylene powder and Irgafos 168 were subjected to dry-blending followed by melt-blending at 200ºC on a Brabender PL 2000-6 single-screw extruder equipped with a 19mm diameter screw, length-to-diameter ratio of 25 and screw speeds of 40–100 rpm. The extrudate was cooled and pelletised.

3.1.3 Compression moulding of films

Both thin films (ca. 160 µm) and thicker polymer plaques (ca. 4mm) were prepared by compression moulding at 190ºC. Weights of 1 and 4g were used for preparation of the thin films and plaques, respectively. A typical compression cycle consisted of melting of the pellets for 1.5 min and compression at 10-12 bar for another 1.5 min, with subsequent rapid cooling in an ice/water mixture.

3.2 Degradation

3.2.1 Accelerated oven ageing

Thin films and plaques were degraded thermo-oxidatively at 90ºC and 110 ºC, respectively, in a heat-circulating oven with digital temperature control, supplied by SMC manufacturing (Cape Town, South Africa). The progress of degradation was followed visually (for physical changes) and by means of FTIR spectroscopy (chemical changes) and samples were removed at regular intervals for further analysis. The degradation process was discontinued when samples snapped or flaked on bending.

3.2.2 Homogenisation of degraded films

A number of films were collected at pre-determined time intervals during the degradation process for further analysis by means of various analytical techniques. Since degradation is a spatially heterogeneous process, one would expect to obtain different results when analysing different areas on one polymer film. Reproducibility of results was ensured by homogenisation of films. The homogenisation process was done by shredding the various films into smaller pieces and re-melting them into a single new film for a very brief time. Films removed from the oven at advanced stages of degradation were brittle and shattered easily. After this remoulding process, however, plasticity was restored.

3.2.3 Abrasion of layers form plaques for depth-profile studies

For the purpose of studying the spatial heterogeneity of degradation in the thick polymer plaques, layers were removed in 100 µm increments from the degraded surface into the core, for further analysis. Abrasion of layers was done mechanically by moving a rotational fly cutter over the width of every plaque. The shavings from every layer were collected and stored for further analysis. The machinery was cleaned after each collection to avoid contamination.

3.3 Characterisation

3.3.1 Size Exclusion Chromatography

Size exclusion chromatography (SEC) separates macromolecules according to their hydrodynamic volume[1] which can be related to their molecular weight through calibration of the system with narrow dispersity standards. SEC has become the dominant method for the determination of molecular weight and molecular weight distribution (MWD) of synthetic polymers. The stationary phase consists of a swollen gel with a defined pore size distribution. Depending on the size or hydrodynamic volume of

macromolecules, they will be able to access a certain fraction of the pores, thereby affecting their retention time within the column[2]. Polyolefins with high tacticity and copolymers of propylene and ethylene and/or higher α-olefins containing long isotactic PP sequences, can only be dissolved under conditions which result in complete melting of crystalline domains. Therefore, SEC of PP and crystalline copolymers of PP is carried out at elevated temperatures by means of 'high temperature SEC' (HT-SEC)[1].

Molecular weight measurements (i.e., average molecular weight, molecular weight distributions) were performed on a Polymer Laboratories PL 220 high-temperature chromatograph (Polymer Laboratories, Varian Inc., Church Stretton, Shropshire, England). The temperature of the injection block and column compartment was set to 150ºC and a flow rate of 1ml.min^{-1} was maintained. The chromatographic system was equipped with three 300 X 7.5mm PLgel Olexis columns (Polymer Laboratories, Varian Inc., Church Stretton, Shropshire, England) and a differential refractive index detector was used. Polymer samples were dissolved in 1,2,4-trichlorobenzene (TCB) for two hours at a concentration of 1mg/ml and 200 µl of each sample was injected. Butylhydroxytoluene (BHT) (Ciba®, Switzerland) was used as antioxidant to prevent further oxidation of samples during SEC analysis. Narrowly distributed polystyrene standards (Polymer Standards Service GmbH, Mainz, Germany) were used for calibration purposes. The WinGPC software (Polymer Standards Service GmbH, Mainz, Germany) was used for data acquisition and processing.

3.3.2 Fourier-Transform Infrared Spectroscopy

Transmission FTIR spectra were recorded on a Perkin Elmer Paragon 1000 FTIR spectrometer (Perkin Elmer, Waltham, USA). Spectra were recorded at a resolution of 2 cm^{-1}, 64 scans were accumulated for each spectrum and automatic background subtraction was performed. Spectrum V2.0 software (Perkin Elmer) was used for data acquisition and processing.

Attenuated total reflectance (ATR) measurements were performed on a Nicolet Nexus 670 (Thermo Electron, Waltham, USA) FTIR spectrometer with SensIR ATR attachment equipped with a diamond reflective crystal. All measurements were performed at an incidence angle of 45º. Spectra (from 4000 to 650cm^{-1}) were obtained from collection of 64 scans at a resolution of 2 cm^{-1}.

3.3.3 Differential Scanning Calorimetry

Melting and crystallisation behaviour was determined using a Mettler 822 DSC instrument (Mettler Toledo, Switzerland), calibrated with indium metal according to standard procedures. The thermal history of samples was removed by a first heating cycle from 25ºC to 200ºC at a heating rate of 10ºC.min^{-1}, after which the temperature was kept isothermally for 3 minutes. Thereafter, the sample was cooled at 10ºC.min^{-1} to 25ºC, kept constant for another 3 minutes, and subsequently heated to 200ºC again. Data obtained during the second heating cycle were used for all thermal analysis

calculations. In all DSC plots presented the upwards curve is associated with exothermic transitions while downwards curves illustrate endothermic thermal transitions. All DSC measurements were conducted in a nitrogen atmosphere at a purge gas flow rate of 20ml.min^{-1}.

3.3.4 Nuclear Magnetic Resonance Spectroscopy

Nuclear magnetic resonance (NMR) has become a valuable and indispensable analytical tool among polymer chemists, especially in the field of copolymers, where the determination of sequence distribution is frequently a pre-requisite in structural characterisation.

High resolution solution ^{13}C-NMR spectra were obtained at 120ºC on a 600 MHz Varian^{unity} INOVA NMR spectrometer operating at 125 MHz for carbon. A 5mm PFG switchable broadband probe was used. Samples were prepared to a concentration of 6 wt% in deuterated tetrachloroethane (d-TCE), (Aldrich, South Africa). Spectra were recorded with a 90º flip angle of approximately 6 µs, with continuous proton decoupling, an acquisition time of 1.8 s and a pulse delay time of 15 s. Under these conditions, spectra were found to be 99% quantitative, provided that only carbon atoms with relaxation delays ($T1$) of less than 3s are taken into account[3].

3.3.5 Temperature Rising Elution Fractionation

Temperature rising elution fractionation (TREF) fractionates semi-crystalline polymers according to their crystallisability or solubility-temperature relationship, which is a function of their molecular structure [4]. Molecules of different structures will each have a distinct crystallinity and dissimilar dissolution temperatures, thereby allowing their separation by TREF. Commercially, there exist two kinds of experimental TREF apparata, analytical and preparative TREF[4-6]. Analytical TREF is generally an automated process, with the separation/fractionation setup directly linked to other analytical instruments such as FTIR or SEC, allowing on-line structural characterisation of polymer fractions. Preparative TREF allows for the collection of larger amounts of fractions which can subsequently be analysed off-line also by means of NMR and/or DSC. Although this is a time-consuming process, it is usually the method of choice when fractionating polypropylene.

During this study an in-house built preparative-TREF setup, utilising sea sand as support medium, was used[7]. The TREF experiment consists of two steps or cycles[8]. The first involves the controlled, slow crystallisation of polymer onto a support (eliminating the previous crystallisation history of the polymer), whereby molecules of different crystallisabilities are packed onto the support particles in a layered structure. It is of the utmost importance that a slow cooling rate is applied during the crystallisation step, since fast cooling may lead to secondary effects such as co-crystallisation of fractions with different crystallisability, and a molecular weight influence on the crystallisation process[4, 5]. Material with the highest crystallisability will crystallise out of solution first at high temperature and form the first layer on the support, followed by layers of continuously decreasing crystallisability. In the subsequent

elution step, the polymer/support mixture is subjected to increasing temperatures in the presence of a suitable solvent, which dissolves the layers off the support in a reversed order to that followed during crystallisation, i.e., least crystallisable material elutes first, followed by fractions of increasing crystallisability. The two steps of a typical TREF experiment are illustrated in Scheme 3.1.

During the crystallisation step 3g of polymer and ca. 2 wt% Irganox 1010 (Ciba® Speciality chemicals, Switzerland) were dissolved in 300 ml xylene at 130ºC in a glass reactor. After complete dissolution, the reactor was transferred to an oil-bath (pre-heated to 130ºC) and pre-heated sea sand (white quartz, Aldrich, South Africa) was added to the solution. The reactor containing the mixture of sand and dissolved polymer was cooled down to room temperature at a rate of 1ºC/hour, to allow for very slow, controlled crystallisation of layers onto the support material. At the end of this stage the polymer exists as segregated layers of different composition and crystallinity[5, 6], which can be separated and collected during the subsequent elution step.

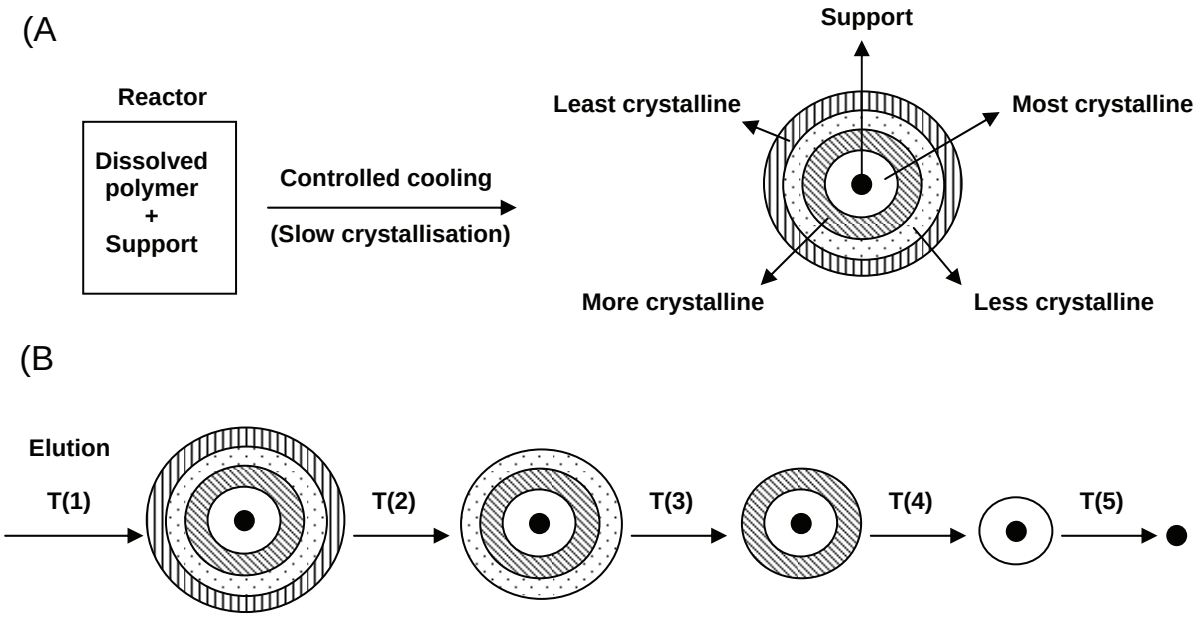

Scheme 3.1: Schematic separation mechanism of TREF where (A) represents the crystallisation and (B) the elution step.

The polymer/sand mixture from the previous step was packed into a stainless steel column and transferred into a modified GC oven. Pre-heated xylene was pumped through the column and the temperature of the oven was increased at a steady rate. As the temperature was increased, fractions of increasing crystallisability became soluble, and were collected at pre-determined temperature intervals (30, 60, 80, 90, 100, 110, 120ºC). Xylene was evaporated and fractions were recovered by precipitation in acetone. Finally, all fractions were dried until no further weight loss was observed and prepared for subsequent analysis by complimentary analytical techniques.

3.3.6 Crystallisation Analysis Fractionation

Crystallisation analysis fractionation (CRYSTAF) is another useful technique for fractionating semi-crystalline polymers, sharing the same fundamentals with TREF on separation according to crystallisability. The process is similar to classical stepwise fractionation by precipitation, the major difference being that the concentration of the polymer still in solution is measured during crystallisation by temperature reduction, rather than the amount of polymer precipitated[6, 8]. It differs from TREF in the sense that, whereas two temperature cycles are applied during a TREF experiment (crystallisation and elution cycles), CRYSTAF is a continuous process during which information is extracted directly during the crystallisation process by monitoring the concentration depression during cooling[8]. CRYSTAF also does not utilise any packing/support material for the crystallisation step and no fraction collection is done for the purpose of further analysis (i.e., not preparative). The CRYSTAF experiment is illustrated in Scheme 3.2.

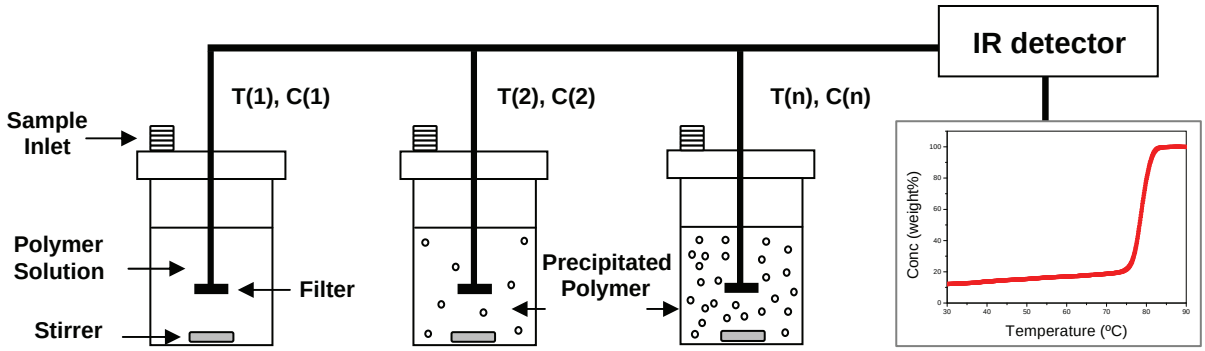

Scheme 3.2: Schematic representation of the CRYSTAF process

CRYSTAF experiments were performed on a commercial CRYSTAF apparatus Model 200 (PolymerChar, Valencia, Spain). For each sample, a weight of 20mg was dissolved in 40 ml 1,2-*ortho*-dichlorobenzene (*o*-DCB). Crystallisation was carried out under agitation in stainless steel reactors, equipped with automatic stirring and filtration devices. After dissolution, the temperature was decreased from 100ºC to approximately 30ºC at a rate of 0.1ºC/min. Fractions were taken automatically and the concentration of the solution was determined by an infrared detector, using 3.5 µm as the chosen wavelength.

3.3.7 SEC-FTIR using the LC-Transform® interface

Size Exclusion Chromatography coupled to infrared spectroscopy (SEC-FTIR) is a valuable technique for studying the chemical heterogeneity of polymers, especially copolymers where each monomer has

its own characteristic groups absorbing in the infrared spectrum, and the chemical composition or heterogeneity can be determined by the IR absorption band ratio of the functional groups of the two monomers[9-13]. This hyphenated technique combines the molecular weight separation capability of SEC with the power of infrared spectroscopy to identify components on the basis of their unique chemical fingerprint. Two experimental approaches have been employed for coupling the two techniques[14], (a) flow cells and (b) solvent evaporative interfaces. Flow-cells provide convenient on-line coupling of the two techniques. The technique is, however, complicated by the presence of the solvent, since most organic solvents absorb strongly in the IR region, which might overlap with signals from the polymer molecules in question. Solvent evaporative interfaces are therefore favoured in this regard, as long as samples are non-volatile and the solvent does not contain any buffer that could precipitate with the sample. The commercial evaporative interface most often employed, is the LC-Transform® device manufactured by Lab Connections (Lab Connections, Carrboro, USA). The principle upon which the LC-Transform® interface operates is illustrated in Scheme 3.3.

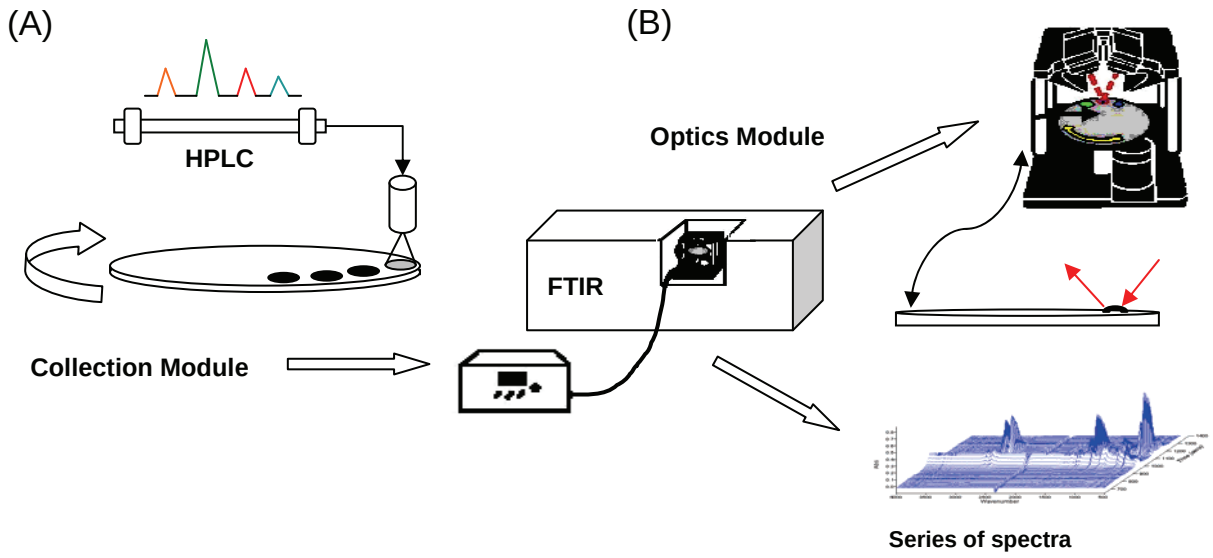

Scheme 3.3: LC-FTIR setup illustrating the collection and optics module

The first step (A) of the SEC-FTIR experiment is the chromatographic separation of molecules according to their hydrodynamic volume by SEC. At the column exit, the SEC eluent containing separated solutes are directed towards the LC-Transform® unit, where it flows into the sealed deposition chamber that is kept under vacuum. Here the eluent flows through a heated nebuliser nozzle which directs the eluent onto a rotating Germanium disc placed on a heated stage for assisted evaporation of the solvent. The species separated during SEC are sprayed continuously onto the perimeter of the Germanium collection disc and subsequently transferred to the optics module (B) of the interface which fits into the sample compartment of the FTIR spectrometer. During the FTIR analysis stage, specialised software is used to rotate the disc at the same speed used during deposition, while recording the infrared spectrum at every spot along the perimeter of the disc.

Processing of the data allows the construction of Gram-Schmidt plots and chemigrams which provide a wealth of information with regards to chemical composition of the material analysed.

A prototype high-temperature gradient HPLC system PL XT-220 (Polymer Laboratories, Varian Inc, Church Stretton, Shropshire, England) was used for the size exclusion chromatography part of the experiment. Dissolution and automated sample injection was performed using a robotic sample handling system (PL-XTR, Polymer Laboratories). The temperature of the sample block, injection needle, injection port and the transfer line between the auto-sampler and column compartment was set at 140ºC. Four PL mixed A columns, column size 250 X 8.0 mm internal diameter, containing packing material particles with an average diameter of 20 µm (Polymer Laboratories) were chosen and TCB was used as mobile phase at a flow rate of 1ml.min^{-1}. Samples were dissolved at 140ºC in TCB at a concentration of 0.5–1.0mg/ml and 50µl of each sample was injected. The column outlet was connected to a solvent evaporation FTIR interface, the LC-Transform® (Series 300, Lab Connections, Carrboro, USA). The stage and nozzle temperatures were set to 160 and 150ºC, respectively, while the transfer line between the SEC column outlet and LC-Transform nebulisation compartment was set to 150ºC. The nebuliser nozzle was cooled by a constant flow of compressed air to avoid overheating. Germanium collection discs were rotated at a speed of 10º.min^{-1} inside the compartment and subsequent FTIR analysis of the deposited trace was performed on a Nicolet Protegè (Thermo Electron, Waltham, USA). Analysis of SEC-FTIR results was performed by means of the Omnic software package supplied by Thermo Electron.

3.3.8 High-Temperature Gradient Liquid Chromatography

The same high-temperature gradient HPLC system described in Section 3.3.7 was used for the separation of carbonyl-containing degradation products from non-degraded material. A Perfectsil 300 Å column with dimensions 250 X 4.6mm internal diameter and particle diameter of 5 µm (MZ Analysentechnik, Mainz, Germany) was used as stationary phase. Decalin and cyclohexanone were used as mobile phase solvents (Merck, Darmstadt, Germany) in the following gradient profile:

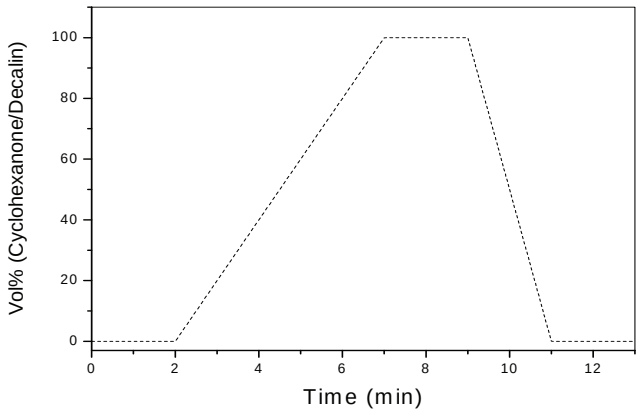

Scheme 3.4: Representation of the cyclohexanone/decalin solvent gradient profile used for HT-gradient HPLC separation.

Samples were dissolved in decalin for 2 hours at a concentration of 1–1.2 mg.ml^{-1} at 140ºC prior to injection. A volume of 50µl was injected for each sample and the column outlet was connected to an evaporative light scattering detector (ELSD), model PL-ELS 1000, supplied by Lab Connections, Carrboro, NC. An ELSD nebuliser temperature of 160ºC and evaporation temperature of 270ºC was employed together with an air flow of 1.5 ml.min^{-1}.

3.3.9 Fourier Transform Infrared microspectroscopy

All FTIR-µS measurements were performed on a Thermo Nicolet Continuµm infrared microscope (Thermo Electron, Waltham, USA) equipped with a cryogenically cooled MCT detector (Mercury cadmium telluride, narrow band mid-IR: 4000–650 cm^{-1}). The microscope was coupled to a Nicolet-Nexus 680 FTIR spectrometer as beam source. The aperture was set to 100 X 100 µm and the step width of the line scans was 50 µm (i.e., a scan is performed at intervals of 50 µm along the line scanned).

Samples were prepared by taking thin slices across the width of degraded plaques (200 ± 5 µm) using a Reichert-Jung rotary microtome. The thickness was measured by means of a micrometer gauge. Each cross-section was clamped in a micro-vice sample holder which fits into the X-Y-movable stage, allowing for precise control over the position of a sample during scanning. All measurements were performed in transition mode at a resolution of 4 cm^{-1} and 100 scans were collected at each point along a line. Data accumulation and processing was done by means of the OMNIC Continuµm software (Thermo Electron, Waltham, USA).

3.4 References

1. Lederer, K., Size exclusion chromatography. In *Polypropylene: An A-Z reference*, Karger-Kocsis, J., Ed. Kluwer Publishers: Dordrecht, 1999; p 736.
2. Pasch, H., Thermodynamics of polymer chromatography. In *HPLC of polymers*, Pasch, H.; Trathnigg, B., Eds. Springer: Berlin, 1998; p 18.
3. Assumption, H. J.; Vermeulen, J. P.; Jarrett, W. L.; Mathias, L. J.; van Reenen, A. J. *Polymer* (2006) 47, p 67.
4. Soares, J. B. P.; Hamielec, A. E. *Polymer* (1995) 36, p 1639.
5. Xu, J.; Feng, L. *Eur. Polym. J.* (2000) 36, p 867.
6. Monrabal, B., Temperature rising elution fractionation and crystallisation analysis fractionation. In *Encycl. Anal. Chem.*, Meyers, R. A., Ed. John Wiley & sons LTD: New York, 2000; Vol. 9, p 8074.
7. Rabie, A. J. *Blends with low density polyethylene (LDPE) and plastomers*. University of Stellenbosch, Stellenbosch, 2004.
8. Monrabal, B. *J. Appl. Pol. Sci.* (1994) 52, p 491.
9. Adrian, J.; Esser, E.; Hellmann, G.; Pasch, H. *Polymer* (2000) 41, p 2439.
10. Pasch, H.; Siewing, A.; Heinz, L.-C. *Macromol. Mater. Eng.* (2003) 288, p 771.
11. Pasch, H.; Adler, M.; Rittig, F.; Becker, S. *Macromol. Rapid Commun.* (2005) 26, p 438.
12. Kok, S. J.; Wold, C. A.; Hankemeier, T.; Schoenmakers, P. J. *J. Chromatogr. A.* (2003) 1017, p 83.

13. Kok, S. J.; Hankemeier, T.; Schoenmakers, P. J. *J. Chromatogr. A.* (2005) 1098, p 104.
14. Somsen, G. W.; Gooijer, C.; Brinkman, U. A. T. *J. Chromatogr. A.* (1999) 856, p 213.

Chapter 4

Results and Discussion

This chapter describes the development of a multi-component analysis approach, combining fractionation and hyphenated techniques for studying the degradation of impact polypropylene copolymers. The degradation behaviour of two copolymers with different ethylene contents is compared and finally, the spatial heterogeneity of the degradation process is studied in both copolymers. All results are accompanied by a discussion of the trends observed.

Introduction

Polyolefin degradation has been a subject of interest since the 1940's when some preliminary investigations were performed by Bolland and Gee[1]. It has, however, become evident over the past few years that conventional analytical techniques are insufficient for assessing degradation in heterogeneous polymers. The need for understanding the effect of degradation on polymer microstructure has lead to new developments in this field, where techniques such as CRYSTAF, TREF and LC-FTIR have recently provided valuable information on the degradation of polyolefins. Whereas conventional techniques such as SEC, FTIR and DSC generally only supply average values of the specific property measured for the bulk material, e.g., average molecular weight, chemical composition and thermal behaviour, these innovative techniques provide the capability to study degradation as a function of the heterogeneity of the sample. Such techniques are of extreme importance when studying samples such as impact PP copolymers, which are known to be highly complex, heterogeneous materials. In this chapter fractionation (TREF and CRYSTAF) and hyphenated techniques (SEC-FTIR) will be used in combination to assess the heterogeneity of degradation within impact PP copolymers. TREF fractionation will also be coupled to conventional techniques (SEC, FTIR, DSC) for studying the degradation behaviour of the individual, more homogeneous morphologies comprising these copolymers.

This chapter will be divided into three major sections according to the three major objectives of this study. The first section contains results obtained by the combination of various techniques into a multi-dimensional analysis procedure developed for studying the heterogeneity of the degradation within a low ethylene content impact polypropylene copolymer. In the second part it is demonstrated how the techniques employed in the first section can be used to highlight the differences in degradation behaviour between two impact PP copolymers based on their primary structure. In the third section the spatial heterogeneity of the degradation in thicker samples of both impact polypropylene grades is studied by means of FTIR-microspectroscopy and these results are compared to those obtained by a conventional technique consisting of layer-by-layer milling followed by ATR-FTIR, SEC and CRYSTAF analysis of the layers. This section illustrates the influence of the morphology of these copolymers and its effect on oxygen diffusion from the surface into the core of thicker samples during degradation. This extends the results of the previous sections, by also taking into account diffusion effects resulting from sample morphology.

4.1 Development of a multi-dimensional analysis approach for studying the degradation behaviour of an impact PP copolymer

Although it is the aim of this study to develop new analytical methods that supply more information on the degradation process than conventional techniques, FTIR and SEC are two conventional techniques still employed for monitoring the progress of polyolefin degradation[2, 3]. Results obtained by these

conventional techniques are presented first before a discussion on novel approaches is given. All results in Section 4.1 were obtained from analyses of sample 3V, which is the copolymer sample of lower ethylene content (10.48%) and higher isotacticity (88.82%), as summarised in Table 3.1.

4.1.1 FTIR analysis of undegraded and degraded samples of copolymer 3V

Transmission FTIR spectroscopy was used to monitor the progress of degradation during accelerated oven ageing of copolymer 3V. FTIR is a useful technique for identification and quantification of degradation products, since oxidation reactions lead to the formation of new functional groups not present within the original, undegraded material. Figure 4.1 illustrates the changes in the FTIR spectrum occurring upon degradation in copolymer 3V. All spectra were normalised to the CH_3 symmetric bending (umbrella) band[4, 5] at 1377 cm^{-1}. The most significant oxygenated products generated by degradation, namely carbonyls and hydroperoxides, are clearly observed in the wavelength ranges 1550–1850 cm^{-1} and 3200–3700 cm^{-1}, respectively. In Figure 4.1 the intensity of these bands are seen to increase with ongoing degradation times, as the concentration of degradation products increases. The broadness of these bands is ascribed to the overlapping absorption of a number of different carbonyl and hydroperoxide-containing products. The hydroperoxide band centred around 3400 cm^{-1} is inherent to the stretching vibrations of both associated (3370 cm^{-1}) and free hydroperoxides (3560 cm^{-1})[6]. Derivatisation reactions have been performed to resolve the overlapping stretching vibrations of various species in the carbonyl region of the FTIR spectrum[7, 8].

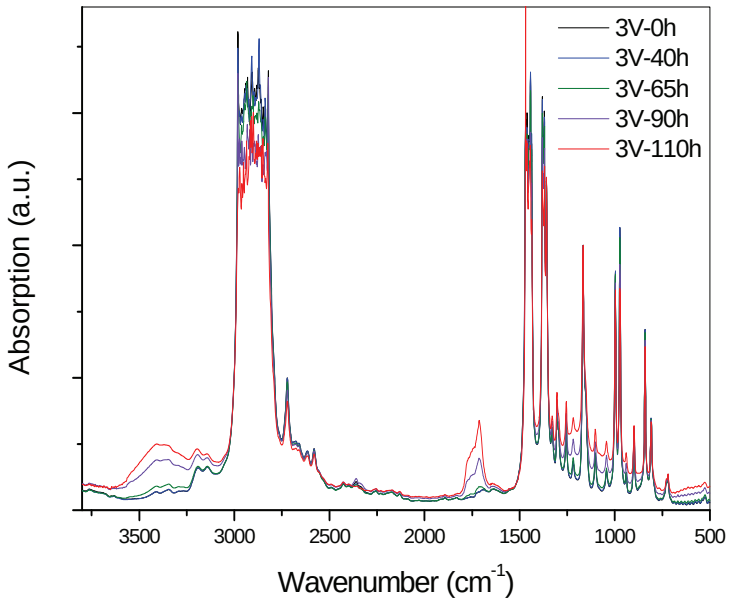

Figure 4.1: Changes in the FTIR spectra of sample 3V during thermo-oxidative degradation.

Carboxylic acids (1705–1710 cm^{-1}), ketones (1715 cm^{-1}), esters (1740 cm^{-1}), aldehydes (1730 cm^{-1}) and γ-lactones (1770–1780 cm^{-1}) have previously been reported to be the major degradation functionalities within this region[9-12]. In Figure 4.2 the FTIR spectral changes in the carbonyl and

hydroperoxide regions are illustrated for different time intervals and the above-mentioned functionalities are clearly observed. The band around 1720cm^{-1}, corresponding to the ketone functionality, is a direct product of β-scission and is the most significant primary degradation product formed during the early stages of degradation within PP. With ongoing degradation times, the γ-lactone band at 1785cm^{-1} becomes most significant with simultaneous increases in all other bands within the carbonyl region as well. This result is consistent with other studies on the thermo-oxidative degradation of PP homopolymer, where the formation of ketones and γ-lactones followed the same order[10, 13]. The presence of a significant γ-lactone band at 1785cm^{-1} is characteristic of the thermo-oxidative degradation of polypropylene homopolymer. Although this band does appear during the photo-degradation of polyethylene[10, 14], it is negligible in polyethylene and EP elastomers subjected to thermo-oxidative degradation[10]. There exist some similarities between the degradation behaviour of ethylene-propylene copolymers and polypropylene homopolymer[15, 16]. This is to be expected, since this particular impact PP copolymer sample consists mainly of PP and it has been reported that, in samples containing ≥ 85% propylene, the degradation is dominated by this repeat unit[16, 17].

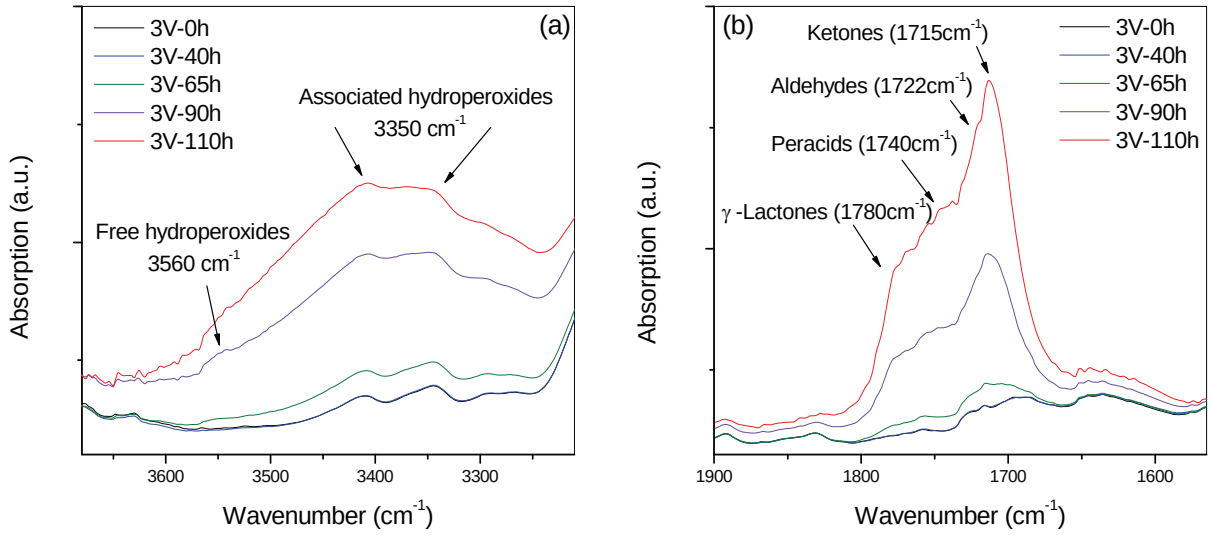

Figure 4.2: An enlargement of the (a) hydroperoxide and (b) carbonyl areas of the FTIR spectrum showing the main degradation products formed.

The degree of oxidation at different times is quantified by the carbonyl index, defined as the ratio between the integrated band absorbance (area or height) of the carbonyl band and that of a reference band, in order to compensate for film thickness variations[18]. The 840cm^{-1} was chosen as the reference band[19] and the increase in the carbonyl index with ongoing degradation time is illustrated in Figure 4.3.

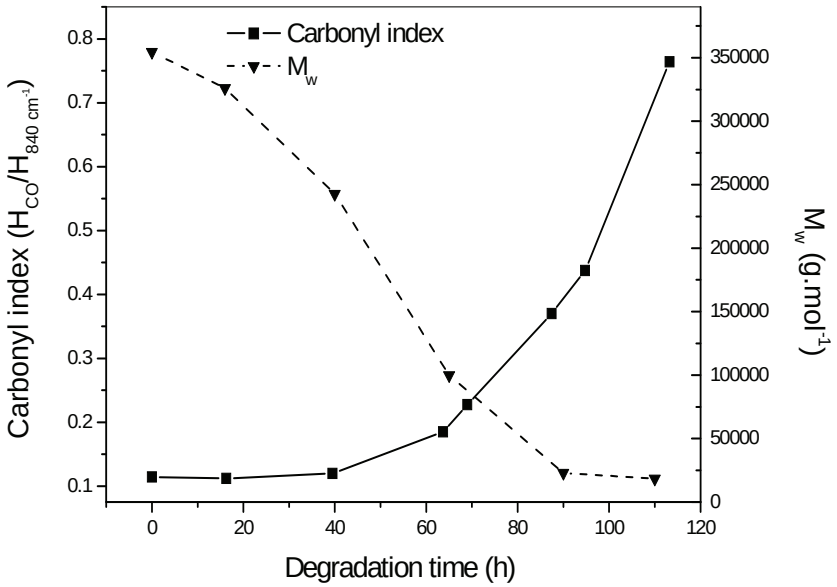

Figure 4.3: Carbonyl content and weight-average molecular weight ($\overline{M}_w$) changes of sample 3V as a function of degradation time.

An induction stage resembling oxygen uptake and diffusion into the polymer is clearly visible until approximately 40 hours, after which there is a steady increase in the carbonyl index caused by the autocatalytic radical-initiated degradation process found in polyolefins. Besides the incorporation of carbonyl functionalities, the molecular weight of polyolefins is also known to be affected by scission reactions during oxidation. The decrease in the weight-average molecular weight ($\overline{M}_w$) and the increase in carbonyl concentration is seen to occur simultaneously, although a decrease in $\overline{M}_w$ is already evident at very short degradation times, even when no carbonyl groups can be detected by FTIR spectroscopy. The change in the molecular weight distribution curves of sample 3V observed upon degradation, will be presented next.

4.1.2 SEC analysis of undegraded and degraded samples of copolymer 3V

Polymer degradation is always accompanied by changes in molecular weight averages and molecular weight distributions[20]. Depending on the nature of the polymer and the type of radical reactions present, either chain branching or chain scission reactions may prevail. In the case of polypropylene, tertiary C-H bonds are preferentially cleaved during the initiation of oxidation and the autocatalytic sequence of reactions leads to chain scission events and polydispersity reduction rather than crosslinking[21]. Figure 4.3 demonstrates the effect of degradation on the molecular weight and carbonyl concentration in copolymer 3V. It is seen that, even when a low concentration of carbonyl species is detected by FTIR, there already seems to be a considerable decrease in the weight-average molecular weight ($\overline{M}_w$) from approximately 354 000 g.mol^{-1} in the undegraded sample to 326 000 and 243 000 g.mol^{-1} after degradation times of 16 and 40 hours, respectively. FTIR is known to detect

carbonyl species immediately after the induction period, although degradation is seen to occur at times shorter than this, since the decrease in molecular weight is undoubtedly related to irreversible chemical changes within the polymer. The molecular weight distribution curves for the various degradation times are illustrated in Figure 4.4.

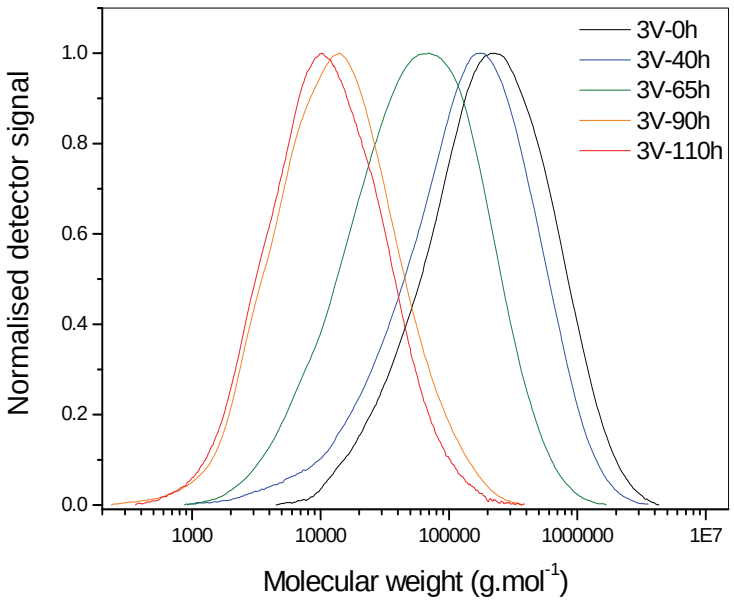

Figure 4.4: Changes in the SEC curves of sample 3V as a function of degradation time.

With ongoing degradation time, molecular weight curves show a general shift towards lower values, indicating that chain scission occurs predominantly in this low ethylene content impact PP copolymer.

The change in the number-average ($\overline{M}_n$) and weight-average ($\overline{M}_w$) molecular weight as well as the polydispersity of sample 3V is illustrated as a function of degradation time in Table 4.1.

Table 4.1: Average molecular weight and polydispersity values for sample 3V as a function of degradation time

Sample	Degradation time (h)	$\overline{M}_n$ (g.mol^{-1})	$\overline{M}_w$ (g.mol^{-1})	PDI
3V-0h	0	111 500	354 400	3.18
3V-40h	40	49 000	242 800	4.96
3V-65h	65	25 400	100 000	3.94
3V-90h	90	6 900	23 000	3.33
3V-110h	110	6 600	18 400	2.79

Although some information on the chemical composition and molecular weight changes brought about by degradation could be obtained for this copolymer, it is clear that new analytical approaches are needed to obtain more detailed information on the degradation process. Since the amount of ethylene within these copolymers is so small, techniques such as FTIR and SEC reflect only the degradation

behaviour of the PP phase. These techniques supply only average chemical composition and molecular weight information for the bulk polymer, without any indication of the degradation of the other components present in smaller amounts within this heterogeneous system.

One approach for obtaining information on the distribution of degradation products across the molecular weight distribution of a polymer, is through hyphenation of SEC and FTIR spectroscopy[22]. The solvent evaporation LC-Transform® interface for semi-online coupling of SEC and FTIR was used to obtain infrared absorption intensities as a function of elution volume. Visually, SEC-FTIR results differ slightly from that obtained by normal SEC equipped with a differential refractive index detector, although the shapes of the curves are comparable. The Gram-Schmidt plot obtained from SEC-FTIR analysis can be defined as a graphical representation of the total infrared absorption over the entire elution volume of the polymer, which can be correlated with its molecular weight distribution. Each point along the Gram-Schmidt constitutes a complete FTIR spectrum and thus, the chemical composition can be determined at every point across the molecular weight or elution volume plot[23]. It is, therefore, possible to obtain the total infrared absorption of specific functional groups as a function of elution volume, which allows for the determination of degradation products[22] or comonomer concentrations[23, 24] across the molecular weight distribution of a polymer.

4.1.3 Fractionation and hyphenated techniques for studying degradation in impact PP copolymers

4.1.3.1 SEC-FTIR results for undegraded and degraded 3V samples

Figures 4.5 (a)–(d) illustrate the SEC-FTIR results obtained for four 3V samples degraded for 0, 60, 90 and 110 hours, respectively. Names of samples are given as 3V, followed by the degradation time in hours, and the extension _GS or _CO/CH to indicate the Gram-Schmidt curve or carbonyl profile, respectively. The sample name 3V-110h_GS therefore signifies that this is the Gram-Schmidt profile of the 3V copolymer sample degraded for 110 hours, whereas the sample name 3V-0h_CO/CH describes the carbonyl profile within the 3V sample degraded for 0 hours, i.e., the undegraded 3V copolymer. Upon degradation a shift in the Gram-Schmidt curve towards larger elution volumes (i.e., lower molecular weight) is observed. This is in agreement with the shift in the SEC results obtained in Section 4.1.2. As the length of long chains decreases due to chain scission, pores from which large, undegraded molecules have been excluded, have now become accessible to them, leading to longer retention times within the porous column packing. For the purpose of determining the distribution of carbonyl-containing degradation products across the molecular weight distribution, the area ratio of the entire carbonyl band (1804–1580 cm^{-1}) with respect to the CH band at 3005–2787cm^{-1} was constructed over the elution volume curve. In Figure 4.5 it can be seen how the carbonyl concentration or index increases from 60 to 110 hours across the Gram-Schmidt curve and reaches a maximum at the low molecular weight side.

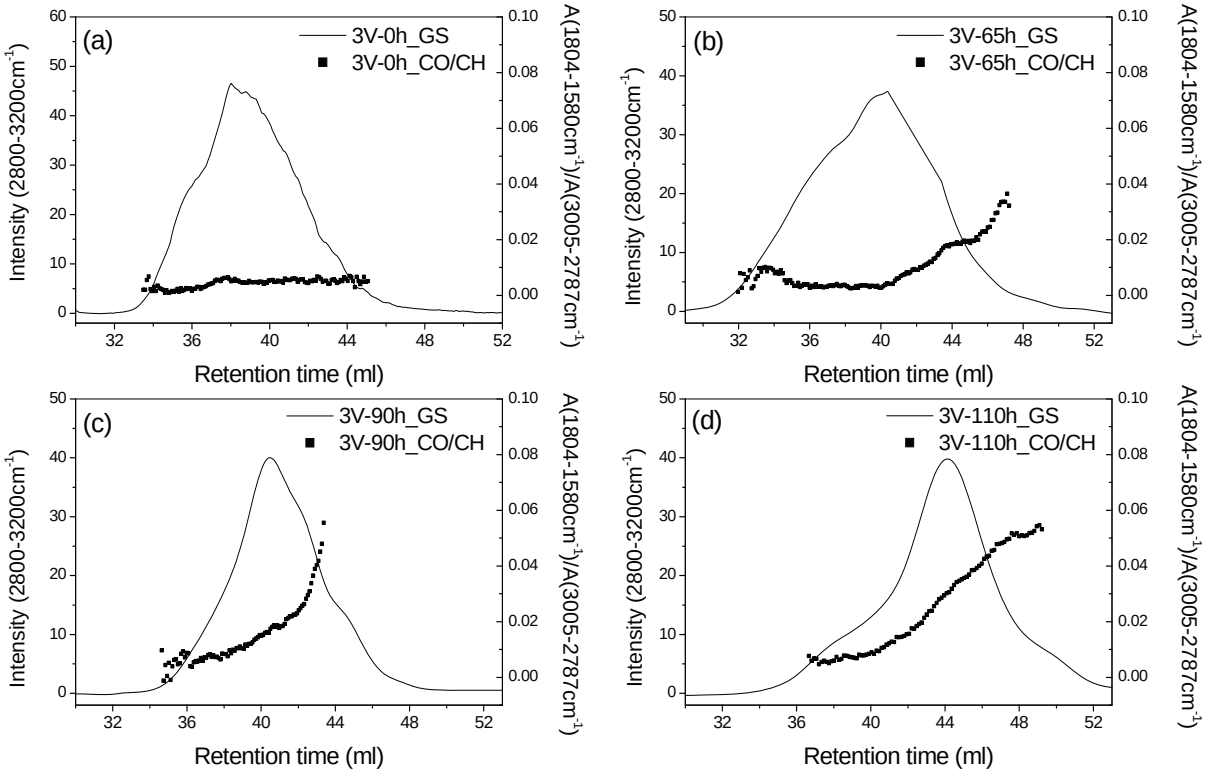

Figure 4.5: SEC-FTIR results for sample 3V degraded for (a) 0, (b) 60, (c) 90 and (d) 110 hours.

The low molecular weight region of the copolymer is therefore rich in carbonyl-containing degradation products, which was also found for a PP homopolymer and PP-1-pentene copolymers upon thermo-oxidative degradation[25]. This technique is therefore valuable in providing information on the distribution of degradation products and confirms the heterogeneity of the degradation process which is not possible with conventional techniques.

Apart from changes in molecular weight and chemical composition, degradation is also known to affect the crystallinity or crystallisability of polymer molecules. These changes in crystallinity and thermal behaviour of degraded polymers are usually studied by DSC[26-30], where the changes in peak melting temperatures and melt enthalpy values can supply valuable information on the effect of degradation on crystallinity. Another technique that has the ability to provide information on the influence of degradation on crystallisability, is CRYSTAF. Although this technique is well-established for studying the crystallisability of semi-crystalline polyolefins, it has only recently found application in the field of polymer degradation[22]. In principle this technique is a fractionation process facilitated by step-by-step precipitation of a semi-crystalline polymer from solution, while monitoring the concentration of polymer in solution[31]. Since crystallisability can also be studied by TREF, which operates on a slightly different principle to CRYSTAF, the effect of degradation on crystallisability as studied by this stepwise crystallisation and subsequent dissolution process will also be studied.

4.1.3.2 CRYSTAF results for the undegraded and degraded 3V samples

Figure 4.6 demonstrates the changes in crystallisation behaviour of impact copolymer 3V as a function of degradation time. The curve labelled 3V-0h, which represents the undegraded 3V copolymer, shows characteristic crystallisation behaviour expected from a semi-crystalline material, with a relatively sharp crystallisation peak centred around 83ºC and a small soluble fraction. The curve of the same 3V copolymer degraded for 90 hours (3V-90h), resembles a broader crystallisation peak commencing at a considerably lower crystallisation temperature than the undegraded sample, together with a significant increase in the soluble fraction. The effect of degradation on crystallisability previously reported for a polypropylene homopolymer and polypropylene-1-pentene copolymer[25], were also visible in this case. The main crystallisation peak is seen to shift towards lower crystallisation temperatures upon degradation, accompanied by a decrease in the peak intensity, indicating a lower concentration of material crystallising out at the maximum crystallisation temperature. An increase in the soluble fraction is also observed, which indicates that oxidation alters the chemical composition of some chains to such an extent that they are no longer crystallisable at higher temperatures.

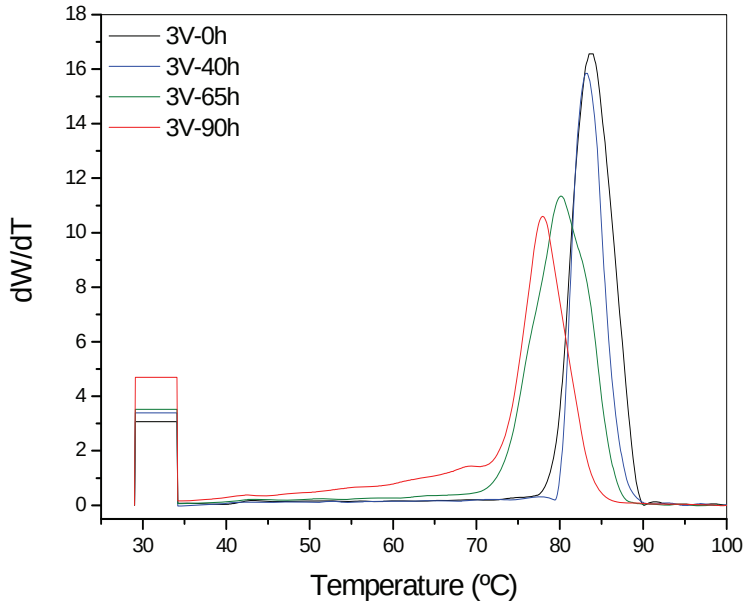

Figure 4.6: Changes in the CRYSTAF results for sample 3V with degradation time.

The crystallisation curve of the sample degraded for 40 hours shows a narrowing of the original sample (3V-0h) on the higher crystallinity side, which might indicate the preferential degradation of higher crystallinity material. Data on the peak crystallisation temperatures and the percentage soluble material in each sample is given in Table 4.2. The peak crystallisation temperature of the sample degraded for 110 hours, is also reported, although its crystallisation was measured over a different temperature range, as can be seen in Figure A1 of Appendix A. Full width at half maximum (FWHM) values supplied here are used as an indication of the amount of peak broadening or narrowing

occurring in CRYSTAF peaks upon degradation. These values were determined by fitting a simple Gaussian distribution to all CRYSTAF curves.

Table 4.2: Peak crystallisation temperatures and soluble fraction percentages of undegraded and degraded samples of 3V determined by CRYSTAF

Sample	T_c (peak maximum) (°C)	Soluble fraction (Wt %)	FWHM
3V-0h	84.0	12.8	4.69
3V-40h	83.2	14.2	3.44
3V-65h	80.2	14.7	6.68
3V-90h	77.9	19.9	5.12
3V-110h	76.2	n.d.	n.d.

n.d. not determined

The oxidation process is known to lead to several reactions in the polymer, including chain scission, crosslinking and insertion of chemical groups such as carbonyl functionalities and hydroperoxides into polymer chains, both of which affect the crystallinity of the polymer[28, 29, 32]. It has been reported that main chain scission leads to the formation of in-chain CO functionalities such as ketones in polypropylene[33], which are partially included in the lamella crystal upon re-crystallisation. These inclusions lead to disruption of the lamellae, causing amongst other things, a broadening of the crystalline distribution, as indicated by broadening of crystallisation peaks. Insertion of chemical groups such as carbonyls and hydroperoxides also disrupts the molecular regularity, thereby limiting secondary crystallisation. It is known that the disruption of the regularity of PP leads to a significant reduction in crystallinity. This effect is illustrated by the decrease in crystallisation peak intensity and temperature, as well as the increase in the soluble fraction observed in Figure 4.6. In Figure 4.3 it is clear that there is an increase in the carbonyl index (i.e., concentration of carbonyl groups) and a decrease in molecular weight with ongoing degradation times. CRYSTAF analysis has, therefore, indicated that a major portion of these carbonyl groups are incorporated into the main chain in order to observe this effect on crystallisability. Owing to the existence of a relationship between crystallinity and both molecular weight and CO concentration, it is necessary to investigate the effect of these two parameters on the crystallisability of this impact PP copolymer. The relationship between crystallisation peak temperature, molecular weight and carbonyl concentration is illustrated in Figure 4.7.

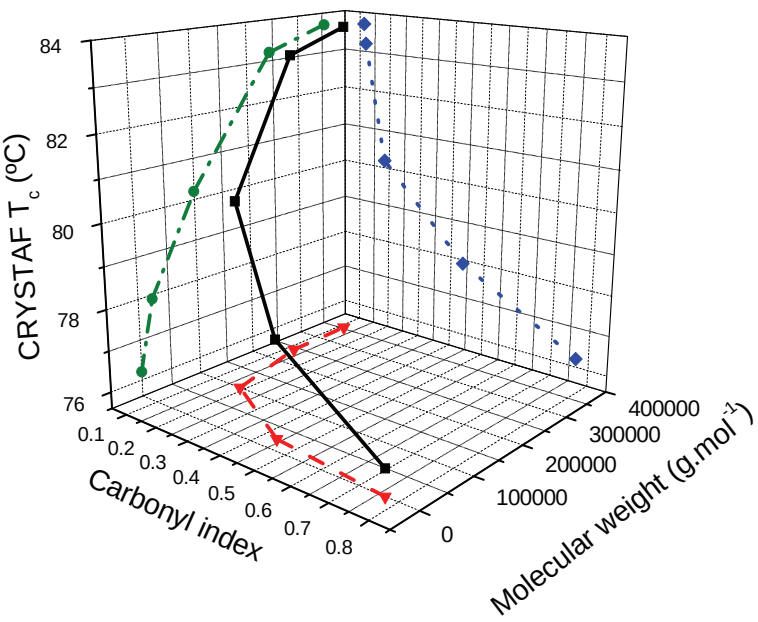

Figure 4.7: Representation of the combined influence of molecular weight and carbonyl concentration on the crystallisation peak temperature in CRYSTAF.

The black curve represents the combined effect of degradation on the three molecular parameters namely molecular weight, carbonyl concentration and crystallisation temperature. The XZ projection (blue) represents the relationship between CRYSTAF crystallisation temperature (T_c) and carbonyl index, whereas the YZ (green) and XY (red) projections display the relationship between molecular weight and T_c and that between molecular weight and carbonyl index, respectively. The blue curve indicates that the highest crystallisation temperatures are present in samples with low carbonyl concentrations, and a non-linear, exponential decrease in crystallisation temperature is observed with increasing carbonyl concentrations. The green curve shows an exponential decrease in crystallisation temperature with decreasing molecular weight and the red curve is similar to Figure 4.3, where an exponential decrease in molecular weight is observed with increasing carbonyl concentrations. The black curve which represents the combined effect of molecular weight and carbonyl concentration on CRYSTAF T_c, follows the shape of the T_c as a function of molecular weight curve (green) up to a certain CO concentration value, after which the curve follows the shape of the carbonyl index versus T_c curve (blue). At low carbonyl index values where a significant decrease in molecular weight is observed for small carbonyl index increases, the crystallisation temperature seems more dependent on molecular weight. At higher CO concentration, however, the carbonyl concentration influence becomes the dominant factor governing the crystallisation temperature. It is known that changes in crystallinity caused by degradation can also be studied by DSC[27-30, 34], therefore the DSC melt and crystallisation curves for the undegraded and degraded samples will be compared next.

4.1.3.3 DSC results for the undegraded and degraded 3V samples

Figure 4.8 shows the differences in the crystallisation and melting behaviour for the undegraded and degraded 3V samples. All melting curves observed here were collected during the second heating cycle after the thermal history of all samples was eliminated.

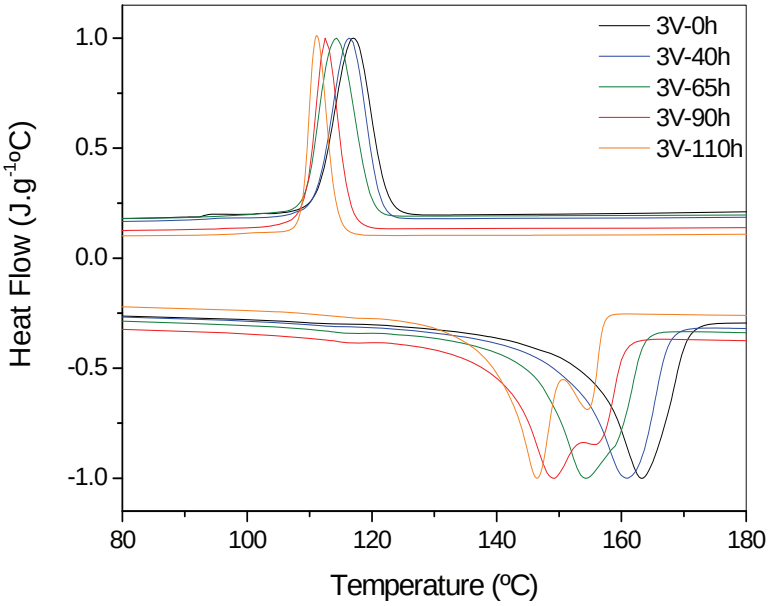

Figure 4.8: DSC results for the undegraded and degraded 3V samples.

The peak maxima of both the crystallisation and melting peaks shift towards lower temperatures with ongoing degradation time. It has been stated that the melting temperature obtained during the second heating cycle of the DSC experiment more accurately reflects the influence of degraded molecules on crystallisation[34]. Crystals formed upon re-crystallisation consists of degraded molecules that are both shorter due to chain scission events and defective due to the incorporation of carbonyls and hydroperoxides. With ongoing degradation times, scission and group insertions lead to crystals that are progressively less perfect, with an accompanied decrease in melting temperatures.

The melt endotherm in Figure 4.8 broadens and splits into two at more advanced stages of degradation. The presence of a second melt endotherm as well as the broadening of the melt endotherm is probably also caused by melting of less perfect crystals formed from defective, oxidised molecules (containing more impurities) under less favourable conditions (i.e., low mobility). The less perfect crystals melt, crystallise again and melt at higher temperatures, where they have more mobility, giving rise to the second melting peak. The onset of melting is also seen to move to lower temperatures as degradation time increases. Continuous melting of both pre-existing and newly-formed, overgrown crystals are supposed to be a continuous melting process, starting with the melting of those crystals deposited last. Since the level of impurity in crystals increases with exposure time,

the onset of melting is expected to shift to lower temperatures[34]. The thermal data for the undegraded and degraded samples are presented in Table 4.3. The T_m values in paretheses represent the melting temperature of the higher melting component observed upon splitting (90 and 110 h) or broadening (65h) of the main melt endotherm at longer degradation times. These changes in the characteristics of the melting peak, therefore, also illustrate the existence of metastable structures caused by the degradation process and emphasise the need for fractionation techniques to better understand the heterogeneity of degradation within impact PP copolymers.

Table 4.3: DSC thermal data for undegraded and degraded 3V samples

Sample	T_m (ºC)	T_c (ºC)	Δh_m ($J.g^{-1}$)
3V-0h	162.6	118.2	94
3V-40h	160.1	117.7	91
3V-65h	154.6 (159.0)	115.5	89
3V-90h	148.6 (155.7)	112.5	89
3V-110h	147.0 (154.6)	110.9	87

In Figure 4.9 the melting and crystallisation temperatures obtained by DSC are presented as a function of carbonyl concentration as determined by FTIR. The crystallisation temperature curve is similar to that observed for the CRYSTAF crystallisation in Figure 4.6. It can therefore be concluded that there is a definite, non-linear relationship between CRYSTAF and DSC crystallisation and DSC melting temperature and the concentration of carbonyl functionalities present in the degraded sample, although molecular weight effects should not be ignored.

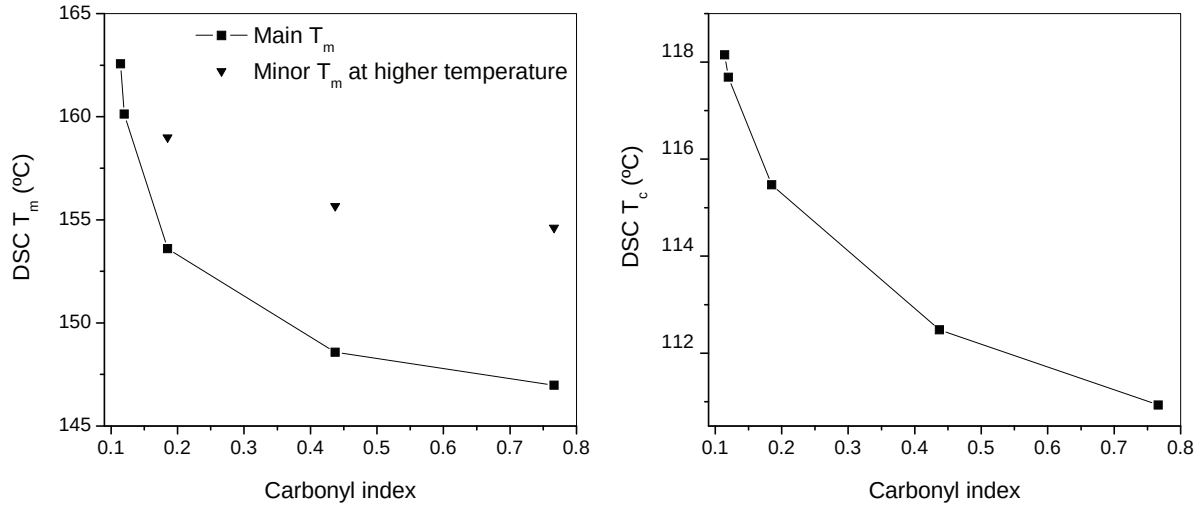

Figure 4.9: DSC melting (T_m) and crystallisation (T_c) values as a function of carbonyl concentration.

The combined effect of molecular weight and CO concentration on DSC crystallisation and melting temperatures are illustrated in Figures 4.10 and 4.11, respectively.

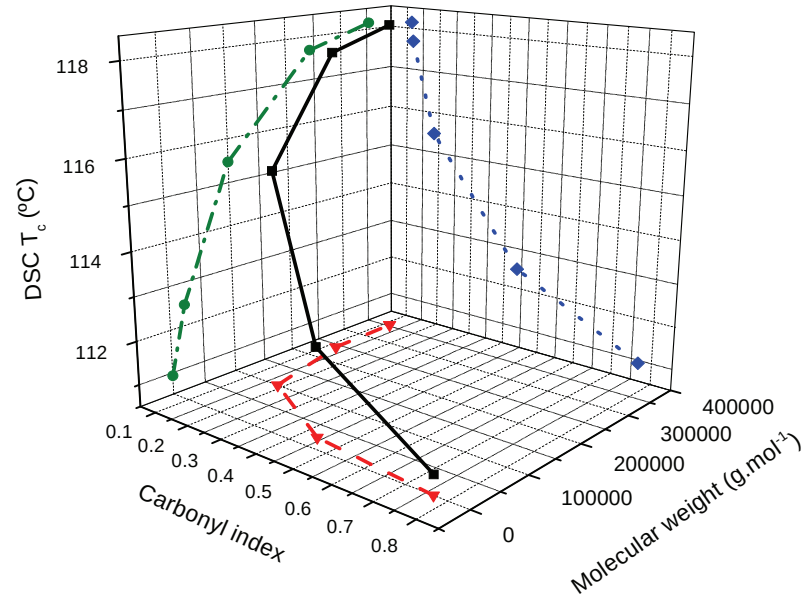

Figure 4.10: Representation of the combined influence of molecular weight and carbonyl concentration on the crystallisation temperature in DSC.

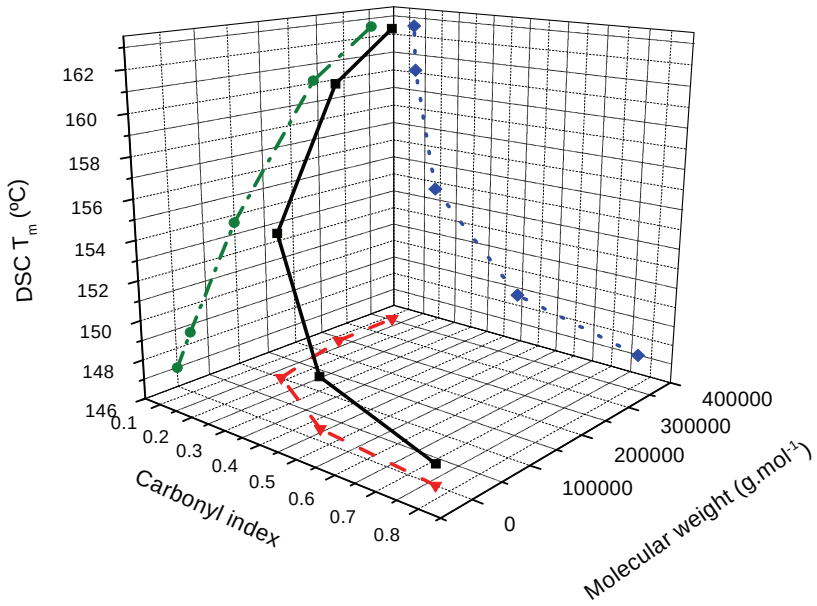

Figure 4.11: Representation of the combined influence of molecular weight and carbonyl concentration on the melting temperature in DSC.

Molecular weight and carbonyl concentration seem to have a similar effect on both DSC and CRYSTAF crystallisation temperatures where, at low carbonyl concentrations crystallisation temperature is governed by molecular weight changes, whereas the level of CO incorporation becomes dominant at higher CO concentrations. The effect is also similar to that observed for DSC melting temperatures, although the black curve follows the molecular weight curve (green) up to a higher CO index than in the case of crystallisation temperature. Here, molecular weight effects remain dominant for longer before the CO concentration effect starts to govern the melting of this copolymer.

From the results in Sections 4.1.3 it can be concluded that combined techniques such as SEC-FTIR and TREF-SEC supply more detailed information on the degradation behaviour of impact PP copolymers than when these techniques are used in isolation. When used in isolation, these two techniques do however, not supply information on the way in which the different components or morphologies in these heterogeneous samples are affected by oxidation. It is clear at this point that the different morphologies would have to be separated from each other and studied in isolation to obtain information on the way in which they degrade. Preparative-TREF is a well-established technique for fractionating semi-crystalline materials according to their crystallisability. The changes in the crystallisability of a polymer as a function of degradation time observed by DSC and CRYSTAF, should therefore also be evident in TREF, while analysis of the fractions obtained from this fractionation procedure should provide information on the susceptibility of the different components to degradation.

A suitable elution temperature program is selected to obtain a range of fractions with different crystallisabilities ranging from highly amorphous material eluting at low temperatures, to highly crystalline material collected at higher temperatures. It is known that impact PP copolymers are highly complex materials consisting of amorphous ethylene-propylene random copolymers (EPR), a range of crystallisable copolymers with different comonomer contents and monomer sequence distributions as well as homopolymers of ethylene and propylene[35-37]. Prep-TREF is, therefore, considered a highly suitable method for separating the different morphologies, and since fractionation depends on both chemical composition and tacticity, FTIR, SEC, DSC and NMR data will supply information on the degradation behaviour of the individual fractions, leading to a better understanding of the degradation process in impact PP copolymers. It will also allow the full characterisation of the undegraded material, since molecular parameters such as comonomer distribution, monomer sequence distribution and tacticity distribution can be obtained as a function of crystallisability.

The next section contains results on the TREF fractionation of the undegraded 3V copolymer sample into its constituting components, and subsequent analysis of the individual components by means of FTIR, SEC, NMR, DSC and SEC-FTIR. The TREF analysis was combined with these techniques to obtain detailed structural information on the composition and heterogeneity of the undegraded material. A proper analysis of the structure and composition of this complex sample in its undegraded state will promote a better understanding of its behaviour upon degradation.

4.1.3.4 Prep-TREF results for the undegraded 3V sample

Undegraded films were fractionated by means of the prep-TREF setup described in Section 3.3.5 of the experimental chapter. An antioxidant stabiliser (Irganox 1010) was added to the polymer to prevent degradation during the dissolution and fractionation steps and fractions were collected at 30, 60, 80, 90, 100, 110, 120 and 130ºC during subsequent re-heating of the pre-crystallised polymer in

incremental steps. Figure 4.12 shows the weight fraction per temperature increment ($W_i\%/\Delta T$) and accumulative weight ($\Sigma W_i\%$) plots for copolymer 3V, as a function of elution temperature. The $W_i\%/\Delta T$ plot approximates the differential curve of the cumulative weight plot. From this curve it is seen that the copolymer dissolves and elutes over a broad range, indicating heterogeneity in both isotacticity and chemical composition. The fractionation data is presented in Table 4.4.

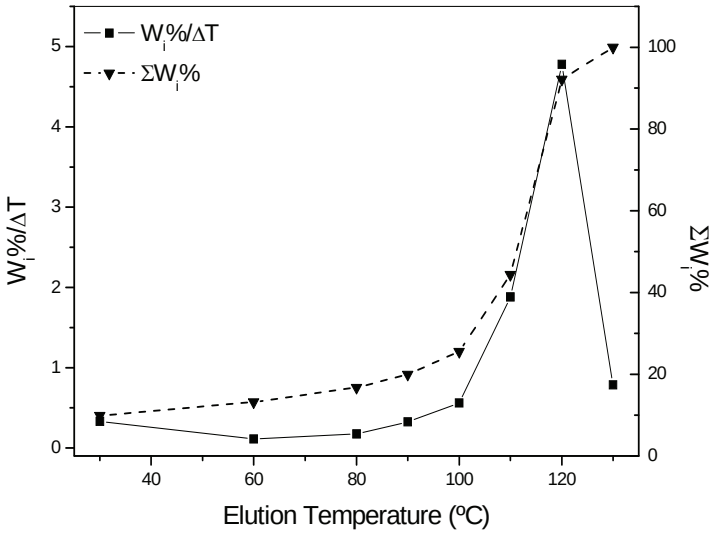

Figure 4.12: TREF curves for the undegraded 3V copolymer sample.

From the fractionation data three main weight fractions can be identified, namely those eluting at 30ºC, 110ºC and 120ºC. Together these three fractions constitute 74.42% of the total sample weight, with the 120ºC fraction alone, constituting 47.77 percent. The composition of these fractions will therefore influence the properties of the bulk copolymer to a large extent. The individual fractions obtained by prep-TREF were analysed by FTIR, DSC, ^{13}C-NMR and SEC-FTIR to determine their chemical composition as well as thermal and morphological properties.

Table 4.4: TREF data for the undegraded 3V sample

Sample	T_e (ºC)	W_i (g)	W_i (%)	ΣW_i (%)	$W_i\%/\Delta T$
3V-0h-30	30	0.303	9.90	9.90	0.330
3V-0h-60	60	0.102	3.36	13.26	0.090
3V-0h-80	80	0.106	3.47	16.73	0.163
3V-0h-90	90	0.100	3.26	19.99	0.307
3V-0h-100	100	0.171	5.60	25.59	0.527
3V-0h-110	110	0.574	18.80	44.39	1.771
3V-0h-120	120	1.459	47.77	92.16	4.498
3V-0h-130	130	0.240	7.85	100.00	0.739

4.1.3.5 TREF-(^{13}C-NMR) results for the undegraded 3V sample

^{13}C-NMR has long been the method of choice for determining the comonomer content, monomer sequence distributions and stereoregularity of the propylene unit in EP copolymers[38] and their fractions of impact copolymers obtained by solvent fractionation or TREF[37, 39-41]. Figure 4.13 represents the ^{13}C-NMR spectrum for the bulk 3V copolymer, which is a typical spectrum for EP copolymers with low ethylene contents[42]. Chemical shifts were referred to isolated methylene groups at 30.0 ppm and assignment of the resonances followed the terminology described by Carman and Wilkes[43] where the letters S, P and T indicate secondary (methylene), primary (methyl) and tertiary (methine) carbon atoms, respectively.

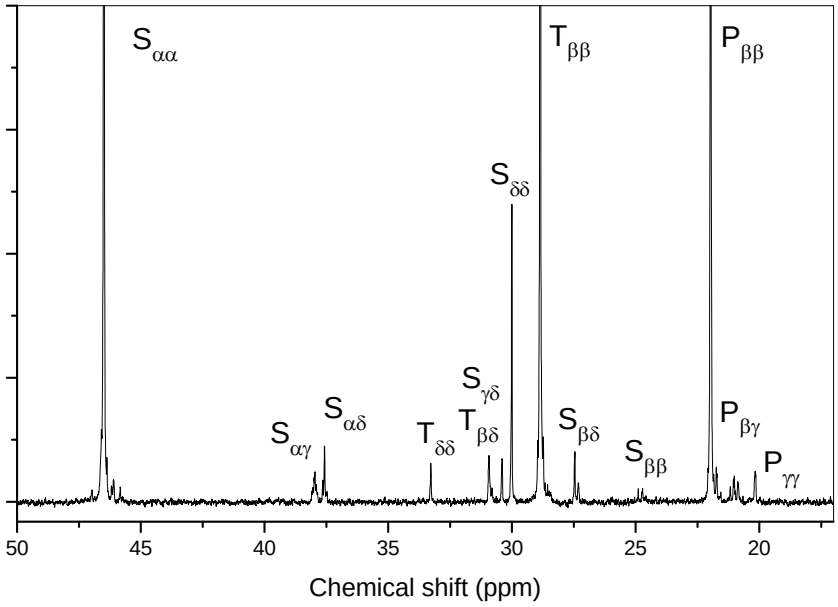

Figure 4.13: ^{13}C-NMR peak assignments for the undegraded 3V sample

Furthermore, the two Greek subscripts refer to the distance, in both directions, of any given carbon to the nearest neighbouring tertiary carbon bearing a methyl side group. Therefore, a carbon labelled $S_{\alpha\alpha}$, is a secondary carbon with two tertiary carbons on either sides, whereas a $S_{\alpha\beta}$ carbon is a secondary carbon with a tertiary carbon on one side and another tertiary carbon found one carbon away, until a $S_{\delta\delta}$ carbon is reached which indicates a secondary carbon with tertiary carbons bearing methyl groups, being four carbons away on both sides. When the distance to the nearest tertiary carbon exceeds four, the δ^+ notation is used. This nomenclature is illustrated in Scheme 4.1 for the methylene carbons in EP copolymers without monomer inversion [44].

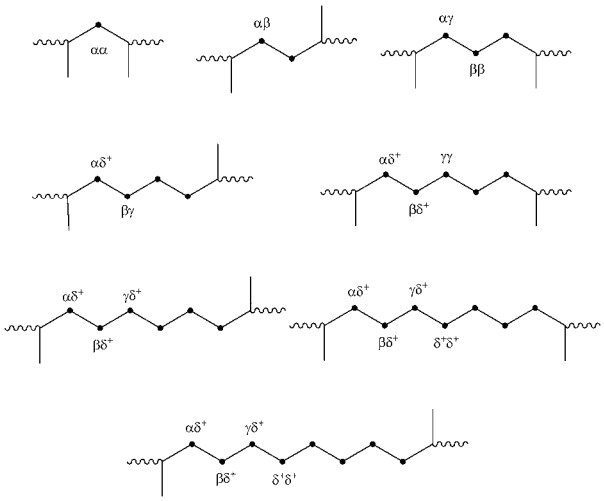

Scheme 4.1: Illustration of the nomenclature used for the methylene carbons in ethylene-propylene copolymers without monomer inversion.

In Figure 4.13 four major peaks are observed, namely the $S_{\alpha\alpha}$ (CH_2), $T_{\beta\beta}$ (CH) and $P_{\beta\beta}$ (CH_3) corresponding to the three distinct carbon atoms in the constitutional base unit of PP, as well as the $S_{\delta\delta}$, representing the CH_2's in PE. Minor peaks ($S_{\alpha\gamma}; S_{\alpha\delta}; S_{\beta\delta}; S_{\gamma\delta}; T_{\delta\delta}; S_{\beta\delta}; P_{\beta\gamma}; P_{\gamma\gamma}$) are also present in the spectrum, indicating that various transition segments such as PEP, EPE, PPE, EEP, are present as junctions in between longer ethylene and propylene segments [42]. The absence of the $S_{\alpha\beta}$ resonance indicates that no inverted propylene units are present. Comonomer content and monomer sequence distributions were calculated according to the following equations [45], based on relationships established by Ray *et al.* [46] and Randall [44].

P'	=	$S_{\alpha\alpha} + ½ (S_{\alpha\gamma} + S_{\alpha\delta})$	(4.1)
E'	=	$½ [S_{\delta\delta} + S_{\beta\delta} + S_{\alpha\gamma} + ½ (S_{\gamma\delta} + S_{\beta\delta} + S_{\alpha\delta})]$	(4.2)
P	=	P'/(P' + E')	(4.3)
E	=	E'/(E' + P')	(4.4)
PP	=	$S_{\alpha\alpha}$/(P' + E')	(4.5)
PE + EP	=	$(S_{\alpha\gamma} + S_{\alpha\delta})$/(P' + E')	(4.6)
EE	=	$½ (S_{\beta\delta} + S_{\delta\delta} + ½ S_{\gamma\delta})$/(P' + E')	(4.7)
PPP	=	P x $T_{\beta\beta}$/ $(T_{\beta\beta} + T_{\beta\delta} + T_{\delta\delta})$	(4.8)
PPE + EPP	=	P x $T_{\beta\delta}$/ $(T_{\beta\beta} + T_{\beta\delta} + T_{\delta\delta})$	(4.9)
EPE	=	P x $T_{\delta\delta}$/ $(T_{\beta\beta} + T_{\beta\delta} + T_{\delta\delta})$	(4.10)
EEE	=	$½ (S_{\delta\delta} + ½ S_{\gamma\delta})$/(P' + E')	(4.11)
EEP + PEE	=	$S_{\alpha\delta}$ / (P' +E')	(4.12)
PEP	=	$½ S_{\alpha\gamma}$/(P' +E')	(4.13)

Results from the sequence analysis of the 3V bulk copolymer and its TREF fractions, are presented in Table 4.5, together with isotacticity (%mmmm) data for the PP part obtained by the ^{13}C-NMR method described by Kanezaki *et al*.[47] Unfortunately, data on the 130ºC fraction was not available, although, based on the knowledge of TREF fractionation it is expected to be similar in composition to the 110 and 120ºC fractions. The sample names of all fractions were given according to the method described in Section 4.1.3.1, followed by -30; -60; -80, etc., to indicate the TREF elution temperature at which each fraction was collected. The sample name 3V-0h-120, therefore, describes the 120ºC fraction of the undegraded 3V copolymer, whereas the 80ºC fraction of the same sample is labeled 3V-0h-80. This nomenclature will be used throughout this dissertation.

Table 4.5: ^{13}C-NMR monomer sequence analysis and tacticity data of the bulk 3V sample and its TREF fractions

Sample	P	E	PP	PE EP	EE	PPP	PPE EPP	EPE	EEE	EEP PEE	PEP	% mmmm
3V-0h	89.52	10.48	86.36	6.34	7.32	84.19	3.63	1.70	5.75	3.18	1.58	88.82
3V-0h-30	49.55	50.45	34.43	30.23	34.39	49.39	0.14	0.02	25.78	13.42	1.80	24.70
3V-0h-60	45.11	54.89	34.15	21.92	43.87	28.74	11.64	4.73	37.56	12.43	1.65	36.13
3V-0h-80	44.46	55.54	38.29	12.32	48.99	37.74	3.96	3.11	44.47	7.47	1.00	64.91
3V-0h-90	54.31	45.69	52.66	3.31	43.83	54.26	0.04	0.01	42.25	2.37	0.06	71.21
3V-0h-100	90.27	9.73	89.96	0.63	9.11	89.37	0.90	0.00	8.50	0.02	0.11	85.74
3V-0h-110	94.85	5.15	94.85	0.00	4.37	91.86	2.99	0.00	2.81	0.00	0.00	86.54
3V-0h-120	99.39	0.61	99.39	0.00	0.61	99.39	0.00	0.00	0.61	0.00	0.00	91.52

From the sequence analysis data it can be seen that, with increasing elution temperature, there is a decrease in ethylene content, with an accompanying increase in the propylene content and isotacticity, which indicates that fractionation is governed mainly by decreasing comonomer content and increasing isotacticity. The content of long ethylene sequences (EEE) also decreases and that of long propylene sequences (PPP) increases with elution temperature, until values of 94,85 and 99.39% are reached for PPP triads in the 110ºC and 120ºC fractions respectively, indicating that these fractions consist mainly of long propylene sequences. The amount of EP junctions and isolated ethylene and propylene units decreases with elution temperature. The high amount of (PE + EP) diads in the first four fractions indicates that ethylene and propylene segments are linked to some degree, whereas this value becomes virtually 0 in the highest eluting fractions, indicating that almost no junctions between the propylene and ethylene is present. These fractions are believed to consist of long propylene homopolymer sequences with a small amount of PE homopolymer.

The first fraction eluting at 30ºC consists of equal amount (ca. 50/50%) of ethylene and propylene and together with the high amount of EP junctions (PE+EP; PPE+EPP; EEP+PEE), it can be assumed that this fraction consists mainly of ethylene-propylene random copolymer (EPR) while atactic PP and some ethylene homopolymer may also form part of this fraction[48]. The following three fractions eluting at 60ºC, 80ºC and 90ºC consist of equally high amounts of long sequences of ethylene and propylene,

with a fair amount of EP junctions also present, thereby indicating that these fractions consist of propylene and ethylene segments that are linked, but since true block structures cannot be produced by the sequential gas-phase polymerisation process in question, these are called 'blocky' copolymers[49]. The 60ºC fraction also exhibits a higher amount of (EEP+PEE) and (PPE + EPP) junctions between the segments than the following 2 fractions, thereby indicating that these fractions might be classified as transition copolymers, i.e., having a structure between that of a random and blocky copolymers[49].

The number average sequence length of the propylene and ethylene segments in the copolymer fractions was calculated from the following relationships[38] and the results are presented in Table 4.6:

$$\overline{n_P} = \frac{(PP) + 1/2(PE)}{1/2(PE)} \tag{4.14}$$

$$\overline{n_E} = \frac{(EE) + 1/2(PE)}{1/2(PE)} \tag{4.15}$$

Average sequence lengths were not determined for the 110 and 120ºC fractions, since the amount of PE sequences is 0 in this case. The concentration of propylene and long propylene sequences (PPP) in these two fractions are close to 100, therefore it can be accepted that these fractions consist mainly of PP homopolymer, in which case the average length of propylene sequences is expected to be infinite.

Table 4.6: The average lengths of ethylene and propylene segments in the bulk 3V sample and its TREF fractions

Sample	$\overline{n_E}$	$\overline{n_P}$
3V-0h	3.31	28.86
3V-0h-30	5.41	3.32
3V-0h-60	5.00	4.12
3V-0h-80	8.95	7.21
3V-0h-90	27.51	32.84
3V-0h-100	29.99	287.23
3V-0h-110	n.d.	n.d.
3V-0h-120	n.d.	n.d.

n.d: not determined

From these results it is clear that the length of both the ethylene and propylene segments increases with elution temperature, with a more marked increase in the length of propylene segments towards higher elution temperatures. This indicates that TREF not only fractionates impact PP copolymers according to the isotacticity of the propylene phase, but also according to the ethylene and propylene

sequence lengths, or isotactic sequence lengths[50], with fractions containing longer sequences, eluting at higher temperatures[39, 51]. This range of copolymers with varied composition is the result of numerous catalyst active sites with different selectivity towards ethylene and propylene during copolymerisation and it is observed that more ethylene inserted into chains with lower stereoregularity. The gradual change in the sequence distribution of propylene and ethylene sequences from the first to the last fraction reveals some continuity in structure, which is known to be characteristic of impact PP copolymers prepared via the *in-situ* co-polymerisation method[40]. SEC analysis of the molecular weight distribution of the TREF fractions of this complex copolymer formed the next step in the multi-step characterization procedure followed to characterize the undegraded 3V-0h copolymer.

4.1.3.6 TREF-SEC results for the undegraded 3V sample

The molecular weight distributions of all TREF fractions of the undegraded sample were determined by SEC and are presented together with the distribution of the bulk 3V-0h sample in Figure 4.14. The 110 and 120ºC fractions exhibit monomodal molecular weight distribution curves, indicating their homogeneity. The 60–90ºC fractions show clear bimodality in their molecular weight distributions with the 30 and 100ºC fractions also having slight shoulders at the lower and higher molecular weight sides, respectively. Such bimodal molecular weight distributions indicate compositional heterogeneity due to the co-elution of non-identical products within these fractions. This phenomenon is often observed for the mid-elution temperature fractions of impact PP copolymers fractionated by TREF[52 53 54,15, 54]. Zacur *et al*.[52, 53] and Usami *et al.*[55] have illustrated the co-elution of semi-crystalline ethylene-propylene copolymers (EPC) and PP homopolymer within this elution range for an impact PP copolymer fractionated by TREF. Since PP is characterised by an isotacticity distribution,[52, 56] not all of the PP homopolymer phase will elute at high temperatures, with PP fractions of lower isotacticity eluting within the same temperature range as the semi-crystalline EPC phase. These authors have concluded that the higher molecular weight component consists of the EP copolymer phase (EPC), while the lower molecular weight distribution belongs to PP homopolymer[52, 53]. The high molecular weight tail in the 100ºC fraction of sample 3V-0h is similar to that observed in the 105ºC fraction of the ICPP fractionated by Zacur, who have, upon comparison of the hydrodynamic volume curve of this fraction with that obtained at 105ºC for the hPP, concluded that the shoulder was indicative of the presence of EPC molecules[52]. Although these fractions of the impact PP copolymer in question seems similar in composition to those analysed by these authors, additional information on the composition of these fractions will be obtained to clarify its composition.

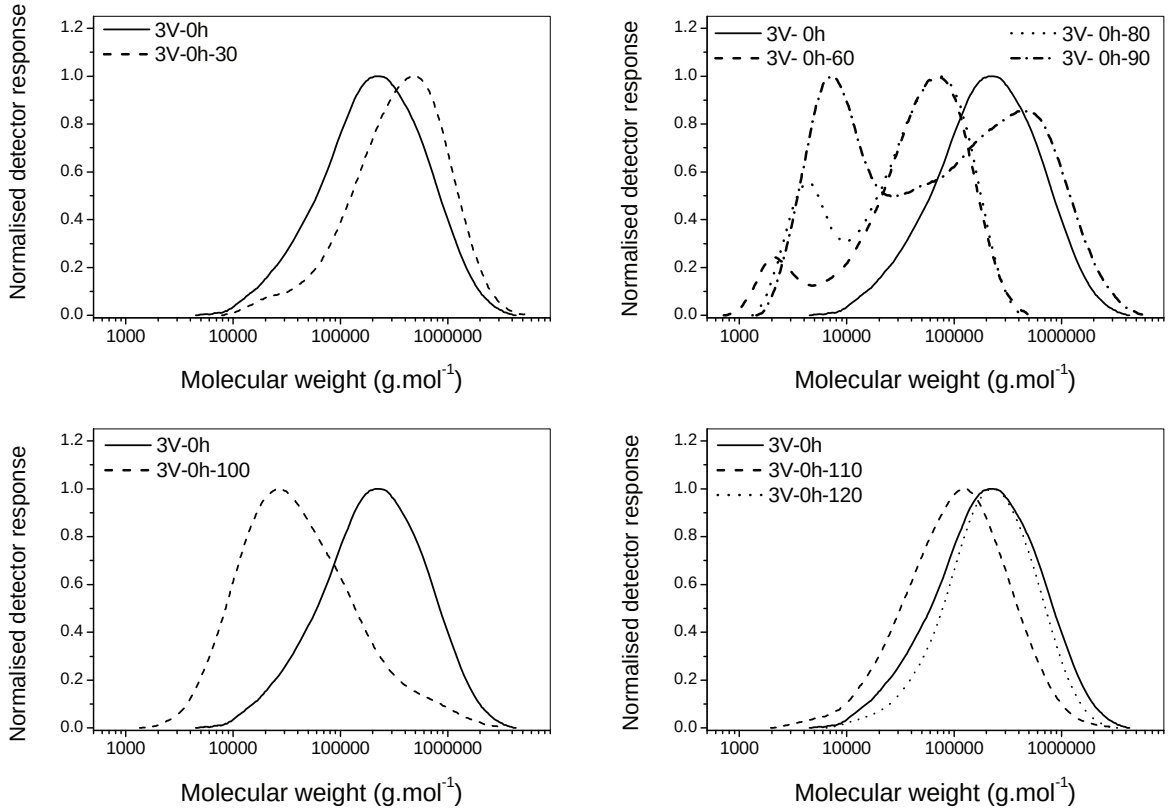

Figure 4.14: SEC curves for the undegraded bulk 3V copolymer sample and its TREF fractions.

From the SEC results of copolymer 3V-0h it is clear that TREF-SEC alone does not supply sufficient information on the composition of the various distributions within the molecular weight curves of these TREF fractions. Therefore, additional techniques are needed for complete characterisation. The overall composition and thermal behaviour of the TREF fractions will now be studied by FTIR-ATR and DSC, and finally, the composition of each fraction will be characterised as a function of its molecular weight distribution by means of SEC-FTIR.

4.1.3.7 TREF-(ATR-FTIR) results for the undegraded 3V sample

The IR bands at 998 cm^{-1} and 841 cm^{-1}, associated with methyl rocking modes, are characteristic of the threefold helix of isotactic PP[57, 58], and only appear for helix segments with at least ~11 and ~14 repeat units, respectively[59]. These bands indicate the presence of long crystallisable PP sequences, whereas the band at 972 cm^{-1} is associated with the methyl rocking vibrations of shorter helix segments. The 720 cm^{-1} band is characteristic of the rocking vibrations of methylene sequences $-(CH_2)_n-$, where $n \geq 5$[58, 60], and is considered an indication of the presence of long ethylene sequences (EEE), while a doublet at 720–740 cm^{-1} indicates the presence of crystalline PE. When PE crystallinity is small, the band at 730 cm^{-1} of the doublet will be reduced to a shoulder of the band at 720 cm^{-1}. Figure 4.15 illustrates the ATR spectra of the TREF fractions of copolymer 3V.

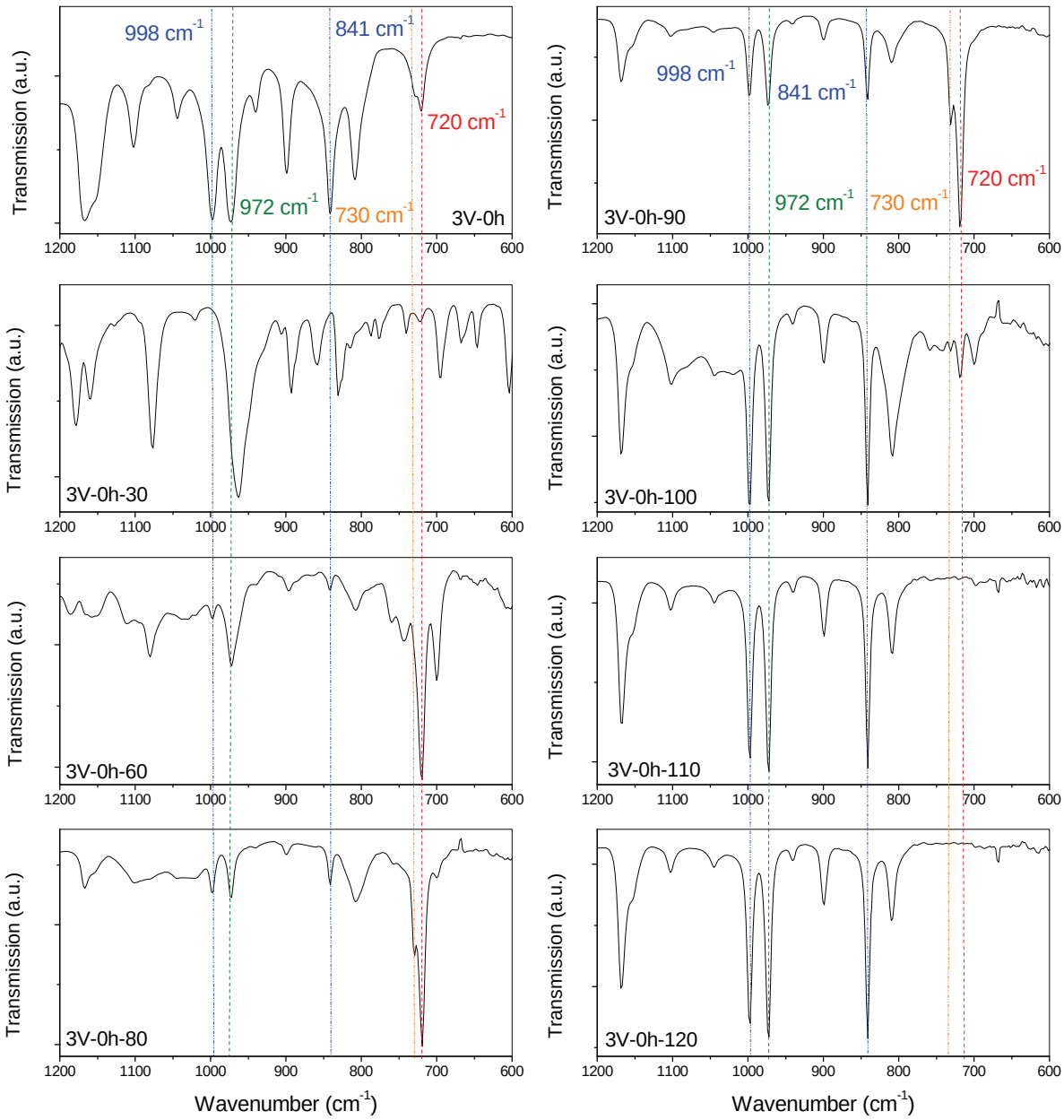

Figure 4.15: A selected area of the FTIR spectrum obtained by ATR-FTIR of the undegraded 3V sample and its TREF fractions.

The attenuated total reflectance infrared (ATR-FTIR) spectrum of the 30ºC fraction is typical for a random copolymer where both the ethylene and propylene segments are too short too crystallise, as indicated by the absence of bands at 998 cm^{-1}, 841 cm^{-1} and 730 cm^{-1}. A small peak at 720 cm^{-1} is observed, which indicates that some longer ethylene sequences (n ≥ 5) are present. This supports the NMR data which indicated that this fraction consists of the EPR and non-crystallisable ethylene and propylene homopolymer part of the copolymer. From elution temperatures of 60 to 120ºC, an increase in the bands at 998 cm^{-1} and 841 cm^{-1} is observed, indicating an increase in the concentration of long crystallisable PP sequences. A shoulder at 730 cm^{-1} in the 60ºC fraction indicates that PE sequences have also reached the required length for crystallisation and this shoulder develops into a distinct, separate band in the 80ºC to 100ºC fractions. These fractions, therefore, consist of crystallisable

segments of both ethylene and propylene. The last two fractions are characteristic of highly crystalline PP (strong intensity bands at 998 cm^{-1} and 841 cm^{-1}) with a small amount of PE homopolymer present too, as indicated by the very small band visible at 720 cm^{-1}. The absence of the band at 730 cm^{-1} indicates that no long, crystallisable PE segments are present.

4.1.3.8 TREF-DSC results for the undegraded 3V sample

The DSC crystallisation and melting curves of all fractions, the latter which were obtained upon the second heating cycle, are presented in Figure 4.16. In the 30ºC fraction, a small crystallisation peak around 37ºC and melt endotherm at 56ºC is observed, which indicates that, even though amorphous random ethylene-propylene copolymers are expected to elute in this fraction, some crystallisable material is present too. The presence of EPR is confirmed by the glass transition (Tg) present below 0ºC[61, 62]. The transition around 40ºC is expected to be caused by long PE segments (evidenced by the relatively large percentage of EEE sequences from NMR results in Table 4.4) that may be arranged in a long-range order[40].

Small melting endotherms at about 90 and 112ºC as well as at 103 and 130ºC are observed in the 60 and 80ºC fractions, respectively. This indicates that both the ethylene and propylene segments have reached a crystallisable length, but the large difference in melting temperatures compared to PE and PP homopolymers, suggests that the amount of long, crystallisable PE and PP sequences is very small. The large amount of shorter sequences disrupts the crystal growth, leading to imperfect crystals. These results are consistent with those obtained by NMR and FTIR and serve as proof that these fractions are segmented or transition copolymers. The following two fractions (90 and 100ºC) also exhibit two melt endotherms, corresponding to the melting of both ethylene and propylene crystallisable sequences[53, 63].

In these two fractions the melting temperatures of the PP segments have increased to 146ºC and 150ºC, respectively, indicating that more prefect crystals are formed in the PP phase. The endotherm associated with the melting of ethylene segments appears at almost the same melting temperature in these two fractions, namely at 118ºC, which is considerably higher than the T_m of the ethylene in the fractions eluting at 60 and 80ºC. This indicates that the ethylene segments of the copolymer phase are also crystallising into more perfect crystals. The intensity of these endotherms do, however, decrease significantly, indicating that there is less ethylene crystallising out in these two fractions, than in the foregoing two, which agrees well with the NMR sequence results for the percentage long ethylene sequences (EEE) provided in Table 4.5. These fractions clearly consist of segmented or ‘blocky’ copolymers (EPC) with longer segments of PE and PP that are able to crystallise at higher temperatures into more perfect crystalline structures.

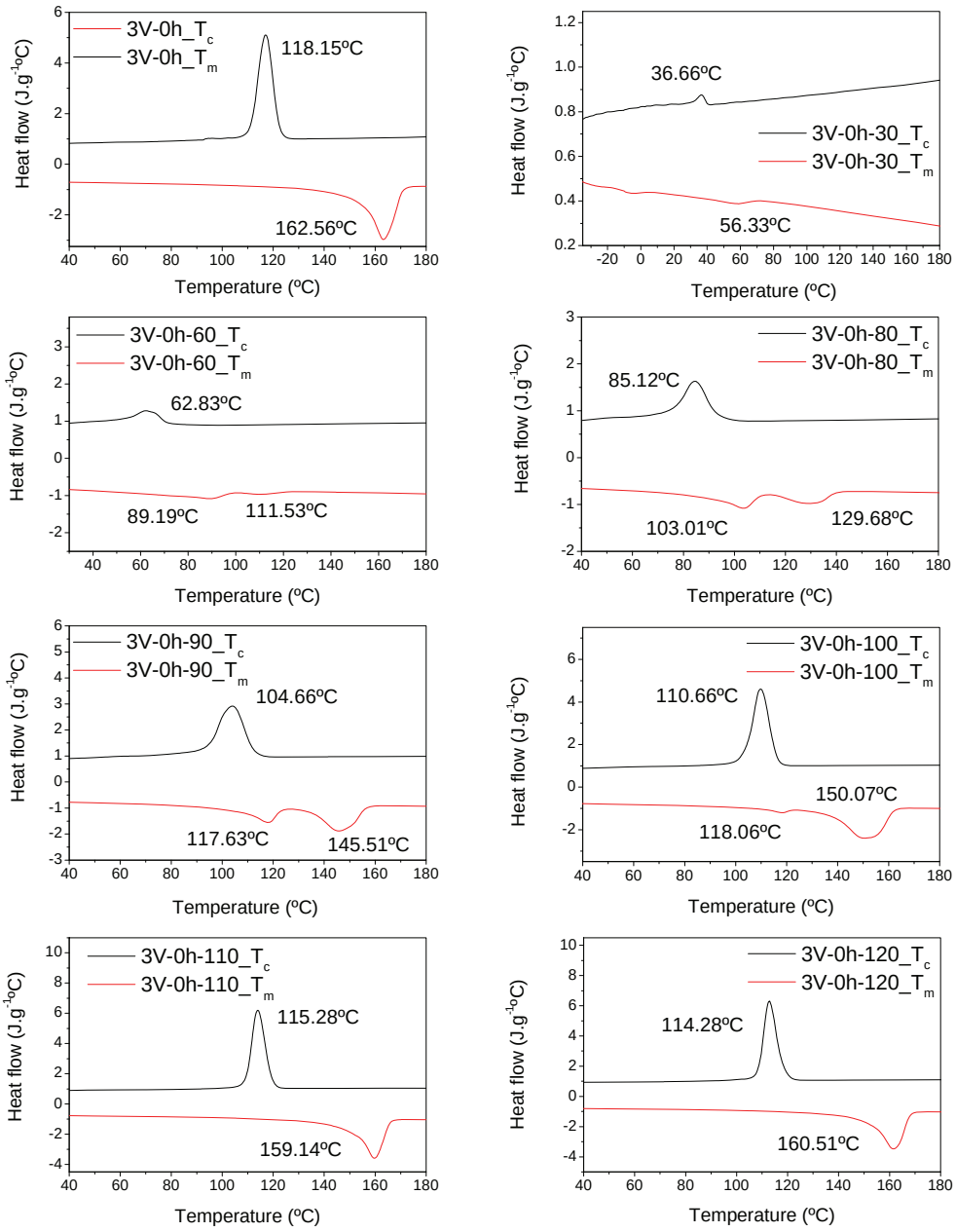

Figure 4.16: DSC crystallisation and melting curves for the undegraded bulk 3V sample and its TREF fractions

In the last two fractions, a single melting endotherm is observed around 160ºC, which agrees with NMR and FTIR results of this fraction being isotactic PP. These melting endotherms are slightly below that expected for the isotactic homopolymer. This is attributed to the presence of a very small amount of ethylene in these fractions, as confirmed by NMR and FTIR. The concentration of long ethylene sequences is, however, too low for a melt endotherm to be observed in DSC.

4.1.3.9 TREF-(SEC-FTIR) results for the undegraded 3V sample

SEC-FTIR analysis of the fractions was performed in order to obtain information on the chemical composition across the molecular weight distribution of each fraction. This is expected to provide

valuable information on the chemical composition of especially those fractions where bimodality was detected in their molecular weight distributions. The SEC-FTIR results of the 60, 80, 90 and 100ºC fractions are presented in Figure 4.17.

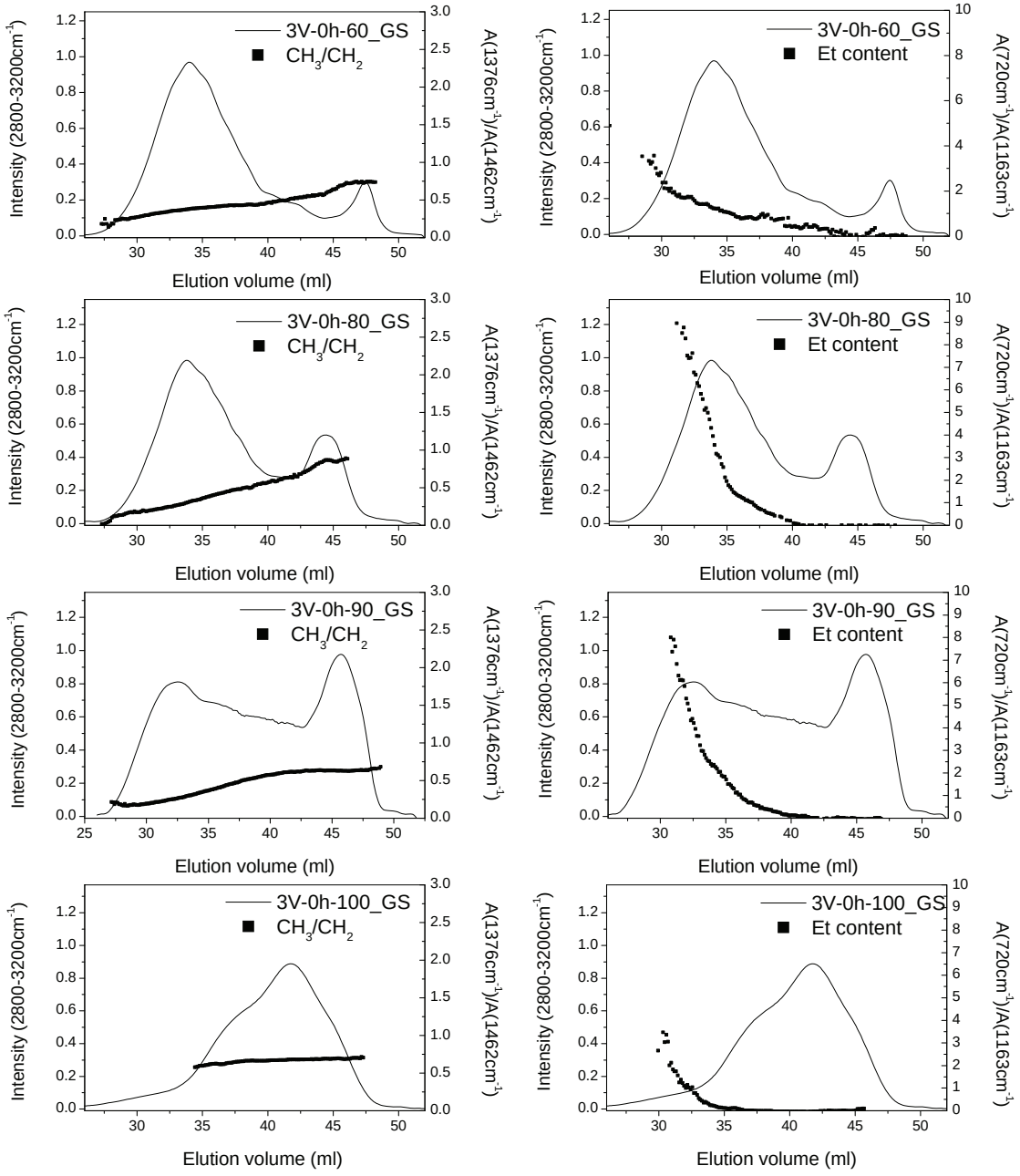

Figure 4.17: SEC-FTIR analysis of the ethylene and propylene distribution within the 60ºC, 80ºC, 90ºC and 100ºC TREF fractions of sample 3V-0h.

As explained previously, the CH_3/CH_2 curve illustrates the propylene distribution across the Gram-Schmidt, while the ethylene content profile is labelled 'Et content'. In all SEC-FTIR results presented in this study, the Gram-Schmidt plot represents the total FTIR absorption over the 2800-3200 cm^{-1} range of the FTIR spectrum. The propylene content is quantified by the ratio of the areas of the bands representing the CH_3 and CH_2 bendings at 1376 cm^{-1} and 1462cm^{-1}, respectively[23, 24, 64]. The presence

of CH_3 groups indicates branching and is characteristic of PP units, whereas the intensity of the CH_2 band is taken as a measure of the total polymer concentration. Since the band at 1378 cm^{-1} may also originate from chain branching in polyethylene[65], the validity of using the 1378cm^{-1}/1462cm^{-1} ratio as an indication of propylene content, was investigated by constructing the ethylene content profile across the molecular weight distribution curves of the 'blocky' or segmented copolymer fractions. The ethylene content was quantified by the area ratio of the bands at 720 cm^{-1} and 1163 cm^{-1}, which is used to determine the comonomer composition within EP block copolymers[66].

The 60, 80 and 90ºC fractions exhibit a gradual increase in the CH_3/CH_2 ratio across the bimodal molecular weight distributions, suggesting a higher propylene content within the low molecular weight component, although this might also originate from branched polyethylene. The 720 cm^{-1}/1162 cm^{-1} ratio of these three fractions, however indicate a gradual decrease in ethylene content from the high molecular weight side of the distribution, until a value of 0 is reached within the lower molecular weight component. This serves as an indication of ethylene-rich chains being present in the high molecular weight component, while no ethylene is found within the lower molecular weight component of the bimodal distribution. The 1378 cm^{-1} band is, therefore, believed to be representative of the methyl groups in polypropylene only. The 1378 cm^{-1}/1462 cm^{-1} ratio will be used in all subsequent SEC-FTIR analyses to characterise the propylene concentration across each Gram-Schmidt profile.

The lower molecular weight component of the bimodal distributions of the blocky and block copolymers seems to consist of propylene homopolymer only, whereas the higher molecular weight component is believed to contain ethylene-propylene copolymers (EPC) with different monomer distributions. The copolymers which are richest in ethylene appear on the higher molecular weight side of the distribution and a gradual increase in propylene concentration is observed towards the lower molecular weight side. These results are in agreement with those obtained by Zacur *et al.*, which indicated the overlap between EPC and hPP within the mid-elution temperature fractions of TREF-fractionated ICPPs[52, 53]. From ^{13}C-NMR it was predicted that the 100ºC fraction forms the transition between the block copolymer and higher eluting iPP fractions. Although the amount of ethylene present within this fraction (ca. 10%) is much lower than in the preceding ones (ca. 50%), the presence of some ethylene-propylene copolymers seems to be indicated by the slight shoulder detected on the high molecular weight side of the SEC curve. The CH_3/CH_2 ratio constructed from the SEC-FTIR results indicate a slightly lower value at the low elution volume (high molecular weight) side of the Gram-Schmidt curve compared to the higher elution volume end, indicating a lower propylene content within this region of the molecular weight distribution. This is also in agreement with the 720 cm^{-1}/1163 cm^{-1} ratio which indicates that the ethylene concentration decreases to 0 across the larger elution volume component of the distribution. SEC-FTIR analysis, therefore, confirms the presence of EPC within the higher molecular weight shoulder to the hPP molecular weight distribution within the 100ºC fraction.

DSC analysis revealed two melt endotherms in each of these fractions, suggesting the presence of both crystalline ethylene and propylene. Since there exist specific infrared bands associated with

crystalline entities for both monomers within the infrared spectrum, it should be possible from SEC-FTIR to construct profiles of ethylene and propylene crystallinity across these bimodal molecular weight distributions. The 998 cm^{-1} and 841 cm^{-1} bands are known to result from long repeating monomer units in the crystalline 3_1 helix of PP[57, 59, 60, 67], while the 972 cm^{-1} band is associated with short helix segments. The intensity of the 998 cm^{-1} and 841 cm^{-1} bands were also found to be linearly related to the density of polypropylene as a measure of its crystallinity[68]. The ratio of the 998 and 972 cm^{-1} bands has, therefore, been used to determine PP tacticity[59, 67, 69, 70], and has been indicated as a measure of the degree of spectral crystallinity in polypropylene[51]. FTIR determination of isotacticity is known to depend on the thermal history of the sample[71], and standardisation via annealing of PP samples at elevated temperatures, has been proposed[70]. The deposition and cooling conditions of all samples were kept identical during SEC-FTIR analysis in order to ensure reliable crystallinity measurements.

Similar to propylene, FTIR spectroscopy should also supply information on the relative crystallinity of ethylene in EP copolymers. As the crystallinity in polyethylene increases, the 720 cm^{-1} band, originating from long continuous methylene sequences, splits and the intensity of the 730 cm^{-1} component increases[72, 73]. The 730 cm^{-1} band produced by crystal-field splitting, has been identified as a true crystallinity band[59] and, therefore, the ratio of the band intensities at 720 cm^{-1} and 730 cm^{-1} is related to the relative crystallinity in polyethylene[73-75]. In Figure 4.18 the 998 cm^{-1}/972 cm^{-1} and 730 cm^{-1}/720 cm^{-1} ratios are constructed across the Gram-Schmidt curves of all fractions in order to study the distribution of ethylene and propylene crystallinity across the molecular weight profiles.

The 60ºC fraction displays a very low level of propylene isotacticity or crystallinity across the low elution volume (high molecular weight) component of the bimodal elution volume curve. The 998 cm^{-1}/972 cm^{-1} ratio across the higher elution volume (lower molecular weight) component is considerably higher, and agrees well with the CH_3/CH_2 ratio which indicated that this component consists of PP homopolymer. The 730 cm^{-1}/720 cm^{-1} ratio profile indicates that crystalline ethylene is only present within the lower elution volume component, which was identified as the semi-crystalline EPC component of this fraction. The discontinuation of this profile result from the absence of the 730 and 720 cm^{-1} bands within the higher elution volume component of the distribution.

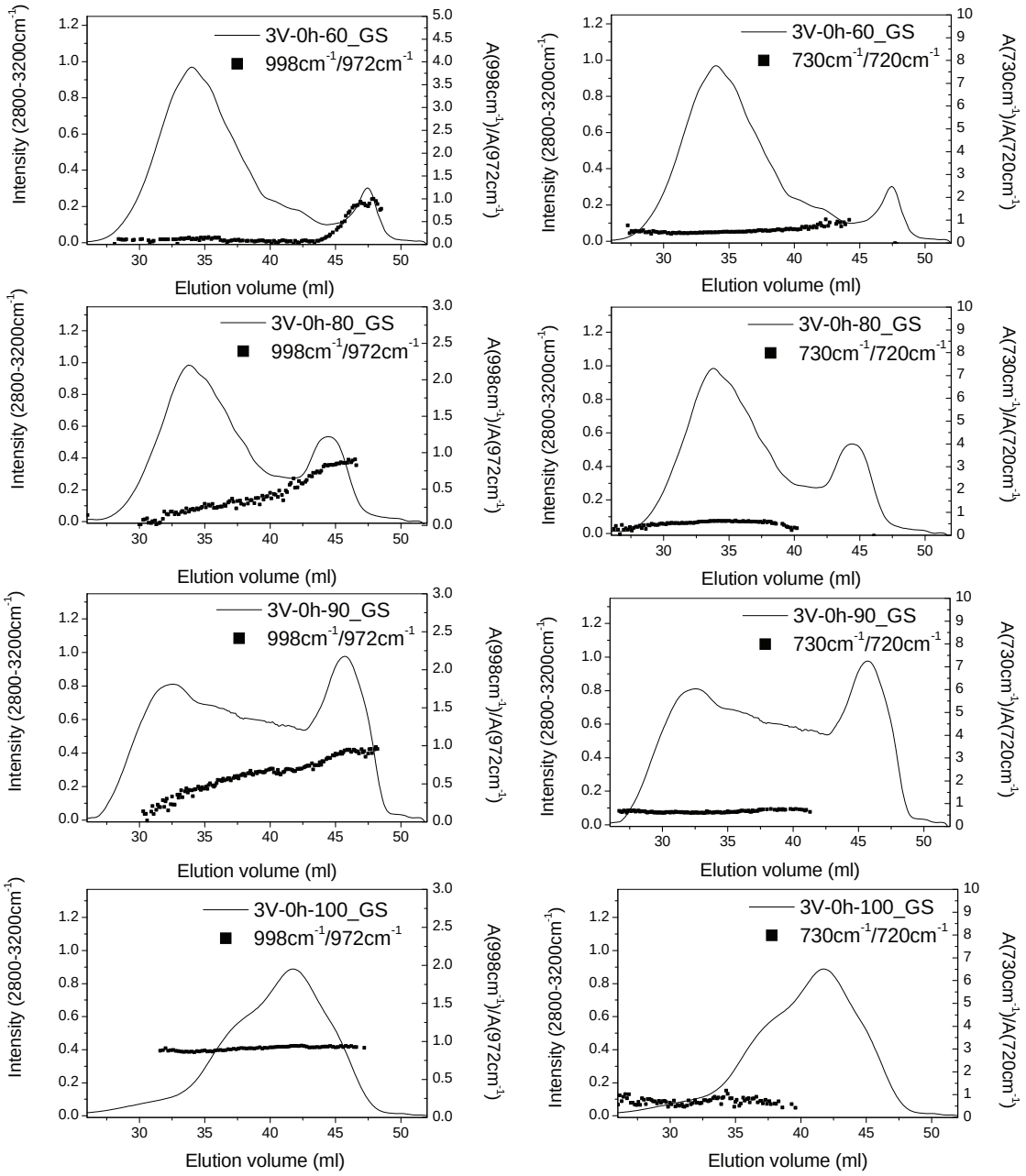

Figure 4.18: SEC-FTIR analysis of the ethylene and propylene crystallinity distributions within the 60ºC, 80ºC, 90ºC and 100ºC TREF fractions of sample 3V-0h.

The 80ºC and 90ºC fractions both show a gradual increase in the 998cm^{-1}/972cm^{-1} ratio across the bimodal elution volume curve, with the highest value reached across the higher elution volume component where PP homopolymer is found. The 80ºC and 90ºC fractions also display ethylene crystallinity only within the lower elution volume component of the distribution, where EPC elutes. It is therefore concluded that, within these fractions, both crystalline ethylene and propylene is found within the EPC phase, while PP of a higher crystallinity is found within the higher elution volume, PP homopolymer component. The two melt endotherms present in the DSC heating curve of these fractions is therefore representative of crystalline ethylene of the EPC phase melting at the lower of the

two melting temperatures, with the propylene segments of the EPC, as well as the homopolymer phase, melting at higher temperatures.

The 100ºC fraction, which consists mainly of PP homopolymer with a very small percentage EPC, exhibits a more or less uniform propylene concentration across the Gram-Schmidt curve. The value for the 998 cm^{-1}/972 cm^{-1} ratio is similar to that observed on the higher elution volume end of the PP homopolymer component of the preceding fractions, with only a slightly lower value present on the lower elution volume end shoulder where the CH_3/CH_2 ratio has indicated the EPC to elute. It is also only within this low elution volume shoulder of the Gram-Schmidt plot that any crystalline ethylene is detected. These results on the ethylene and propylene crystallinity determined by SEC-FTIR appear to agree well with the compositional information obtained by SEC and the thermal behaviour of the fractions detected by DSC. The propylene (1376 cm^{-1}/1462 cm^{-1}) and ethylene content (720 cm^{-1}/1163cm^{-1}) of the 30, 110 and 120ºC fractions were determined by the same SEC-FTIR procedure as described for the preceding fractions and the results are presented in Figure 4.19.

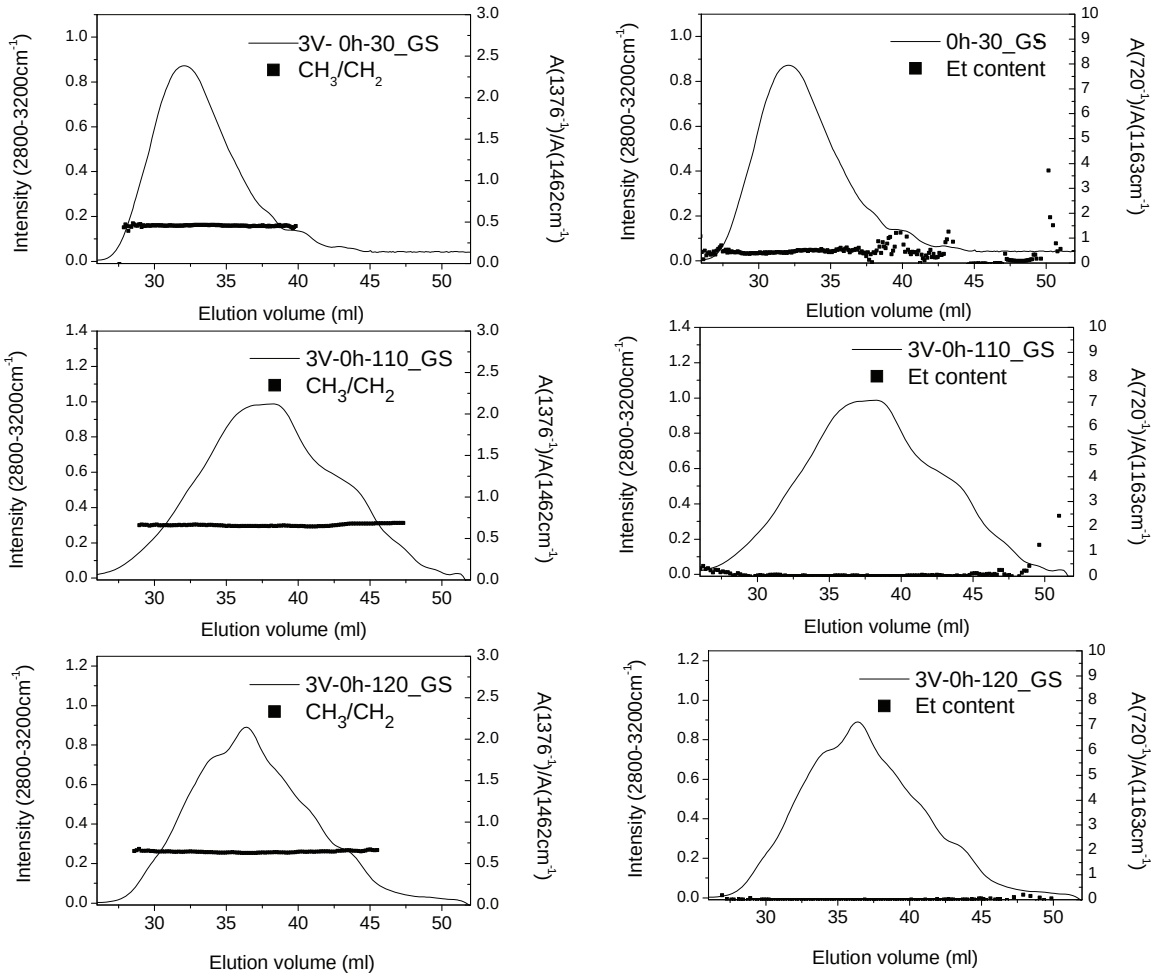

Figure 4.19: SEC-FTIR analysis of the ethylene and propylene contents distributions within the 30ºC 110ºC and 120ºC TREF fractions of sample 3V-0h.

The 30ºC fraction, which consists mainly of EPR, shows uniform concentration profiles for both ethylene and propylene across the main elution volume curve, with a decrease in the ethylene content on the larger elution volume side, where atactic PP is expected to elute. The 110 and 120ºC fractions are known to consist almost exclusively of iPP, which is also reflected in the uniform CH_3/CH_2 ratio across the elution volume curve of these two fractions, and the ethylene content profiles approaching 0. The crystallinity of both monomers was also profiled across the elution volume curves of these fractions and the results appear in Figure 4.20. In the 30ºC fraction ethylene crystallinity seems to decrease slightly towards larger elution volumes, with a substantial decrease at the largest elution volume end of the curve, where atactic PP elutes. No 998 cm^{-1} band was present across the entire Gram-Schmidt plot, indicating the absence of any crystalline propylene within this fraction. It can, therefore, be concluded that the crystallisation and melting transitions visible in the DSC result of this fraction, originate from low crystallinity polyethylene alone.

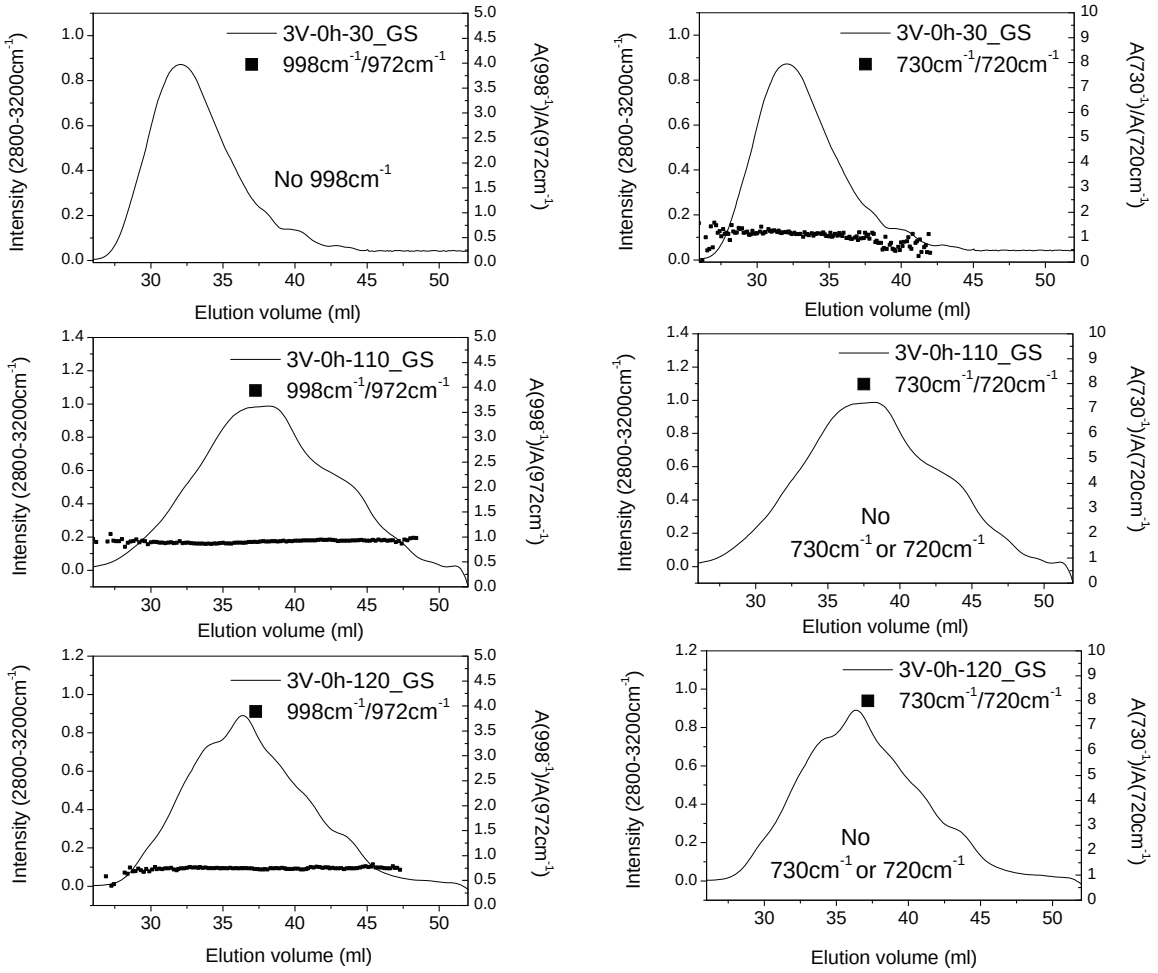

Figure 4.20: SEC-FTIR analysis of the ethylene and propylene crystallinity distributions within the 30ºC 110ºC and 120ºC TREF fractions of sample 3V-0h.

The 110 and 120ºC fractions are known to consist mainly of iPP, which is reflected in their uniform propylene crystallinity profiles across the elution volume curve of both. Ethylene crystallinity profiles

were not constructed for these fractions, due to the absence of the ethylene bands at 730 cm^{-1} and 720 cm^{-1}.

Analysis of the TREF fractions of the undegraded 3V copolymer by SEC, FTIR, DSC, ^{13}C-NMR and SEC-FTIR revealed the 30ºC fraction to consist of EPR and atactic PP, the 60 and 80ºC fractions contain transition EPC copolymers consisting of shorter, low crystallinity segments of ethylene and propylene, as well as low isotacticity PP. The 90 and 100ºC fractions contain 'blocky EPC copolymers' with longer crystallisable segments of ethylene and propylene, as well as low isotacticity PP homopolymer. The 110 and 120ºC fractions consist mainly of isotactic PP with a very small amount of ethylene homopolymer. The 130ºC fraction is expected to be similar in composition to the two foregoing fractions, therefore, the weight percentage of this fraction is included in the total weight percentage of material eluting within the highest (110–130ºC) elution range. The weight percentage of material collected within each of the 4 major elution ranges, is presented in Table 4.7.

Table 4.7: Weight percentages of the 4 major fractions constituting sample 3V

T_e	30ºC	(60–80ºC)	(90–100ºC)	(110–130ºC)
Sample	**EPR + aPP**	**'Transition' EPC + low isotacticity PP**	**'Blocky' EPC + higher isotacticity PP**	**Isotactic PP + hPE**
3V-0h	9.90	6.83	8.86	74.72

It can be seen here that the highest eluting fractions consisted mostly of isotactic PP, account for almost 75% of the bulk sample, with the EPR and atactic PP being the second largest component at 10% and those fractions consisting of the transition and blocky EPC copolymers and low isotactictiy PP, constitute only 6.83 and 8.86% of the total sample mass, respectively. This explains why bulk characterisation techniques mostly reflect the behaviour of the iPP phase upon degradation and emphasises the fact that fractionation and hyphenation of techniques are needed in order to study the degradation behaviour of all morphologies present.

4.1.4 TREF results for the degraded 3V samples

After oven ageing, degraded samples were re-crystallised according to the TREF crystallisation step described in Section 3.3.5 of the experimental chapter, after which fractions of the degraded samples were collected at the same elution temperatures used in the fractionation step of the undegraded sample in the previous section. In Figure 4.21 the weight fraction per temperature increment ($W_i\%/\Delta T$) of the undegraded 3V copolymer is compared to those of the same copolymer degraded for 40, 65 and 90 hours respectively. A shift in the peak dissolution temperature is observed from 120ºC in the undegraded and only slightly degraded samples (3V-40h) to 110ºC in the samples degraded for 65 and 90 hours. This shift also indicates the selective degradation of the higher isotacticity fraction which was observed in the CRYSTAF results in Section 4.1.3.2. The shift in dissolution temperature towards

lower temperature and the decrease in its intensity, together with the increase in the amount of material eluting at the lowest elution temperature (soluble fraction) also agrees with the CRYSTAF results obtained in Section 4.1.3.2.

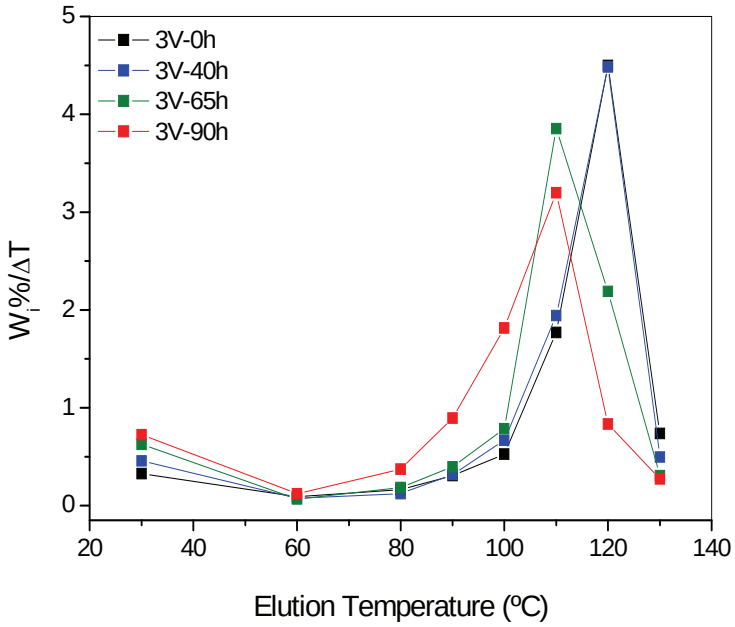

Figure 4.21: TREF weight fraction per temperature increment curves ($W_i\%/\Delta T$) for the undegraded and degraded 3V samples.

Both these techniques, therefore, indicate changes in the solution crystallisation of the impact PP copolymer upon degradation. TREF, however, provides the advantage of obtaining additional information on the structural or compositional changes caused by degradation, through off-line analysis of the collected fractions by other techniques. Figure 4.22 displays the change in the weight percentage of each TREF fraction as a function of degradation time, where the bulk sample was fractionated after 0, 40, 65 and 90 hours of degradation.

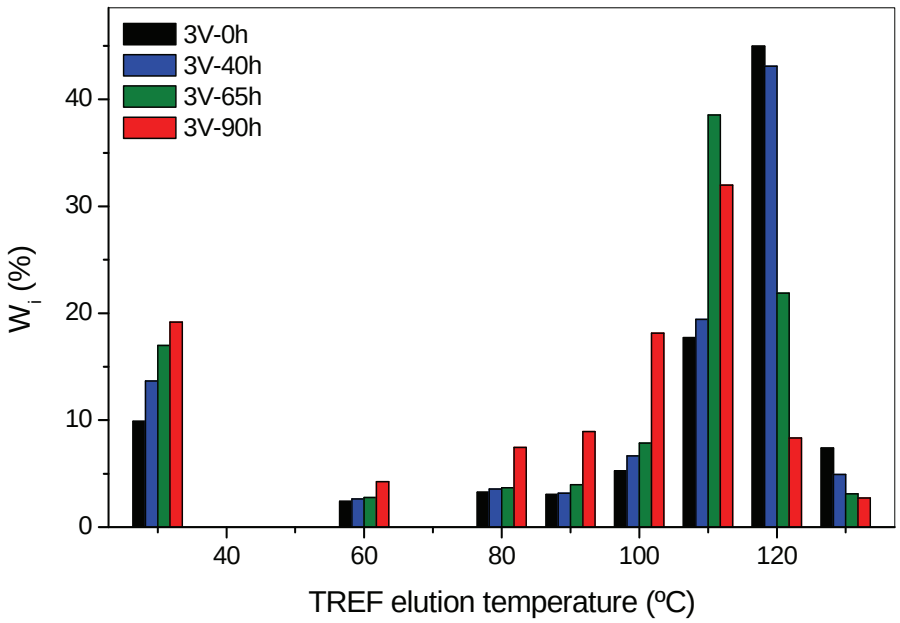

Figure 4.22: Changes in the weight percent (W_i%) of all TREF fractions of sample 3V obtained after degradation times of 0, 40, 65 and 90 hours.

The fractions eluting from 30 to 100ºC show an increase in weight percentage with ongoing degradation time, whereas a decrease is observed for the 120 and 130ºC fractions. The 110ºC fraction shows an initial increase in weight percentage from degradation times of 0 to 65 hours, followed by a decrease in the sample degraded for 90 hours. These changes are also illustrated by the line graphs in Figure 4.23, where the changes in weight percentage of each fraction with ongoing degradation time can be seen more clearly.

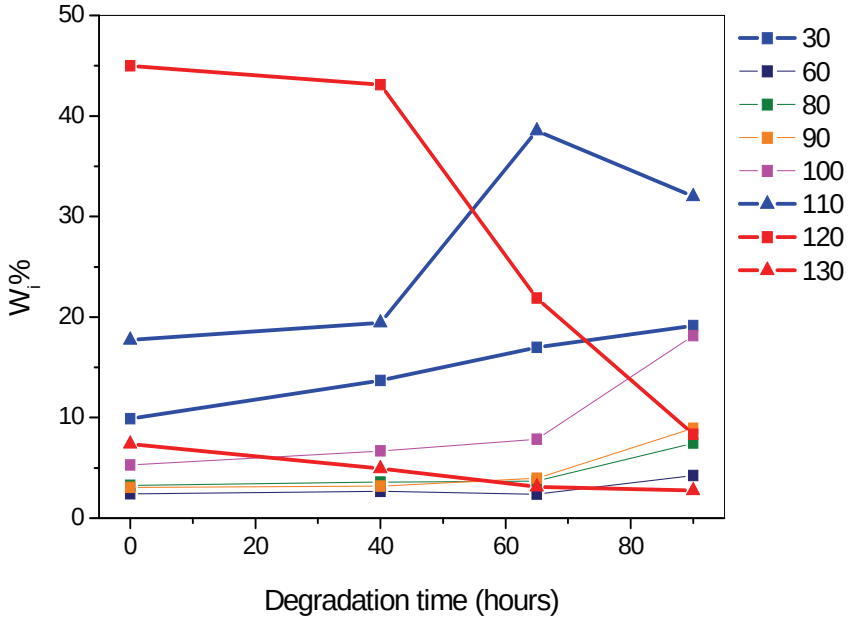

Figure 4.23: Weight percent (W_i%) changes of all TREF fractions as a function of degradation time.

The 120ºC fraction, which comprises the largest weight fraction of sample 3V, shows the most significant decrease in weight percent with ongoing degradation time, followed by the 130ºC fraction. The most significant increases in weight percentage is observed in the 30 and 110ºC fractions, whereas a more gradual increase is seen in the weight percentage of all fractions eluting from 60 to 100ºC for degradation times up to 65 hours. A more significant increase in the amount of material eluting in these fractions is only observed at a degradation time of 90 hours. The increase in the amount of material eluting at 30ºC, together with the decrease in the 120 and 130ºC fractions also suggests that the fractions with higher isotacticity are more susceptible to degradation.

From a theoretical point of view, the chemical composition effect accounts for PP being more degradable than PE, due to the presence of numerous highly reactive tertiary C-H bonds which can be cleaved in the presence of oxygen [76-78], despite its crystalline nature. From the analysis of the TREF fractions of the undegraded material, it was concluded that the highest eluting fractions are those consisting of isotactic PP with only a very small amount of PE homopolymer. The initial increase in the amount of material eluting in the 110ºC fraction suggests that some portion of the original 120ºC and 130ºC fractions was modified by degradation to a relatively small extent to ensure its elution at 110ºC, rather than at 30ºC at degradation times up to 65 hours. At 90 hours, however, a considerable portion of the 110ºC fraction has been modified to an extent where it is no longer crystallisable at 110ºC, and is presumed to elute at lower elution temperatures, as indicated by the decrease in the amount of material eluting within this fraction and the increase in the amount of material eluting at lower temperatures.

The TREF results therefore suggest that the PP fraction is more susceptible to degradation than the amorphous EPR and the range of semi-crystalline EP copolymers, and it's crystallisability is significantly affected by degradation. The preferential degradation of the PP phase in impact PP copolymers, has also been demonstrated by other authors[54, 76, 77, 79], but it is still unclear as to how the EPR and segmented copolymers are affected by the degradation process and whether it is only the PP being modified. The TREF fractions of the samples degraded for 40, 65 and 90 hours, obtained by fractionation after degradation, will now be analysed by SEC, SEC-FTIR and ^{13}C-NMR and compared to those of the undegraded copolymer, to obtain more detailed information on the compositional changes occurring in the different fractions upon degradation and to better understand the changes in crystallisability of the bulk sample observed by the TREF analysis of degraded samples.

4.1.4.1 TREF-SEC results for the degraded 3V samples

The molecular weight distributions of the TREF fractions of the undegraded 3V-0h sample have been presented in Section 4.1.3.6. Figure 4.25 shows the SEC curves for the undegraded and degraded bulk 3V samples, each with the individual SEC distributions of their TREF fractions. The SEC molecular weight distribution curve of the bulk 3V sample shifts towards lower molecular weight with increasing degradation times from 0 to 90 hours as has been demonstrated in Figure 4.4. Shifts in the

SEC curves of the individual TREF fractions of each sample are also observed. Individual molecular weight distributions are also seen to shift towards lower values. The bimodal distributions show an increase in the intensity of the lower molecular weight component with ongoing degradation time, with an accompanying decrease in the intensity of the higher molecular weight distribution. The higher molecular weight component shows an initial increase in molecular weight after a degradation time of 40 hours, followed by a decrease at longer degradation times. The lower molecular weight component shows molecular weight shifts even at 40 hours. Overlays of the molecular weight distribution changes of each TREF fraction, as a function of degradation time, are presented in Figure 4.25.

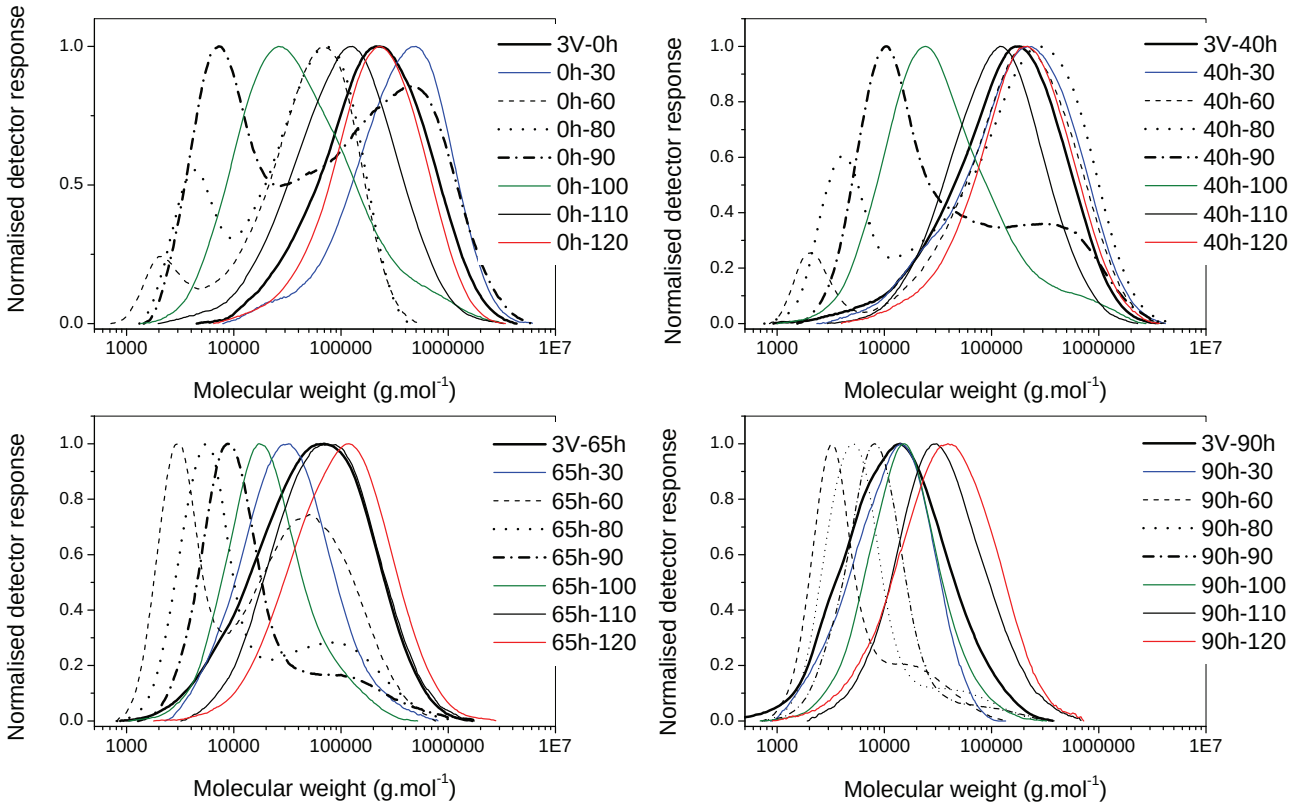

Figure 4.24: SEC curves for the bulk undegraded and degraded 3V samples and the individual SEC distributions of the TREF fractions of each.

The 30, 110 and 120ºC fractions show a definite shift towards lower molecular weight with ongoing degradation of the bulk 3V sample. The high molecular weight side of the 100ºC fraction also shifts towards lower values. The molecular weight curves of the degraded transition and blocky copolymer fractions (60–90ºC), however, display more complicated changes, where, in general, the MWD of the lower molecular weight component is seen to remain constant, whereas a shift in the distribution of the higher molecular weight component is observed. It has to be taken into account that the shifts observed here are not those of the isolated fractions being degraded, but rather represent the changes occurring in the bulk sample upon degradation, since re-crystallisation and fractionation was performed after degradation. It also has to be remembered that, upon degradation, some material shift into other

fractions due to changes in crystallisability, therefore the material giving rise to the molecular weight distribution in the 0h sample of a certain fraction, may not be of the same chemical composition as the fraction eluting at the same temperature within the 3V-90h sample after TREF re-crystallisation and fractionation.

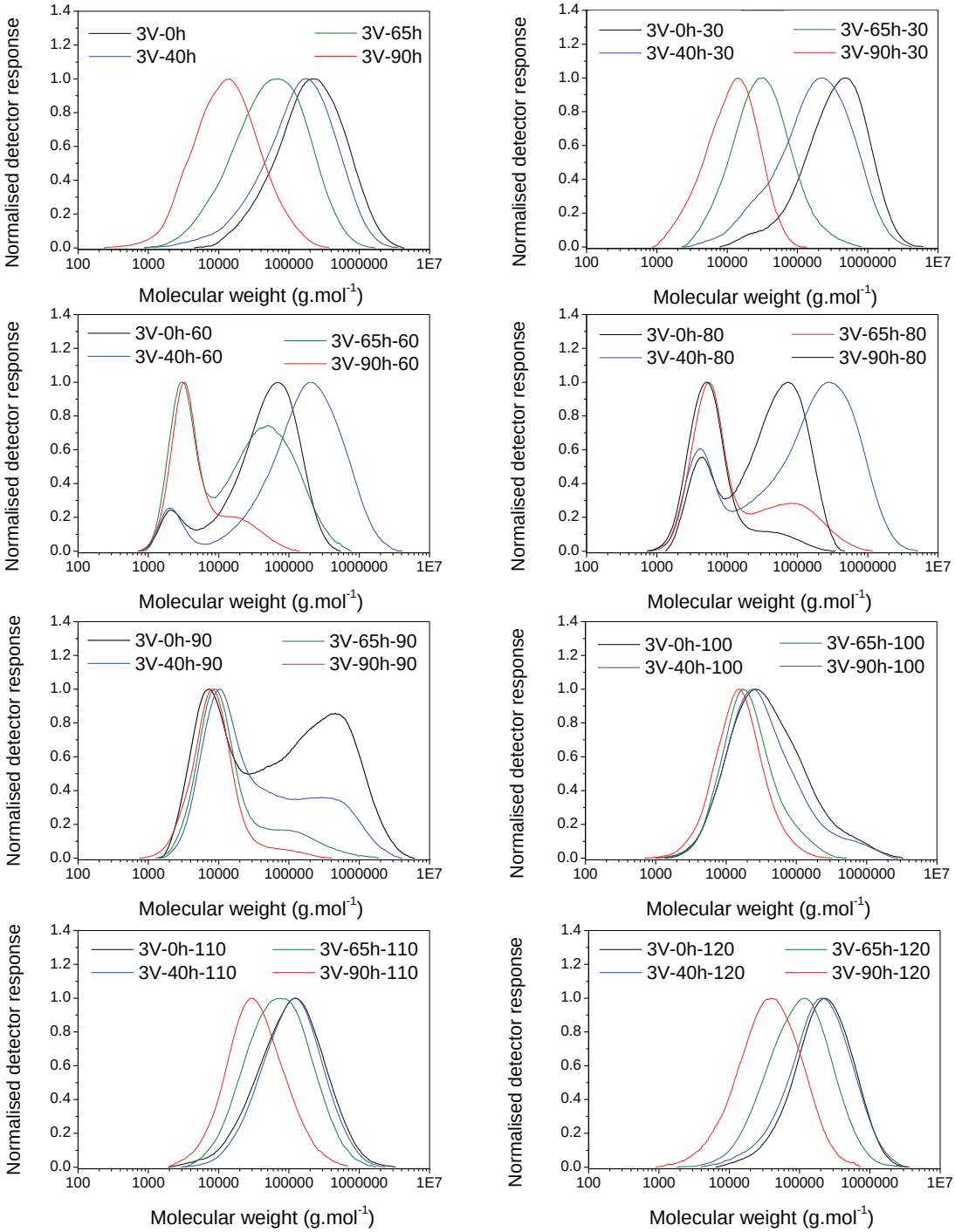

Figure 4.25: Changes in the SEC curves of the bulk 3V samples and their TREF fractions with ongoing degradation times.

In Figure 4.25 the shift in the molecular weight curves of the 100, 110 and 120ºC fractions can be ascribed to the comonomer content and tacticity of the undegraded sample (0h), which is considerably higher than that of the preceding fractions. According to theory, the 30ºC fraction is expected to be extremely stable, since it has the highest ethylene content and lowest isotacticity of all the fractions. This fraction, however, exhibits the largest shift in molecular weight with ongoing degradation time. From TREF analysis we have observed a considerable increase in the amount of material eluting at 30ºC with ongoing degradation times, with an accompanying decrease in the amount eluting at 110 and 120ºC. This shift in the molecular weight curve is therefore expected not only to be caused by changes in the EPR originally present in the 30ºC fraction of the undegraded material, but mainly by the fractions of higher elution temperatures (110ºC, 120ºC) that have moved into the soluble fraction as a result of considerable modification of their structure, that has rendered them non-crystallisable.

As has been mentioned before, more complicated changes in molecular weight are observed for the 60-90ºC fractions, where the lower molecular weight component of the bimodal distribution remains at more or less the same molecular weight, whereas the higher molecular weight component shows noticeable shifts. ^{13}C-NMR revealed these fractions to consist of almost equal amounts of ethylene and propylene, and isotacticity values between that of the 30ºC fraction and that of the 100–120ºC fractions. DSC and FTIR have also further indicated that these fractions are segmented or blocky copolymers of ethylene and propylene. As mentioned before, the two components in the bimodal distribution of these fractions are expected to be EPC and PP homopolymer, but further analysis is needed to confirm the chemical composition of the overlapping distributions.

From these results, it can be seen that off-line coupling of TREF and SEC supplies information on the molecular weight shifts occurring in the individual fractions obtained by fractionation after degradation of the bulk 3V sample. Conventional SEC only gives an average molecular weight result for the bulk material, without any indication of the susceptibility of the different components to oxidation. The TREF-SEC technique does, however, not supply information on the distribution of degradation products or the chemical composition across the molecular weight distribution of each fraction. The next step in the development of the multi-dimensional analysis technique for studying the degradation of impact PP copolymers is, therefore, the hyphenation of TREF with SEC-FTIR. This will be useful especially for determining the distribution of degradation products across molecular weight distributions and for confirming compositional changes within fractions as a result of degradation.

4.1.4.2 TREF-(SEC-FTIR) results for the degraded 3V samples

The SEC-FTIR results of the TREF fractions obtained by fractionation of the bulk samples after degradation will now be discussed. In the following figures the concentration of degradation products was calculated by the ratio of the carbonyl band area (1804–1580cm^{-1}) and that of the CH band in the region 3005–2787 cm^{-1}. The propylene content was quantified by the ratio of the CH_3 and CH_2 bendings at 1376 cm^{-1} and 1462 cm^{-1}, respectively [23, 24, 64]. In Section 4.1.3.9 it was proven that the

1376 cm^{-1} band is not the result of branching in PE and, therefore, only representative of PP units. Chain branching is, however, also known to occur during PE degradation,[80] therefore, the validity of using the 1376 cm^{-1} band as an indication of CH_3 groups in PP, was once again investigated by profiling the ethylene contents across the Gram-Schmidt plots of the degraded 80ºC TREF fraction. The 720 cm^{-1}/1163 cm^{-1} band area ratio was once again used to quantify the ethylene contents within this blocky copolymer fraction. The comparison of the propylene (1378 cm^{-1}/1462 cm^{-1}) and ethylene contents (1163 cm^{-1}/720 cm^{-1}) within the 80ºC fraction of the undegraded and degraded samples, are presented in Figure 4.26.

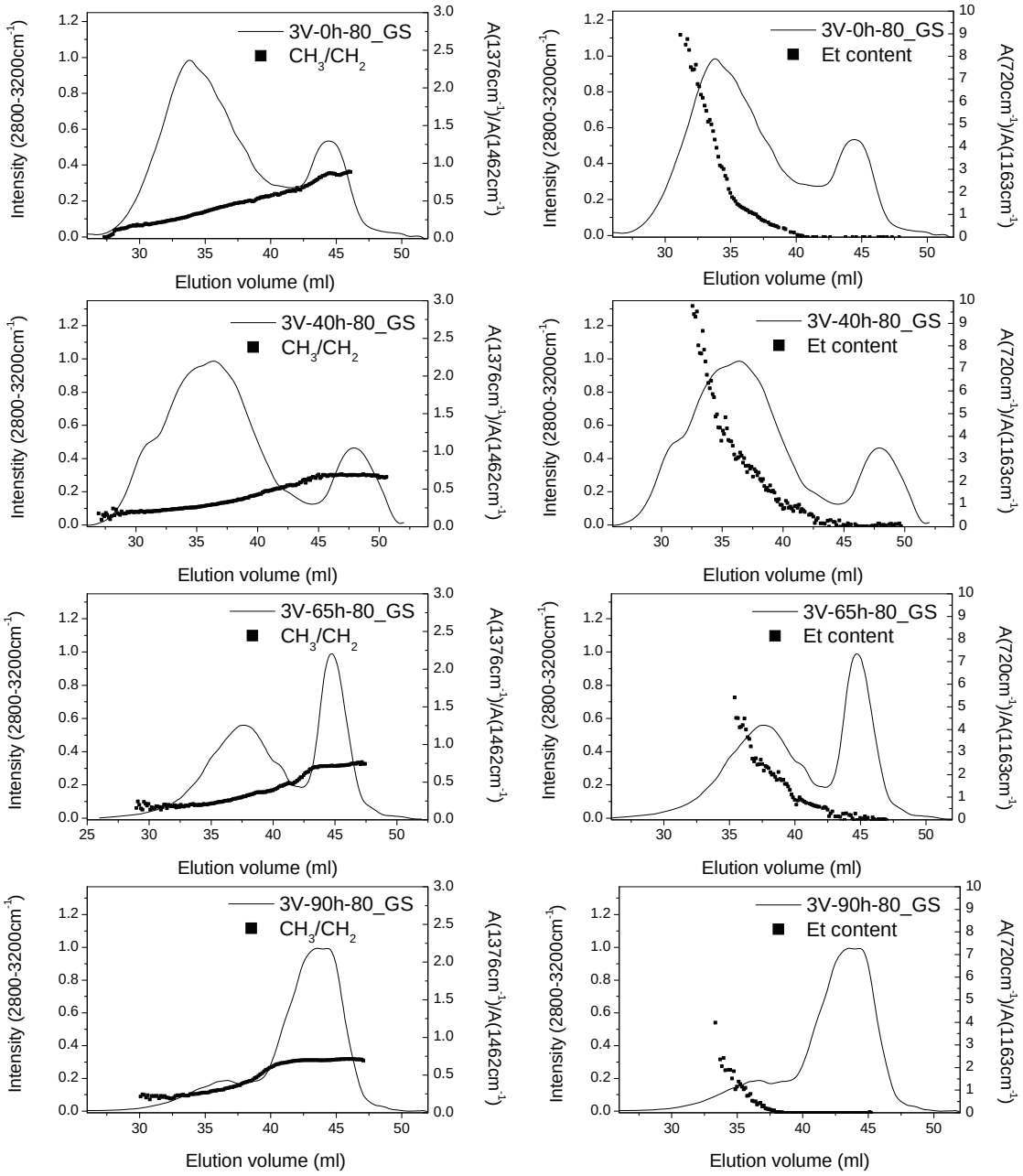

Figure 4.26: Comparison of the ethylene and propylene concentration profiles within the 80ºC fraction of the undegraded and degraded 3V copolymer samples.

The ethylene and propylene content profiles for the 80ºC fraction of the undegraded sample (3V-0h) have already been discussed in Section 4.1.3.9, where it was concluded that the lower elution volume component contains semi-crystalline EP copolymers, whereas the higher elution volume component consists of PP homopolymer exclusively. Within the samples degraded for 40, 65 and 90 hours, the gradual increase in propylene content towards the higher elution volume component originally visible within the undegraded sample, still exists, with this ratio reaching a plateau across the higher elution volume component in the degraded samples. This indicates that, even in the degraded samples, only PP is to be found within this component of the bimodal distribution. When comparing this to the ethylene content profiles of this fraction, it is seen that, even after degradation, this higher elution volume component still contains no ethylene. Therefore, the CH_3 groups present here, are not part of branched PE within this component and must be inherent to the PP units only. The 1378 cm^{-1}/1462 cm^{-1} ratio will, therefore, be used as an indication of the propylene content in all subsequent SEC-FTIR results of the degraded fractions as well.

The carbonyl concentration and propylene content will now be profiled across the molecular weight distribution of each TREF fraction in the undegraded and degraded samples. The distribution of degradation products across the molecular weight distribution of each fraction will be studied, together with changes in its chemical composition. The SEC-FTIR results of the highest eluting iPP fractions (120 and 110ºC) will be presented first, followed by that of the 60-100ºC fractions (co-eluting low isotacticity PP and EPC), and finally, that of the EPR-rich 30ºC fraction. Figure 4.27 shows the SEC-FTIR results obtained for the 120ºC fraction in samples degraded for 0, 40, 65 and 90 hours, obtained after re-crystallisation of the bulk, degraded samples and fractionation by TREF.

The Gram-Schmidt curve shifts to higher elution volumes from 0 to 90 hours, which is in agreement with the decrease in molecular weight observed in the SEC results for this fraction (Section 4.1.4.1). As degradation proceeds, chain scission of longer, entangled chains renders shorter molecules that are capable of entering some of the pores in the column packing material from which they were previously excluded in their undegraded state. This leads to an increase in the elution volume necessary to elute these molecules. The Gram-Schmidt curves also broaden towards longer degradation times. There also seems to be a slight broadening in the SEC curves in Section 4.1.4.1, but the effect is much less pronounced. This is ascribed to the fact that a certain degree of spreading always accompanies the deposition onto the Germanium disc in the LC-Transform® interface.

In the 0 hours fraction a uniform CO/CH ratio distribution of value close to 0 is observed across the molecular weight distribution curve. In the 120ºC fraction of the sample degraded for 90 hours, this ratio curve is seen to have shifted to a slightly higher value across the entire distribution, with a marked increase at the higher elution volume end, indicating a higher concentration of degradation products within the lower molecular weight end of the curve. The ratio in the 40 and 65 hours samples also displays a uniform profile close to 0 across the entire molecular weight distribution, which indicates that only undegraded material remains in the 120ºC fraction of bulk samples degraded for 40 and 65 hours.

All degraded molecules containing substantial amounts of carbonyl functionalities have been rendered non-crystallisable, causing them to elute at lower temperatures, except at longer degradation times (90h), where carbonyls are clearly incorporated into chains, but they are still crystallisable and elute at 120ºC.

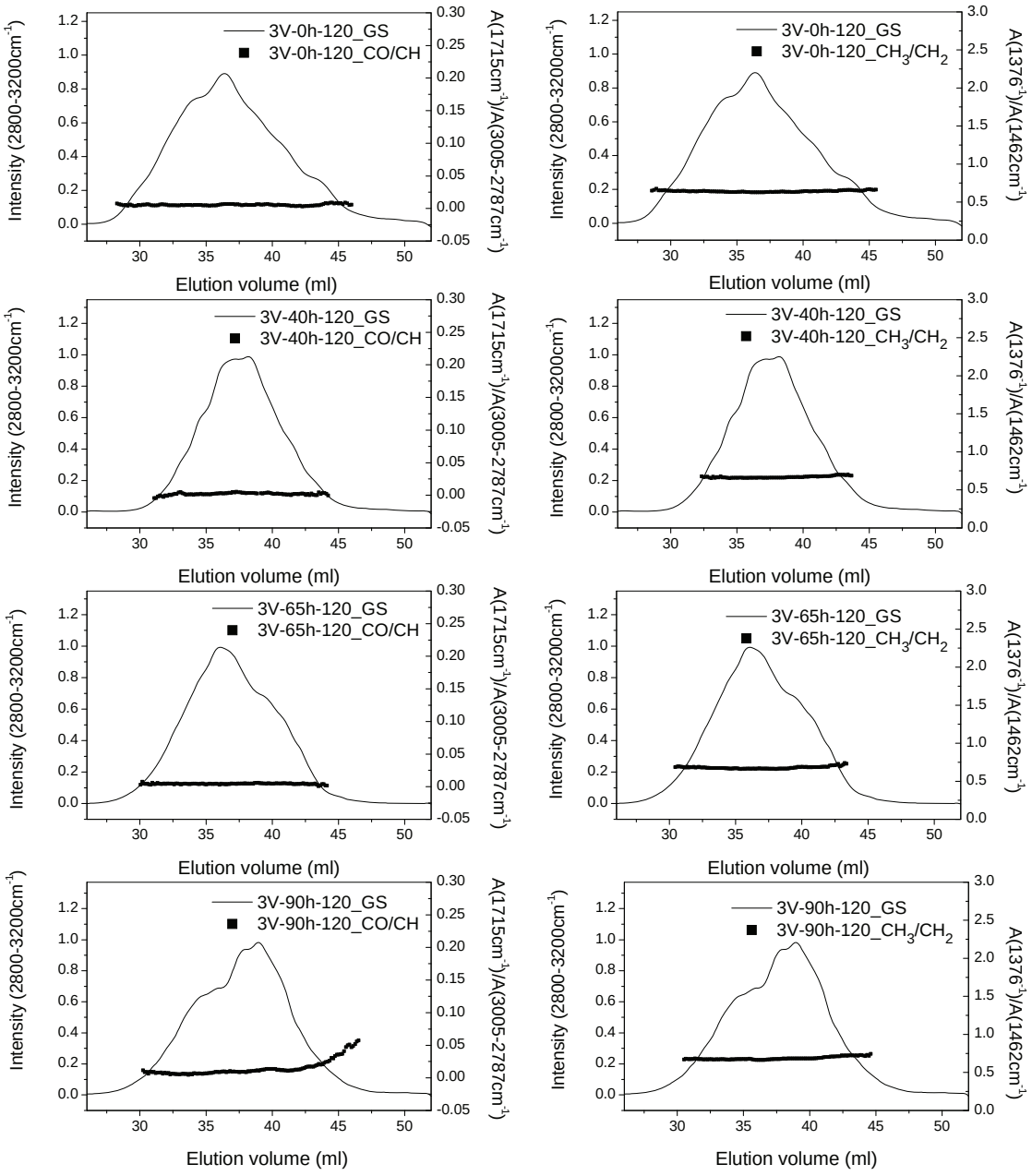

Figure 4.27: SEC-FTIR results for the 120ºC TREF fraction of sample 3V degraded for 0, 40, 65 and 90 hours, where fractionation was performed after degradation.

It has already been mentioned that the CH_3/CH_2 ratio gives an indication of the distribution of propylene across the molecular weight distribution of this fraction. This ratio appears to remain unchanged during all stages of degradation, i.e., there does not seem to be a significant change in the chemical composition of this fraction as a function of degradation. This ratio indicates that, even after

degradation, this sample still consists predominantly of PP, even though some part of the iPP phase is degraded preferentially. The ethylene concentration is presumed to be too low to have a marked influence on the CH_3/CH_2 ratio.

Individual FTIR spectra can be extracted from the Gram-Schmidt profile in order to examine the chemical composition at any point along the elution volume curve. The individual FTIR spectra at the maximum of the Gram-Schmidt curves of the 120ºC fraction in the undegraded sample and that degraded for 90 hours, appear in Figure 4.28.

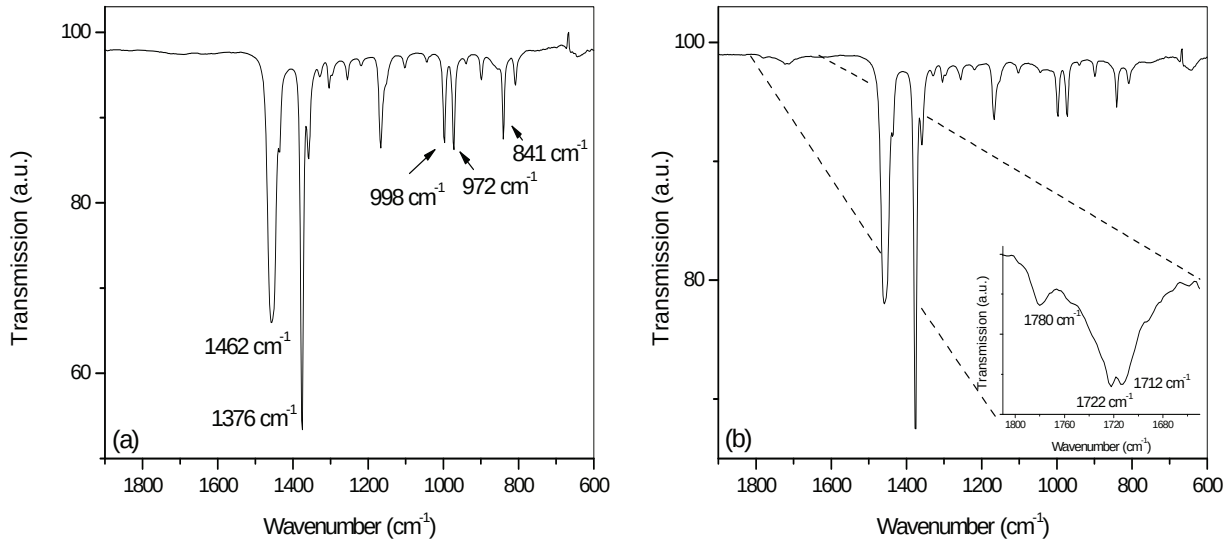

Figure 4.28: Individual FTIR spectra extracted from the Gram-Schmidt profiles of sample 3V-0h-120ºC(a) and sample 3V-90h-120ºC(b) at 36.2 ml and 38.9 ml, respectively.

The FTIR spectra in the 1900–600 cm^{-1} region of Figure 4.28 (a) and (b) are characteristic of isotactic PP. The absence of the 720 cm^{-1} and 730 cm^{-1} bands indicate that, even though the presence of ethylene is detected by ^{13}C-NMR, the concentration of long ethylene sequences is not high enough to be visible in the FTIR spectrum. The two spectra display a difference in the intensity of the carbonyl band in the area 1805–1580 cm^{-1}, which is reflected in the CO/CH ratio's in Figure 4.27, (3V-90h-120_CO/CH), already starting at this point along the distribution, although the most significant increase only occurs at the lower molecular weight edge of the Gram-Schmidt curve. The insert in Figure 4.28(b) is an enlargement of the carbonyl absorption area, where peak intensities are clearly visible at approximately 1780 cm^{-1}, 1722 cm^{-1} and 1712 cm^{-1}, corresponding to the main carbonyl functionalities formed during PP degradation.

Figure 4.29 shows the SEC-FTIR results for the 110ºC fraction in samples degraded for 0, 40, 65 and 90 hours, obtained after re-crystallisation and fractionation by TREF. The results for the 110ºC fraction are similar to that of the 120ºC, where the Gram-Schmidt plot is seen to shift towards slightly longer elution volumes at longer degradation times. Similar shifts in SEC curves were also observed for the 120ºC and 110ºC fractions in Section 4.1.4.1. A CO/CH ratio of approximately 0 is also observed up to

65 hours, whereas this ratio curve shifts to a higher value across the entire Gram-Schmidt plot at 90 hours, with a marked increase at the lower elution volume end. The CH_3/CH_2 ratio remains unchanged from 0 to 90 hours, as was also seen in the 120ºC fraction.

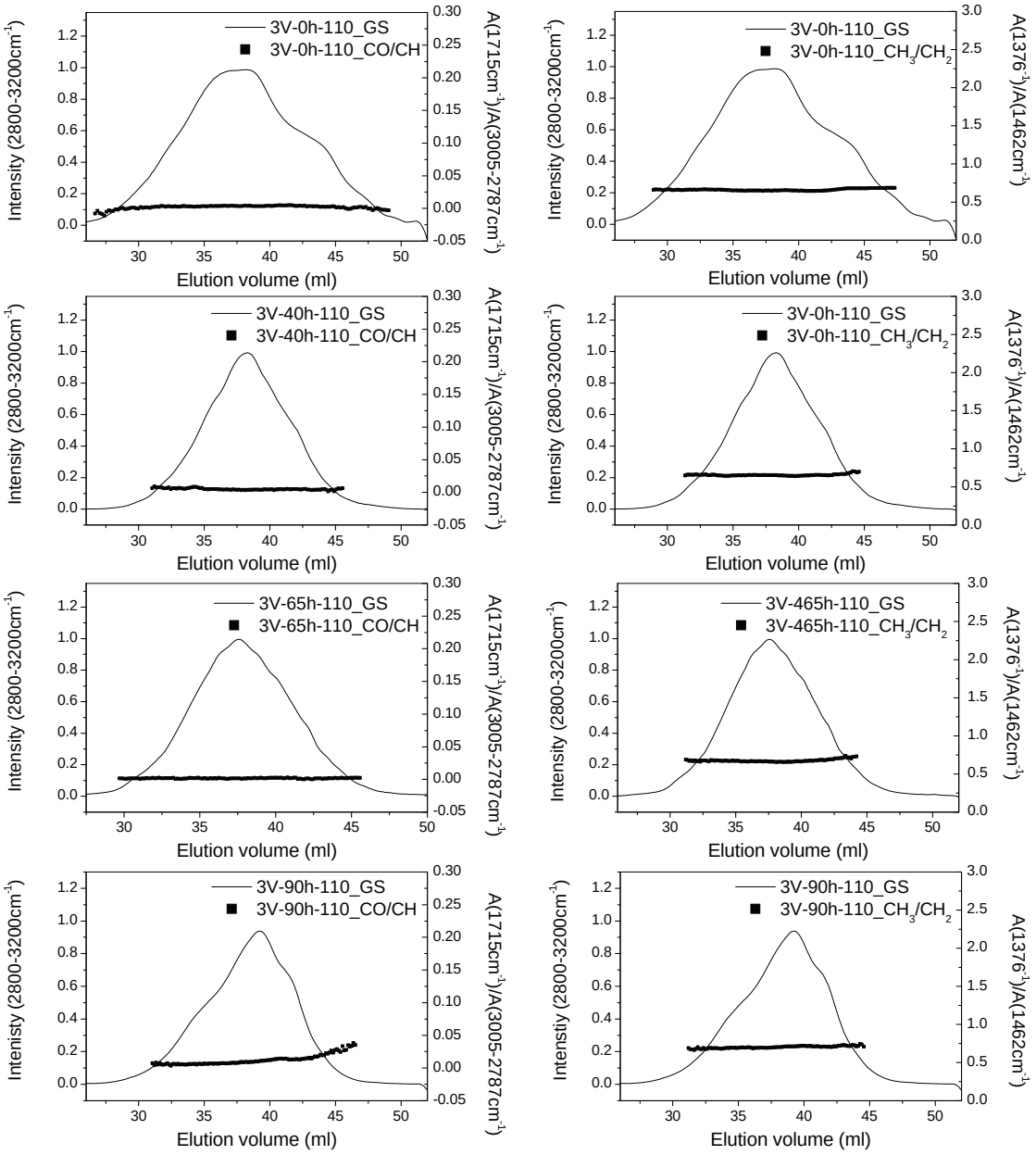

Figure 4.29: SEC-FTIR results for the 110ºC TREF fraction of sample 3V degraded for 0, 40, 65 and 90 hours, where fractionation was performed after degradation.

Next, the SEC-FTIR results of the blocky and segmented copolymer fractions were studied. The 80ºC fraction is presented first within this series to illustrate the changes occurring upon degradation within the fractions consisting of co-eluting low isotacticity PP and EPC. The SEC-FTIR results for the 80ºC fraction of the undegraded and degraded samples are presented in Figure 4.30.

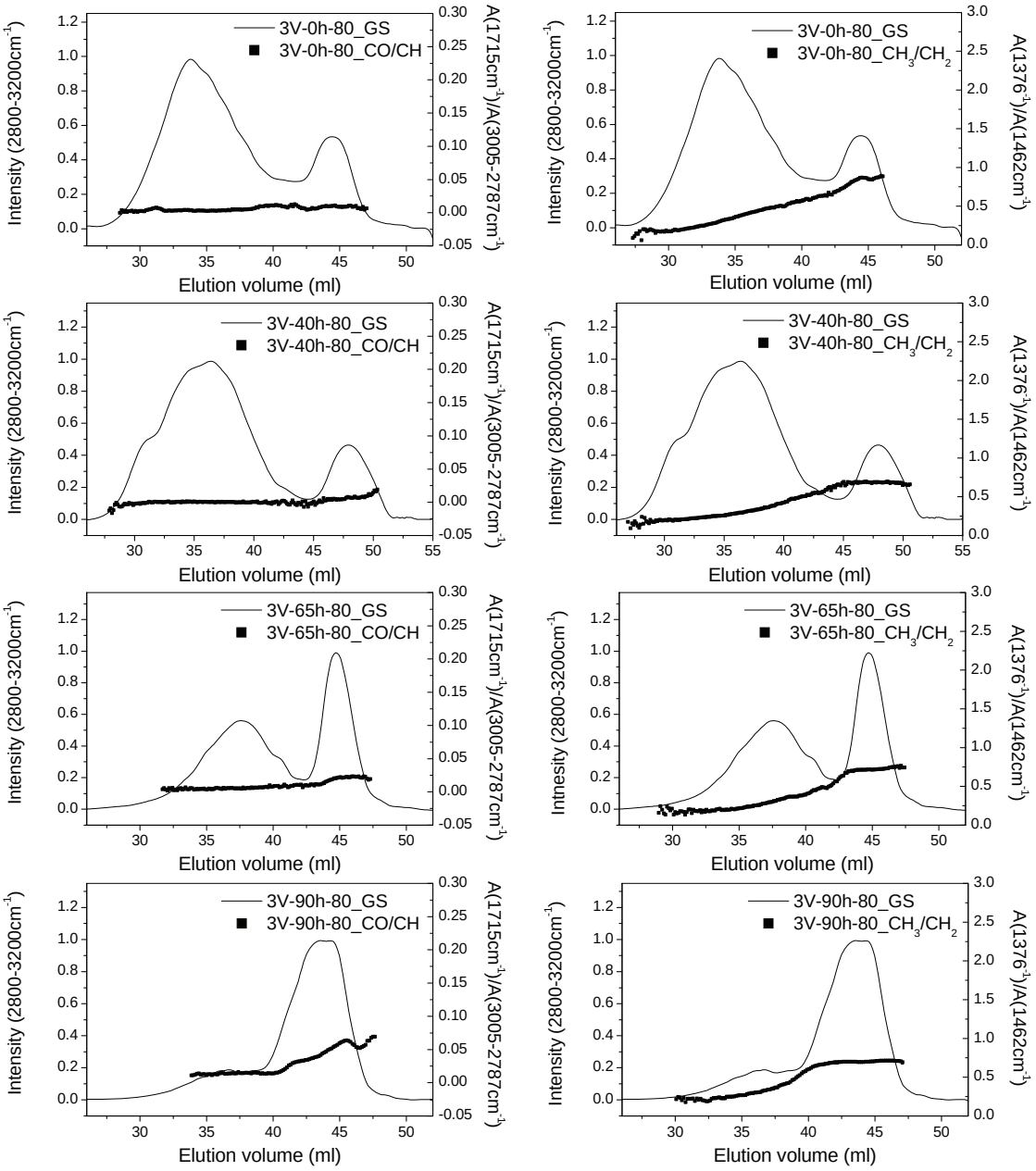

Figure 4.30: SEC-FTIR results for the 80ºC fraction of the 0h, 40h, 65h and 90h samples of copolymer 3V, obtained by TREF analysis after degradation.

The chemical composition of the bimodal molecular weight distribution of the 80ºC fraction of the undegraded sample was studied by SEC-FTIR in Section 4.1.3.9 and it was found that the lower elution volume component consists of semi-crystalline EP copolymers, which co-elute with low isotacticity PP homopolymer present within the higher elution volume component. With degradation times from 0 to 90 hours, the lower elution volume component is seen to shift towards larger elution volumes, whereas the higher elution volume component remains at an approximately constant elution volume. The intensity of the higher elution volume component also increases within the Gram-Schmidt profile with ongoing degradation times, whereas the lower elution volume component, which is the dominant component within the undegraded sample, is reduced to a very small intensity within the

sample degraded for 90 hours. The CH_3/CH_2 ratio which increases gradually towards the higher elution volume end of the undegraded sample, reaches a plateau which spreads across the entire higher elution volume component of the samples degraded for 40, 65 and 90 hours. The value for this ratio is approximately 0.65, which agrees with the value obtained for the CH_3/CH_2 ratio within the isotactic PP fraction (120ºC). The increase in the amount of PP eluting within this component might less likely be caused by degraded PP originally present within the lower elution volume EPC component of this fraction that has been reduced in molecular weight by chain scission, or more likely by isotactic PP from higher eluting fractions (120ºC, 130ºC of sample 3V-0h) that has been degraded and rendered less crystallisable upon re-crystallisation. TREF analysis indicated an increase in the weight percentage of this fraction from 3.26% in the undegraded material to 7.46% in the sample degraded for 90 hours. This increase was accompanied by a considerable decrease in the amount of material eluting at 120 and 130ºC in the degraded sample, therefore the SEC-FTIR result suggests that the iPP phase degrades preferentially and elutes at lower temperatures in the TREF experiment after re-crystallisation of the degraded chains.

The carbonyl concentration of approximately 0 is observed across the entire bimodal molecular weight distribution of the sample labelled 3V-0h-80 hours. A slight increase in this profile is seen at the lower molecular weight side in the sample degraded for 40 hours, and becomes more pronounced across a larger portion of the higher elution volume component in the 65 and 90 hours samples. The drastic increase in the slope of the ratio curve indicates that a considerable amount of carbonyl-containing degradation products are present within this lower molecular weight component of the 80ºC fraction of the sample degraded for 90 hours, although the CO/CH ratio across the higher molecular weight component also increases from approximately 0.003 to values between 0.0127 and 0.0159 in the sample degraded for 90 hours. This component continuously elutes in the 80ºC fraction with ongoing degradation times, but its intensity (amount of material) appears to decrease due to PP degradation products moving into this fraction at longer degradation times.

Figure 4.31 shows an overlay of the individual infrared spectra obtained at the maxima (34.0 ml and 44.1 ml) of the two components of the bimodal distribution of the 80ºC fraction of the undegraded 3V sample. It is clear that the spectrum at 34.0 ml contains a considerable amount of long ethylene segments, some of which are crystallisable, as seen by the strong absorption band present as a doublet at 720cm^{-1} and 730cm^{-1}. Bands associated with PP, i.e., 972 cm^{-1} and 998 cm^{-1} are also present. The spectrum at 44.1 ml is characteristic of PP with bands at 998 cm^{-1}, 972 cm^{-1} and 841 cm^{-1}. These spectra confirm that the two components in the bimodal distribution are EPC and PP homopolymer.

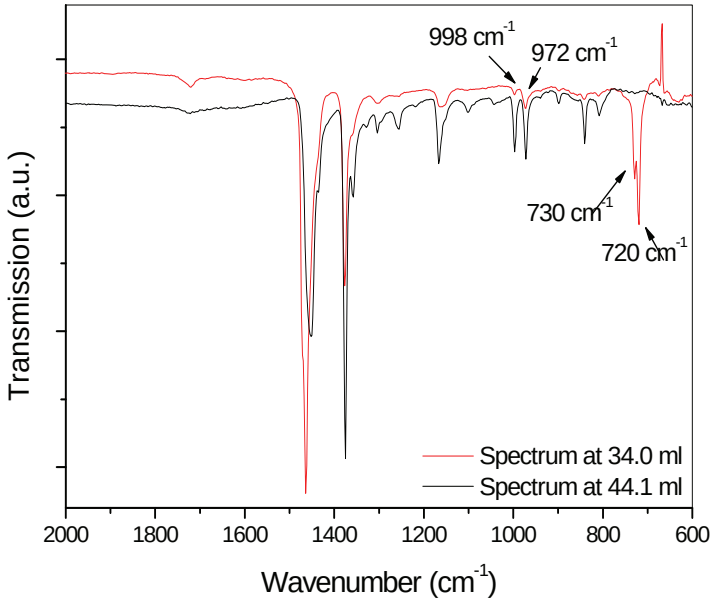

Figure 4.31: Individual FTIR spectra extracted from the Gram-Schmidt profile at the maxima of the two peaks in sample 3V-0h-80ºC.

The spectra extracted from the maxima of the two components in the Gram-Schmidt of the 80ºC fraction of the sample degraded for 90 hours, are presented in Figure 4.32.

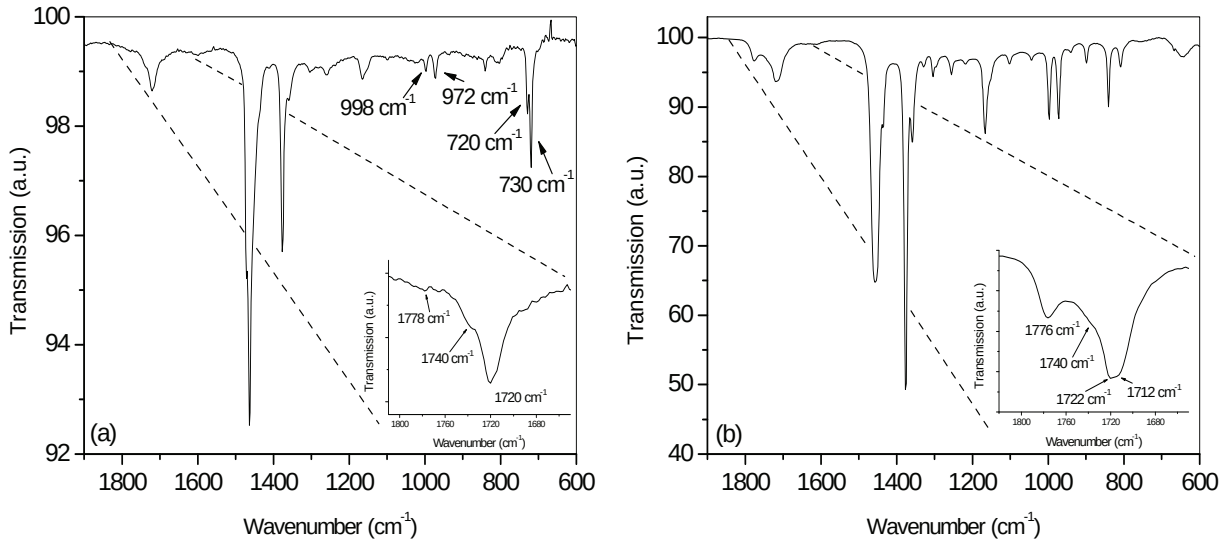

Figure 4.32: Individual FTIR spectra extracted at 36.7 ml (a) and 43.8 ml (b) of the Gram-Schmidt profile of sample 3V-90h-80ºC.

The spectrum at 36.7 ml contains bands associated with both ethylene and propylene, with a considerable amount of both longer and crystallisable ethylene segments, as indicated by the doublet at 720 cm^{-1} and 730 cm^{-1}. The spectrum at 43.8 ml seems to contain only PP, with no bands at 720 cm^{-1} or 730 cm^{-1} to indicate the presence of longer or crystallisable ethylene sequences. The spectrum at 36.7 ml also contains a sharp carbonyl band with a maximum intensity at approximately

1722 cm^{-1}, which is characteristic of ketones, the major primary degradation product formed in PP, although the narrowness of the carbonyl region and the negligible γ–lactone band at 1780 cm^{-1} might indicate that carbonyl groups have been inserted into PE chains too. The carbonyl band is considerably broader in the spectrum at 43.8 ml, with definite bands at 1722 cm^{-1} and 1776 cm^{-1}, the latter which is associated with γ-lactones, a degradation product formed during degradation in PP. The presence of a significant carbonyl band in both spectra indicates that at 90 hours, carbonyl functionalities are present across both components of the bimodal distribution. The transition and blocky copolymer fractions (60–100ºC) all showed bimodal molecular weight distributions in SEC, although the higher molecular weight component was reduced to a shoulder in the 100ºC fraction. The SEC-FTIR results for the 60 and 90ºC fractions were similar to those of the 80ºC and are presented in Figure 4.33 and Figure 4.34, respectively.

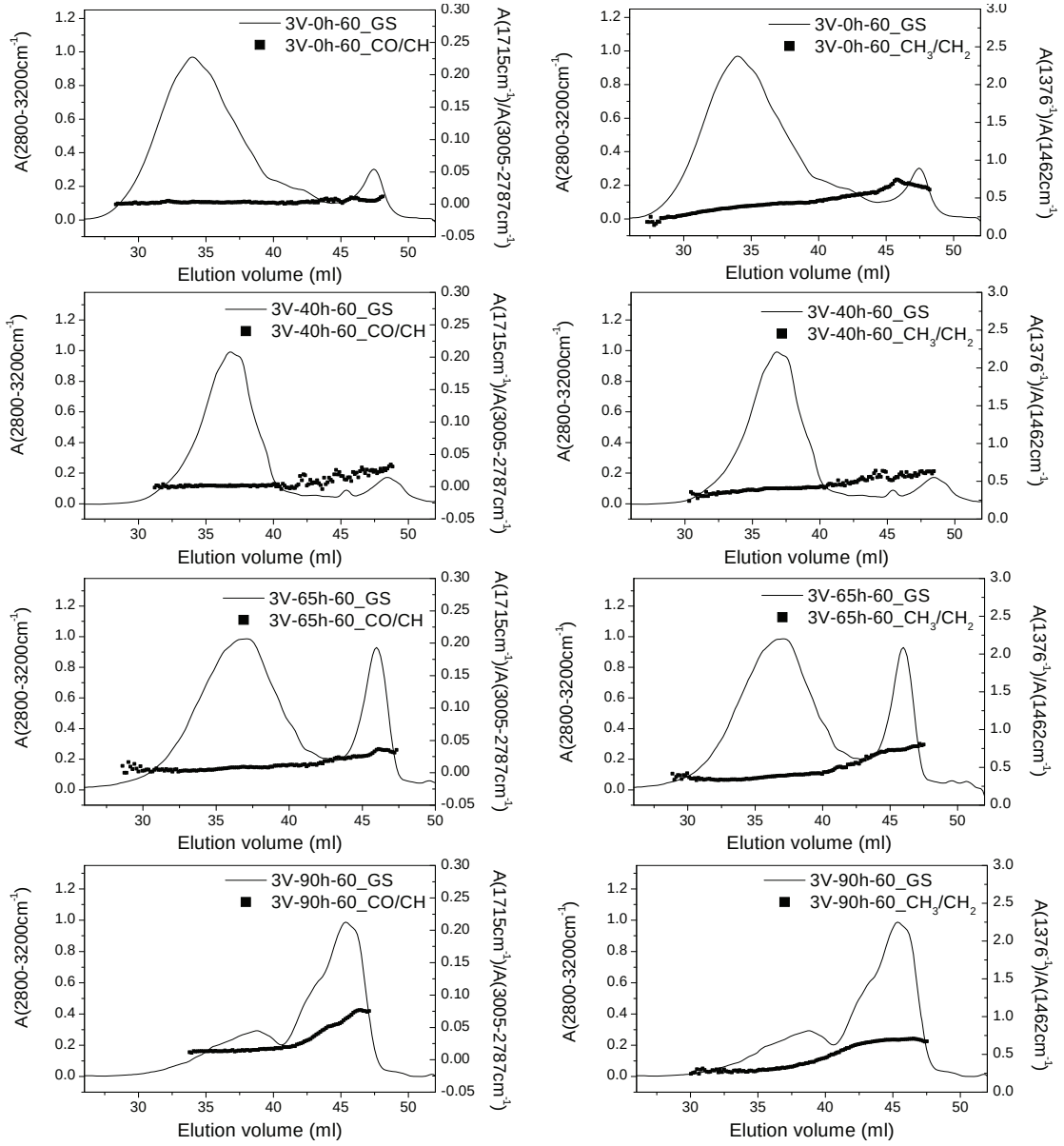

Figure 4.33: SEC-FTIR results for the 60ºC fraction of the 0h, 40h, 65h and 90h samples of copolymer 3V, obtained by TREF analysis after degradation.

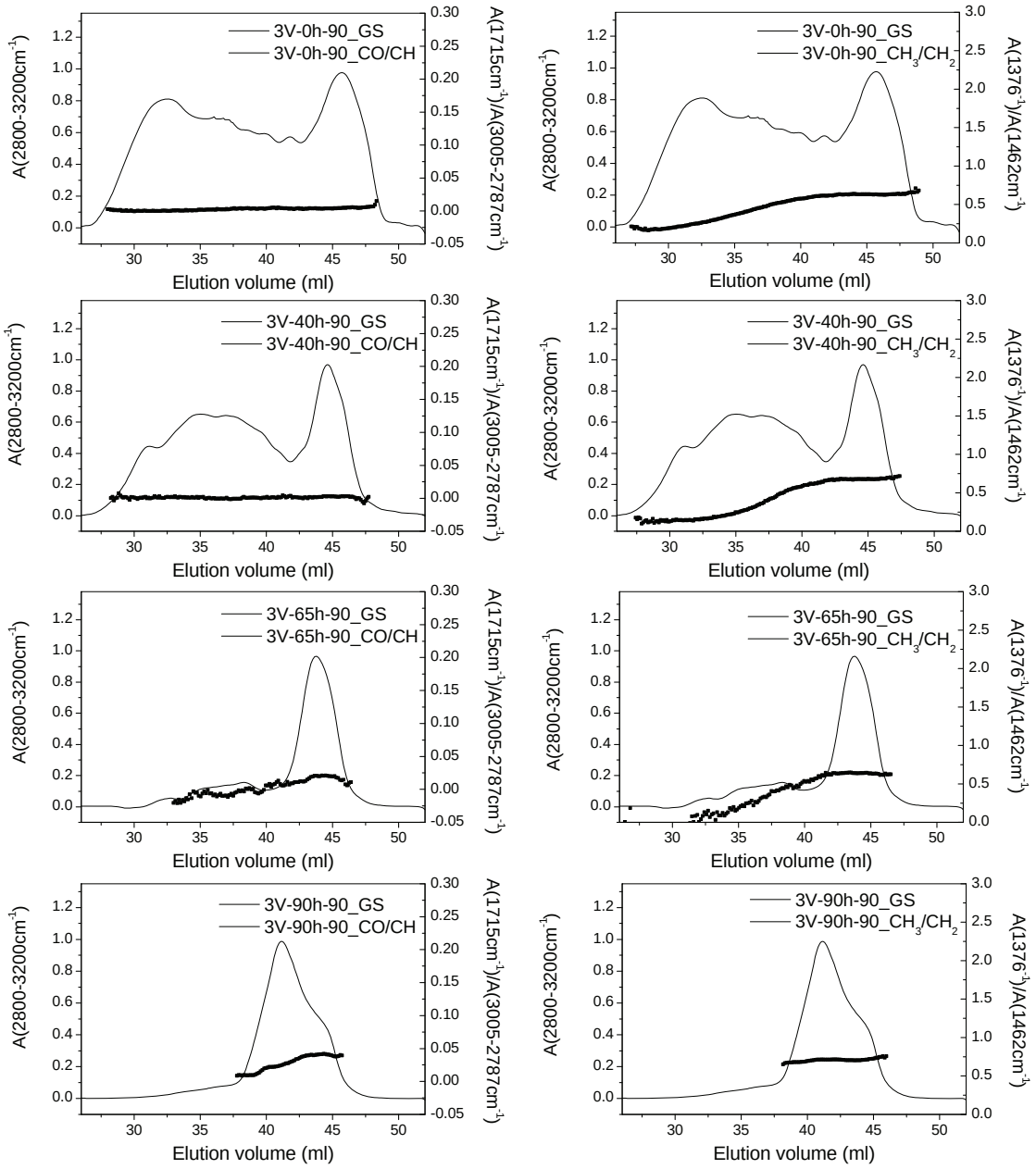

Figure 4.34: SEC-FTIR results for the 90ºC fraction of the 0h, 40h, 65h and 90h samples of copolymer 3V, obtained by TREF analysis after degradation.

The CH_3/CH_2 ratio in the undegraded sample of both of these fractions (3V-0h-60; 3V-0h-90) also increases towards the lower elution volume side of the Gram-Schmidt plot, indicating that the propylene content increases towards the lower molecular weight side of the distribution. As was seen for the 80ºC fraction, this ratio also reaches a plateau across the higher elution volume component with ongoing degradation times, indicating an increase in the propylene content. Degraded, less crystallisable PP that was originally present within higher eluting fractions is, therefore, seen to elute in all lower eluting, copolymer fractions with ongoing degradation times. The CO/CH ratio also increased on the higher elution volume side of all degraded samples, indicating that degraded molecules containing carbonyl functionalities are found mainly on the lower molecular weight side of the

distribution. At 90 hours, this ratio is seen to have increased across both components of the bimodal distribution, but a much higher concentration of degradation products is seen within the higher elution volume component. The SEC-FTIR results of the 100ºC fraction are presented in Figure 4.35.

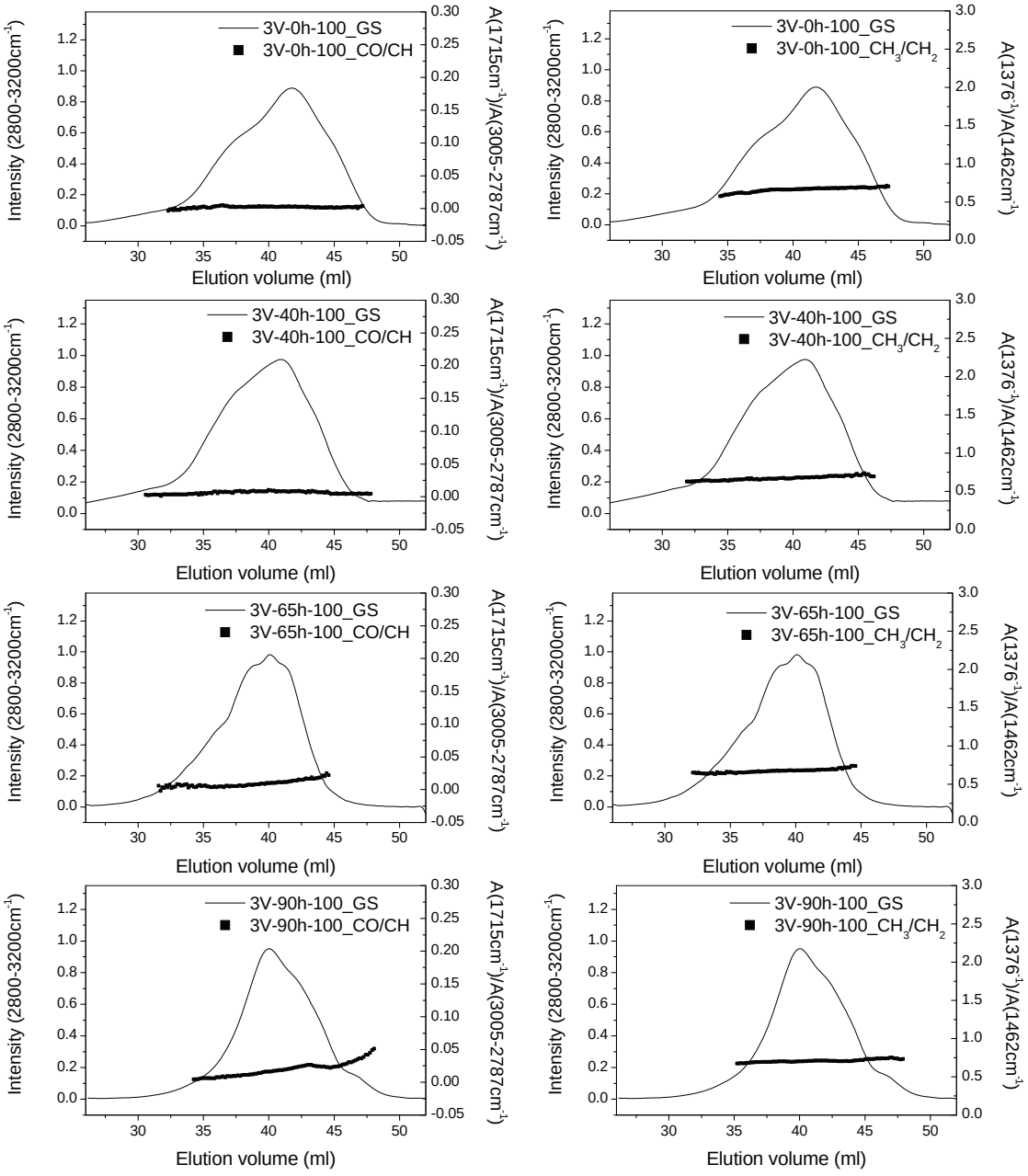

Figure 4.35: SEC-FTIR results for the 100ºC fraction of the 0h, 40h, 65h and 90h samples of copolymer 3V, obtained by TREF analysis after degradation.

The Gram-Schmidt curve moves to slightly larger elution volumes with ongoing degradation times with the most significant change or decrease at the low elution volume side. This result agrees with the SEC data where a decrease was mainly seen on the high molecular weight side of the molecular weight distribution curve. At a degradation time of 65 hours, the CO/CH ratio curve shows an increase at the larger elution volume side of the Gram-Schmidt curve which becomes even more pronounced in

the 90h sample. A uniform CH_3/CH_2 ratio is observed across the entire elution volume curve of the undegraded sample and it remains unchanged throughout all degradation times.

The individual spectra extracted at elution volumes of 36.5 ml and 41.4 ml in the Gram-Schmidt plot are presented in Figure 4.36. The main difference between the two spectra, is the presence of the 720 cm^{-1} and 730 cm^{-1} bands, presenting long, crystallisable ethylene sequences, in the 36.5 ml spectrum. The lower elution volume component of the 100ºC fraction is therefore also EPC, whereas the higher elution volume component consists of semi-crystalline PP, as indicated by the spectrum at 41.4 ml. This fraction is therefore, also accepted as part of the range of EP copolymers, which co-elutes with PP homopolymer, although, in comparison to the 60–90ºC fractions, a much lower ethylene content and concentration of long ethylene sequences were detected by ^{13}C-NMR. The appearance of the EPC as just a shoulder to the PP distribution, is ascribed to the low amount of EPC within this fraction, compared to the PP homopolymer. ^{13}C-NMR has illustrated that this fraction contains only 0.63% of EP sequences, whereas the concentration of long PPP sequences equals 89.37%. This fraction is therefore the highest eluting fraction containing EPC before the predominantly isotactic PP-containing fractions eluting at 110 and 120ºC.

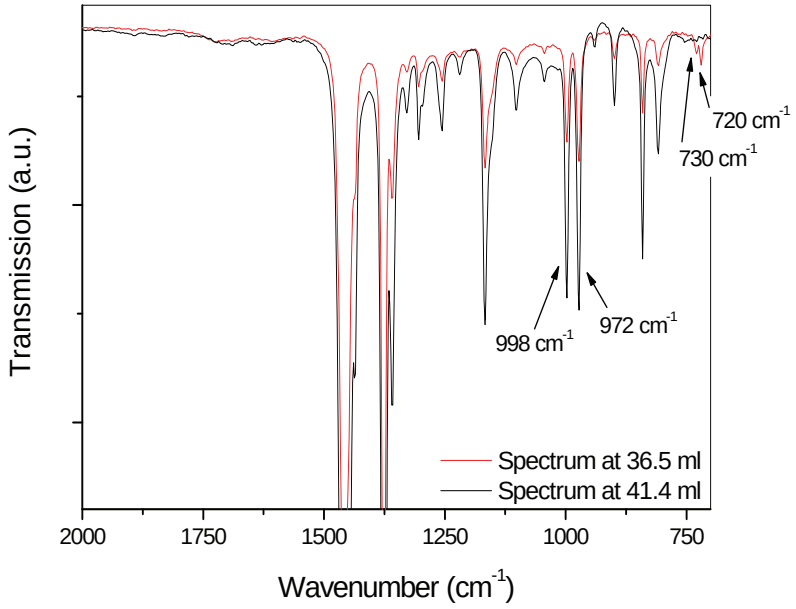

Figure 4.36: Individual FTIR spectra extracted from the Gram-Schmidt profile at 36.5 ml and 41.4 ml in sample 3V-0h-100ºC.

The spectra extracted at the maximum intensity of the Gram-Schmidt curve (elution volume of 38.2 ml) and a point close to the lowest elution volume end (43.1 ml) of the 100ºC fraction of the 90h sample, is presented in Figure 4.37.

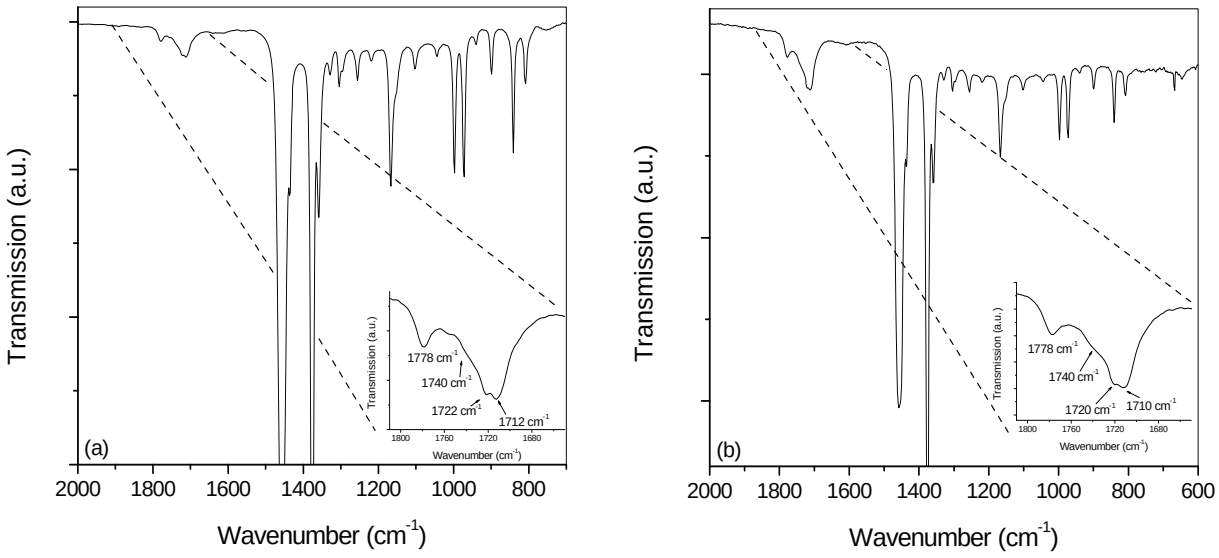

Figure 4.37: Individual FTIR spectra extracted at 38.2 ml (a) and 43.1 ml (b) of the Gram-Schmidt profile of sample 3V-90h-100ºC.

The spectrum at 38.2 ml is similar to that extracted at 36.5 ml in the 0h sample, although a much smaller 720 cm^{-1} band is present in the 90h sample. In Figure 4.22 it was seen that the weight percentage of the 100ºC fraction increased from 5.27% in the 0h sample to 18.16% in the sample degraded for 90 hours, therefore a considerable amount of degraded PP has moved into this fraction upon degradation. This is proven by the spectrum at 43.1 ml showing that only PP is present at the larger elution volume end where the highest CO concentration is found. Finally, the SEC-FTIR results of the EPR-rich fraction will be presented. The SEC-FTIR results for the 30ºC fraction at the various stages of degradation are presented in Figure 4.38.

The Gram-Schmidt plot of the 30ºC fraction of the undegraded sample contains a single broad component centred around an elution volume of 32.1 ml. The Gram-Schmidt plot shifts to larger elution volumes with ongoing degradation times, indicating a decrease in molecular weight, which was also observed in the SEC results in Section 4.1.4.1. The CO/CH ratio shows a slight increase towards the higher elution volume side of the Gram-Schmidt of the 65h sample, while it forms a steeper slope across the entire molecular weight distribution in the sample degraded for 90 hours, where it reaches a maximum at the lower molecular weight side. In this case, degradation products are present across the complete molecular weight distribution. The CH_3/CH_2 ratio is uniform across the entire molecular weight range in the undegraded and 40h samples, whereas a slight increase is observed in the samples degraded for 65 and 90 hours. The extraction of individual spectra from the Gram-Schmidt plot is necessary to gain insight into the chemical composition changes of this fraction resulting from degradation.

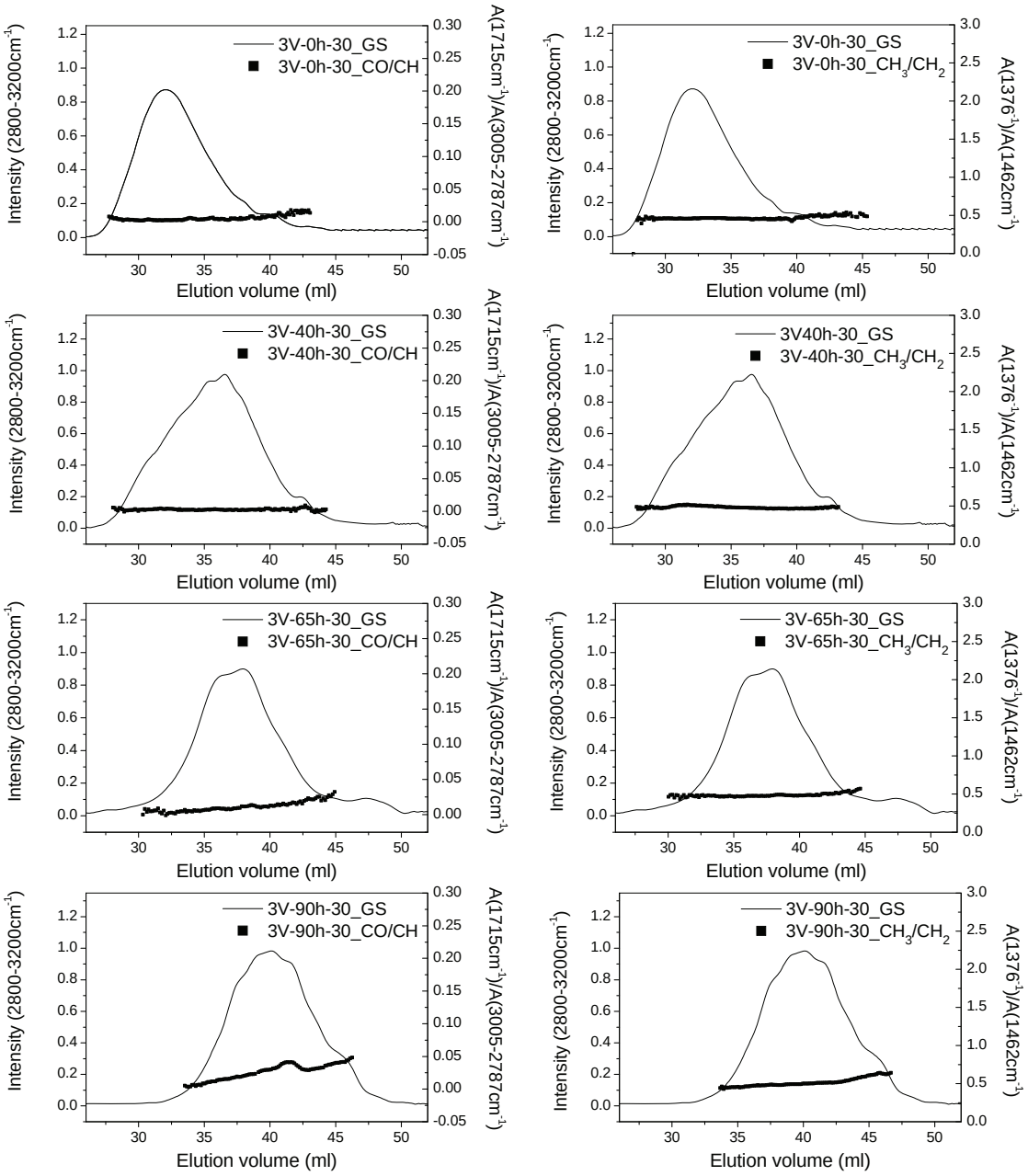

Figure 4.38: SEC-FTIR results for the 30ºC fraction of the 0h, 40h, 65h and 90h samples of copolymer 3V, obtained by TREF analysis after degradation.

Figure 4.39 shows the spectrum extracted at the maximum (32.1 ml) of the Gram-Schmidt plot of the 30ºC fraction of the undegraded sample. This fraction clearly consists of amorphous ethylene and propylene, with no crystalline PP bands visible at 998 cm^{-1} and 841 cm^{-1}. A shoulder to the 720 cm^{-1} band around 730 cm^{-1}, suggests that some crystallisable ethylene is present, which was also seen from the SEC-FTIR results of the 730 cm^{-1}/720 cm^{-1} ratio of this fraction in Figure 4.20. The spectra extracted at the maximum (40.0 ml) as well as a point close to the higher elution volume end of the molecular weight distribution (48.0 ml) of the 90 hours sample, appear in Figure 4.40.

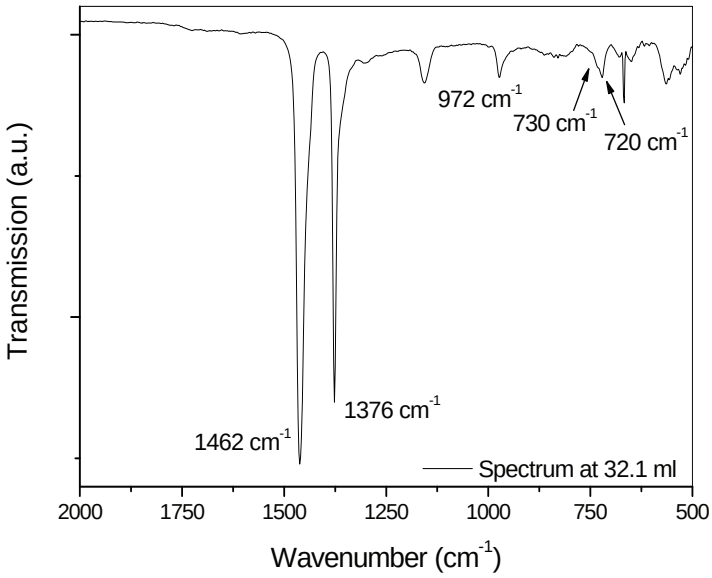

Figure 4.39: Individual FTIR spectra extracted from the Gram-Schmidt profile at the maximum of the main peak at 32.1 ml in sample 3V-0h-30ºC.

The spectrum at 40.0 ml is similar to that at the maximum of the undegraded sample, which is characteristic of EPR. The spectrum at 48.0 ml, however, is that of PP with characteristic bands at 972 cm^{-1}, as well as 1462cm^{-1} and 1376 cm^{-1}. Strong carbonyl bands commonly observed upon thermo-oxidative degradation in PP are also present at 1780 cm^{-1}, 1740 cm^{-1} and 1712 cm^{-1} and 1720 cm^{-1}. There does not seem to be any ethylene present in this part of the Gram-Schmidt, although its presence might be obscured by the abundance of polypropylene. These results prove that PP found at higher T_e in the undegraded sample had been modified by carbonyl group insertion, to such an extent that it is no longer crystallisable at higher temperatures. This accounts for the increase in the weight percentage of material eluting in the 30ºC fraction from 0 to 90 hours.

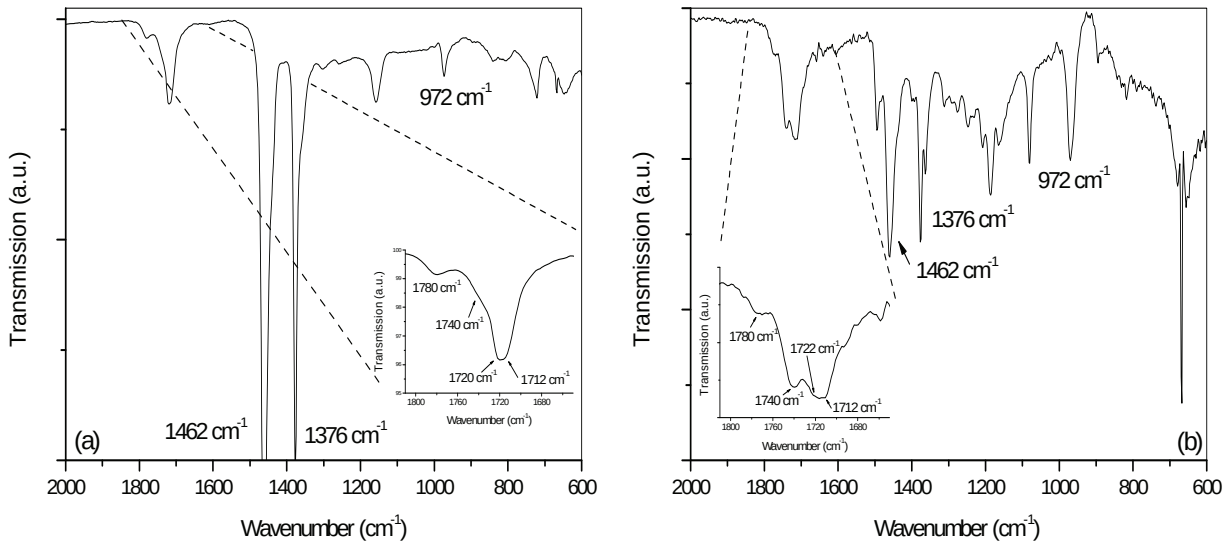

Figure 4.40: Individual FTIR spectra extracted at 40.0 ml (a) and 48.0 ml (b) of the Gram-Schmidt profile of sample 3V-90h-30ºC.

4.1.4.3 TREF-(^{13}C-NMR) results for the degraded 3V samples

^{13}C-NMR analysis was performed on the fractions of all degraded samples after fractionation by TREF. Sequence analysis of these fractions was done in order to obtain information on the changes in the distribution of ethylene and propylene caused by degradation. The complete sequence analysis and propylene tacticity results of the TREF fractions of the undegraded material have already been presented in Table 4.4, while those for the most degraded sample (90h) are presented in Table 4.8.

Table 4.8: ^{13}C-NMR monomer sequence analysis and tacticity data of the bulk 3V-90h sample and its TREF fractions

Sample	P	E	PP	PE EP	EE	PPP	PPE EPP	EPE	EEE	EEP PEE	PEP	% mmmm
3V-90h	88.35	11.65	84.95	6.79	8.29	83.15	3.57	1.63	6.57	3.57	1.61	84.80
3V-90h-30	46.89	53.11	30.63	32.53	35.46	15.10	26.71	5.08	0.02	0.01	0.01	21.80
3V-90h-60	61.14	38.86	55.27	11.74	32.74	50.32	7.62	3.20	28.63	7.25	0.88	67.41
3V-90h-80	80.29	19.71	78.73	3.12	18.10	77.88	1.58	0.83	16.88	2.24	0.17	87.91
3V-90h-90	91.88	8.12	91.62	0.52	7.79	91.59	0.27	0.03	0.02	0.00	0.00	91.18
3V-90h-100	98.07	1.93	98.07	0.00	1.93	98.07	0.00	0.00	1.93	0.00	0.00	96.03
3V-90h-110	99.01	0.99	99.01	0.00	0.99	99.01	0.00	0.00	0.98	0.00	0.00	98.15
3V-90h-120	93.30	6.70	93.30	0.00	6.70	93.30	0.00	0.00	6.70	0.00	0.00	96.28

Changes in the total amount and the distribution of the monomers, as well as the isotacticity of the PP phase, are observed. Interpretation of these results was simplified by plotting the most important changes as a function of degradation time. The changes in the weight percentages of all fractions of the 0 and 90 hours samples obtained by TREF, are presented together with the changes in monomer sequence distributions. Figure 4.41 illustrates the changes in the propylene concentration with elution temperature for the undegraded and most degraded (3V-90h) samples. An increase in the mole percentage of propylene is observed for all fractions from 30–110ºC, with drastic increases in especially the 60–90ºC fractions. A decrease is observed in the 120ºC fraction. This is also the fraction in which a significantly smaller weight percentage of material eluted in the degraded (3V-90h) sample after re-crystallisation and fractionation by TREF.

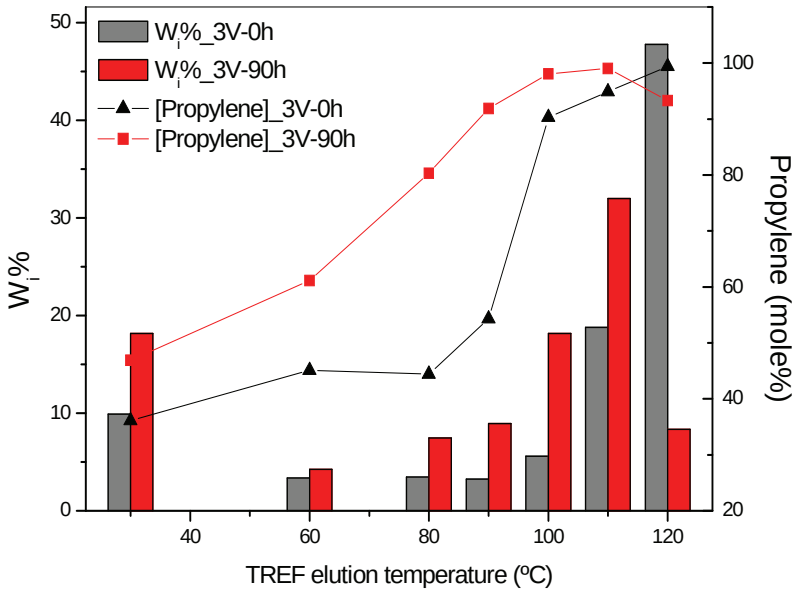

Figure 4.41: Weight percent (W_i%) and propylene content (mole%) per TREF elution temperature for the 3V-0h and 3V-90h samples.

This result, therefore, also indicates the selective degradation of the isotactic PP phase. Those fractions presenting an increase in propylene also show an increase in the amount of material eluting upon degradation. Degraded isotactic PP is therefore believed to elute within these fractions as a result of changes to its structure, rendering chains less crystallisable. Some chains are, therefore, unable to crystallise at higher temperatures, which prevents them from eluting at 120ºC, as was the case in the undegraded sample. As seen from the data in Table 4.8, the distribution of long PP sequences (PPP) follows the same tendency as the total amount of PP in the undegraded and degraded samples. The number average sequence length of the propylene and ethylene segments in the fractions was once again calculated and the results appear in Table 4.9.

Table 4.9: The number-average lengths of ethylene and propylene segments in the bulk 3V-90h sample and its TREF fractions

Sample	$\overline{n_E}$	$\overline{n_P}$	**Sample**	$\overline{n_E}$	$\overline{n_P}$
3V-0h	3.31	28.86	**3V-90h**	3.44	26.02
3V-0h-30	5.41	3.32	**3V-90h-30**	3.18	2.88
3V-0h-60	5.00	4.12	**3V-90h-60**	6.58	10.42
3V-0h-80	8.95	7.21	**3V-90h-80**	12.58	51.39
3V-0h-90	27.51	32.84	**3V-90h-90**	30.95	353.45
3V-0h-100	29.99	287.23	**3V-90h-100**	n.d.	n.d.
3V-0h-110	n.d.	n.d.	**3V-90h-110**	n.d.	n.d.
3V-0h-120	n.d.	n.d.	**3V-90h-120**	n.d.	n.d.

n.d: not determined

Compared to the average sequence lengths for ethylene and propylene determined in Section 4.1.3.5 (Table 4.6), it is observed that both the ethylene and propylene sequence length increases in the 60-90ºC fractions upon degradation. Shorter sequence lengths are observed for both monomers in the 30ºC fraction. The change in the tacticity of the PP phase in each fraction is illustrated in Figure 4.42. All fractions from 60 to 100ºC exhibit an increase in isotacticity as PP from higher fractions has moved into these fractions, causing an increase in the amount of PP, as well as its isotacticity.

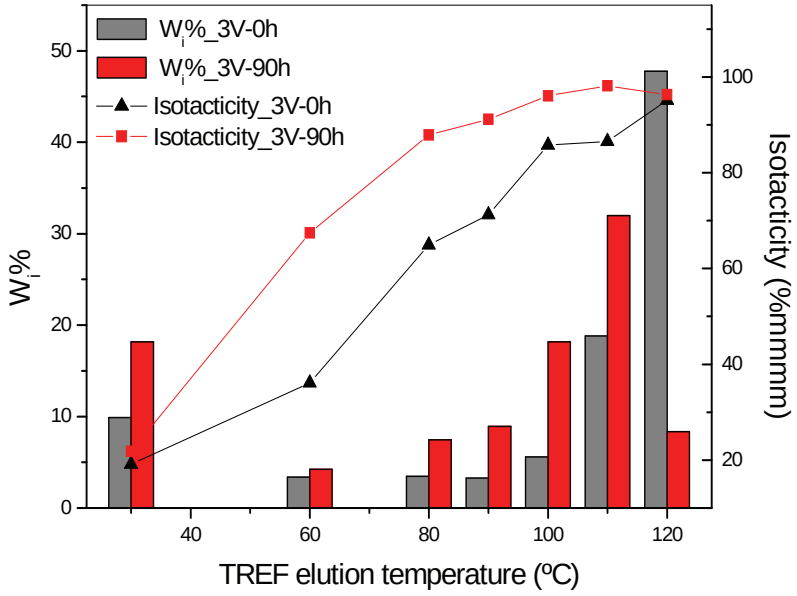

Figure 4.42: Weight percent (W_i%) and tacticity values per TREF elution temperature for the 3V-0h and 3V-90h samples.

It can, therefore, be concluded that the iPP phase of this impact PP copolymer is degraded preferentially, and the change in crystallisability of the bulk sample, is caused by a significant change in the crystallisability of this phase. Chain scission and carbonyl group insertion alters the crystallisability of PP chains, causing them to elute at lower elution temperatures after re-crystallisation in the TREF experiment. The degree to which chains have been modified, determines the temperature at which degraded molecules will elute, i.e., severely degraded material will elute as part of the soluble fraction, whereas less degraded material will elute at temperatures between 30ºC and 110ºC, according to the extent of their degradation. In the following section, the degradation study of impact PP copolymers will be extended to a second, higher ethylene content impact PP copolymer grade and TREF fractionation combined with other techniques will be used to investigate the difference in degradation behaviour based on sample heterogeneity, i.e., the distribution in molecular weight, tacticity and comonomer contents.

4.2 Comparison of the degradation behaviour of two impact PP copolymers with different ethylene contents

4.2.1 Properties of the bulk 3V and 4V copolymer samples

In Section 4.1 it was concluded that the degradation of the impact PP copolymer in question is governed by chemical composition. Of all the components present in copolymer 3V, the iPP phase was seen to degrade preferentially due to its low ethylene contents (high concentration of tertiary carbons) and its high isotacticity, despite the amorphous nature of the EPR which promotes oxygen diffusion. A grade of higher comonomer content was selected to investigate the combined effect of comonomer content, isotacticity and a higher weight percentage of amorphous material on the degradation behaviour of impact PP copolymers. The changes in crystallisability observed for sample 3V in Section 4.1 will also be studied for the higher ethylene content copolymer grade.

In addition to the impact PP copolymer sample, 3V, described in Section 4.1, a second grade with a higher comonomer content and lower isotacticity, named 4V, was also obtained as unstabilised reactor powder. Both materials were prepared via copolymerisation of propylene with ethylene for production of a PP with increased toughness at temperatures ranging from ambient to below zero temperatures. For commercial purposes sample 3V is produced as a high flow (MFR = 16g.10min^{-1}), narrow molecular weight distribution material suitable for injection moulding of thin-walled articles requiring good impact resistance and stiffness. Such products include stadium seating, caps and closures, boxes and containers, indoor furniture and cosmetic containers. Sample 4V is a very high flow (MFR = 50g.10 min^{-1}), narrow molecular weight distribution copolymer, normally formulated with antistatic additives. This grade is particularly suitable for injection moulding of thin-walled articles with long flow paths, and is known for its superior impact strength at low temperatures. Typical high flow path-to-wall thickness applications of this grade include basins, laundry baskets and silicone/filler tubes, whereas its most common thin-walled products are yoghurt cups, margarine tubs and domestic household articles.

The properties of the two impact PP grades are summarised in Table 4.10. The major differences observed here are the comonomer content, which is approximately 10.5 mole% and 16.4 mole% for the 3V and 4V samples, respectively. This is accompanied by a difference in propylene isotacticity (%mmmm) of approximately 88.8% and 83.2% for the respective samples. Weight-average molecular weight values ($\overline{M_w}$) are similar, whereas a slightly higher polydispersity is detected in sample 4V. Slightly lower melting and crystallisation temperatures (T_m, T_c) and a considerably lower melt enthalpy (ΔH_m) value is also observed for sample 4V, indicating a lower percentage crystallinity within this copolymer.

Table 4.10: Summary of the molecular properties of impact PP copolymer samples 3V and 4V

Sample	[Ethylene] (mole%)	Isotacticity (%mmmm)	$\overline{M}_w$ (g.mol^{-1})	$\overline{M}_n$ (g.mol^{-1})	PDI	T_c (ºC)	T_m (ºC)	Δh_m (J.g^{-1})
3V-0h	10.48	88.82	354 400	114 600	3.18	118.2	162.6	94
4V-0h	16.42	83.17	351 900	86 600	4.06	116.3	160.7	72

The difference in crystallisability of the two samples investigated by CRYSTAF, prep-TREF and DSC are presented in Figure 4.43 and Figure C.3 (Appendix C). It is noted here that the peak crystallisation temperature (T_c) in CRYSTAF is considerably lower than the dissolution temperature in prep-TREF. This temperature difference is referred to as the 'undercooling' effect, as described by Monrabal[81]. It is stated that, although CRYSTAF and TREF both separate according to crystallisability, and a slow cooling process is applied in both cases, the difference arises from the undercooling needed to start nucleation and further crystallisation in CRYSTAF, compared to the dissolution step alone in TREF. This is also the case in crystallisation from the melt with subsequent melting measured by DSC. The effect of different solvents used for CRYSTAF and TREF analysis, namely 1,2,4-trichlorobenzene (TCB) or *ortho*-dichlorobenzene (*o*-DCB) and xylene can, however, also not be ruled out.

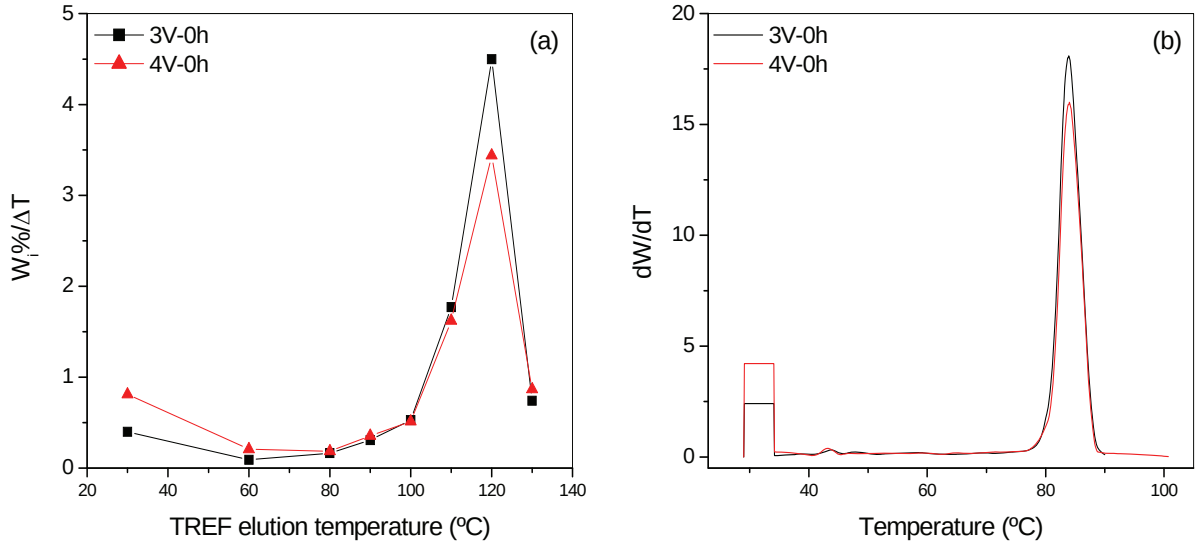

Figure 4.43: Dissolution and crystallisation curves of samples 3V and 4V obtained by (a) TREF (W_i%/ΔT) and (b) CRYSTAF, respectively.

Although the CRYSTAF peak crystallisation temperatures and the maximum of the TREF (W_i%/ΔT) curves at 120ºC are similar for the two samples, the intensity of the 4V crystallisation peak is lower than that of sample 3V in both experiments, and a larger CRYSTAF soluble fraction and TREF W_i%/ΔT-value at 30ºC is detected for the 4V sample. This sample contains a higher percentage of ethylene comonomer, and therefore is expected to contain a larger amount of non-crystallisable

material. The CRYSTAF T_c and soluble fraction data, together with the TREF dissolution temperatures (T_d) and $W_i\%/\Delta T$ values at 30ºC and 120ºC are given in Table 4.11.

Table 4.11: Comparison of CRYSTAF and TREF data for the undegraded 3V and 4V samples

Sample	CRYSTAF T_c (ºC)	Soluble fraction (Wt %)	TREF peak T_d (ºC)	$W_i\%/\Delta T$ at peak max	$W_i\%/\Delta T$ at 30ºC
3V-0h	84.0	12.8	120	4.498	0.330
4V-0h	83.9	21.0	120	3.439	0.845

Analysis of the bulk samples has indicated a difference in ethylene content and isotacticity, as well as a reasonable difference in the amount of amorphous material present in the two materials. In Section 4.1 fractionation techniques were used to study the heterogeneity of copolymer 3V. It was seen that ICPP's are highly complex materials exhibiting distributions in a number molecular properties such as molecular weight, comonomer content, isotacticity and monomer sequence lengths and distributions. ^{13}C-NMR, SEC, and DSC analysis of the TREF fractions of the undegraded 4V copolymer will now be compared to those of copolymer 3V.

4.2.2 Characterisation of the TREF fractions of the undegraded 3V and 4V samples

Sample 4V was fractionated according to the same TREF conditions used for copolymer 3V in Section 4.1 and the fractionation data, i.e., the weight in grams (W_i), weight percent ($W_i\%$), accumulative weight percent ($\Sigma W_i\%$) and weight percent per temperature increment ($W_i\%/\Delta T$) for all fractions of the two copolymers are presented in Table B.1 of Appendix B. The weight percentage ($W_i\%$) and weight percentage per temperature increment ($W_i\%/\Delta T$) data for the two copolymers are compared in Figure 4.44. Here it can be seen that the major differences in the weight percentage of the fractions of the two copolymers are present within the lowest elution temperature fractions, namely those eluting at 30 and 60ºC, as well as the higher eluting 110ºC and 120ºC fractions. A larger weight percentage of material elutes at 30 and 60ºC in copolymer 4V, accompanied by smaller weight percentages of the fractions eluting at 110 and 120ºC. Very small variations in the weight percentages of fractions eluting at 80–100ºC and 130ºC are detected for the two copolymers.

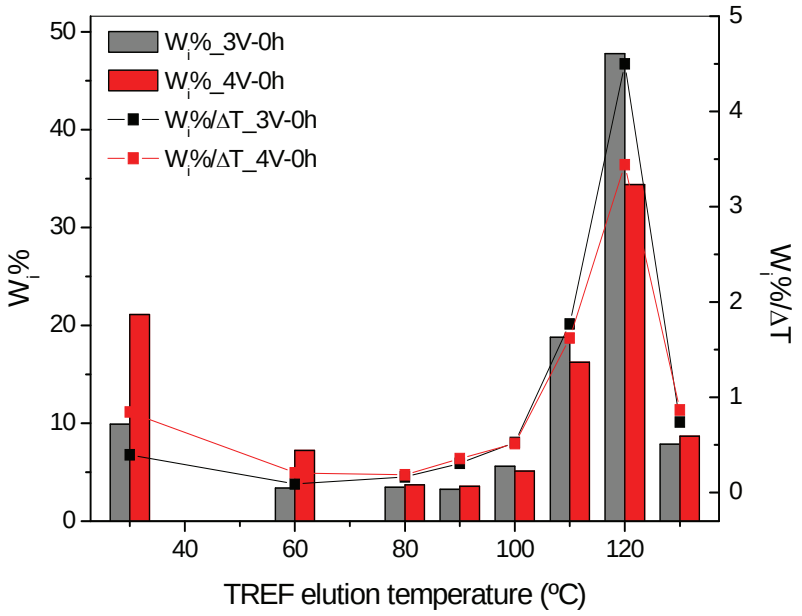

Figure 4.44: Comparison of the weight percentage (W_i%) and weight percentage per temperature increment (W_i%/ΔT) of the fractions of samples 3V and 4V as a function of TREF elution temperature.

In Section 4.1 it was concluded that the 30ºC and 60ºC fractions of copolymer 3V consisted mainly of EPR (30ºC) and transition EP copolymers (60ºC) of short ethylene and propylene sequences, which co-elutes with a small amount of atactic PP. ^{13}C-NMR, DSC, and SEC of the fractions of copolymer 4V will now be presented in order to compare their chemical composition, molecular weight and thermal properties to those of sample 3V.

4.2.2.1 TREF-(^{13}C-NMR) analysis of the undegraded 3V and 4V samples

The comonomer content and tacticity of the two grades have already been presented in Table 4.9. The diad and triad sequence distributions of the two monomers as well as the number-average sequence length of ethylene ($\overline{n_E}$) and propylene ($\overline{n_P}$) are presented in Table 4.12.

Table 4.12: ^{13}C-NMR sequence analysis and average sequence lengths for samples 3V and 4V

Sample	PP	PE EP	EE	PPP	PPE EPP	EPE	EEE	EEP PEE	PEP	$\overline{n_E}$	$\overline{n_P}$
3V-0h	86.36	6.34	7.32	84.19	3.63	1.70	5.75	3.18	1.58	3.31	28.26
4V-0h	78.31	10.54	11.17	74.95	5.81	2.82	8.56	5.32	2.61	3.12	15.86

Apart from the higher ethylene content and lower isotacticity of copolymer 4V previously mentioned, a higher EEE and lower PPP triad concentration is also observed. A higher concentration of long ethylene sequences is, therefore, found within copolymer 4V, accompanied by a lower concentration of long propylene sequences. Furthermore, a higher concentration of all connecting units found in E and

P sequences (EP, PPE, EPE, EEP, PEP) are also present in this copolymer. These results suggest that the excess ethylene present in the bulk 4V copolymer is located both in longer ethylene homopolymer sequences and within the random and semi-crystalline EP copolymers. The average length of ethylene sequences is similar in the two grades, whereas a longer propylene average sequence length is present in copolymer 3V. The comonomer content, tacticity and monomer sequence distribution data of the TREF fractions of sample 3V have been presented in Table 4.5 of Section 4.2.6.1, whereas the data for sample 4V is presented in Table 4.13. All calculations were done according to the methods described in Section 4.1.3.5.

Table 4.13: ^{13}C-NMR sequence analysis and tacticity data for sample 4V and its TREF fractions

Sample	P	E	PP	PE EP	EE	PPP	PPE EPP	EPE	EEE	EEP PEE	PEP	% mmmm
4V-0h-30	36.11	63.89	25.23	21.77	47.94	7.89	27.44	0.78	33.32	9.02	3.21	19.16
4V-0h-60	34.33	65.67	20.69	27.27	52.30	13.70	12.95	7.67	44.32	17.01	3.50	31.53
4V-0h-80	33.25	66.75	27.36	11.77	60.68	24.83	5.54	2.88	56.40	7.80	1.19	55.99
4V-0h-90	51.39	48.61	48.65	5.48	45.83	51.21	0.13	0.05	44.00	3.46	0.54	67.73
4V-0h-100	92.70	7.30	92.24	0.92	6.80	91.39	1.13	0.17	6.47	0.46	0.08	87.74
4V-0h-110	99.05	0.95	99.05	0.00	0.95	99.05	0.00	0.00	0.95	0.00	0.00	94.52
4V-0h-120	99.76	0.24	99.58	0.37	0.13	99.76	0.00	0.00	0.13	0.28	0.00	92.99

In both samples, the isotacticity of the fractions increases with T_e from 30ºC to 120ºC, indicating that the fractionation of the polypropylene phase is governed by tacticity. The ethylene content within the 30–90ºC fractions is also higher than that of the 100–120ºC fractions of both copolymers. The distribution of ethylene as a function of TREF elution temperature is presented in Figure 4.45.

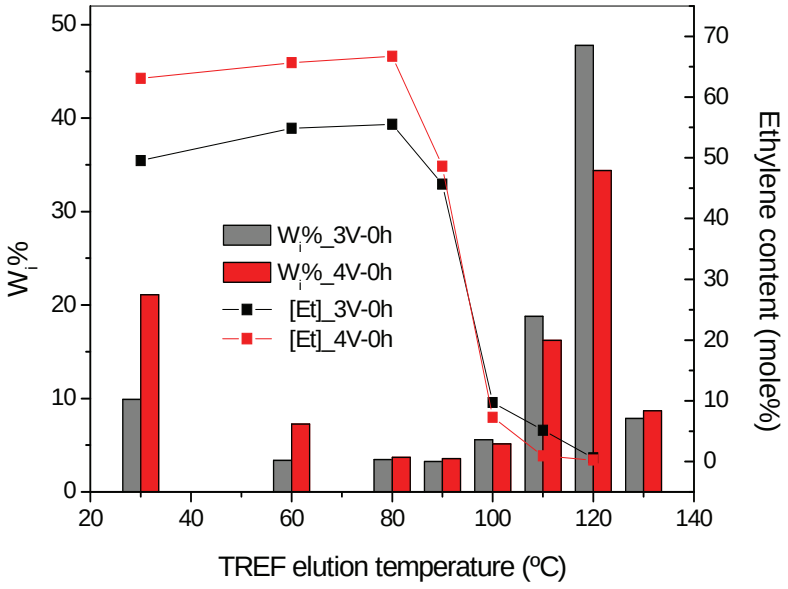

Figure 4.45: Comparison of the weight percentage and ethylene content of samples 3V and 4V as a function of TREF elution temperature.

Figure 4.45 shows that the ethylene contents of both copolymers decrease towards higher elution temperatures. A considerably higher ethylene concentration is present in the first three fractions of copolymer 4V, whereas the ethylene content of the following 4 fractions is similar to that of copolymer 3V. The excess ethylene comonomer added during polymerisation, therefore, seems to be incorporated into the random copolymer fractions, i.e., the EPR and 'transition' copolymers consisting of shorter segments of ethylene and propylene. According to these results, a higher comonomer content should affect the nature of the random and semi-crystalline EP copolymers produced, without having much influence on the PP matrix. Since, during the ICPP polymerisation process ethylene is only introduced into the second reactor, after hPP synthesis in the first, this can be expected. Zacur *et al.* have also found, when comparing the TREF profiles of an iPP sample and an impact PP copolymer, the higher cumulative weight at low T_e of the impact copolymer resulted from the presence of EP copolymers[52]. The isotacticity of the fractions of the two grades are presented as a function of TREF elution temperature in Figure 4.46.

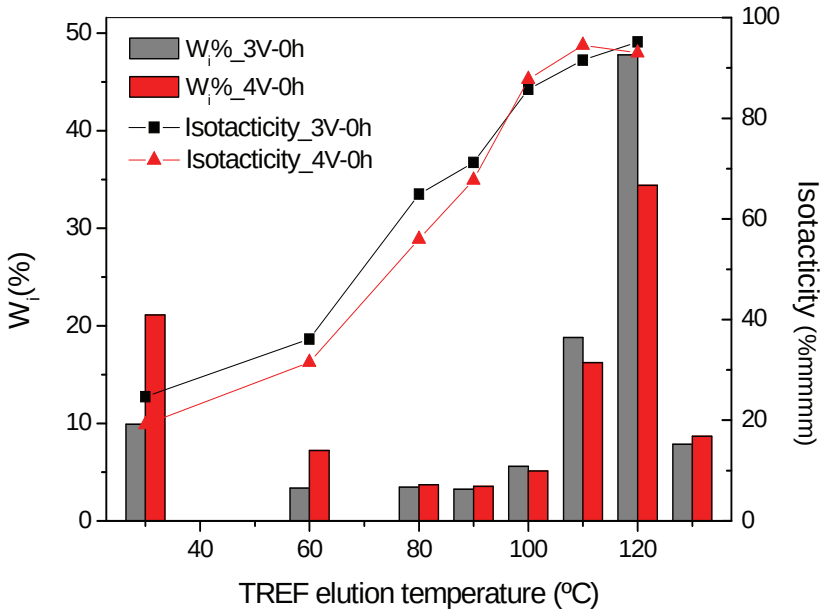

Figure 4.46: Weight percentage and propylene isotacticity of samples 3V and 4V as a function of TREF elution temperature.

The tacticity distribution is also similar in the two copolymers, with a slightly lower isotacticity detected in the fractions eluting between 30 and 90ºC of sample 4V, which are also the fractions containing a higher ethylene content than the corresponding fractions in copolymer 3V. TREF-(^{13}C-NMR) have indicated that the excess ethylene detected in the bulk 4V sample is mainly incorporated into the EPR and transition copolymer fractions eluting between 30 and 90ºC, and the isotacticity of the PP within these fractions is also slightly lower than that of copolymer 3V.

4.2.2.2 TREF-SEC and TREF-DSC analysis of the undegraded 3V and 4V samples

Molecular weight and thermal parameters of the TREF fractions of the two copolymers were obtained by SEC and DSC analysis. The molecular weight distribution curves for all fractions of the two copolymers are displayed in Figure B.1 of Appendix B, while $\overline{M}_w$ and $\overline{M}_n$ values are given in Table B.2 of the same appendix. The $\overline{M}_w$ values of the fractions of both copolymers are plotted against TREF elution temperature in Figure 4.47. Only the molecular weight values of the higher molecular weight EPC component of the 60–90ºC fractions are included here due to the similarity in molecular weight observed for the low isotacticity PP homopolymer part of these fractions eluting at corresponding temperatures within the two copolymers.

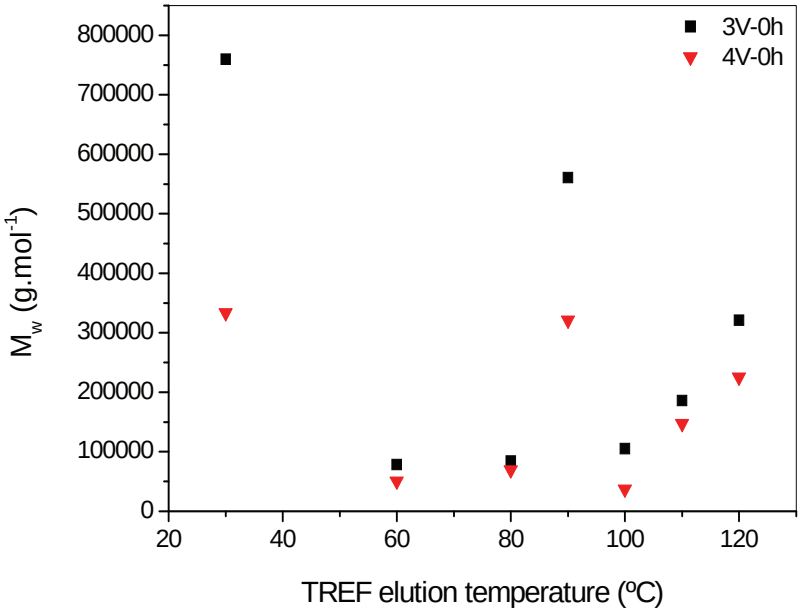

Figure 4.47: $\overline{M}_w$ values of all TREF fractions of the undegraded 3V and 4V samples as a function of TREF elution temperature.

The $\overline{M}_w$ values of fractions eluting at 60, 80, 100, 110 and 120ºC are fairly similar in the two copolymers, whereas differences are observed in the 30ºC and 90ºC fractions. In these three fractions higher $\overline{M}_w$ values are observed for those fractions belonging to copolymer 3V.

The values of the DSC thermal parameters, T_c, T_m and ΔH_m, of all TREF fractions of the undegraded 3V and 4V copolymers are given in Table B.3 of Appendix B. The DSC T_m and T_c values of the fractions of both copolymers are compared in Figure 4.48. Two melt endotherms were observed in the 60–100ºC fractions of both copolymers, and the T_m values of both the higher and lower melting components are included in Figure 4.48.

The melting temperatures of both the lower and higher melting components of all fractions of the two copolymers are almost identical. In Section 4.1 the 60ºC, 80ºC, 90ºC and 100ºC fractions were seen to consist of co-eluting lower isotacticity PP homopolymer as well as semi-crystalline EP copolymers. The lower of the two melt endotherms were assigned to the melting of the crystallisable ethylene in the EPC phase, whereas propylene from both the EPC and PP homopolymer phase was seen to melt at higher temperatures.

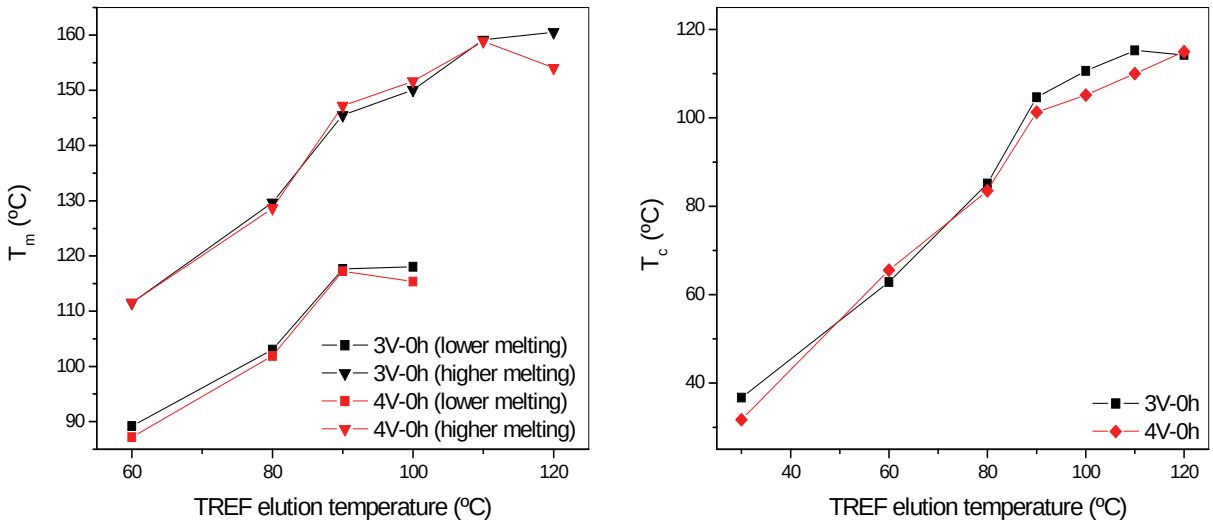

Figure 4.48: DSC melting and crystallisation temperatures for all fractions of the undegraded 3V and 4V copolymers.

The similarity in the melting temperatures of the lower melting component indicates that the sequence length of the crystallisable ethylene sequences in the EP copolymers eluting at corresponding temperatures in the two copolymers is very similar. The similarity in the melting temperatures of the higher melting component suggests that the PP phase of the two copolymers is of similar isotacticity distributions across the elution temperature range, as was also seen in Figure 4.46 from ^{13}C-NMR analysis. Furthermore, it also suggests that the propylene sequence lengths of the EPC phase is similar in fractions of corresponding elution temperatures. These results show that components of almost identical thermal behaviour are found in fractions of corresponding elution temperatures within the two copolymer grades, regardless of differences in ethylene content and molecular weight. The degradation behaviour of the two copolymers will now be compared.

4.2.3 Analysis of the degradation behaviour of the bulk 3V and 4V samples by FTIR and SEC

Thin films of samples 3V and 4V were subjected to the same conditions of accelerated thermo-oxidative degradation. Samples of both grades were extracted from the oven at pre-determined time intervals and saved for further analysis. The progress of degradation was studied by means of FTIR analysis and the ageing procedure was terminated when embrittlement of a complete film area

occurred in each grade. It was observed that embrittlement of the 3V films occurred at an earlier degradation time than those of sample 4V, therefore, the rate and extent of degradation was compared quantitatively by means of the carbonyl index. This was calculated as the ratio of the peak height at the maximum of the carbonyl band (1804–1580 cm^{-1}) and that of the reference band at 840cm^{-1}, as was done in Section 4.1.1. Since the intensity of the 840 cm^{-1} band is influenced by sample crystallinity and there is a difference in crystallinity between the two copolymer grades, the carbonyl index was also calculated relative to the 972 cm^{-1} band. These results are displayed for both samples in Figure 4.49.

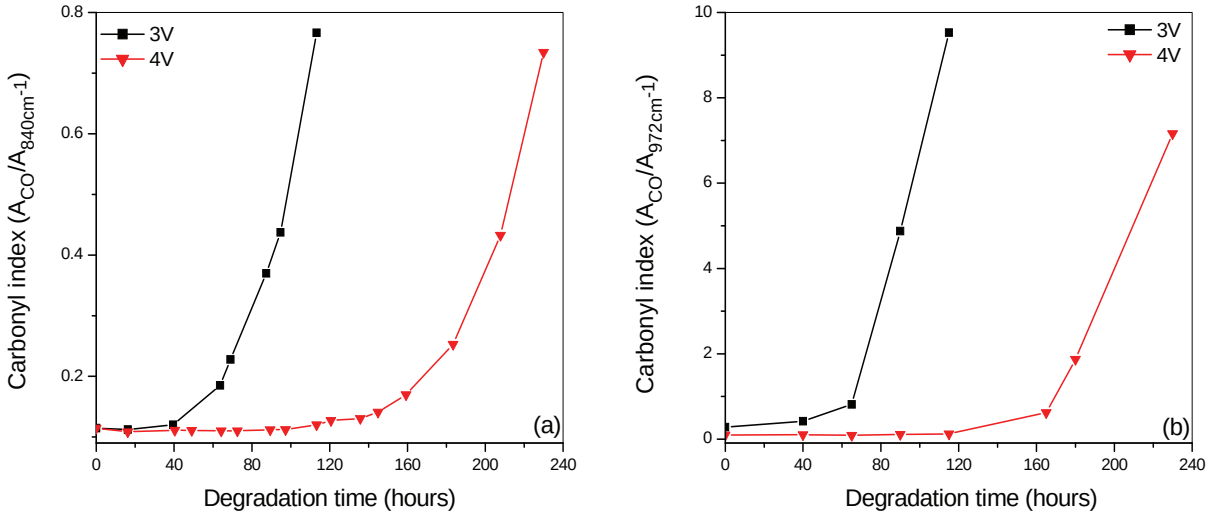

Figure 4.49: Comparison of the carbonyl index changes in samples 3V and 4V, as calculated relative to the 840 cm^{-1} (a) and 972 cm^{-1} (b) bands of the infrared spectrum.

The 3V sample displays a significantly shorter induction period (ca. 40 hours) than sample 4V, for which a gradual increase in carbonyl index is only observed after 100 hours of ageing. After the induction period, degradation is seen to spread through both samples at a steady rate, although a faster rate is observed in sample 3V, as indicated by the steeper slope of the carbonyl index curve. A maximum carbonyl index value is reached after 110 hours for sample 3V and approximately 230 hours for sample 4V. For comparison of the degradation behaviour of the two samples, sampling intervals or degradation times were chosen that correlate to approximately the same carbonyl index. Samples of copolymer 3V taken at 0, 40, 65 and 90 and 110 hours were therefore compared to those sampled at 0, 115, 179 and 195 and 230 hours for sample 4V. The decrease in weight-average molecular weight, $\overline{M}_w$, with ongoing degradation time is presented in Figure 4.50 (a). Figure 4.50 (b) illustrates the $\overline{M}_w$ change of both copolymers as a function of the carbonyl index values obtained with ongoing degradation.

Although the two copolymers are of almost identical molecular weight in their undegraded state, the change in molecular weight with ongoing degradation time is dissimilar. During the first stages of degradation (up to 40 and 115 hours for samples 3V and 4V, respectively), the molecular weight of

both copolymers decrease to approximately 250 000 g.mol^{-1}. At longer degradation times, however, the decrease in $\overline{M}_w$ for sample 3V is considerably faster, confirming the faster rate of degradation in the sample of lower comonomer content and isotacticity.

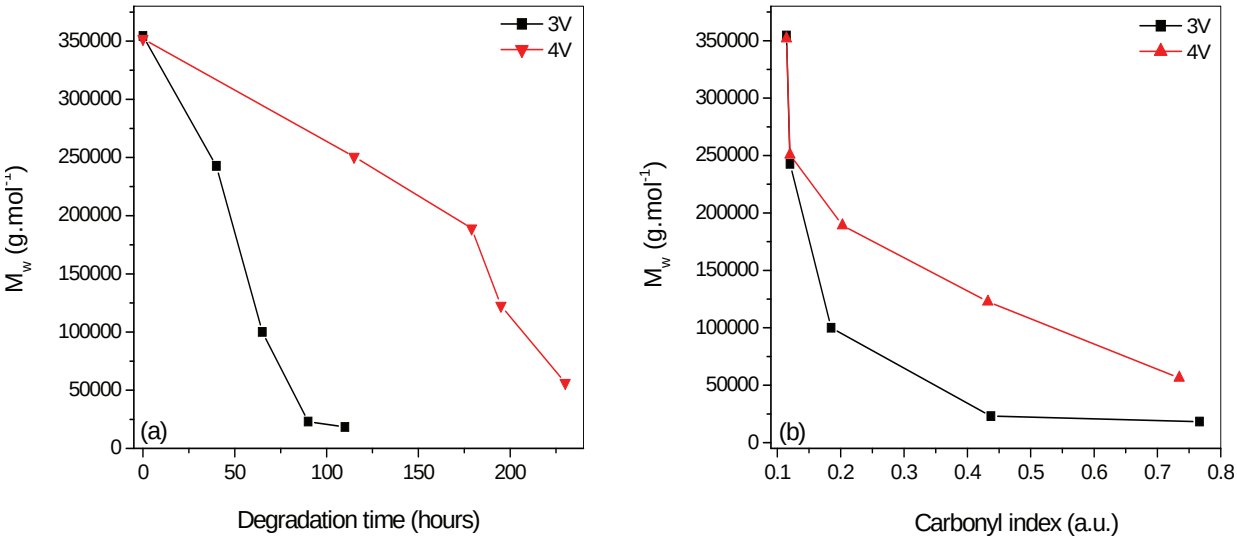

Figure 4.50: Comparison of $\overline{M}_w$ decreases of samples 3V and 4V as a function of (a) degradation time and (b) carbonyl index.

Figure 4.50 (b) also illustrates a similar relationship between $\overline{M}_w$ and carbonyl during early stages of degradation (low carbonyl index values) for the two samples. At more advanced stages of degradation, however, for the same carbonyl index values, sample 3V shows a more significant decrease in molecular weight than sample 4V. The molecular weight distribution curves of the different samples are presented in Figure C.1 of Appendix C and the average molecular weight and polydispersity values of all samples of the two grades are presented in Table C.1 of Appendix C.

4.2.4 Changes in crystallisability of the degraded 3V and 4V copolymers studied by CRYSTAF, DSC and TREF

In Sections 4.1.3.2 and 4.1.3.3 it was demonstrated how the CRYSTAF T_c and DSC melting and crystallisation temperatures of copolymer 3V are influenced by degradation. The CRYSTAF results of copolymer 4V were consistent with those obtained for copolymer 3V, where the peak crystallisation temperature decreased, the intensity of the crystallisation peak decreased and an increase in the soluble fraction was observed with ongoing degradation times. The CRYSTAF crystallisation curves of the degraded 4V copolymer are presented in Figure C.2 of Appendix C, whereas the crystallisation data, soluble fraction weight percentages and FWHM values are supplied in Table C.2 of the same appendix. The DSC curves of the two copolymers are presented in Figure C.3 and the melting and crystallisation data is supplied in Table C.3 of Appendix C. The changes in CRYSTAF T_c, as well as

DSC T_c, T_m and ΔH_m of the two copolymers with ongoing degradation time are summarised in Figure 4.51. Each coloured arrow points in the direction of the Y-axis belonging to the curve of the same colour, i.e., the CRYSTAF T_c (black) and DSC ΔH_m (blue) curves are associated with the Y-axis on the left hand side of each plot, whereas the DSC T_c (red) and T_m (green) curves correspond to the Y-axis on the right.

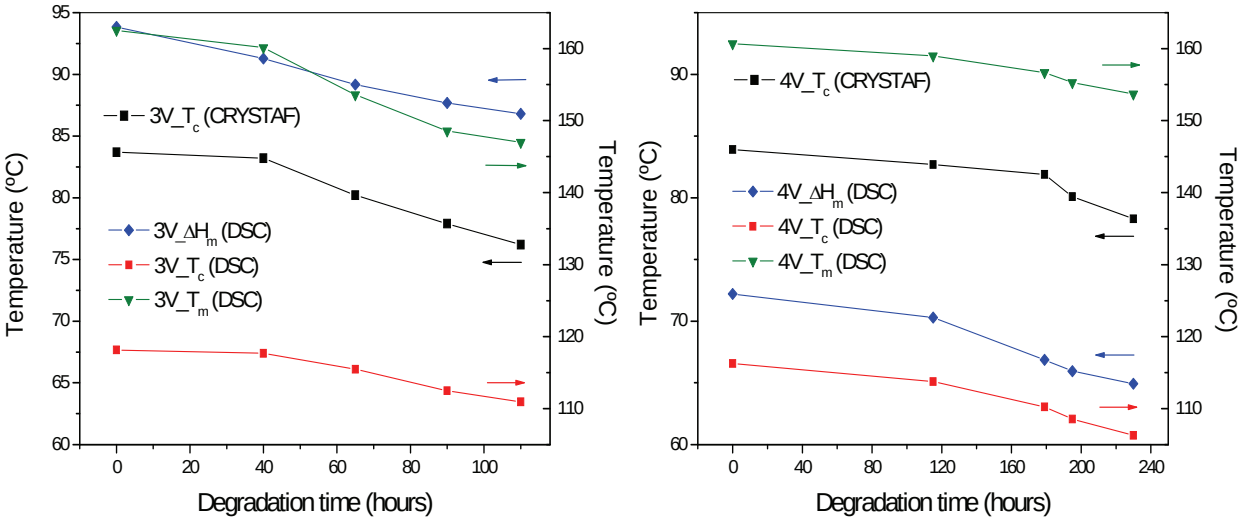

Figure 4.51: Comparison of the changes in crystallisation and melting behaviour of the two copolymers as a function of degradation time.

Similar changes in the crystallisation parameters are observed for the two copolymers. Copolymer 3V shows very little change in these parameters from 0 to 40 hours of degradation, after which the melting and crystallisation as well as melt enthalpy values decrease steadily. Copolymer 4V, which was seen only to start degrading after approximately 115 hours, also shows a minor change in these parameters during the induction period, after which the decrease in the melting and crystallisation temperatures follow a similar pattern to those of copolymer 3V. In Sections 4.1.3.2 and 4.1.3.3 it was demonstrated how three molecular parameters, namely the carbonyl index, molecular weight and either the CRYSTAF T_c or DSC T_c or T_m could be combined to study the effect of molecular weight and carbonyl concentration on the crystallisation and melting temperature of the degraded 3V copolymer. These plots were also constructed for copolymer 4V. The combined effect of carbonyl index and molecular weight on the CRYSTAF crystallisation temperature of this sample is demonstrated in Figure 4.52, while the effect of these two parameters on the DSC T_m and T_c are illustrated in Figure 4.53.

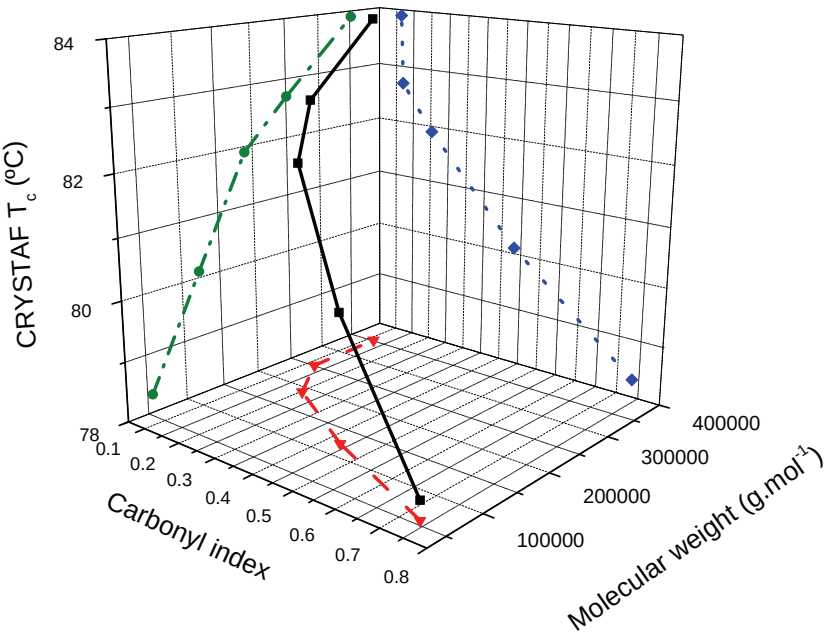

Figure 4.52: Representation of the combined influence of molecular weight and carbonyl concentration on the CRYSTAF crystallisation temperature of copolymer 4V.

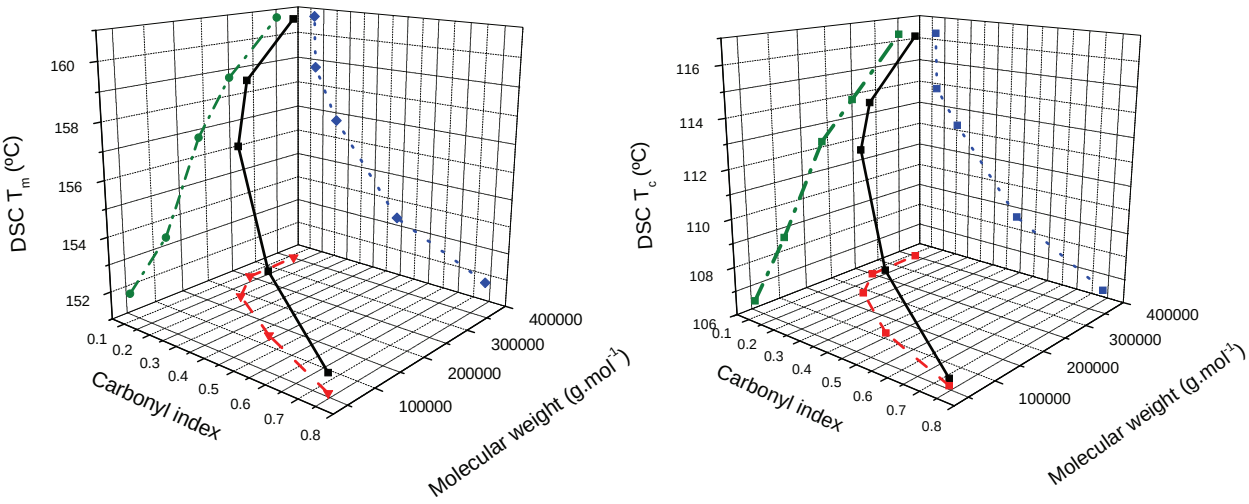

Figure 4.53: Representation of the combined influence of molecular weight and carbonyl concentration on DSC melting and crystallisation temperatures of copolymer 4V.

For copolymer 4V it can also be seen that there exists some correlation between the three independent parameters presented here. The combination curve (black) indicates that the T_m and T_c values of degraded samples of copolymer 4V are also influenced predominantly by molecular weight effects during early stages of degradation (low carbonyl concentrations), whereas the carbonyl concentration dominates thermal parameters during advanced stages of degradation when the molecular weight is reduced significantly by scission and a large number of carbonyl functionalities are incorporated into

oxidised chains. The CRYSTAF T_c and DSC T_m combination curves (black), together with their XY, YZ and XZ projections, for samples 3V and 4V are compared in Figures 4.54 and 4.55, respectively.

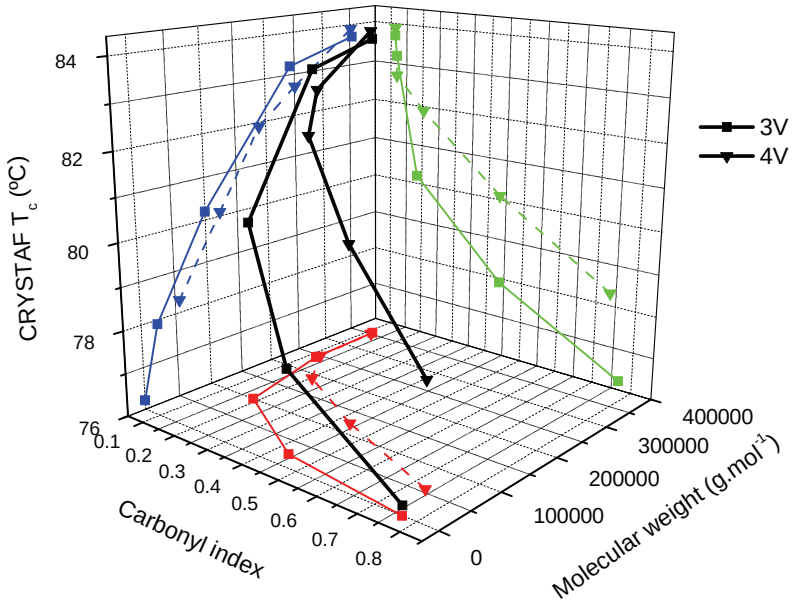

Figure 4.54: Comparison of differences in the relationships between carbonyl index, molecular weight and CRYSTAF T_c for samples 3V and 4V.

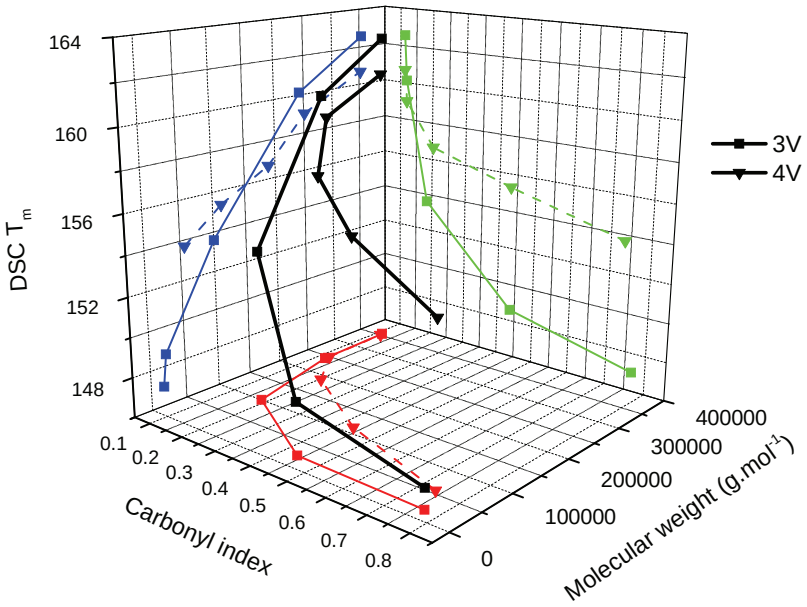

Figure 4.55: Comparison of differences in the relationships between carbonyl index, molecular weight and DSC T_m for samples 3V and 4V.

Differences in the shape of the combination curves of the two copolymers are observed for both the CRYSTAF T_c and DSC T_m data. Compared to copolymer 3V, the combination curves for copolymer 4V appear to follow the molecular weight curve for a shorter period of the degradation process before the carbonyl concentration becomes dominant. The difference in the combination curves of the two samples is related to differences in the individual projections. The relationship between T_c and T_m and

molecular weight are very similar for the two copolymers, whereas differences are observed for the molecular weight versus carbonyl index and T_c or T_m versus carbonyl index projections. Although similar relationships between these parameters are seen initially, it can be seen at higher carbonyl index values that for approximately the same carbonyl index, copolymer 4V has higher molecular weight and T_m values than sample 3V. In Figure 4.44 (b) it was seen that the relationship between carbonyl index and $\overline{M}_w$, which is almost identical at low carbonyl index values, is steeper in copolymer 4V, indicating that, for the same carbonyl index, $\overline{M}_w$ is higher in copolymer 4V. The molecular weight decrease is small compared to the increase in carbonyl concentration, which explains the steeper slope of the combination curves of copolymer 4V at higher carbonyl index values in Figures 4.54 and 4.55. These presentations allow the comparison of the degradation of ICPP copolymers 3V and 4V irrespective of the difference in the time scale of their degradation and clearly indicate the influence of degradation on the interrelationship between three seemingly independent molecular parameters.

To conclude the results on the degraded bulk 3V and 4V samples, degraded samples of copolymer 4V were also re-crystallised and fractionated by TREF. The preparative TREF results for both copolymers are shown in Figure 4.56.

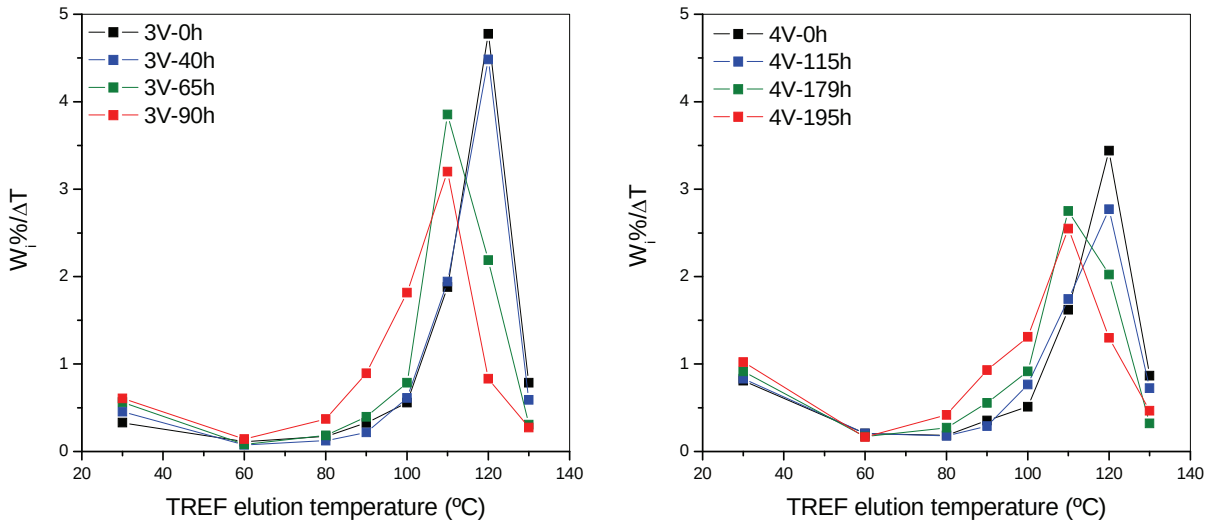

Figure 4.56: TREF weight fraction per temperature increment curves ($W_i\%/\Delta T$) for the degraded 3V and 4V samples.

Although the TREF dissolution profiles of the two samples differ slightly in terms of the intensity and broadness of the main dissolution peak and the amount of material eluting in the soluble fraction at 30ºC, the changes observed, are similar. The dissolution curve of sample 4V is also seen to shift towards lower temperatures and decrease in intensity with ongoing degradation time while there is an increase in the $W_i\%/\Delta T$ value of the 30ºC fraction. These results indicate that, although there is a difference in the amount of iPP of copolymer 4V relative to that of the amorphous material eluting at lower temperatures, the iPP phase is still degraded preferentially. The changes in the weight

percentages of the material eluting in every fraction of the undegraded and degraded 4V copolymer, are illustrated in Figure 4.57.

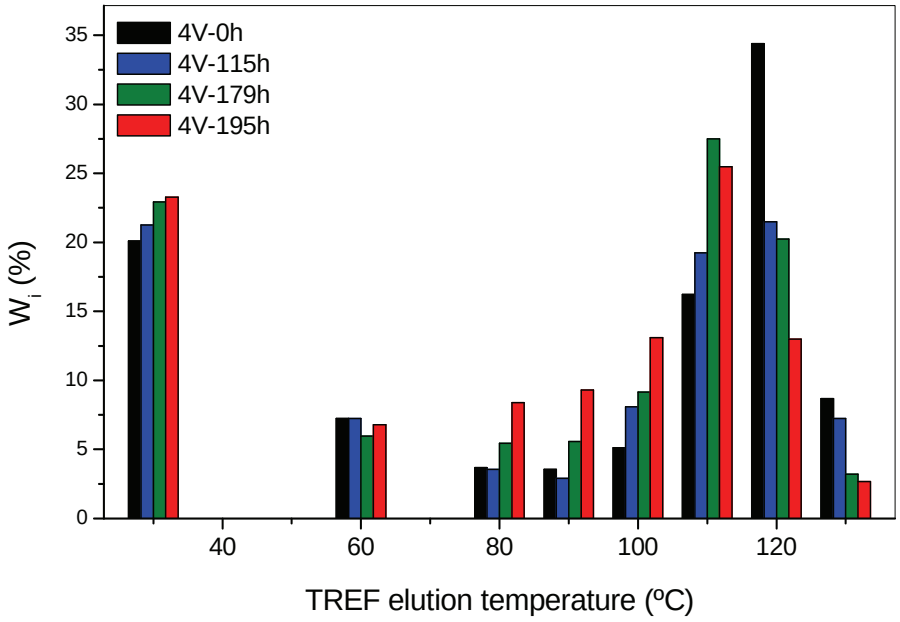

Figure 4.57: Changes in the weight percentage (W_i%) of all TREF fractions of sample 4V obtained after degradation times of 0, 115, 179 and 195 hours.

Similar to what was observed for sample 3V in Figure 4.22, a decrease in the amount of material eluting in the 120 and 130ºC fractions with ongoing degradation times occurs, accompanied by an increase in the amount of material eluting in most of the fractions between 30 and 110ºC. Degradation seems to affect the crystallisability of the degraded 4V sample to the same extent as in sample 3V, where degraded iPP molecules were modified by scission and carbonyl group insertion to such an extent that they were no longer crystallisable at higher temperatures (110 and 120ºC), resulting in the increase in the amount of material dissolving and eluting at lower elution temperatures. The SEC results of all fractions of the two copolymers are presented in Figures 4.58 and 4.59. Although these results have already been presented for sample 3V in Section 4.1.4.1, it is included here for comparative purposes.

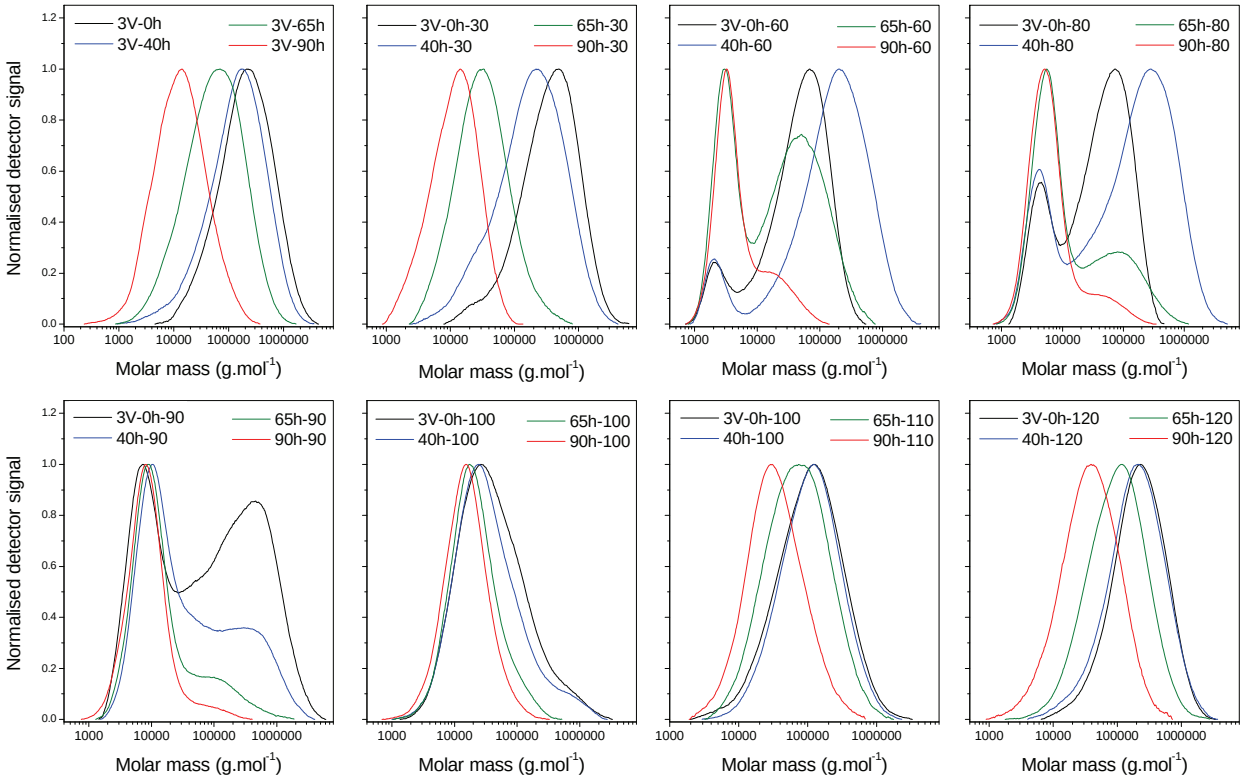

Figure 4.58: Changes in the SEC curves of the bulk 3V samples and each of its TREF fractions obtained after re-crystallisation of samples degraded for 40, 65 and 90 hours.

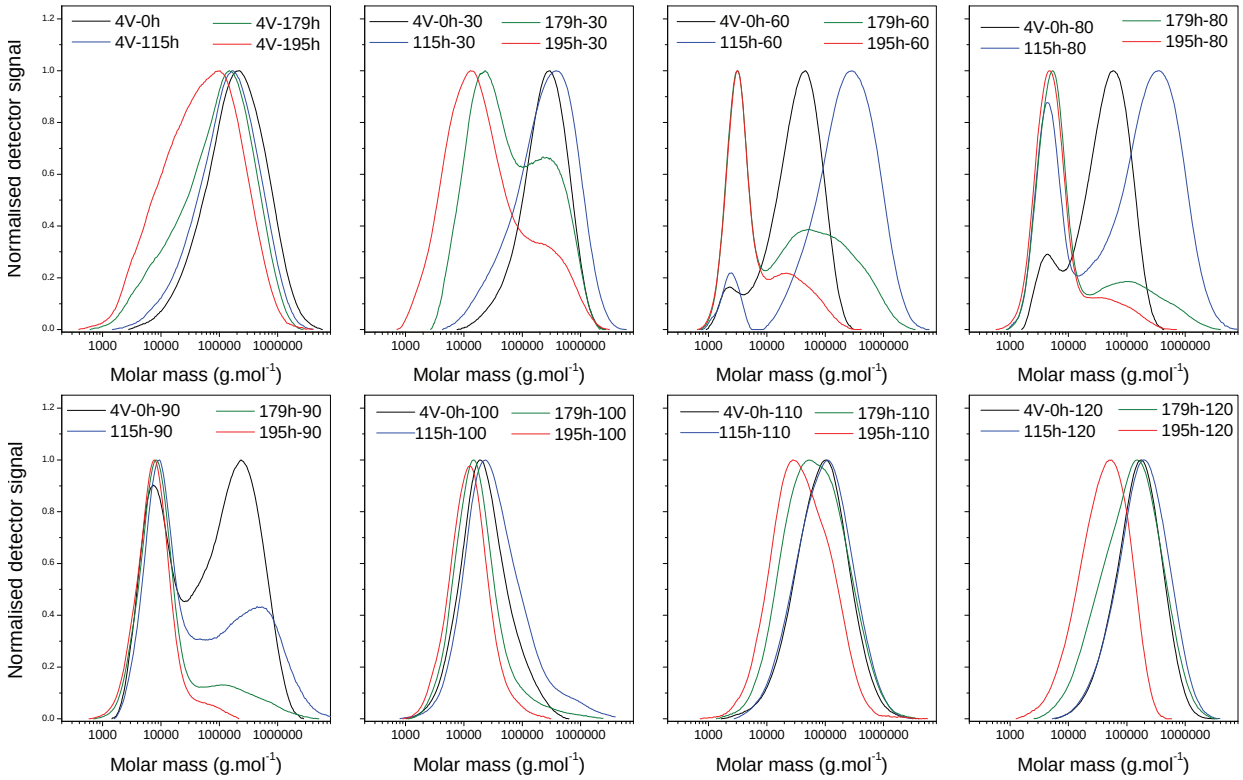

Figure 4.59: Changes in the SEC curves of the bulk 4V samples and each of its TREF fractions obtained after re-crystallisation of samples degraded for 115, 179 and 195 hours.

The shifts in molecular weight distributions of the highest eluting fractions of the two copolymers are very similar. This is to be expected, since these fractions consist mainly of iPP, and since the polymerisation of propylene in the first reactor of the synthesis of impact PP is not affected by ethylene content, the characteristics (e.g., molecular weight and isotacticity distribution) of the hPP phase is accepted to be fairly similar in the two copolymers. In Section 4.1 the 60–90ºC fractions were found to consist of two co-eluting components, i.e., low isotacticity PP and EPC. If the molecular weight shifts of these fractions eluting at corresponding temperatures in the two grades are compared, it is seen that there is very little difference in the molecular weight changes of the low isotacticity PP component (at lower molecular weight) of these fractions in the two grades. The EPC component, however, shows slightly different molecular weight shifts in the two copolymers. In the 60 and 80ºC fractions of sample 3V, the molecular weight distribution curve of the higher molecular weight EPC component is seen to shift towards higher values in the sample degraded for 40 hours, after which the complete molecular weight distribution curve shifts back to lower values after 65 and 90 hours. This component of the 60 and 80ºC fractions of copolymer 4V is seen to shift to even higher molecular weight values in the sample degraded for 115 hours, after which the molecular weight distribution curve also shifts back to lower values, but compared to sample 3V, a higher molecular weight shoulder remains where the EPC distribution was seen in the fractions degraded for 115 hours. A more gradual shift towards lower molecular weight values is seen with ongoing degradation time in sample 4V. These fractions of sample 4V were also seen to contain a higher mole percentage of ethylene than the corresponding fractions of sample 3V, and since it is known that PE degrades mainly via a cross-linking mechanism at moderate temperatures, this might be an indication of partial cross-linking of the ethylene sequences in the EP copolymers.

The most significant difference in the molecular weight changes of the fractions of the two copolymers is, however, seen within the 30ºC fraction. SEC-FTIR analysis in Section 4.1 indicated this fraction to consist mainly of EPR, with a minor aPP component present as a low molecular weight shoulder to the molecular weight distribution curve of the EPR. From Section 4.1 it was also concluded that degraded iPP from higher eluting fractions is found in the 30ºC fraction upon re-crystallisation and fractionation of degraded samples by TREF, therefore the concentration of low molecular weight material is expected to increase within these fractions. The entire molecular weight distribution curve of this fraction shifts to lower values in sample 3V, whereas some part of the original distribution in the undegraded material remains and overlaps with the distribution of low molecular weight degradation products in sample 4V. The EPR of this fraction of copolymer 4V, therefore, seems to be more stable than that of sample 3V, possibly due to its chemical composition, .i.e., higher comonomer content and lower isotacticity. The higher ethylene in the 60–90ºC fractions of sample 4V also seems to improve the stability of these fractions in copolymer 4V.

In Section 4.2 FTIR and SEC results have indicated a longer induction period and slower increase in carbonyl functionalities, as well as a slower decrease in $\overline{M}_w$ values for copolymer 4V. A longer

induction period and slower degradation rates in impact PP copolymers with higher ethylene contents and isotacticity has been reported by a number of authors[10, 54, 79], whereas the opposite result was obtained by others[4, 5, 82]. The introduction of more stable methylene units from ethylene is believed to be the reason for the delayed onset and slower rate of oxidation in ICPP's of higher ethylene contents. The presence of ethylene units is believed to eliminate the number of tertiary PP carbons that can undergo dissociation reactions. Higher isotacticity of the PP unit also increases the rate of oxidation, since the presence of the 3_1 helix in crystalline PP promotes the bimolecular decomposition reaction which is of lower activation energy than the unimolecular equivalent occurring in more random conformations[54]. The preferential attack of tertiary carbons of the PP phase in ICPP's is not denied by Kruczala *et al*.[5, 82], although the rate of degradation is reported to be influenced by the amount of EPR. Thermal degradation at 393 and 433K indicated the copolymer of higher ethylene content (25%) to degrade more rapidly than the sample containing only 10% ethylene, due to the higher rate of oxygen diffusion in the EPR phase at elevated temperatures[5].

In Figures 4.49 and 4.50 a considerable difference in degradation behaviour is observed for the two copolymers with only a small difference in ethylene contents and isotacticity, but a relatively large difference in the amount of amorphous material. TREF fractionation combined with ^{13}C-NMR, DSC and SEC was used to investigate the microstructural properties of the two copolymers. SEC and DSC results of the corresponding fractions of both copolymers agreed well, with only minor differences in the SEC values for the 30 and 90ºC fractions of samples 3V and 4V. Almost identical T_m and T_c values were observed for all fractions eluting at corresponding TREF elution temperatures within the two copolymer grades. This illustrates the similarity in the isotacticity distribution of the hPP phase of the two copolymers as well as the similarity in ethylene and propylene sequence lengths of the EPC component of corresponding fractions.

Differences are, however, observed in the weight percentages of the fractions eluting at corresponding elution temperatures for the two samples. Larger amounts of the amorphous fractions (30ºC–90ºC) are collected during prep-TREF of sample 4V, accompanied by a smaller amount of the more crystalline ones eluting at 110 and 120ºC. Similar amounts are collected for the 100ºC fraction of both copolymers. From ^{13}C-NMR, DSC, SEC and CRYSTAF results it was concluded that the four major constituents identified in sample 3V are also present within the same elution ranges for sample 4V. In Section 4.1 the major constituent of the 30ºC fraction was identified as EPR, the 60ºC and 80ºC fractions consists of co-eluting components of EPC and low isotacticity hPP, where the ethylene and propylene sequences are very short and of low crystallinity. The 90 and 100ºC fractions also consist of these two components, although the isotacticity of the hPP within these fractions is higher and the ethylene and propylene sequence lengths are longer, resulting in EP copolymers of higher crystallinity. The 110–130ºC fractions were found to consist mainly of isotactic PP, with a very low concentration of hPE present too. According to these classifications, the total amount of material (W_i%) eluting within each of the elution ranges mentioned here, was calculated from TREF data and the results are presented in Table 4.14.

Table 4.14: Weight percentages of the four major constituents of samples 3V and 4V

T_e	30ºC	(60–80ºC)	(90–100ºC)	(110–130ºC)
Sample	**EPR + aPP**	**'Transition' EPC + low isotacticity PP**	**'Blocky' EPC + higher isotacticity PP**	**Isotactic PP + hPE**
3V-0h	9.90	6.83	8.86	74.72
4V-0h	21.11	10.94	8.67	59.28

It is seen here that similar amounts of material elute between 90ºC and 100ºC within the two copolymers, whereas significant differences are seen for the other three elution ranges. The combined weight percentage of the 60 and 80ºC fractions constitutes 6.83% and 10.94% of sample 3V and 4V, respectively. The most significant differences are, however, observed in the 30ºC fraction, as well as the highest eluting (110–130ºC) fractions. The PP phase is considered unaffected by the ethylene content during copolymerisation. This PP phase, ranging from aPP in the lowest eluting fractions, through semi-crystalline propylene within the mid-eluting EP copolymers to highly isotactic PP in the highest eluting fractions, is indicated to be very similar in the two copolymers, with regard to istoacticity and thermal behaviour. It is, therefore, assumed that similar weight percentages of PP will elute in corresponding fractions of the two copolymers where PP was seen to co-elute with EPC. A difference in the weight percentage of the 60–80ºC elution range is, therefore, expected to result from a difference in the concentration of the EPC, rather than the low isotacticity PP. The aPP in the 30ºC fraction and the hPE in the highest elution range (110–130ºC) are present in such small amounts, that the differences observed for these fractions can confidently be ascribed to a difference in the amount of EPR and iPP present within the two copolymers. It is seen that the amount of EPR in copolymer 4V is more than double the amount in sample 3V, whereas the amount of iPP in sample 4V is only 59.28%, compared to 74.72% in sample 3V.

The delayed induction and slower oxidation rate portrayed by sample 4V is believed, not only to be the result of the higher ethylene content and lower isotacticity of the bulk sample, but also the relative amounts of the four major components present within the two impact copolymers. TREF fractionation of the undegraded samples has indicated that sample 4V also contains a larger concentration of amorphous EPR and transition EPC accompanied by a lower concentration of iPP, which is the component that degrades preferentially in this copolymer too, despite its higher concentration of amorphous material. TREF fractionation combined with ^{13}C-NMR has also indicated that the excess ethylene added during the second stage of the polymerisation of sample 4V is located within the EPR and transition EPC fractions. Upon re-crystallisation and fractionation of degraded samples by TREF, similar molecular weight shifts were seen within the iPP fractions of the two copolymers. The behaviour within the EPR and co-eluting EPC and low isotacticity PP fractions were, however, different for the two copolymers, where these fractions of copolymer 4V appeared to be more stable than those of sample 3V. The higher ethylene content within copolymer 4V is, therefore, considered to be

responsible for the higher stability of the bulk 4V copolymer, mainly due to an increased stability of the lower eluting fractions containing the excess ethylene.

It seems interesting that, although degradation initiates within the PP phase, the amount of ethylene and its distribution within the four components of an ICPP seems to be the most important factor determining the degradation behaviour of the two copolymers. An increase in the oxidation induction time with increasing ethylene content is accounted for by the higher chemical stability of its methylene units as well as the barrier effect of the comonomer in intra-chain hydroperoxide formation[76-79]. It is also known that the amount of ethylene affects the morphology of impact PP copolymers, e.g., the shape and size distribution of the dispersed EPR phase as well as the nature of the segmented EP copolymers acting as a compatibiliser at the interface between the EPR inclusions and the iPP matrix[36, 40]. This interface has been suggested to play a vital role in the migration and combination of free radicals during the degradation of heterophase EP copolymers[83]. Therefore, the difference in stability between the two copolymers might be the result of the difference in morphology between the two grades. These results have indicated that, although chemical composition is still the most important factor governing the degradation of impact PP copolymers, the unique morphology of these copolymers plays a very important role. In the following section the degradation of impact PP copolymer thin films studied in the previous two sections, will be expanded to thicker specimens where oxygen diffusion is expected to play a bigger role. The spatial heterogeneity of degradation within copolymers 3V and 4V will be studied by FTIR-μS and a conventional technique consisting of layer-by layer milling followed by SEC, FTIR and CRYSTAF analysis.

4.3 Studying the spatial heterogeneity of thermo-oxidative degradation in impact PP copolymers 3V and 4V

As explained in Section 2.5.5, polymer degradation is not always homogeneous on the macroscopic scale. Degradation under accelerated conditions often occurs as a heterogeneous process controlled by oxygen diffusion [84-94]. In thick polymer samples, where oxygen consumption exceeds the rate of oxygen permeation, oxidation of the surface layers is generally observed, with the core of the sample remaining unaffected. The heterogeneity of the degradation process depends on various factors. Intrinsic sample parameters responsible for heterogeneous degradation behaviour in polymers include: sample thickness; comonomer distribution and stereoregularity as well as sample morphology, which governs the solubility and permeability of oxygen in the polymer. Heterogeneity is also caused by differences in radical mobility throughout the sample, although the effect of additives and catalyst residues on the degradation behaviour of polymers is also not to be ignored.

The spatial heterogeneity of the degradation process leads to depth-varying concentrations of oxidation products across thick polymer specimens. Depth profiling of degradation products can be done by a number of analytical techniques, including FTIR and GPC analysis over a cross-section of

the degraded polymer obtained by microtoming[95] or layer-by-layer milling[96,97]. It is clear that, when studying the heterogeneity of the degradation process, techniques are needed that take into account the spatial variation in degradation product concentrations as well as the intrinsic heterogeneity of the sample. FTIR microspectroscopy (FTIR-µS) is a very powerful technique currently used for studying the heterogeneity of degraded samples on the micrometer scale. Depth profiling of degradation products are done by analysing the oxidised sample in the plane perpendicular to the axis of exposure [98]. Slices are positioned under the objective of the FTIR microscope and analysed by transmission of light through a restricted area, the size and dimensions of which are determined by the pre-defined image-masking aperture. The sample is secured onto a precision-controlled movable sample stage that allows accurate, reproducible analysis of each slice at a number of points across the sample width, as determined by the step-width selected for the experiment. Individual IR spectra are recorded at a single point or a number of points or zones across the sample width, as determined by the selected step-width and are subsequently analysed by suitable IR software to create a profile of oxidation product concentration across the sample width. Single point analyses are, however, of limited use when studying heterogeneous or multi-component samples. Point-by-point analysis of larger, continuous areas is possible by moving the specimen in a known, pre-determined manner relative to the aperture. This technique is known as FTIR mapping and, by plotting the absorbance magnitude of a specific vibrational mode over the area analysed, a concentration map or profile of a specific chemical species can be obtained. Such maps are generally referred to as functional group maps and are extremely useful when studying the distribution of carbonyl, hydroperoxide and carboxylic groups in heterogeneously degraded polymer samples[99].

4.3.1 Optimisation of experimental conditions

To ensure reliable, reproducible results from FTIR-µS analysis, a few experimental parameters need to be considered. One of the biggest sources of error in FTIR-µS originates from the microspectroscopy apertures chosen. Opaque apertures are applied to ensure that radiation reaching the detector is representative only of the sample area of interest, and that stray light from areas surrounding the defined sample area is excluded. The spatial resolution of the FTIR microscope can be controlled by the aperture size and dimensions, however, the highest spatial resolution is not determined by the apertures, but rather by the diffraction limit of the radiation[100]. Figure 4.60 shows the results of selected area of the FTIR spectrum obtained from analysis of an EP copolymer, using three different aperture dimensions.

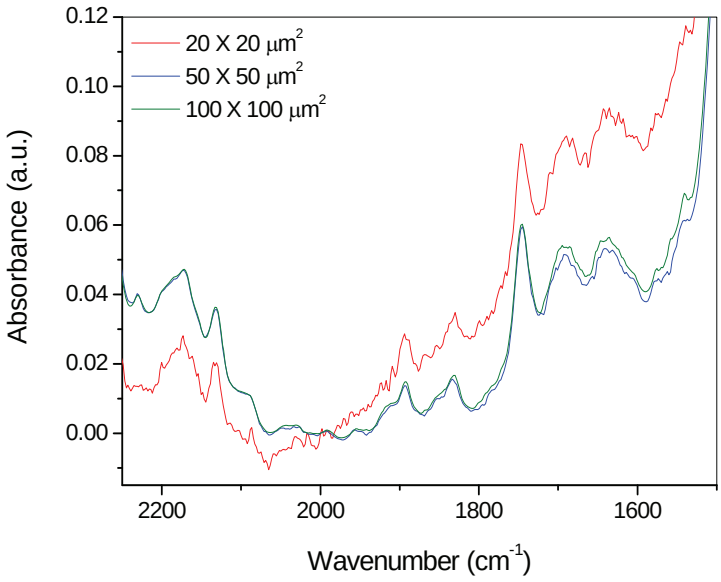

Figure 4.60: The comparison of different aperture dimensions on the quality of FTIR-μS results obtained.

It is evident that the signal-to-noise level improves from the smallest aperture size to the largest. It has been stated that small aperture sizes are responsible for an increase in the noise level and distortion of the relative intensities observed in the FTIR spectra. An aperture size of 100 X 100 μm^2, which is similar to that used by Ellis *et al*. [100] for the analysis of a heterogeneous EP copolymer system, was selected for all analyses.

Finally, the step-size or step-width between measurement points in line scans or maps needed to be selected. Figure 4.61 shows the results obtained for the CO peak area measured in sample 4V at step-widths of 10, 20, 50 and 100 μm.

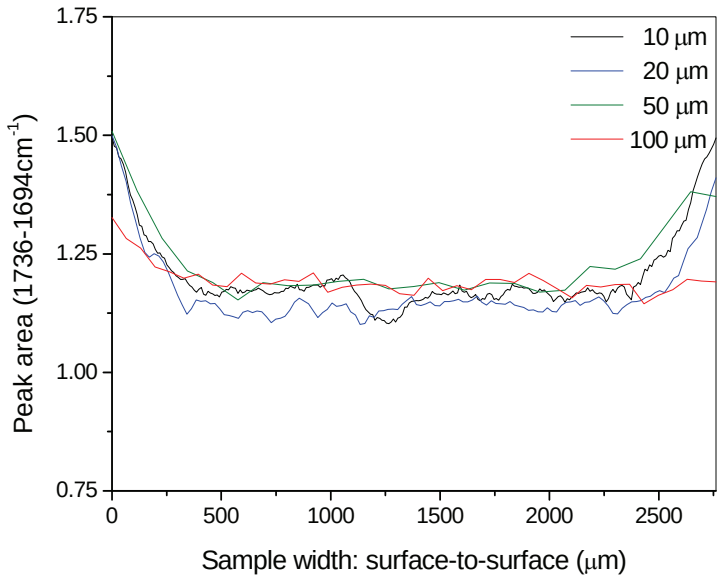

Figure 4.61: Comparison of the effect of the step-width on the concentration profile of the carbonyl functionality.

It is clear that larger step-widths result in similar concentration profile trends than smaller ones, with the advantage of saving valuable analysis time. The step-width is usually smaller than or equal to the aperture dimensions chosen [100]. Over-sampling, i.e., when the step-width is smaller than the aperture size, is often applied for obtaining sharper mapping data when studying details close to the diffraction limit. Step-widths of 100 µm and 50 µm were chosen respectively, for collecting the maps and line scans presented in this section.

4.3.2 Determination of carbonyl oxidation product profiles by FTIR-µS

For the purpose of obtaining CO concentration profiles within heterogeneous samples, one can perform FTIR-µS analyses both by means of line scans, i.e., where a number of points are scanned across the width of a specimen at a pre-determined step-width in the Y direction, and area maps, where an area of pre-defined size is scanned at a specified step-width in both the X and Y directions. FTIR maps of the CO band intensity over areas of both an undegraded (3V-0h) and degraded (3V-170h) sample of copolymer 3V are presented in Figure 4.62.

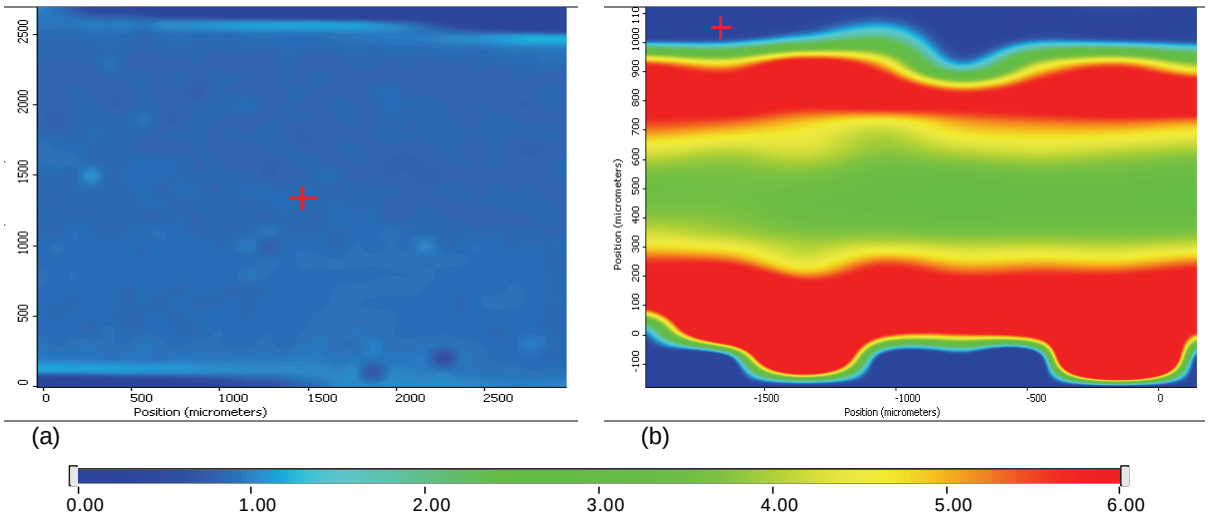

Figure 4.62: Carbonyl group maps of a microtomed slice of (a) the undegraded (3V-0h) and (b) a degraded sample (3V-170h).

The concentration of carbonyl-containing degradation products was measured by the area of the CO band between 1736 cm^{-1} and 1694 cm^{-1}. A reference band was not chosen in this case, since the thickness of all microtomed slices varied by less than 5%. As seen from the scale attached, the dark blue areas are representative of areas containing no carbonyl functionalities, whereas the green, yellow and red areas represent those portions of the sample that contain increasing amounts of CO degradation products, with red areas being the most degraded. In the undegraded sample, the dark blue area is indicative of the air surrounding the microtomed slice and the lighter blue areas represent the very low concentration of CO functionalities formed during sample preparation, which are in this

case, seen to be uniformly distributed across the entire sample area. In the degraded sample, the dark blue area on both sides of the specimen are once again representative of the air surrounding the sample, whereas the green, yellow and red zones indicate a low to high concentration of CO degradation products. The highest concentration of carbonyl-containing functionalities can be observed close to the edges, with the core of the sample also being degraded (no blue area present in the centre as in the undegraded sample). The narrow light blue, green and yellow areas at the edges of the degraded sample are an artefact caused by overlap of the film edge (red) and surrounding air (dark blue) within the 100 µm slices recorded. FTIR maps are useful for extracting individual spectra from areas of dissimilar colours, therefore the difference in the CO peak intensity of any point on the undegraded sample can be compared to those found in the degraded sample. These maps also give an indication of the thickness of the surface area affected by degradation. The width of the microtomed slice of the undegraded sample is approximately 2700 µm, which is subsequently reduced to only 1240 µm in the sample degraded for 170 hours, which indicates the loss of the surface layers due to severe embrittlement caused by prolonged degradation. Different embedding media such as paraffin wax and epoxy resins were attempted to ensure adhesion of the brittle layer to the undegraded material during microtoming, but sufficient adhesion was not achieved by any of these media.

In the following analyses, line scans were performed for the purpose of constructing CO concentration profiles for the different degradation times of both copolymers. The reproducibility of the technique was investigated by comparing several line scans recorded at different positions on the same microtomed slice to the concentration profiles obtained from a number of different microtomed slices. Figure 4.63 (a) contains the CO concentration profile of the undegraded 3V copolymer obtained at six different positions on the same microtomed slice. A step-width of 100 µm was applied. The average of the six curves is presented in Figure 4.63 (b) and error bars are fitted to indicate the deviation of each point from the average.

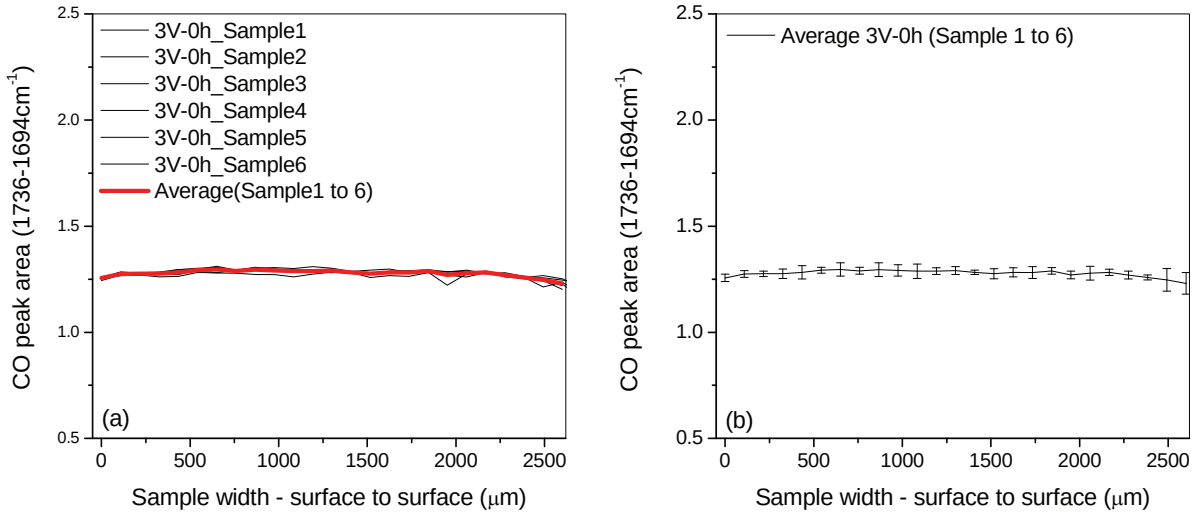

Figure 4.63: Evaluation of the reproducibility of the CO group concentration profiles measured at different points on a microtomed slice of the undegraded (3V-0h) sample.

Figure 4.64 (a) contains the CO concentration profile obtained from line scans performed on three different microtomed slices. Here, a step-width of 50µm was applied. The average curve is also shown in Figure 4.64 (b), with error bars indicating the deviation of individual curves from the average value. It can be seen here that CO concentration values obtained in the three separate scans deviate more from the average values than in Figure 4.63 (b), but the deviation observed here, is still within acceptable limits.

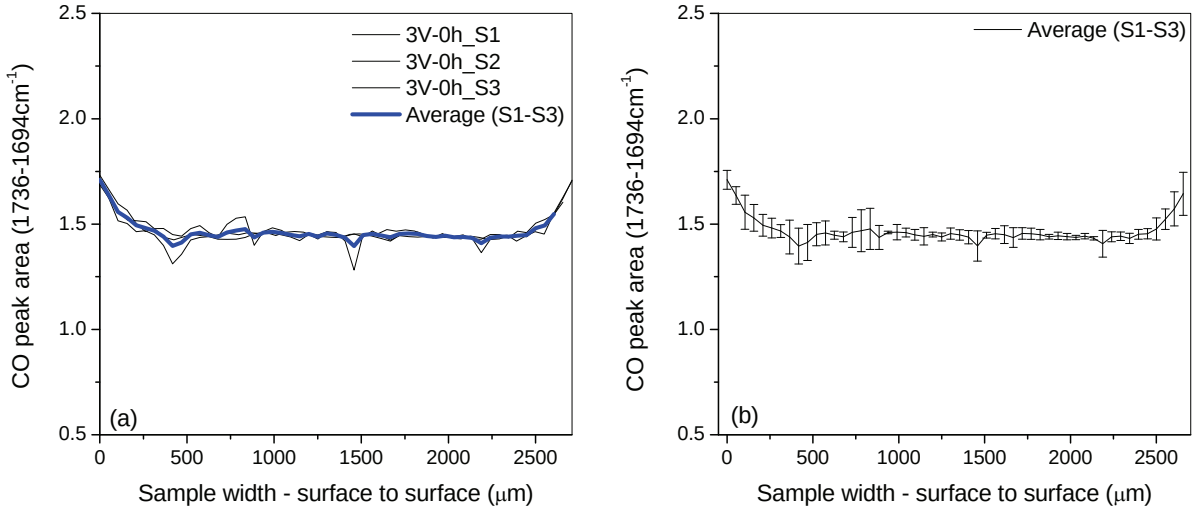

Figure 4.64: Evaluation of the reproducibility of the CO group concentration profiles measured on different microtomed slices of the undegraded (3V-0h) sample.

Since thick samples such as these in question are known to degrade heterogeneously, a larger deviation between measurements of degraded samples was expected. CO concentration profiles obtained from three separate line scans performed on three different slices of 3V-96h plaques are presented in Figure 4.65 (a) and the average curve with fitted error bars are once again shown in Figure 4.65 (b). A relatively small deviation from the average values is seen for data points collected within the core of the three plaques (500 to 1500 µm). A larger deviation between points is however seen close to both edges (0 to 450 µm and 1600 to 2250 µm). From Figure 4.62 it is clear that a more advanced level of degradation is detected at the edges compared to the core of the sample. In samples degraded for 96 hours, it can be seen that the core of all three are still relatively undegraded compared to the edges. Since degradation is a heterogeneous process, the edges of the three samples are expected to degrade somewhat differently depending on the characteristics of each plaque, and the deviation from the average value at each point is expected to be noticeable.

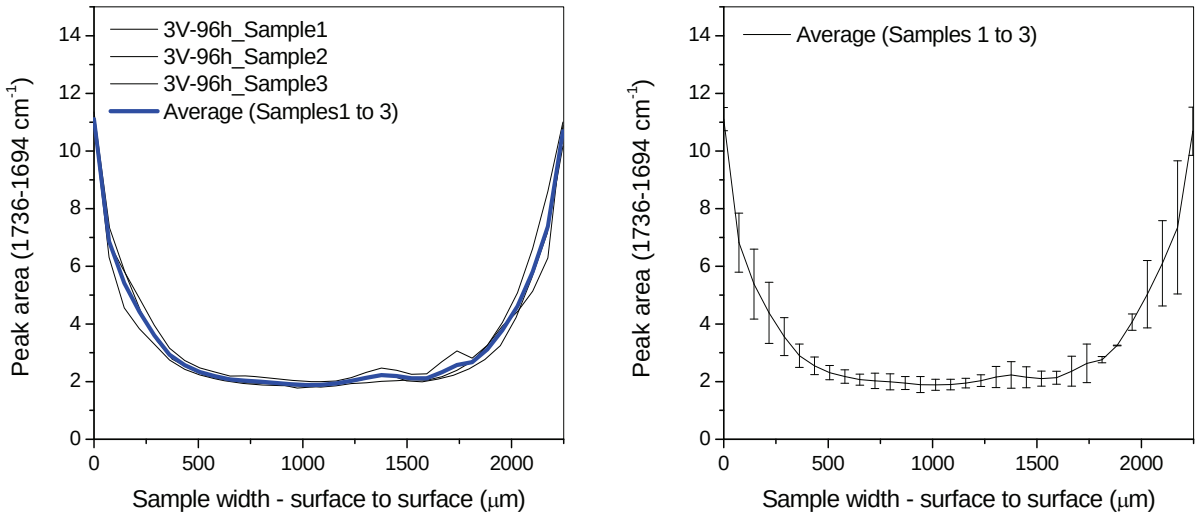

Figure 4.65: Evaluation of the reproducibility of the CO group concentration profiles measured on different microtomed slices of a degraded (3V-96h) sample.

It was, therefore, concluded that results from a number of analyses performed on separate microtomed slices would have to be performed to obtain reliable results. Each CO concentration profile presented in the following graphs represents the average curve obtained for a number of individual measurements performed on different microtomed specimens.

The carbonyl concentration profiles for the various degradation times obtained across the width of each microtomed slice of sample 3V, are presented in Figure 4.66. All profiles were constructed around the centre of each sample, which is indicated by the point, X=0.

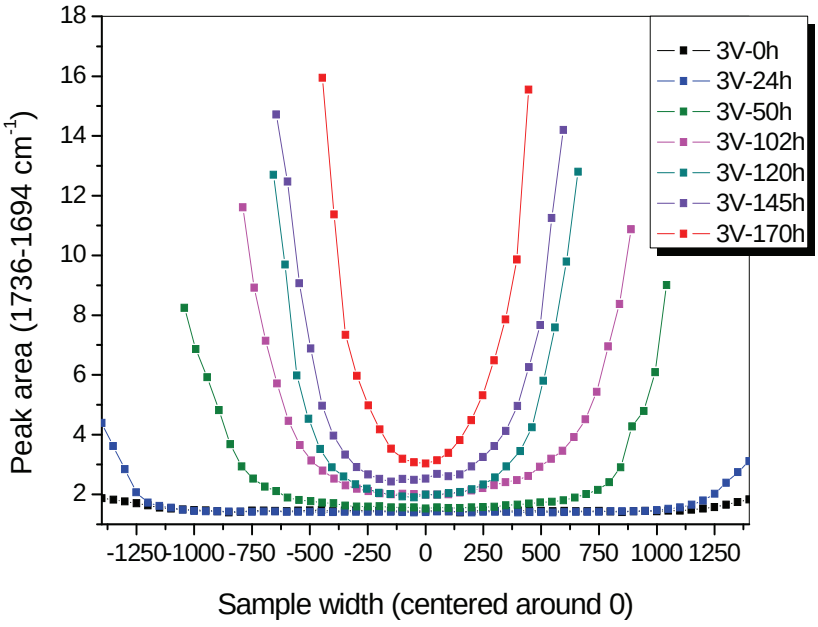

Figure 4.66: Averaged CO group concentration profiles obtained at different times during the degradation of sample 3V.

The concentration profiles obtained at all time intervals are symmetrical, indicating that degradation proceeds in a similar way starting from both surfaces. The undegraded sample shows a uniform distribution of carbonyl functionalities across the entire width of the sample. During the early stages of degradation (3V-24h), a slight increase in the CO concentration is observed at distances close to the two edges first, with the core of the sample appearing to be unaffected, as seen by the plateau region in the middle of the CO concentration profile. This is typically found during the degradation of thicker samples where oxygen is consumed within the surface layers before it can diffuse into the core layers[97, 101]. At longer degradation times, degradation is seen to spread further into the bulk of the sample, as a drastic increase in the CO concentration values at the two edges is observed. A decrease in the width of the plateau section in the core of the sample (distances close to 0 µm on either side) also gets increasingly narrower as the edges degrade away. This can be seen by the CO concentration profile changing its shape from a U to a sharper V-shaped curve. It is also interesting to note that, although the edges are considerably more degraded than the bulk of the sample at all degradation times, the core also seems to degrade gradually with ongoing degradation times, as is visible from the increase in the y-offset of all curves at X = 0 µm (centre or core of the sample) with ongoing degradation time. The CO concentration profiles of sample 4V obtained at the various degradation times are presented in Figure 4.67.

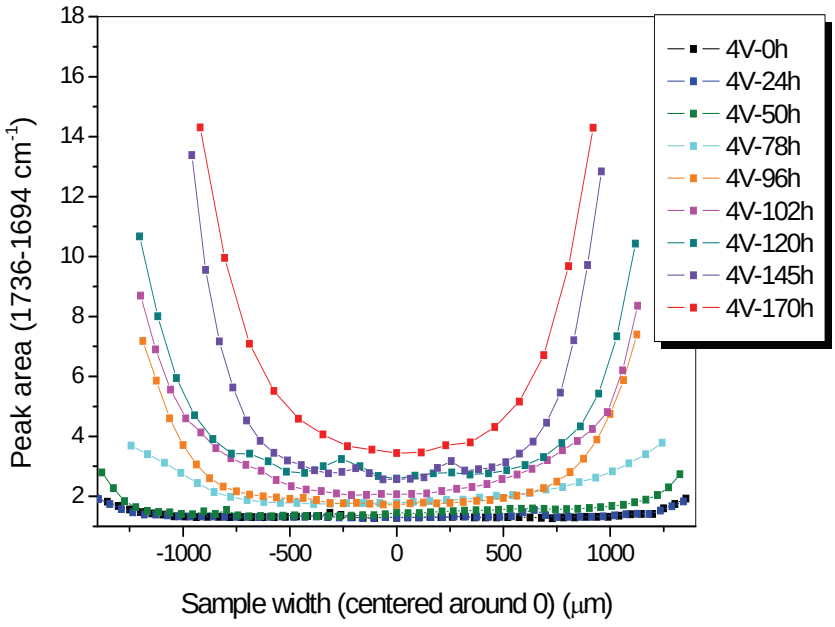

Figure 4.67: Averaged CO group concentration profiles obtained at different times during the degradation of sample 4V.

The CO concentration profiles of sample 4V are similar in shape to those of sample 3V, with the edges at all degradation times containing a higher concentration of CO functionalities and therefore being more degraded than the bulk or core. The increase in CO concentration at the edges seems more gradual than in sample 3V and the U-shaped curve never really develops into a V-shaped one at longer degradation times. This indicates that, at longer degradation times, (especially 4V-145h and

4V-170h), the core of the 4V slices are still substantially less degraded than the edges. It can therefore be concluded that the CO concentration profile across the width of sample 3V is much steeper than in sample 4V, at longer degradation times. These results are consistent with those obtained for the degradation of the thin 3V and 4V films in Section 4.2, where a steeper increase in the carbonyl index with ongoing degradation time was observed for sample 3V.

The CO concentration at different distances from the core to the surface of all 3V and 4V samples is presented as a function of degradation time in Figure 4.68. Here, d indicates the distance of each point from the core of the sample where the CO peak area (1736–1694cm^{-1}) was measured and d = 0 signifies the point exactly at the centre of each plaque. Therefore, the curve labelled d = 0 µm illustrates how the CO concentration profile changes in the exact centre or core of the sample with ongoing degradation time. The curves labelled d = 1400 µm in sample 3V and d = 1350 µm in sample 4V, represent the CO concentration curves taking place at the edges of the two samples with ongoing degradation times. Unfortunately these two curves only contain a limited number of points, since the edges degrade completely within a fairly short time and are lost due to embrittlement. Furthermore, curves labelled d = 100 µm, d = 250 µm, d = 450 µm, which are closest to d = 0 µm, can also be regarded as layers found within the core of the plaques, whereas those labelled d = 800 µm, d = 1000 µm and d = 1200 µm are regarded to be representative of the CO concentration changes happening at the edges.

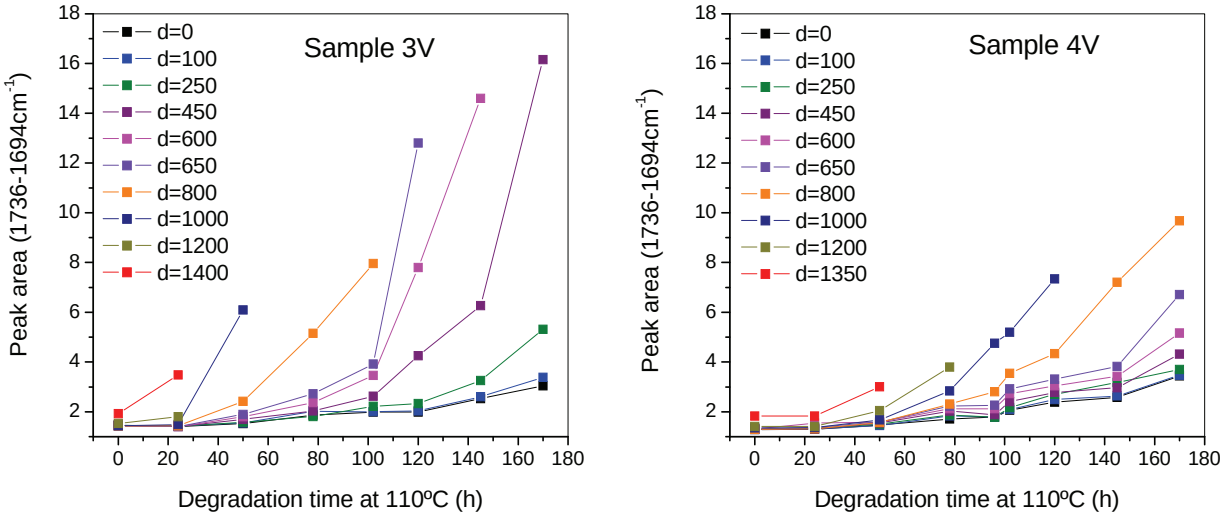

Figure 4.68: The CO concentration value at different distances from the core to the surface of all 3V and 4V samples, as a function of degradation time.

It can be seen in Figure 4.68 that the difference in the CO concentration profiles of the core and the edges of sample 4V is less significant than those of sample 3V, where the CO concentration profiles of the layers close to the edge are much steeper than those in the bulk. In sample 4V, the layers at d = 0 µm to d = 650µm all have similar concentration profiles, with the biggest difference seen only from 100-170h, where there is a significant increase in CO concentration with ongoing degradation

time. The layers found at 800–1350 µm from the core show an increase in CO concentration commencing at shorter degradation times, with significantly higher CO values reached at longer degradation times. The outermost layers (d = 1000 µm; d = 1200 µm; d = 1350 µm) of sample 4V show a gradual increase in CO concentration after 20h, with a drastic increase only observed after 50h, at which point there seems to be very little change in the CO profiles of the core layers.

In sample 3V, a gradual increase in CO concentration with ongoing degradation times is only observed for the core layers from 0 to 250 µm. All layers closer to the edge, starting at a distance of 450 µm from the core show a drastic increase in CO concentration from a degradation time of 78h. The outermost layers of sample 3V show a drastic increase in CO concentration from as early as 20h of degradation, with the layer at d = 1400 µm, showing no induction period at all, as indicated by the increase in CO concentration seen from 0h already.

From the above it can be concluded that degradation starts earlier in sample 3V (as seen from the increase in the CO profile of the layer at 1400 µm from 0h already) and it spreads more quickly towards the core layers than in sample 4V. However, when comparing the degradation behaviour of the core of both samples (d = 0), a similar CO concentration is detected for sample 4V than 3V with ongoing degradation time.

In Section 4.2 the degradation behaviour of thin films of samples 3V and 4V were compared and it was seen that degradation also started earlier in sample 3V and proceeded more quickly with ongoing degradation time. This difference in stability was ascribed to the higher ethylene content (less tertiary carbons originating from propylene) and accompanying lower isotacticity of sample 4V, both factors which render this material more stable as a result of its chemical structure. In terms of the 4 major components found in the two impact PP copolymers, it was also confirmed that sample 4V contained a higher amount of amorphous copolymer (EPR) and transition copolymers, and a smaller amount of highly crystalline isotactic PP than sample 3V. The degradation behaviour observed for the thicker plaques is consistent with the results observed for the thin films of the two copolymers. What is observed here, however, is that oxygen diffusion effects might also play a role, since the core of both samples seem to degrade similarly. Oxygen diffusion effects are expected here, since these plaques are considerably thicker, and the difference in the amount of amorphous material in the two films might be responsible for the slightly different degradation behaviour than that observed in Section 4.2. Information on the crystallinity or morphology of the thicker samples is needed to confirm the contribution of morphology to the difference in degradation behaviour between the core and surface of these samples. This is also needed to justify why, although the edges of the two grades behave as expected, there is a similarity in the degradation behaviour of their core layers.

4.3.3 Spatial heterogeneity of thermo-oxidative degradation in ICPPs studied by SEC, FTIR and CRYSTAF after layer-by-layer milling

The FTIR micro-spectroscopy results will now be compared to a conventional technique of layer-by-layer milling with subsequent analysis of the layers by ATR-FTIR, SEC and CRYSTAF. Three different degradation time intervals were chosen for comparison by this conventional technique, 0h, 50h and 102h. Longer degradation times were omitted due to the difficulty of accurately milling severely degraded samples to the desired thickness, due to their brittleness. The top layers of all plaques were mechanically removed in thickness steps of 100 µm to a distance of 700 µm into the bulk. The ATR-FTIR results of the layers obtained from undegraded and degraded samples of samples 3V and 4V are presented in Figure 4.69. The peak area from 1736 cm^{-1} to 1670 cm^{-1} was taken as an indication of the concentration of carbonyl-containing degradation products found in each layer.

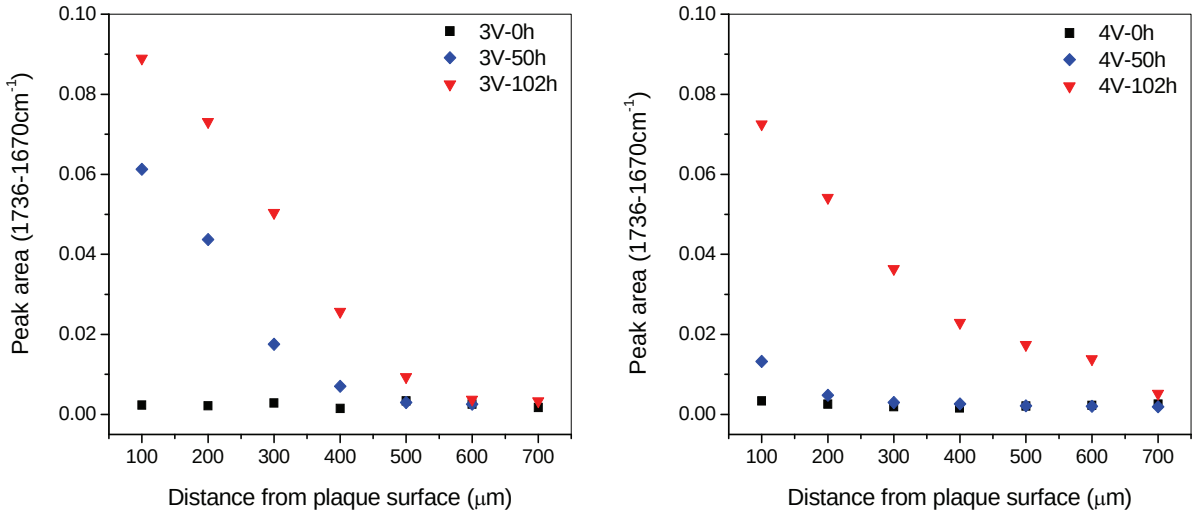

Figure 4.69: ATR-FTIR results of the CO concentration of the layers of copolymers 3V and 4V obtained by abrasion from the surface.

Both undegraded samples show a uniform distribution of a very low concentration of CO species from the surface to a distance of 700 µm into the core. After 50 hours, a significant concentration of CO species is detected in the 100 to 700 µm layers of sample 3V, whereas a small increase in CO concentration is visible only in the surface layer (100 µm) of sample 4V. After 102 hours, however, a considerable increase in the CO concentration of all layers from the surface to a distance of 700 µm of sample 4V is observed. In sample 3V, a higher CO concentration is observed in the surface layers compared to those in sample 4V, but the CO concentration of the 500-700 µm layers is smaller than in the case of sample 4V. This agrees well with the FTIR-µS results which indicate that the surface layers of sample 3V is more degraded than those of sample 4V, whereas the layers around the core of sample 4V seem to be degraded to a greater extent than those in sample 3V. The SEC results for the layers of the two copolymers are presented in Figure 4.70.

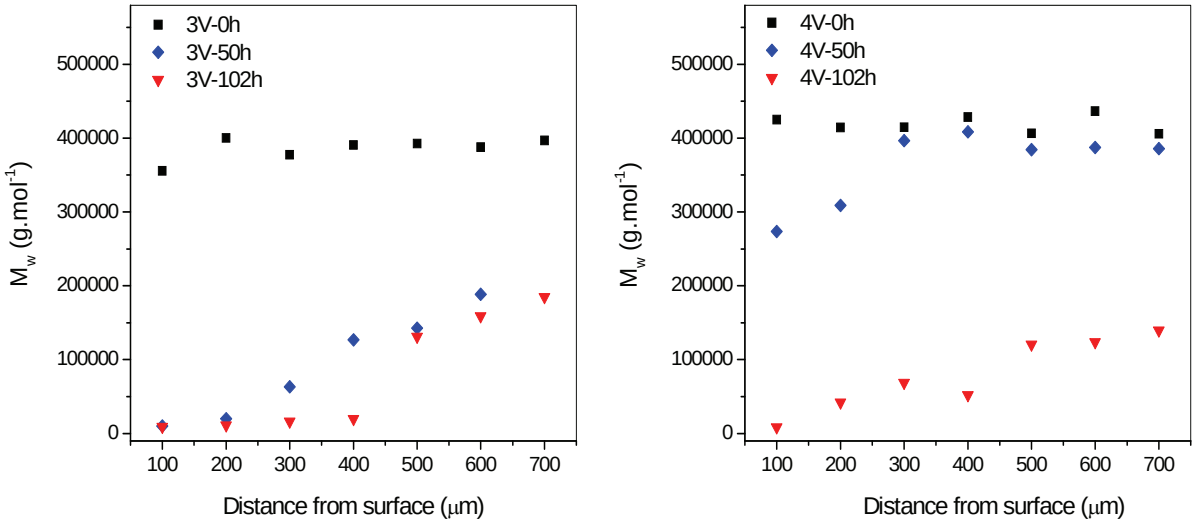

Figure 4.70: SEC results of the molecular weight changes within the layers of copolymers 3V and 4V obtained by abrasion from the surface.

Similar molecular weights are seen for all layers of the two undegraded samples. At 50 hours, a significant decrease is seen in all layers of sample 3V, whereas only the 100 and 200 μm layers of sample 4V show a molecular weight decrease. At 102h, a drastic decrease in molecular weight is seen in all layers of sample 4V too, and the molecular weight of the 500–700 μm layers is slightly lower than the corresponding layers in sample 3V. This is once again consistent with the ATR-FTIR and FTIR-μS results presented before.

Finally, CRYSTAF analysis of the layers was performed to investigate possible differences in crystallinity and crystallisability of the surface and core layers of both copolymers, and to investigate whether differences in morphology could be related to the degradation behaviour observed by FTIR-μS. The CRYSTAF crystallisation curves of the layers of the undegraded 3V and 4V copolymers, as well as those of the samples degraded for 50 and 102 hours, are presented in Figure 4.71.

Similar crystallisation curves are observed for the core and surface layers of both the undegraded 3V and 4V copolymer samples. At a degradation time of 50 hours, a decrease in the peak maximum of the crystallisation curves of sample 3V is seen with increasing distance towards the surface of the sample. A significant increase in the soluble fraction of the surface layers is also observed. These results indicate that the crystallisability of the surface layers has been changed by degradation, while very little shift in the 3V-50h_500 and 3V-50h_700 core layers indicate that these layers have remained fairly undegraded. A very small shift in the crystallisation curves of the 4V layers are seen at 50 hours, with the layers at 100-300 um appearing at only a slightly lower crystallisation temperature than the core layer (4V-50h_600 μm).

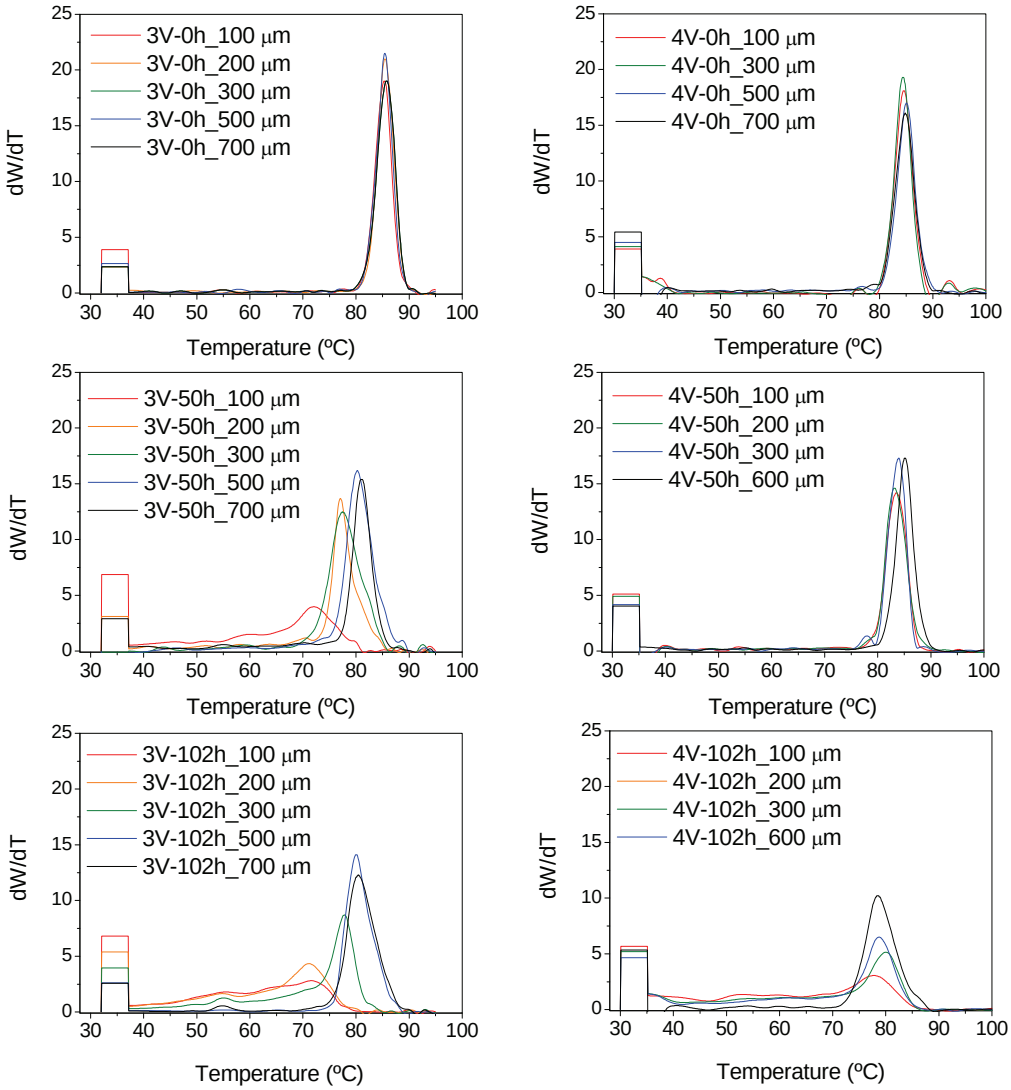

Figure 4.71: CRYSTAF crystallisation curves of the different layers of the undegraded and degraded 3V and 4V copolymers.

At a degradation time of 102 hours, the degradation within sample 3V has spread even further into the core, as indicated by the shift in the crystallisation curve of the 200 and 300 μm layers to even lower crystallisation temperatures, and the significant increase in their soluble fractions, compared to the 50 hours sample. However, the core layers (3V-102h_500 and 3V-102h_700 μm) still appear at a crystallisation temperature close to that of the sample degraded for 50 hours. At 102 hours, the crystallisation curves of all layers of sample 4V have shifted towards lower crystallisation temperatures, indicating that degradation spreads through all surface and core layers at longer degradation times. These results indicate that, at longer degradation times, degradation spreads equally through all layers of sample 4V, whereas the core layers of sample 3V are affected to a smaller extent. The peak crystallisation temperatures (T_c) of the undegraded and degraded 3V and 4V samples are presented as a function of depth Figure 4.72.

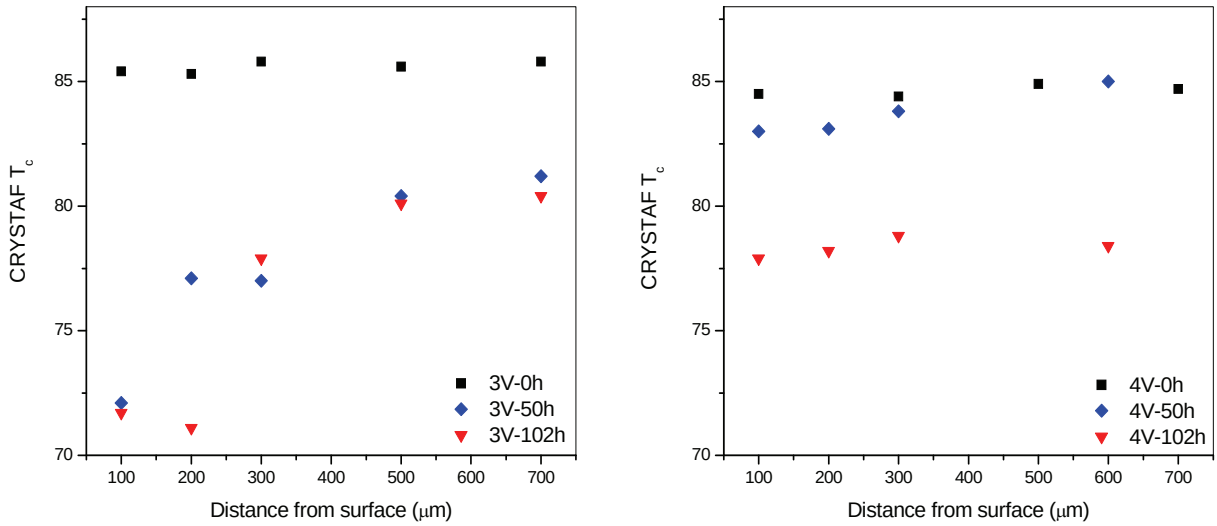

Figure 4.72: CRYSTAF crystallisation temperatures of the different layers of the undegraded and degraded 3V and 4V copolymers.

The CRYSTAF T_c results of the layers of the two copolymers agree well with the FTIR and SEC results presented in Figures 4.70 and 4.71. At a degradation time of 50 hours, a decrease in the T_c of all layers of copolymer 3V from 100 to 700 μm into the core are observed, with the lowest T_c within the most degraded surface layers (100 and 200 μm). At this stage of degradation, the T_c of all 4V layers are similar to those of the undegraded material. After 102 hours of degradation, however, the Tc of all 4V layers have decreased to values below that of the layers of sample 3V-102h, indicating that a higher level of degradation is now present within all layers of sample 4V. It is also noted here that the T_c values of the 4V layers at different distances from the surface are very similar within the 102h sample, whereas a gradient is still present within sample 3V, where the T_c value increases from the surface towards the less degraded core. These results are taken as an indication that oxygen diffusion effects do play a role in the degradation of thicker specimens of the two copolymers. The higher amount of amorphous material present in sample 4V is considered to improve oxygen permeability through the layers, resulting in a more uniform degradation profile from the surface to the core layers.

In Section 4.3 it was illustrated that the degradation principles observed for the thin films in Sections 4.1 and 4.2 still apply in the case of thicker specimens, although sample morphology also starts to play a role, possibly due to oxygen diffusion effects. Chemical composition, i.e., the concentration of tertiary carbons and isotacticity is still the driving force governing the onset and the rate of degradation as was seen for thin films of the two copolymers, although morphological effects also seem to become important at longer degradation times.

4.5 References

1. Bolland, J. L.; Gee, G. *Trans. Faraday Soc.* (1946) 42, p 236.
2. Luzuriaga, S.; Kovárová, J.; Fortelny, I. *Polym. Degrad. Stab.* (2006) 91, p 1226.
3. Alariqi, S. A. S.; Pratheep Kumar, A.; Rao, B. S. M.; Singh, R. P. *Polym. Degrad. Stab.* (2007) 92, p 299.
4. Schlick, S.; Kruczala, K. *JCT Research* (2005) 2, p 389.
5. Kruczala, K.; Bokria, F. G.; Schlick, S. *Macromolecules* (2003) 36, p 1909.
6. Rugg, F. H.; Smith, J. J.; Bacon, R. C. *J. Polym. Sci.* (1954) 13, p 535.
7. Adams, J. H. *J. Polym. Sci., Poylm. Chem. Edn.* (1970) 8, p 1279.
8. Carlsson, D. J.; Brousseau, R.; Zhang, C.; Wiles, D. *ACS Symp. Ser.* (1988) 364, p 676.
9. Mani, R.; Singh, R. P.; Sivaram, S. *Polym. Int.* (1997) 44, p 137.
10. Singh, R. P.; Mani, R.; Sivaram, S.; Lacoste, J.; Lemaire, J. *Polym. Int.* (1993) 32, p 189.
11. Gulmine, J. V.; Janissek, P. R.; Heise, H. M.; Akselrud, L. *Polym. Degrad. Stab.* (2003) 79, p 385.
12. Luongo, J. P. *J. Polym. Sci.* (1960) 42, p 139.
13. Lacoste, J.; Singh, R. P.; Boussand, J.; Arnaud, R. *J. Polym. Sci., Poylm. Chem. Edn.* (1987) 25, p 2799.
14. Valadez-Gonzalez, A.; Gervantes-Uc, J. M.; Veleva, L. *Polym. Degrad. Stab.* (1999) 63, p 253.
15. Tocháchek, J.; Jancár, J.; Kalfus, J.; Zborilová, P.; Burán, Z. *Polym. Degrad. Stab.* (2008) 93, p 770.
16. Delprat, P.; Duteurtre, X.; Gardette, J.-L. *Polym. Degrad. Stab.* (1995) 50, p 1.
17. Gensler, R.; Plummer, C. J. G.; Kausch, H.-H.; Kramer, E.; Pauquet, J.-R.; Zweifel, H. *Polym. Degrad. Stab.* (2000) 67, p 195.
18. Edge, M., Infrared spectroscopy in analysis of polymer degradation. In *Encycl. Anal. Chem.*, Meyers, R. A., Ed. John Wiley and Sons Ltd.: Chichester, 2000; p 7658.
19. Santos, A. S. F.; Agnelli, J. A. M.; Trevisan, D. W.; Manrich, S. *Polym. Degrad. Stab.* (2002) 77, p 441.
20. Lew, R.; Suwanda, D.; Balke, S. T. *J. Appl. Polym. Sci.* (1988) 35, p 1049.
21. Ying, Q.; Zhao, Y.; Liu, Y. *Makromol. Chem.* (1991) 192, p 1041.
22. De Goede, S.; Brüll, R.; Pasch, H.; Marshall, N. *Macromol. Symp.* (2003) 193, p 35.
23. Ver Strate, G.; Cozewith, C.; West, R. K.; Davis, W. M.; Capone, G. A. *Macromolecules* (1999) 32, p 3837.
24. Albrecht, A.; Heinz, L.-C.; Lilge, D.; Pasch, H. *Macromol. Symp.* (2007) 257, p 46.
25. De Goede, S. *Novel Analytical approaches for studying Degradation in PP and PP-1-Pentene Copolymers*. University of Stellenbosch, Stellenbosch, 2006.
26. Li, J.; Yang, R.; Yu, J.; Liu, Y. *Polym. Degrad. Stab.* (2008) 93, p 84.
27. Gallo, R.; Brambilla, L.; Castiglioni, C.; Ipsale, S.; Severini, F.; Quasso, F.; Consolati, G. *Eur. Polym. J.* (2005) 41, p 359.
28. Elvira, M.; Tiemblo, P.; Gómez-Elvira, J. M. *Polym. Degrad. Stab.* (2004) 83, p 509.
29. Guisández, J.; Tiemblo, P.; Gómez-Elvira, J. M. *Polym. Degrad. Stab.* (2005) 87, p 543.
30. Da Costa, H. M.; Ramos, V. D.; de Oliveira, M. G. *Polym. Test.* (2007) 26, p 676.
31. Britto, L. J. D.; Soares, J. B. P.; Penlidids, A.; Monrabal, B. *J. Polym. Sci., Part B: Polym. Phys.* (1999) 37, p 539.
32. Olivares, N.; Tiemblo, P.; Gómez-Elvira, J. M. *Polym. Degrad. Stab.* (1999) 65, p 297.
33. Alam, M. S.; Nakatani, H.; Goss, B. G. S.; Ichiki, T.; Liu, B.; Terano, M. *J. Appl. Polym. Sci.* (2002) 86, p 1863.
34. Rabello, M. S.; White, J. R. *Polymer* (1997) 38, p 6379.
35. Fan, Z.; Zhang, Y.; Xu, J.; Wang, H.; Feng, L. *Polymer* (2001) 42, p 5559.
36. Fu, Z.-S.; Fan, Z.-Q.; Zhang, Y.-Q.; Feng, L.-X. *Eur. Polym. J.* (2003) 39, p 795.
37. Xu, J.; Feng, L.; Yang, S.; Wu, Y. *Polymer* (1997) 38, p 4381.
38. Randall, J. C. *JMS-Rev. Macromol. Chem. Phys.* (1989) C29, p 201.
39. Feng, Y.; Hay, J. N. *Polymer* (1998) 39, p 6723.
40. Hongjun, C.; Xiaolie, L.; Dezhu, M.; Jianmin, W.; Hongsheng, T. *J. Appl. Polym. Sci.* (1999) 71, p 93.
41. Tan, H.; Li, L.; Chen, Z.; Song, Y.; Zheng, Q. *Polymer* (2005) 46, p 3522.
42. Paxson, J. R.; Randall, J. C. *Anal. Chem.* (1978) 50, p 1777.
43. Carman, C. J.; Wilkes, C. E. *Rubber Chem. Technol.* (1971) 44, p 781.

44. Randall, J. C. *Macromolecules* (1978) 11, p 33.
45. Sun, Z.; Yu, F.; Qi, Y. *Polymer* (1991) 32, p 1059.
46. Ray, G. J.; Johnson, P. E.; Knox, J. R. *Macromolecules* (1977) 10, p 773.
47. Kanezaki, T.; Kume, K.; Sato, K.; Asakura, T. *Polymer* (1993) 34, p 3129.
48. Mirabella, F. M. *Polymer* (1993) 34, p 1729.
49. Xu, J.; Feng, L. *Eur. Polym. J.* (2000) 36, p 867.
50. Liu, Y.; Bo, S.; Zhu, Y.; Zhang, W. *J. Appl. Polym. Sci.* (2005) 97, p 232.
51. Mierau, U.; Voigt, D.; Böhme, F.; Brauer, E. *J. Appl. Polym. Sci.* (1997) 63, p 283.
52. Zacur, R.; Goizueta, G.; Capiati, N. *Polym. Eng. Sci.* (1999) 39, p 921.
53. Zacur, R.; Goizueta, G.; Capiati, N. *Polym. Eng. Sci.* (2000) 40, p 1921.
54. Nakatani, H.; Manabe, N.; Yokota, Y.; Minami, H.; Suzuki, S.; Yamaguchi, F.; Terano, M. *Polym. Int.* (2007) 56, p 1152.
55. Usami, T.; Gotoh, Y.; Unemoto, H.; Takayama, S. *Appl. Polym. Sci.: Appl. Polym. Symp.* (1993) 52, p 145.
56. Kakugo, M.; Miyatake, T.; Mizunuma, K.; Kawai, Y. *Macromolecules* (1988) 21, p 2309.
57. Painter, P. C.; Watzek, M.; Koenig, J. L. *Polymer* (1977) 18, p 1169.
58. Baker, B. B.; Bonesteel, J. K.; Keating, M. Y. *Thermochim. Acta* (1990) 166, p 53.
59. Andreassen, E., Infrared and Raman spectroscopy of polypropylene. In *Polypropylene: An A-Z reference*, Karger-Kocsis, J., Ed. Kluwer Publishers: Dordrecht, 1999 p320.
60. Monasse, B.; Haudin, J. M., Molecular structure of polypropylene homo- and copolymers. In *Polypropylene: Structure, blends and composites*, Karger-Kocsis, J., Ed. Chapman & Hall: London, 1995; p 3.
61. Wang, L.; Huang, B. *J. Polym. Sci., Part B: Polym. Phys.* (1990) 28, p 937.
62. Paukkeri, R.; Lethtinen, A. *Polymer* (1994) 35, p 1673.
63. Pires, M.; Mauler, R. S.; Liberman, S. A. *J. Appl. Polym. Sci.* (2004) 92, p 2155.
64. Ozzetti, R. A.; De Oliveira Filho, A. P.; Schuchardt, U.; Mandelli, D. *J. Appl. Polym. Sci.* (2002) 85, p 734.
65. Cross, L. H.; Richards, R. B.; Willis, H. A. *Discuss. Faraday Soc.* (1950) 9, p 235.
66. Bly, R. M.; Kiener, P. E.; Fries, B. A. *Anal. Chem.* (1966) 38, p 217.
67. Luongo, J. P. *J. Appl. Polym. Sci.* (1960) 3, p 302.
68. Quynn, R. G.; Riley, J. L.; Young, D. A.; Noether, H. D. *J. Appl. Polym. Sci.* (1959) 2, p 166.
69. Sibilia, J. P.; Winklehofer, R. C. *J. Appl. Polym. Sci.* (1962) 6, p S56.
70. Brader, I. I. *J. Appl. Polym. Sci.* (1960) 3, p 370.
71. Krimm, S. *Adv. Polym. Sci.* (1960) 2, p 51.
72. Stein, R. S.; Sutherland, G. B. B. M. *J. Chem. Phys.* (1953) 21, p 370.
73. Tobin, M. C.; Carrano, M. J. *J. Polym. Sci.* (1957) 24, p 93.
74. Drushel, H. V.; Iddings, F. A. *Anal. Chem.* (1963) 35, p 28.
75. Snyder, R. G.; Maroncelli, M.; Strauss, H. L.; Hallmark, V. M. *J. Phys. Chem.* (1986) 90, p 5623.
76. Manabe, N.; Yokota, H.; Nakatani, H.; Suzuki, S.; Liu, B.; Terano, M. *Polym. Bull.* (2005) 54, p 141.
77. Manabe, N.; Yokota, H.; Suzuki, S.; Liu, b.; Terano, M. *J. Appl. Polym. Sci.* (2006) 100, p 1831.
78. Terano, M.; Liu, B.; Nakatani, H. *Makromol. Symp.* (2004) 214, p 299.
79. Suzuki, S.; Liu, B.; Terano, M.; Manabe, N.; Kawamura, K.; Ishikawa, M.; Nakatani, H. *Polym. Bull.* (2005) 55, p 141.
80. Pinheiro, L. A.; Chinelatto, M. A.; Canevarolo, S. V. *Polym. Degrad. Stab.* (2004) 86, p 445.
81. Monrabal, B., Temperature Rising Elution Fractionation and Crystallisation analysis fractionation. In *Encycl. Anal. Chem.*, Meyers, R. A., Ed. John Wiley & sons LTD: New York, 2000; Vol. 9, p 8074.
82. Kruczala, K.; Aris, W.; Schlick, S. *Macromolecules* (2005) 38, p 6979.
83. Sarwade, B. D.; Singh, R. P. *J. Appl. Polym. Sci.* (1999) 72, p 215.
84. Cunliffe, A. V.; Davis, A. *Polym. Degrad. Stab.* (1982) 4, p 17.
85. Allen, N. S.; Palmer, S. J.; Marshall, G. P.; Gardette, J.-L. *Polym. Degrad. Stab.* (1997) 56, p 265.
86. Jouan, X.; Gardette, J.-L. *Polym. Commun.* (1987) 28, p 329.
87. Knight, J. B.; Calvert, P. D.; Billingham, N. C. *Polymer* (1985) 26, p 1713.
88. Scheirs, J.; Delatycki, O.; Bigger, S. W.; Billingham, N. C. *Polym. Int.* (1991) 36, p 187.
89. Livanova, N. M. *Polym. Sci. Ser. A* (1994) 36, p 32.
90. Lemaire, J.; Gardette, J.-L.; Lacoste, J. *Macromol. Chem., Macromol. Symp.* (1993) 70, p 419.
91. Celina, M.; George, G. A.; Billingham, N. C. *Polym. Degrad. Stab.* (1993) 42, p 335.

92. Livanova, N. M.; Zaikov, G. E. *Polym. Degrad. Stab.* (1997) 57, p 1.
93. George, G. A.; Celina, M.; Lerf, C.; Cash, G.; Weddell, D. *Macromol. Symp.* (1997) 115, p 69.
94. George, G. A.; Ghaemy, M. *Polym. Degrad. Stab.* (1991) 33, p 411.
95. Girois, S.; Audouin, L.; Verdu, J.; Delprat, P.; Marot, G. *Polym. Degrad. Stab.* (1996) 51, p 125.
96. Turton, T. J.; Okumura, H.; Nishiyama, I. *Polym. Degrad. Stab.* (2003) 81, p 491.
97. Turton, T. J.; White, J. R. *Polym. Degrad. Stab.* (2001) 74, p 559.
98. Rivaton, A.; Gardette, J.-L.; Mailhot, B.; Morlat-Therlas, S. *Macromol. Symp.* (2005) 225, p 129.
99. Shyichuk, A. V.; Ehite, J. R.; Craig, I. H.; Syrotynska, I. D. *Polym. Degrad. Stab.* (2005) 88, p 415.
100. Ellis, G.; Marco, C.; Gòmez, M. *Infrared Phys. Technol.* (2004) 45, p 349.
101. Audouin, L.; Langlois, V.; Verdu, J.; De Bruihn, J. C. M. *J. Mater. Sci.* (1994) 29, p 584.

Chapter 5

Conclusions and Recommendations

In this chapter the overall conclusions of this study are formulated and discussed and some recommendations for future work in this field of study are proposed.

5.1 Conclusions

In Section 4.1 it was illustrated that fractionation (TREF, CRYSTAF) and hyphenated techniques (SEC-FTIR) could be used successfully to obtain information on the heterogeneity of the degradation of bulk impact PP copolymers. The combination of TREF with conventional techniques such as ^{13}C-NMR, FTIR, SEC and DSC into a multi-component analysis procedure proved to be highly suitable for extensive characterisation of the undegraded material and for assessing the degradation behaviour of the individual components of this complex copolymer. The final step of the multi-analysis procedure comprised the combination of TREF with SEC-FTIR, which provided valuable information on the chemical composition of all fractions as a function of molecular weight. This allowed unprecedented insight into the chemical composition distribution as well as ethylene and propylene crystallinity distributions as a function of molecular weight for the fractions of the undegraded material. The distribution of carbonyl-containing degradation products as well as chemical composition changes caused by degradation, could also be evaluated within the TREF fractions of the degraded samples.

The following individual conclusions were also obtained from this section:

- Prep-TREF combined with ^{13}C-NMR, DSC, FTIR and SEC was highly successful at identifying the major components of this heterogeneous copolymer system based on chemical composition, molecular weight, thermal properties and crystallinity. It was concluded that the PP homopolymer phase, ranging from highly amorphous aPP in the lowest elution temperature (T_e) fraction, to highly iPP in the highest fractions, eluted across the entire TREF elution range as a result of its tacticity distribution. Copolymers of ethylene and propylene, ranging from EPR to a range of semi-crystalline copolymers of different monomer sequence lengths and distributions were found to co-elute with the PP phase across the same TREF elution profile, with the result that bimodal molecular weight distributions were present within most fractions of this copolymer. This effect was most pronounced within the mid-eluting fractions. Chemical composition analysis by TREF-(SEC-FTIR) was successful at identifying the lower molecular weight component as low isotacticity PP and the higher molecular weight component as the EP copolymer part. Construction of crystallinity profiles across the bimodal distribution indicated the presence of both crystalline ethylene and propylene within the higher molecular weight EPC component, while a low level of crystallinity of only PP was identified within the low molecular weight component. This was the first time where the chemical composition of TREF fractions of impact PP copolymers had been confirmed by means of SEC-FTIR. This offers a powerful alternative to methods used by other authors for investigating the composition of these copolymers. Prep-TREF combined with the complimentary techniques mentioned above, indicated the 30ºC fraction to consist of EPR with a minor aPP component, the 110–130ºC fractions to consist of highly isotactic PP with a minor hPE component present too, while the mid-eluting 60–100ºC fractions were identified to consist of co-eluting EPC and low isotacticity PP.

- Conventional SEC and FTIR analysis of the bulk 3V copolymer indicated a similarity in thermo-oxidative degradation behaviour to that of hPP, i.e. molecular weight changes resulting mainly from chain scission and the formation of carbonyl functionalities usually found in hPP.

- SEC-FTIR illustrated both shifts in molecular weight distribution curves to lower values as a result of chain scission, and indicated an inhomogeneous distribution of degradation products across the molecular weight distribution of the degraded bulk sample, where the highest concentration of degradation products were located at the low molecular weight side of the molecular weight distribution of degraded samples.

- CRYSTAF analysis indicated a change in the crystallisability of the bulk 3V copolymer as a function of degradation time. Degradation was seen to cause a shift in the peak crystallisation temperature towards lower values, accompanied by an increase in the weight percentage of the soluble fraction. This suggests that degradation mainly affects the more crystalline material, altering the crystallisability of highly isotactic material in such a way that renders some chains completely non-crystallisable.

- Similar changes in crystallinity of the bulk sample were also observed by prep-TREF. Re-crystallisation of degraded bulk samples and their fractionation by TREF, revealed an increase in the weight of material eluting within the lower T_e fractions (30–100ºC), accompanied by a decrease in the amount of the highest eluting fractions (110–130ºC), indicating the preferential degradation of the higher isotactic material within this copolymer. TREF-SEC indicated the biggest shift in molecular weight distribution of the fractions of the degraded samples to be present within the iPP fractions, as well as the 30ºC fraction. Within the bimodal molecular weight distribution fractions, the lower PP molecular weight component showed very little shift in its molecular weight distribution, while the higher EPC component shifted to some extent. SEC-FTIR analysis of the TREF fractions of the degraded samples provided valuable information on the molecular weight and chemical composition changes responsible for the crystallisability changes observed in the TREF curves of the bulk samples. Carbonyl concentration and propylene content profiles were constructed across the molecular weight distribution of each fraction of the undegraded and degraded samples in order to evaluate the distribution of degradation products as well as any chemical composition changes occurring within each fraction. A uniform CO profile with a value close to 0 was observed across the molecular weight distribution curves of all fractions of the undegraded material. Upon degradation, an increase in the CO profile could be observed at the lower molecular weight end of the Gram-Schmidt plot of fractions. The concentration of CO species remained mostly unchanged in the 110ºC and 120ºC fractions, but together with the decrease in the weight of material eluting within these fractions upon degradation, it was believed that degraded material was no longer eluting within this fraction of the degraded material due to a change in crystallisability. The 30ºC fraction, which showed a significant increase in the amount of amorphous material eluting here as a function of degradation time, showed a significant increase in

its CO concentration profile towards the lower molecular weight end of the distribution. The propylene concentration profile indicated the elution of hPP within this fraction upon degradation and, therefore, it was concluded that degraded iPP from higher eluting fractions eluted at 30ºC within the degraded samples. Within the fractions exhibiting bimodal molecular weight distributions of hPP and EPC, an apparent increase in the intensity of the lower molecular weight component was detected, accompanied by an apparent decrease in the intensity of the EPC distribution. The propylene content profile indicated the lower molecular weight component to still only consist of PP, even in the degraded samples. CO functionalities are also mainly found within this component. These results suggest that degraded iPP from higher fractions not only eluted within the soluble fraction (30ºC) after degradation, but also in the 60–100ºC fractions. The elution temperature of the degraded iPP chains, therefore, depends on the level of molecular weight and chemical composition modification brought about by degradation, when degraded bulk sample are re-crystallised and fractionated by TREF.

- CRYSTAF, TREF and SEC proved to be more successful at detecting the onset of degradation than FTIR. Although no carbonyl functionalities could be detected by FTIR during early stages of degradation within the bulk sample (40 hours), CRYSTAF, TREF and SEC indicated changes in crystallisability and molecular weight.

In Section 4.2 it was concluded that TREF combined with ^{13}C-NMR, SEC, and DSC is highly suitable for studying differences in chemical composition, molecular weight, thermal behaviour and monomer sequence distributions and lengths in impact PP copolymers of different comonomer, isotacticity and crystallinity. Although conventional SEC and FTIR analysis illustrated the main differences in degradation behaviour between two copolymer grades, TREF once again succeeded in identifying micro-structural differences between the two undegraded samples in order to explain their difference in degradation behaviour. TREF-SEC also indicated how these micro-structural differences can be correlated to the difference in degradation behaviour of fractions of the two copolymers observed after recrystallisation and fractionation of bulk samples by TREF. The following conclusions were made in this section:

- A large difference in the degradation behaviour of the two copolymers was observed by FTIR and SEC. Conventional techniques indicated a difference in ethylene content, isotacticity and crystallinity between the two copolymers, with a higher ethylene content and lower isotacticity and higher amount of amorphous material by weight than copolymer 3V. Similar changes in crystallisability were also observed by CRYSTAF, TREF and DSC of the bulk copolymers, despite the significant difference in the time scale of the degradation within the two grades.

- TREF fractionation of the two copolymers indicated similar isotacticity distributions as well as DSC T_m and T_c values for corresponding fractions of the undegraded copolymers, indicating that the PP phase is very similar in composition and that the ethylene and propylene sequence distributions of

the EPC phase are very similar in the two copolymers. Only minor differences in molecular weight values were detected in selected fractions. There was, however, a difference in the weight percentage of the fractions eluting in the various elution ranges of the two copolymers. The weight percentage of the lower T_e fractions of copolymer 4V (30ºC and 60ºC) were larger than that of copolymer 3V, and a higher ethylene content was also detected within these fractions as expected.

- TREF analysis of the degraded 4V copolymer illustrated similar changes in the weight percentage of individual fractions to those observed for copolymer 3V, where the amount of material within higher eluting fractions also decreases with an accompanying increase in the amount of material eluting at lower temperatures. It is, therefore, also observed in this case, that the crystallisability of the iPP phase is altered by degradation to such an extent that some part of the original iPP phase is no longer at higher T_e, causing it to elute either at 30ºC or slightly higher T_e, according to the extent of structural modification by scission and CO group insertion reactions. The iPP phase is still degraded preferentially, despite the larger amount of amorphous material present within the bulk 4V sample.

- TREF-SEC of degraded samples, however, indicated differences in the degradation behaviour of some fractions of the two copolymers. The molecular weight shifts observed for the higher eluting (iPP) fractions of the two copolymers are similar, which is to be expected, since the hPP phase seems to be very similar in composition and isotacticity, which are the two major influences governing degradation within PP. The mid-eluting fractions of sample 4V, consisting of low isotacticity PP and EPC, show slight differences in molecular weight shifts to those of sample 3V. Similar changes are observed for the low isotacticity PP component of the fractions of corresponding elution temperatures, whereas the EPC component of copolymer 4V shows slightly higher stability than that of sample 3V. The biggest difference in molecular weight shifts are, however, observed within the 30ºC sample of the two copolymers. In sample 3V, the entire molecular weight distribution of this fraction is seen to shift to lower values with ongoing degradation time, indicating that, although degraded iPP elutes here within the degraded samples, there also seems to be some degradation of the EPR phase. In copolymer 4V, some part of the original molecular weight distribution remains at longer degradation times, indicating a higher stability of the EPR phase observed for this copolymer.

- The higher stability of copolymer 4V is concluded to result not only from differences in comonomer content and isotacticity within the bulk samples, but also from the relative amounts of EPR and iPP as well as the amount of ethylene within the EPR and transition copolymer fractions. Since the ethylene content and amount of EPR has a significant influence on the morphology of the bulk sample, the difference in the stability of the two copolymers is also believed to be related to a difference in the morphology. The EPR promotes mobility of oxygen, causing the core layers of 4V to degrade to a larger extent than that of 3V, but the larger amount of EPR will also restrict

cracking, flaking and loss of surface material, thereby slowing down surface attack during early stages of degradation.

In Section 4.3 the spatial heterogeneity of degradation within thicker samples of both copolymers were studied in order to investigate the influence of morphology (i.e., oxygen diffusion), which might be more significant for these samples compared to the thin films studied in the previous section. FTIR-μS proved to be a suitable method for studying CO concentration profiles across the width of thicker specimens of both samples. The following conclusions were obtained:

- Functional group maps constructed for the CO degradation products indicated a higher level of degradation within the surface layers of thick samples, compared to the core.

- The degradation product profiles were symmetrical for all degradation times studied in the two copolymers, suggesting similar rates of degradation from both surfaces for each plaque. The shape of the profiles were slightly different in the two copolymers, where the CO concentration profiles at longer degradation times were V-shaped in sample 3V, compared to flatter, U-shaped profiles in the 4V grade. These results suggested an earlier onset of degradation at the edges of sample 3V, and quicker spread of degradation from the edges towards the core of this copolymer compared to sample 4V. These results are consistent with those observed for thin films of the two copolymers studied in the previous section, where chemical composition (i.e., concentration of tertiary carbons and isotacticity) was concluded to be the main force governing the earlier degradation in sample 3V. Despite this difference in degradation behaviour at the surface of the two copolymers, the level and the increase in the carbonyl concentration within the core layers of the two samples appeared similar as degradation time increased.

- Layer-by-layer milling from the surface towards the core of thick degraded specimens, followed by FTIR of the layers, confirmed the earlier onset of degradation within the surface layers of sample 3V at degradation time of 50 hours, when hardly any CO functionalities could be detected for sample 4V. At a degradation time of 102 hours, however, similar degradation behaviour is observed throughout the surface layers of both copolymers. SEC analysis of the layers also confirmed the larger extent of degradation in sample 3V at 50 hours, followed by a drastic increase the level of degradation observed for sample 4V at 102 hours.

- CRYSTAF analysis suggested the similarity in degradation of the core layers of the two copolymers to be the result of the similar crystallinity or crystallisability of the core layers of the two copolymers, compared to the bulk. It can, therefore, be concluded that the differences in degradation behaviour of the surfaces of the two copolymers is the result of chemical structure, whereas the similarity in degradation behaviour between the core layers are the result of morphology, where similar crystallisability are detected for the core layers of the two grades, suggesting similar oxygen diffusion effects, which did not play a significant role in the degradation of the thin films.

In general, it is concluded that fractionation and hyphenated techniques, combined with conventional characterisation techniques are highly suitable for studying the microstructure of undegraded impact PP copolymers. These techniques are equally informative of the degradation behaviour of impact PP copolymers as a function of their chemical composition and crystallinity or morphology. These techniques have suggested that chemical structure, i.e., comonomer content and isotacticity of the PP phase governs the degradation behaviour of impact PP copolymer thin films. It was also illustrated how degradation leads to a change in the crystallisability of the iPP phase through chain scission and CO group insertion. The spatial heterogeneity of the degradation process was studied by FTIR-μS and analysis of mechanically abrased layers, which suggested that the degradation of surface layers of thick samples is governed by chemical composition, whereas morphological effects also become important in the degradation of the core layers.

5.2 Recommendations

In this study it was seen how TREF combined with SEC-FTIR can be used to study the degradation of the individual fractions within heterophase EP copolymers. The co-elution of degraded higher isotacticity material from higher eluting fractions together with non-degraded material could, however, obscure changes in the lower eluting fractions. It would, therefore, be useful to separate the degraded molecules from the non-degraded material within each TREF fraction. For this purpose, high-temperature gradient HPLC separation combined with TREF is proposed. Some preliminary investigations for future work in this regard have been performed and the results are presented here.

A sample of copolymer 3V, degraded for 115 hours was fractionated by TREF into three fractions, according to the major components identified within this copolymer within Section 4.1 of this study. The EPR, iPP and co-eluting EPC and low isotacticity fractions were collected at 30, 100 and 130ºC, respectively, in both samples. The TREF fractions of these two samples were analysed by the HT-HPLC procedure described in Section 3.3.8 of the experimental chapter. Considering that the main functionalities formed by degradation are polar in nature, a polar stationary phase was selected to facilitate interaction with degraded molecules. Therefore, non-degraded material was expected to elute first, followed by the more polar, degraded molecules. The 30ºC fraction of the undegraded 3V copolymer, which is known to consist mainly of soluble, non-degraded EPR, was used as reference to investigate the separation of the fractions of the degraded sample according to their degree of degradation. The HT-HPLC results of the undegraded and three degraded fractions are presented in the following figure.

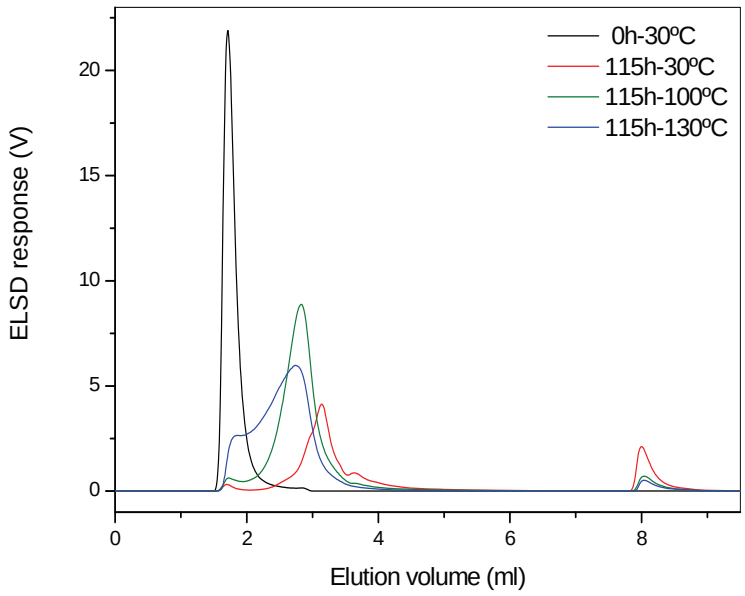

Figure R.1: HT-gradient-HPLC curves of the various TREF fractions of a degraded and undegraded 3V sample.

The undegraded 0h-30ºC fraction elutes within a single, uniform peak at an elution volume close to the dead volume of the column. This indicates that only non-polar material, which does not interact with the stationary phase is present within this fraction. Contrary to this, all fractions of the degraded sample have a main elution peak at slightly higher elution volumes than the single peak eluting in the undegraded fraction, as well as an additional peak at a considerably larger elution volume. The peak at higher elution volume is expected to contain the most degraded, polar molecules retained within the column. The intensity of this peak indicates that the highest concentration of degradation products is present within the 30ºC fraction of the degraded sample, followed by the 100 and 130ºC fractions. The 30ºC fraction also contains the lowest concentration of the original undegraded material, as can be seen from the really small intensity of the blue peak at an elution volume of approximately 1.8 ml. The intensity of this peak decreases in the order 0h-30ºC > 115h-130ºC > 115h-100ºC > 115h-30ºC, indicating that the amount of undegraded material also decreases from the highest to lowest eluting fraction within the degraded sample, and that all fractions contain a smaller concentration of undegraded material than the 0h-30ºC fraction. The degraded fractions all have an additional peak eluting around 3 ml, which is believed to consist of degraded material which is of lower polarity (i.e., lower carbonyl concentration) than the highest eluting peak at 8 ml. The elution order of this peak increases from the 115h-130ºC to the 115h-30ºC fractions, thereby, also indicating that the highest concentration of degradation products is found within the lowest eluting fraction.

It is suggested that, for future work, the HT-HPLC system should be coupled to spectroscopic techniques such as FTIR and NMR for identification of the separated components. Some preliminary results were obtained through coupling of the HT-HPLC to FTIR via the LC-Transform® interface. The (HT-HPLC)-FTIR results of the 115h-30ºC fraction is displayed in Figure R.2.

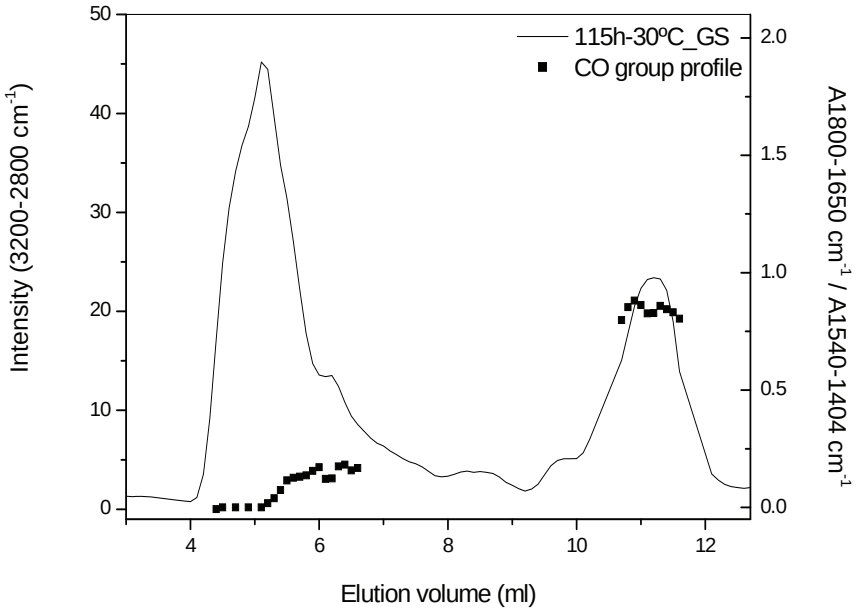

Figure R.2: (HT-HPLC)-FTIR results illustrating the carbonyl concentration profile within the 30ºC fraction of a degraded (115h) sample of copolymer 3V.

These results indicate that carbonyl functionalities are found within both the lower and higher elution volume peaks and that the carbonyl concentration increases with increasing elution volume. This combination of HT-HPLC separation and FTIR can, therefore, be used successfully for separating degraded from non-degraded material within each component of impact PP copolymers fractionated by TREF and for identifying the components separated. Future studies will be directed towards the optimisation of the HT-HPLC-FTIR system as well as the coupling of NMR to HT-HPLC as an alternative method for the identification of the degradation products separated.

Appendix

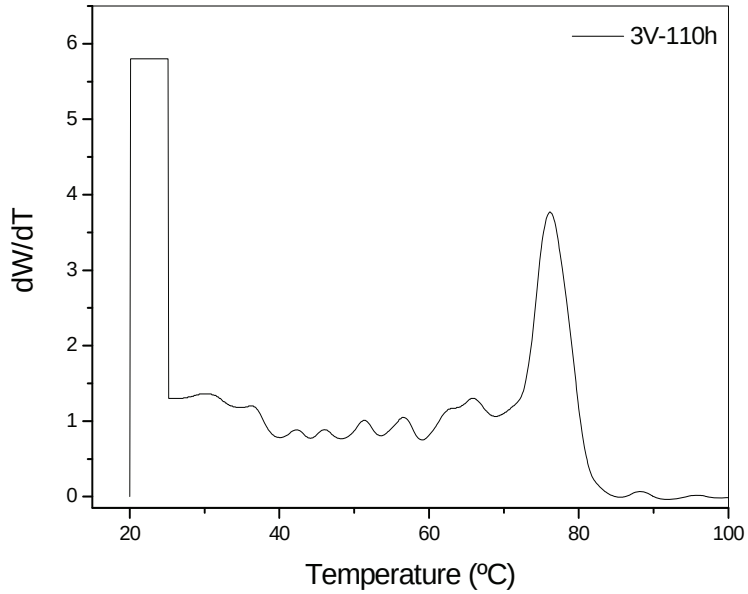

Figure A.1: CRYSTAF curve of the 3V sample degraded for 110 hours.

Table B.1: TREF data for the undegraded 3V and 4V copolymers

Sample	T_e	W_i	W_i	ΣW_i	$Wi\%/\Delta T$
	(°C)	(g)	(%)	(%)	
3V-0h-30	30	0.303	9.90	9.90	0.330
3V-0h-60	60	0.102	3.36	13.26	0.090
3V-0h-80	80	0.106	3.47	16.73	0.163
3V-0h-90	90	0.100	3.26	19.99	0.307
3V-0h-100	100	0.171	5.60	25.59	0.527
3V-0h-110	110	0.574	18.80	44.39	1.771
3V-0h-120	120	1.459	47.77	92.16	4.498
3V-0h-130	130	0.240	7.85	100.00	0.739
4V-0h-30	30	0.7498	21.11	21.11	0.8445
4V-0h-60	60	0.2573	7.24	28.36	0.2070
4V-0h-80	80	0.1312	3.69	32.05	0.1847
4V-0h-90	90	0.1260	3.55	35.60	0.3548
4V-0h-100	100	0.1820	5.12	40.72	0.5125
4V-0h-110	110	0.5759	16.22	56.94	1.6216
4V-0h-120	120	1.2215	34.39	91.33	3.4394
4V-0h-130	130	0.3078	8.67	100.00	0.8667

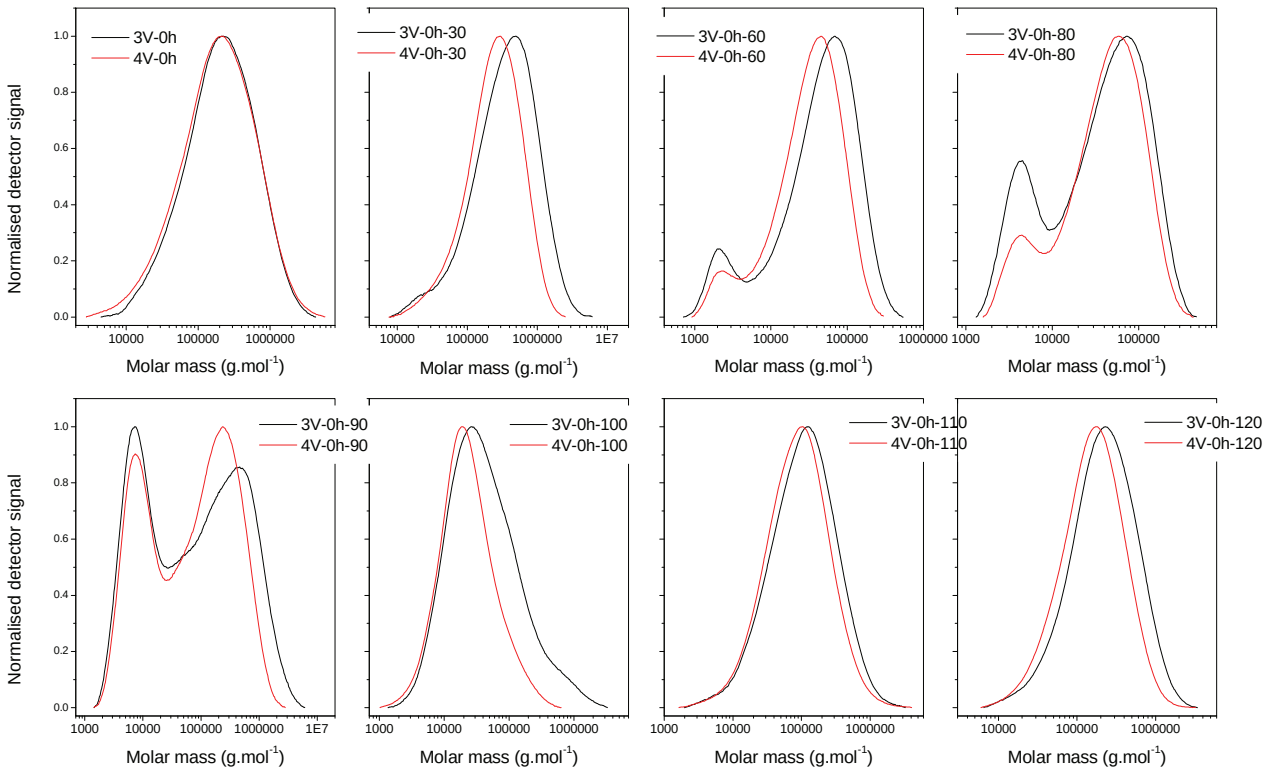

Figure B.1: Molecular weight distribution curves for all TREF fractions of the undegraded 3V and 4V copolymers.

Table B.2: Molecular weight values for all TREF fractions of the undegraded 3V and 4V copolymers

Sample	T_e (ºC)	$\overline{M_n}$ (g.mol^{-1})		$\overline{M_w}$ (g.mol^{-1})	
3V-0h-30	30		750 500		166 600
3V-0h-60	60	2 200	78 500	2 000	42 500
3V-0h-80	80	4 100	84 500	3 600	53 200
3V-0h-90	90	7 500	560 900	5 900	233 900
3V-0h-100	100		105 400		21 600
3V-0h-110	110		186 000		53 100
3V-0h-120	120		321 200		127 500
4V-0h-30	30		333 300		132 600
4V-0h-60	60	2 100	50 700	2 000	30 000
4V-0h-80	80	4 000	69 600	3 600	44 600
4V-0h-90	90	7 800	321 000	6 300	172 300
4V-0h-100	100		37 400		14 900
4V-0h-110	110		147 600		47 600
4V-0h-120	120		225 000		99 300

Table B.3: DSC T_c, T_m and ΔH_m values for all TREF fractions of the undegraded 3V and 4V samples

Sample	T_e (ºC)	T_m (ºC)		T_c (ºC)	Δh_m ($J.g^{-1}$)	
3V-0h-30	30	56.3		36.7	2	
3V-0h-60	60	89.2	111.5	62.8	6	0
3V-0h-80	80	103.0	129.7	85.1	13	10
3V-0h-90	90	117.6	145.5	104.7	16	38
3V-0h-100	100	118.1	150.1	110.7	3	66
3V-0h-110	110		159.1	115.3		92
3V-0h-120	120		160.5	114.3		99
4V-0h-30	30	52.3		31.7	1	
4V-0h-60	60	87.2	111.5	65.5	13	3
4V-0h-80	80	101.9	128.6	83.5	19	6
4V-0h-90	90	117.3	147.2	101.3	17	33
4V-0h-100	100	115.4	151.6	105.2	5	48
4V-0h-110	110		158.9	110.0		88
4V-0h-120	120		154.1	115.0		70

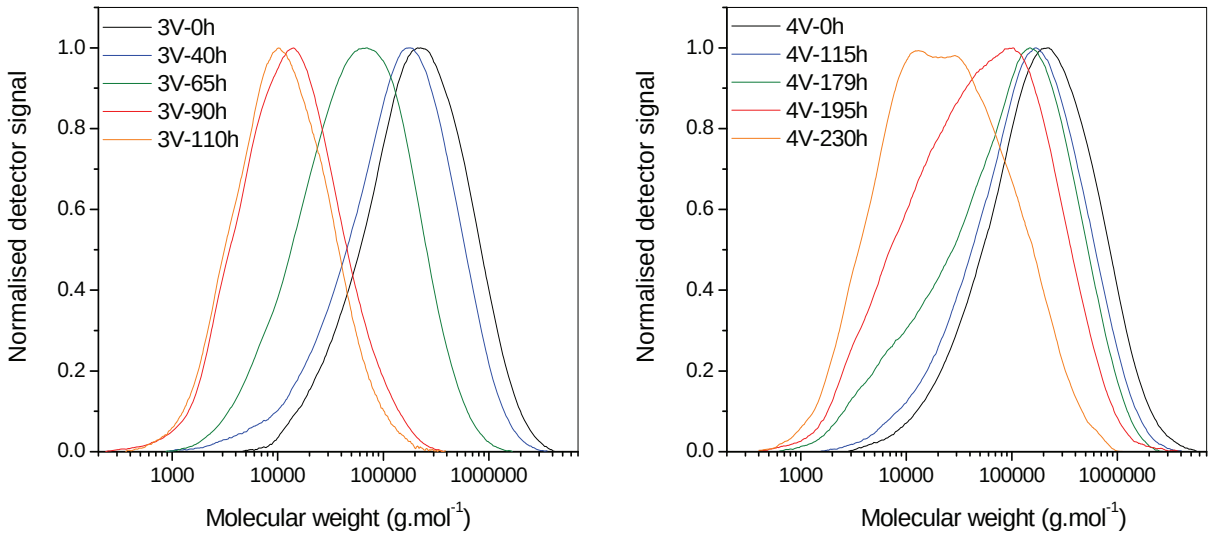

Figure C.1: Comparison of the shift in molecular weight curves of samples 3V and 4V after degradation.

Table C.1: Molecular weight and polydispersity values for the various stages of degradation in copolymers 3V and 4V

Sample	Degradation time (h)	$\overline{M}_n$ (g.mol^{-1})	$\overline{M}_w$ (g.mol^{-1})	PDI
3V-0h	0	111 500	354 400	3.18
3V-40h	40	49 000	242 800	4.96
3V-65h	65	25 400	100 000	3.94
3V-90h	90	6 900	23 000	3.33
3V-110h	110	6 600	18 400	2.79
4V-0h	0	86 600	351 900	4.06
4V-115h	115	40 000	250 800	6.26
4V-179h	179	23 100	189 100	8.18
4V-195h	195	16 300	122 700	7.52
4V-230h	230	10 000	56 400	5.63

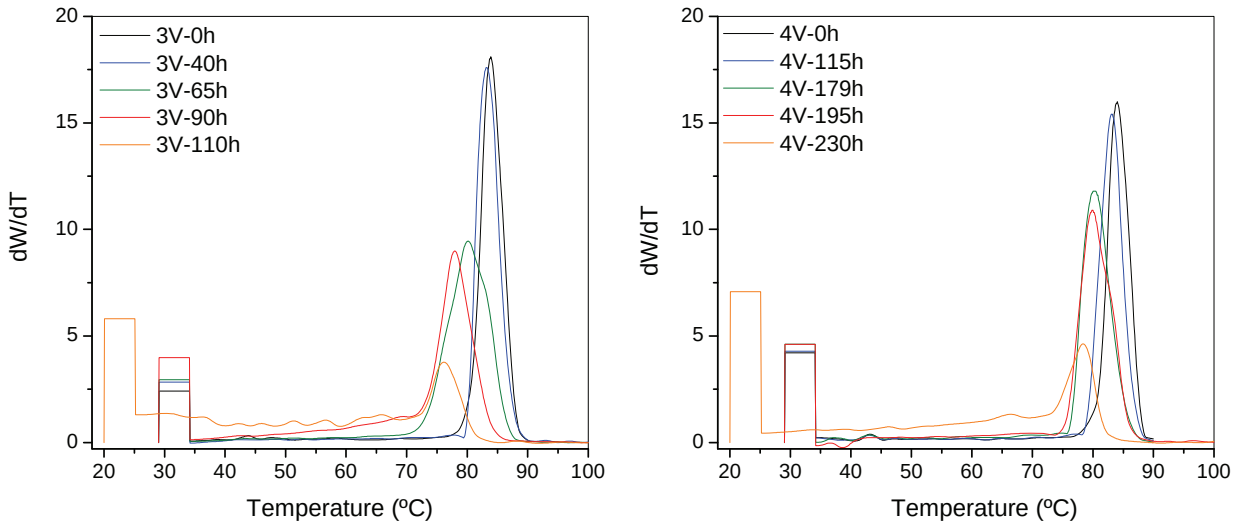

Figure C.2: CRYSTAF results for the various stages of degradation in copolymers 3V and 4V.

Table C.2: CRYSTAF data of the bulk 3V and 4V copolymer samples

Sample	T_c (peak maximum) (ºC)	Soluble fraction (Weight %)	FWHM
3V-0h	84.0	12.8	4.69
3V-40h	83.2	14.2	3.44
3V-65h	80.2	14.7	6.68
3V-90h	77.9	19.9	5.12
3V-110h	76.2	n.d.	n.d.
4V-0h	83.9	21.0	3.41
4V-115h	82.7	22.5	3.61
4V-179h	81.9	23.0	5.07
4V-195h	80.1	23.9	4.39
4V-230h	78.3	n.d.	n.d.

n.d. not determined

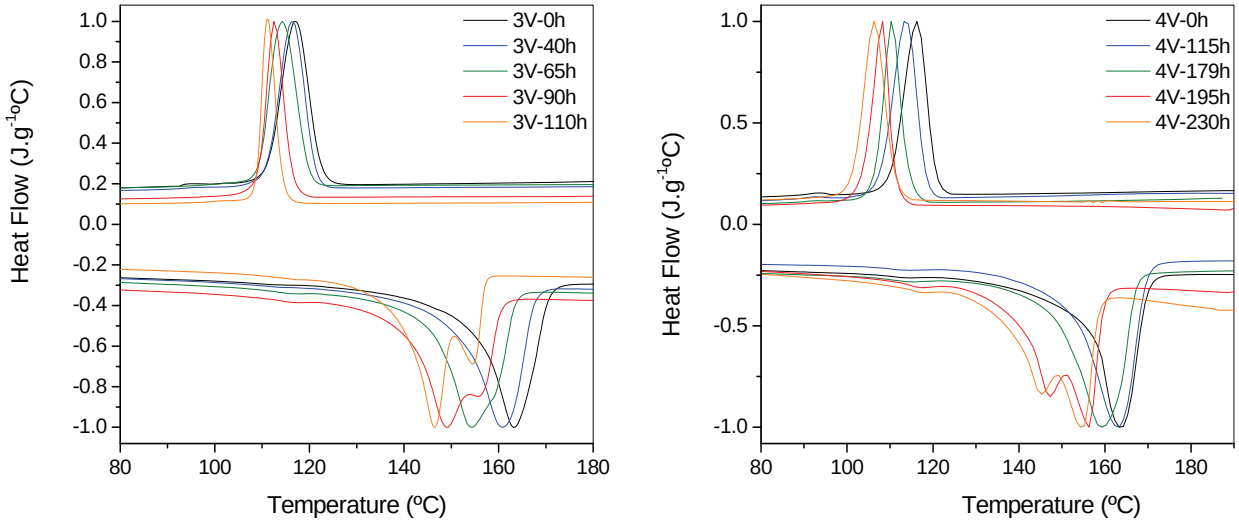

Figure C.3: DSC melting and crystallisation curves obtained at the various stages of degradation in copolymers 3V and 4V.

Table C.3: DSC thermal data for the various stages of degradation in copolymers 3V and 4V

Sample	T_m (°C)	T_c (°C)	Δh_m ($J.g^{-1}$)
3V-0h	162.6	118.2	94
3V-40h	160.1	117.7	91
3V-65h	153.6	115.5	89
3V-90h	148.6	112.5	88
3V-110h	147.0	110.9	87
4V-0h	160.7	116.3	72
4V-115h	159.0	113.8	70
4V-179h	156.7	110.2	67
4V-195h	155.3	108.3	66
4V-230h	153.7	106.5	65